Prediction of the Binding Mode of Suberone-Inhibitors in the p38 MAP Kinase with Molecular Modeling Studies

Ermittlung des Bindemodus von Suberon-Inhibitoren in der p38 MAP Kinase mit Methoden des Molecular Modelings

DISSERTATION

der Fakultät für Chemie und Pharmazie

der Eberhard-Karls-Universität Tübingen

zur Erlangung des Grades eines Doktors

der Naturwissenschaften

2008

vorgelegt von

Katrin Kinkel

Diese Arbeit wurde in der Zeit vom 01.12.2005 bis 31.03.2008 unter der Anleitung von Prof. Dr. Stefan Laufer am Pharmazeutischen Institut der Universität Tübingen angefertigt.

Tag der mündlichen Prüfung: 16.05.2008

Dekan: Prof. Dr. L. Wesemann
Erster Berichterstatter: Prof. Dr. S. Laufer
Zweiter Berichterstatter: Prof. Dr. O. Werz

Quidquis agis, prudenter agas et respice finem.

Was immer du auch tust, tue es klug und denk daran, wie es ausgeht.

Contents

1. Abbrevations **xx**

2. Zusammenfassung **xxiii**

3. Introduction **1**

3.1. Proteins . . . 1

3.1.1. Basics . . . 1

3.1.2. Determining Protein Structure . . . 3

3.1.2.1. X-ray crystallography . . . 3

3.1.2.2. NMR . . . 4

3.1.2.3. Protein Kinases . . . 5

3.2. The p38 MAP kinase . . . 6

3.2.1. The p38 MAP kinase pathway . . . 10

3.2.2. Inhibition of the p38 MAP kinase . . . 11

3.2.3. p38 MAP kinase as a target in the treatment of inflammatory diseases 11

3.2.4. X-ray crystal structures of the p38α MAP kinase; DFG-IN Binders . . . 12

3.2.4.1. DFG motif . . . 12

3.2.4.2. PDB 1W84 . . . 13

3.2.4.3. PDB 1OZ1 . . . 14

3.2.4.4. PDB 2GTN . . . 15

3.2.4.5. PDB 2GFS . . . 15

3.2.4.6. PDB 2I0H . . . 16

3.2.4.7. PDB 2QD9 . . . 17

3.2.5. X-ray crystal structures of the p38 MAP kinase; DFG-OUT Binders . . . 18

3.2.5.1. PDB 1W82 and PDB 1WBS . . . 18

3.2.6. DFG-IN and DFG-OUT . . . 19

3.2.6.1. PDB 2EWA . . . 19

3.2.7. X-ray crystal structures without a ligand . . . 20

3.2.7.1. PDB 2FSO . . . 20
3.2.7.2. PDB 2PKJ . . . 21
3.3. JNK . . . 21
3.3.1. The JNK pathway . . . 23
3.3.2. Inhibition of JNK . . . 24
3.3.3. Ligands of JNK3 . . . 25
3.3.3.1. PDB 1PMN and PDB 1PMQ . . . 25
3.3.3.2. PDB 2B1P . . . 25
3.3.3.3. PDB 2O0U . . . 26
3.4. Ottosen *et al.* . . . 27
3.5. Revesz *et al.* . . . 29
3.6. The Suberones . . . 34

4. Aim of the study **36**

5. Results **40**
5.1. Validation of X-ray crystal structures: What is a good model? . . . 40
5.1.1. WHAT IF . . . 43
5.1.2. Experimental data check: R-value, ProSA, PDBSUM, Ramachandran plot . . . 46
5.1.2.1. R-Value . . . 46
5.1.2.2. ProSA . . . 47
5.1.2.3. PDBSUM . . . 53
5.1.2.4. Ramachandran Plot . . . 54
5.1.3. Chosen PDB structures . . . 58
5.1.4. Alignments by homology of the models . . . 60
5.1.5. PDB 2GTN . . . 70
5.2. Creating databases for Docking . . . 71
5.2.1. The ligands for the docking studies . . . 71
5.2.1.1. Ligands of the chosen PDB structures . . . 72
5.2.2. Properties of the Compounds . . . 72
5.3. GRID . . . 77
5.4. Docking . . . 82
5.4.1. FlexX . . . 83
5.4.1.1. Re-docking . . . 83

5.4.1.2. Cross-docking . . . 83
5.4.1.3. Docking of the Suberones . . . 85
5.4.2. Flexidock . . . 102
5.4.3. GLIDE . . . 102
5.4.3.1. Re-docking . . . 103
5.4.3.2. Cross-docking . . . 103
5.4.3.3. Docking of the Suberones . . . 106
5.4.4. eHITS . . . 115
5.4.4.1. Defining the docking options . . . 115
5.4.4.2. Re-docking . . . 115
5.4.4.3. Cross-docking . . . 116
5.4.4.4. Docking of the Suberones . . . 118
5.5. X-ray crystal structure 278SLS . . . 129
5.5.1. Docking studies with 278SLS . . . 141
5.5.1.1. FlexX . . . 141
5.5.1.2. GLIDE . . . 141
5.5.1.3. eHITS . . . 143
5.6. MORE2 compounds . . . 147

6. Conclusions and discussion **149**

7. Materials and Methods **155**
7.1. PDB structures . . . 155
7.2. Quality Check . . . 155
7.2.1. WHAT IF . . . 155
7.2.2. ProSA . . . 159
7.2.3. PDBSUM and PROCHECK . . . 159
7.3. Modeling . . . 160
7.3.1. SYBYL7.2 . . . 160
7.3.1.1. Databases . . . 160
7.3.2. GRID . . . 161
7.4. Docking . . . 164
7.4.1. FlexiDock . . . 164
7.4.2. FlexX . . . 165
7.4.3. GLIDE . . . 167

7.4.4. eHITS . . . 171
7.4.5. Pictures . . . 172

References **184**

A. Databases **185**
A.1. Ligands for docking . . . 185
A.2. Compounds for docking: Suberones, Revesz and Ottosen compounds . . . 187
A.2.1. Suberone scaffold type GA . . . 187
A.2.2. Suberone scaffold type JH . . . 190
A.2.3. Suberone scaffold type MORE . . . 190
A.2.4. Suberone scaffold type MORE2 . . . 197
A.2.5. Scaffold type OTTO . . . 198
A.2.6. Scaffold type REV . . . 199
A.2.7. Suberone scaffold type RN . . . 200
A.2.8. Suberone scaffold type SK . . . 201
A.2.9. Suberone scaffold type SG . . . 206
A.2.10. Suberone scaffold type GA . . . 209
A.2.11. Suberone scaffold type JH . . . 209
A.2.12. Suberone scaffold type MORE . . . 210
A.2.13. Suberone scaffold type MORE2 . . . 211
A.2.14. Scaffold OTTOSEN compounds . . . 211
A.2.15. Scaffold REVESZ compounds . . . 212
A.2.16. Suberone scaffold type RN . . . 212
A.2.17. Suberone scaffold type SG . . . 212
A.2.18. Suberone scaffold type SK . . . 213
A.3. Comparisons of the different Suberone scaffolds; Angles . . . 214
A.3.1. Suberone scaffold type GA . . . 214
A.3.2. Suberone scaffold type JH . . . 216
A.3.3. Suberone scaffold type MORE . . . 216
A.3.4. Suberone scaffold type MORE2 . . . 219
A.3.5. Scaffold type OTTOSEN . . . 219
A.3.6. Scaffold type REVESZ . . . 220
A.3.7. Suberone scaffold type SG . . . 221
A.3.8. Suberone scaffold type SK . . . 222

List of Figures

3.1. Protein structure, picture taken from www.contexo.info 2
3.2. X-ray crystallography 3
3.3. Rheumatoide Arthritis; picture taken from http://www.orthoteers.com 5
3.4. ATP-binding site of protein kinases 6
3.5. The Human Kinome Project, picture taken from www.kinase.com/human/kinome 7
3.6. Structure of the p38α MAP kinase, PDB 2EWA [1] 9
3.7. p38 MAPK pathway 10
3.8. Ligand L12 bound to p38α MAP kinasein DFG-IN conformation (PDB 1W84 coloured in blue) and ligand LI2 bound to p38α MAP kinasein DFG-OUT conformation (PDB 1WBS coloured in red); the DFG-OUT loop is situated above the DFG-IN loop 13
3.9. Ligand of PDB 1W84 14
3.10. Ligand of PDB 1OZ1 14
3.11. Ligand of PDB 2GTN 15
3.12. Ligand of PDB 2GFS (compound 63) 16
3.13. Ligand of PDB 2I0H 17
3.14. Ligand of PDB 2QD9 17
3.15. Ligand of 1WBS (left) and ligand of 1W82 (right) 18
3.16. SB203580 in PDB 2EWA 19
3.17. L16 loop in PDB 2FSO 20
3.18. Structure of the JNK3, PDB 2B1P [2] 22
3.19. JNK pathway 23
3.20. First reported selective JNK small molecule inhibitor SP600125 24
3.21. Left: ligand of PDB 1PMN, right: ligand of PDB 1PMQ 25
3.22. Ligand of PDB 2B1P 26
3.23. Ligand of 2O0U 26

3.24. Proposed binding mode of the Ottosen compound 45 in the ATP binding pocket of the p38α MAP kinase 28
3.25. Left: Revesz scaffold A, right: Revesz scaffold B 29
3.26. Proposed binding mode of compound 6b, which is the most potent benzoylpyridine with an IC_{50} of 8 nM 30
3.27. Left: Revesz compound 19a, right: Revesz scaffold 3 31
3.28. Left: Revesz compound 18c, right: Revesz compound 18d 32
3.29. Proposed binding mode of 18c 33
3.30. Suberone scaffold: X=O,Y=CH_2; X=CH_2,Y=O; X=CH_2, Y=CH_2, X=CH, Y=CH; X=S, Y=CH_2 34

4.1. Binding modes proposed by Ottosen *et al.* (in red) and Revesz *et al.* (in green) 37
4.2. Workflow: Aim of the study 39

5.1. Local model quality of PDB 1OZ1, red: areas of high energy, blue: areas of low energy 52
5.2. Local model quality of PDB 2GTN, red: areas of high energy, blue: areas of low energy 52
5.3. Local model quality of PDB 1W84, red: areas of high energy, blue: areas of low energy 53
5.4. Local model quality of PDB 1W82, red: areas of high energy, blue: areas of low energy 53
5.5. Torsion angles of protein backbone 54
5.6. Ramachandran plot of PDB 1PMN (left) and PDB 1PMQ (right) created by PROCHECK 55
5.7. Ramachandran plot of PDB 2B1P (left) and PDB 2O0U (right) created by PROCHECK 55
5.8. Ramachandran plot of PDB 1W82 (left) and PDB 1WBS (right) created by PROCHECK 56
5.9. Ramachandran plot of PDB 1OZ1 (left) and PDB 1W84 (right) created by PROCHECK 56
5.10. Ramachandran plot of PDB 2GFS (left) and PDB 2GTN (right) created by PROCHECK 57
5.11. Ramachandran plot of PDB 2QD9 (left) and PDB 2I0H (right) created by PROCHECK 57

5.12. Ramachandran plot of PDB 2FSO (left) and PDB 2PKJ (right) created by PROCHECK 58
5.13. Alignment of PDB 1PMQ, PDB 2O0U is fixed, RMSD 0.6043 60
5.14. Alignment of PDB 1PMN, PDB 2O0U is fixed, RMSD 0.5922 61
5.15. Alignment of PDB 2B1P, PDB 2O0U is fixed, RMSD 0.6206 61
5.16. Alignment of PDB 1PMN, PDB 2O0U is fixed, RMSD 1.1179 62
5.17. Alignment of PDB 1PMQ, PDB 2O0U is fixed, RMSD 1.1158 62
5.18. Alignment of PDB 2B1P, PDB 2O0U is fixed, RMSD 1.0904 63
5.19. Alignment of PDB 1PMN (green), PDB 1PMQ (blue) and PDB 2B1P (red); PDB 2O0U (yellow) is fixed 63
5.20. Alignment the Gly-rich loop atoms of PDB 2PKJ to all other chosen PDBs of the p38α MAP kinase 64
5.21. Alignment the hinge region atoms of PDB 2PKJ to all other chosen PDBs of the p38α MAP kinase 66
5.22. Alignment the DFG atoms of PDB 2PKJ to all other chosen PDBs of the p38α MAP kinase 69
5.23. Alignment by homology in SYBYL of PDB 1W84 to PDB 2GTN (fixed) . . . 71
5.24. Measurement of distances in Å (a-f) and angles in $^\circ$ (α-κ), B=C and A=0 or B=O and A=C 73
5.25. Measurement of distances 73
5.26. Measurement of the angles in $^\circ$ (α-ς) 74
5.27. Measurement of the angles in $^\circ$ (η-κ) 75
5.28. Angles of selected compounds GA1min, GA430min, JH30min, MO15min, MO16min, RN13amin, RN14amin, SK288min, SK362min 76
5.29. GRID: Calculated MIF of oxygen probe in PDB 2QD9 80
5.30. GRID: Calculated MIF of amine probe in PDB 2QD9 81
5.31. GRID: Calculated MIF of phosphate probe in PDB 2QD9 81
5.32. Ligands (from left: BMU (PDB 1KV1 [3]), B96 (PDB 1KV2 [3]), LI2 (PDB 1WBS [4]), L10 (PDB 1W82 [4]) 85
5.33. Docking of PDB 1PMN, pose of REV9min, left: stick representation, right: MOLCAD surface representation 86
5.34. Docking of PDB 1PMN, pose of RN15min, left: stick representation, right: MOLCAD surface representation 87
5.35. Docking of PDB 2O0U, pose of REV10min in stick representation 88

5.36. Docking of PDB 2O0U, left: pose of REV6min in stick representation, right: pose of OTTO4min in stick representation 89
5.37. Docking of PDB 1W84, pose of GA11min, left: stick representation, right: MOLCAD surface representation 90
5.38. Docking of PDB 1OZ1, pose of REV6min, left: stick representation, right: in MOLCAD surface representation 91
5.39. Docking of PDB 1OZ1, pose of GA4min, left: stick representation, right: in MOLCAD surface representation 92
5.40. Docking of PDB 2GFS, pose of OTTO1min, left: stick representation, right: in MOLCAD surface representation 93
5.41. Docking of PDB 2GFS, pose of GA7min, left: stick representation, right: in MOLCAD surface representation 94
5.42. Docking of PDB 2GTN-modified (without Phe169-Ala172), pose of OTTO1min, left: stick representation, right: in MOLCAD surface representation 95
5.43. Docking of PDB 2I0H , pose of REV6min, left: stick representation, right: in MOLCAD surface representation 96
5.44. Docking of the MORE database to PDB 2GTN (left stick representation) and PDB 2I0H (right stick representation). The distance between Thr106 and the amine of MO25min (0.4 Å) and the way MO9min is posed are unrealistic. . . . 98
5.45. Docking to PDB 2QD9, pose of OTTO2min, left: stick representation, right: MOLCAD surface representation 99
5.46. Docking to PDB 2QD9, pose of RN14min, left: stick representation, right: MOLCAD surface representation 100
5.47. Docking of PDB 1W82, pose of OTTO3min, left: stick representation, right: MOLCAD surface representation 100
5.48. Docking of PDB 1WBS, pose of REV5min, left stick: representation, right: MOLCAD surface representation 101
5.49. Docking to PDB 2GTN (green stick representation): GA17min; rank 5; (grey stick representation), Val30 was left out to ensure a clear view, its position is represented by the label 108
5.50. Docking to PDB 2QD9 (green stick representation): left REV1min; rank one; (grey stick representation), right SK510min; rank 44 (grey stick representation) 109
5.51. Docking to PDB 1W84 (green stick representation): REV3min; rank one; (grey stick representation) 111

5.52. Docking to PDB 1W84 (green stick representation): MO23min; rank 7; (grey stick representation) . . . 112
5.53. Docking to 2FSO (green stick representation): GA17min; rank 2; (grey stick representation) . . . 113
5.54. Left re-docking of ligand L12 (pink stick representation) of PDB 1W84, rank 9(green stick representation) and right re-docking PDB 1WBS, native ligand pose (pink stick representation) and docked ligand pose (green stick representation) . . . 116
5.55. Cross-docking study: ligand LIE301 (pink stick representation) of PDB 2GTN in PDB 2QD9 (ligand LGF in green stick representation), rank 2 . . . 118
5.56. Docking to PDB 2I0H: left proposed pose of REV8min rank one and right proposed pose of REV4min rank 2 (no hydrogens were added for this representation) 119
5.57. Docking to PDB 2I0H: proposed pose of Mo15min rank 11 . . . 120
5.58. Docking to PDB 2I0H: left proposed pose of OTTO1min rank 12 and right proposed pose of JH31min rank 81 . . . 121
5.59. Docking of the Suberones in PDB 2I0H: proposed pose of GA17min rank 137 (left) and rank 148 (right) . . . 122
5.60. Docking of the Suberones in PDB 2GTN: proposed pose of REV9min rank 12 123
5.61. Docking to PDB 2QD9: left proposed pose of REV9min rank one and right proposed pose of REV4min rank 37 . . . 125
5.62. Docking to PDB 2QD9: proposed pose of GA425min rank 2 . . . 126
5.63. Docking to PDB 2FSO yielded in very poor results, left RN14min, middle GA17min, right MO23min . . . 127
5.64. Docking to PDB 1WBS, REV6min, rank one . . . 128
5.65. Docking to PDB 1WBS, left docked binding poses are all alike MO39min (rank 7) and right MO36min (rank 8) . . . 128
5.66. Binding mode of NR13a in 278SLS, shot taken in SYBYL7.2 . . . 129
5.67. Binding mode of NR13a in the refined 278SLS (now MK38), shot taken in GLIDE 130
5.68. Left: 278SLS (colored by atom) and PDB 2GTN (purple) aligned by homology; right: 278SLS (colored by atom) and PDB 1W84 (orange) aligned by homology, shots taken in SYBYL7.2 . . . 134
5.69. Lys53, Thr106, Met109 and Gly110 of PDB 2I0H (red), PDB 2QD9 (green) and 278SLS (colored by atom) aligned by homology, shot taken in SYBYL7.2 . 135
5.70. Alignment by homology of all atoms of the hinge region, 278SLS is fixed . . . 135

5.71. Alignment by homology of all DFG atoms, 278SLS is fixed 139
5.72. 278SLS (MOLCAD surface representation) with ligand (stick representation), ring B marked with red arrow, shot taken in SYBYL7.2 140
5.73. Docking of 278SLS (green stick representation): REV4min; rank one (grey stick representation) 142
5.74. Docking of 278SLS (green stick representation): REV4min; rank one (grey stick representation) 142
5.75. Docking of 278SLS (green stick representation): left SK539min; rank 50 (grey stick representation), right SK508min; rank 77 (grey stick representation) . . . 143
5.76. Re-docking studies of 278SLS: docking result with unmodified ligand (left blue stick representation original ligand) and result with modified ligand (right pink stick representation docked ligand) 144
5.77. Docking of the Suberones to 278SLS: MO38min (rank one) has three H-bonds; to Met109 distance: 2,9383Å to Gly110 distance: 2,3915Å and to Asp168 distance: 1,1317 Å 145
5.78. Docking of the Suberones to 278SLS: RN14amin (orange stick representation, rank 48) has one H-bond to Gly110: distance 2,192Å, and the ligand of 278SLS (pink stick represenation) 146
5.79. Docking of the Suberones type SG in 278SLS; left rank one (SK541min) and right rank two (SK468min) 147
5.80. Docking of the MORE2 compounds to PDB 2QD9 and 278SLS (green stick representation); left MORE2min (grey stick representation) in PDB 2QD9; rank one, right MORE3min (grey stick representation) in 278SLS; rank 4 . . . 148

6.1. Binding mode of the Suberones proposed by the modeling studies 150
6.2. Possible modificatons of the Suberones proposed by the modeling studies . . . 153

7.1. SYBYL minimization protocol 160
7.2. GREATER interface 161
7.3. GRID workflow 163
7.4. FlexiDock workflow 165
7.5. FlexX docking algorithm (lecture slide by O.Kohlbacher) 166
7.6. The GLIDE docking hierarchy 169
7.7. eHITS surface points 172

List of Tables

5.1. PDB structures of JNK3 (Status: November 2007) 40
5.2. PDB structures of the p38α MAP kinase (Status: November 2007) 42
5.3. Chosen PDB structures of the p38α MAP kinase and JNK3 after validation, first 5 values represent Structure Z-scores (positive is better than average) following represent RMS Z-scores (should be close to 1.0), part 1 44
5.4. Chosen PDB structures of the p38α MAP kinase and JNK3 after validation, first 5 values represent Structure Z-scores (positive is better than average) following represent RMS Z-scores (should be close to 1.0), part 2 45
5.5. Overall model quality of JNK3 models expressed by the Z-scores 48
5.6. Overall model quality of p38α MAP kinase models expressed by the Z-scores . 51
5.7. Chosen PDB structures of the p38 MAP kinase and JNK3 after validation with X-ray parameters and Rachmachandran plot values 59
5.8. Data of the alignment of the Gly-rich loop atoms of PDB 2PKJ to all other chosen PDBs of the p38α MAP kinase 65
5.9. Datatable: Alignment of the hinge region atoms of PDB 2PKJ to all other chosen PDBs of the p38α MAP kinase 68
5.10. Data of the alignment of the hinge region atoms of PDB 2PKJ to all other chosen PDBs of the p38α MAP kinase 70
5.11. RMSD values of all atoms of PDB 2GTN aligned by homology to all atoms of PDB 2I0H, PDB 1W84 and PDB 1OZ1 70
5.12. Calculated GRIN charges 77
5.13. GLIDE evaluation with PDB 2B1P 105
5.14. Alignment by homology of all hinge region atoms, 278SLS is fixed 133
5.15. Alignment by homology of all DFG atoms, 278SLS is fixed 138
5.16. WHAT IF report of 278SLS; the first 5 values represent Structure Z-scores (positive is better than average) following represent RMS Z-scores (should be close to 1.0) 141

7.1. Chosen probes for the GRID calculations 162

A.1. Ligands for docking evaluation 186
A.2. Suberone scaffold type GA 189
A.3. Suberone scaffold type JH 190
A.4. Suberone scaffold type MORE 197
A.5. Suberone scaffold type MORE2 197
A.6. Scaffold type OTTO 198
A.7. Scaffold type REVESZ 200
A.8. Suberone scaffold type RN 201
A.9. Suberone scaffold type SK 205
A.10. Suberone scaffold type SG 208
A.11. Distances of the Suberone scaffold type GA 209
A.12. Distances of the Suberone scaffold type JH 209
A.13. Distances of the Suberone scaffold type MORE 211
A.14. Distances of the Suberone scaffold type MORE2 211
A.15. Distances of the scaffold type OTTOSEN 211
A.16. Distances of the scaffold type REVESZ 212
A.17. Distances of the Suberone scaffold type RN 212
A.18. Distances of the Suberone scaffold type SG 213
A.19. Distances of the Suberone scaffold type SK 214
A.20. Angles of the Suberone scaffold type GA (α-ς) 215
A.21. Angles of the Suberone scaffold type GA (η-κ) 215
A.22. Angles of the Suberone scaffold type JH (α-ς) 216
A.23. Angles of the Suberone scaffold type JH (η-κ) 216
A.24. Angles of the Suberone scaffold type MORE (α-ς) 217
A.25. Angles of the Suberone scaffold type MORE (η-κ) 219
A.26. Angles of the Suberone scaffold type MORE2 (α-ς) 219
A.27. Angles of the Suberone scaffold type MORE2 (η-κ) 219
A.28. Angles of the scaffold type OTTOSEN (α-ς) 219
A.29. Angles of the scaffold type OTTOSEN (η-κ) 220
A.30. Angles of the scaffold type REVESZ (α-ς) 220
A.31. Angles of the scaffold type REVESZ(η-κ) 221
A.32. Angles of the Suberone scaffold type SG (α-ς) 221
A.33. Angles of the Suberone scaffold type SG (η-κ) 222

A.34. Angles of the Suberone scaffold type SK (α-ς) 223
A.35. Angles of the Suberone scaffold type SK (η-κ) 224

Mein Dank geht an:

... Meinen Doktorvater Prof. Dr. Stefan Laufer für die Betreuung der Arbeit, die Auswahl des Themas und seine Unterstützung auch in Form kostspieliger Programme und sehr lehrreicher Workshops.

... Prof. Dr. O. Werz für die Erstellung des Zweitgutachtens.

... Dr. C. Peifer für seine mitreißende Freunde am Forschen, sein immer offenes Ohr für Ideen oder Probleme.

... Prof. Dr. O. Kohlbacher und M. Röttig für die Benutzung der Modeling Programme auf dem Sand, letzterem für seine Einführung in die Programme, die Beantwortung vieler Fragen und das Lösen vieler kleiner Problemen.

... Dr. R. Niess, Dr. J.S. Hering, G. Ahrens und S. Karcher für das Synthetisieren der Suberone und S. Linsenmeier, S. Luik, M. Göttert und K. Bauer fürs Testen.

... Prof. Dr. T. Stehle, J. Romir und M. Fecker (Interfakultäres Institut für Biochemie, Universität Tübingen) für die Erstellung der Röntgenkristallstruktur von der p38 MAP Kinase mit RN13a.

... Den AK Laufer für die freundliche Aufnahme.

... G. Helms, K. Ward, H. Kahnt und D. Domeyer für ihren administrativen Einsatz in ihren jeweiligen Bereichen.

... Meine Diplom-Informatikerinnen und Bürokolleginnen über die Jahre A. Krasowski, D. Sirim, N. Hämmerle und V. Schattel für informative Gespräche über Computer und vieles andere.

... A. Dorn für die tolle Zusammenarbeit im 8. Semester und auch meinen Studenten des 8. Semesters, die mir immer einen Ausgleich zu meiner rein theoretischen Arbeit gegeben haben.

... P. Keck für Tricks und Tipps im Umgang mit LaTeX.

... Allen Mitbewohnern der vierten Ebene des AK Laufers und Werz für die entspannte Arbeitsatmosphäre!

... Meinen fernen (ehemaligen) Mitpromovierenden Dr. A. Frickenschmidt, M. Eickernjäger und L. Schiefelbein für ihre Unterstützung in allen Lebenslagen.

... Den weiteren vielen lieben Leuten aus dem Norden UND jetzt auch aus dem Süden für ihre Unterstützung in jeglicher Lebenslage!

... Meinem Papa für alles.

1. Abbrevations

A	Alanine
Å	Angström
Ala	Alanine
Arg	Arginine
AP-1	activator protein-1
Asp	Aspartate
Asn	Asparagine
ATP	Adenosintriphosphate
C	Cysteine
CD	Crohn's disease
DHFR	dihydrofolate reductase
COX	Cyclooxygenase
Cys	Cysteine
D	Aspartate
DMARDs	Disease-modifying anti-rheumatic drugs
E	Glutamate
EN	Energy
ERK	Extracellular signal-regulated kinase
F	Phenylalanine
G	Glycine
Glu	Glutamate
Gln	Glutamine
Gly	Glycine
H	Histidine
H-bond	Hydrogen-bond
His	Histidine
HTS	High-Troughput-Screening

I	Isoleucine
IBD	Inflammatory Bowel Disease
IL	Interleukin
Ile	Isoleucine
JNK	c-Jun NH_2-terminal kinase
JIP	JNK-interacting proteins
K	Lysine
L	Leucine
LC/MS	Liquid Chromatography/Mass Spectrometery
Leu	Leucine
Lys	Lysine
M	Methionine
Met	Methionine
MAPK	Mitogen-activated protein kinase
MAPKAP K2	MAPK activated protein kinase 2
MAPKK	Mitogen-activated protein kinase kinase
MAPKKK	Mitogen-activated protein kinase kinase kinase
MIF	Molecular Interaction Fields
MKK	MAP Kinase Kinase
MKP	MAP kinase phosphatase
mol2	mol2 (file format)
MTX	Methotrexate
MW	Molecular Weight
N	Asparagine
NMR	Nuclear magnetic resonance
NSAIDs	Non-steroidal anti-inflammatory drugs
n.t.	not tested
P	Proline
p38 MAP kinase	p38 mitogen-activated protein kinase
PDB	protein database bank (file format)
PPAR-γ	peroxisome proliferators-activated receptor ligand-γ
PGE2	Prostaglandine E2
Phe	Phenylalanine
Pro	Proline

Q	Glutamine
R	Arginine
RA	Rheumatoide Arthritis
RDF	Receptor description file
RMSD	Root mean square deviation
RNA	Ribonucleic acid
S	Serine
SAR	Structure Activity Relationship
Ser	Serine
SP	standard-precision (GLIDE)
T	Threonine
TAB	transforming growth factor-β-activated protein kinase binding protein
TAK	transforming growth factor-β-activated kinase 1
Thr	Threonine
TNF-α	Tumor necrosis factor-α
Trp	Tryptophane
Tyr	Tyrosine
UC	Ulcerative Colitis
V	Valine
Val	Valine
VS	Virtual Screening
W	Tryptophane
WT	Wild type
XP	extra-precision (GLIDE)
Y	Tyrosine

2. Zusammenfassung

Die p38 MAP Kinase and JNK3 gehören zur Familie der MAP Kinasen und steuern die Freisetzung verschiedener entzündungsfördernder Zytokine, die bei chronisch entzündlichen Erkrankungen wie Rheumatoide Arthritis, Morbus Crohn, Psoriasis, Asthma oder Alzheimer, sowie Krebs eine entscheidene Rolle spielen. Die medikamentöse Therapie ist in vielen Fällen noch unzureichend. Die Hemmung der p38 MAP Kinase mit sogenannten "small molecule inhibitors" stellt eine Kontrolle der Biosynthese und Freisetzung der entzündungsfördernden Faktoren in Aussicht. Verschiedene pharmazeutische Unternehmen arbeiten an der Entwicklung derartiger Inhibitoren. In unserem Arbeitskreis wurden die "Suberone" als neue Klasse von Liganden entwickelt. Ihre Wirksamkeit wurde in verschiedenen Testsystemen nachgewiesen. Da es sich hierbei um neue Leitstrukturen handelt, war bis jetzt der genaue Bindemodus noch nicht bekannt und die Synthese verscheidener Derivate konnte noch nicht gezielt nach Struktur-Aktivitäts-Beziehungen erfolgen. Die vorliegende Arbeit befasst sich mit der Untersuchung des Bindemodus der "Suberone" mit verschiedenen Methoden des Molecular Modeling. Die von anderen Gruppen veröffentlichten dreidimensionalen Röntgen-Kristallstrukturen der p38 MAP Kinase und JNK3 wurden in Bezug auf ihre Qualität verglichen. Die besten verschiedenen Konformationen wurden ermittelt und für die weiteren Studien verwendet. Mit dem Programm GRID wurden innerhalb der ausgewählten Proteinstrukturen die energetisch günstigsten Positionen berechnet, an denen bestimmte Strukturfragmente, wie sie auch im "Suberone"-Gerüst (z.B. Carbonyle) vorhanden sind, am wahrscheinlichsten vorkommen werden. Im Anschluss wurden verschiedene Dockingstudien durchgeführt. Mit jedem verwendeten Dockingprogramm wurde zuerst Re-Docking- und Cross-Docking-Versuche vorgenommen. Dafür wurden die in den Proteinstrukturen vorhandenen Liganden unverändert in einer Liganden-Datenbank gespeichert und zum Docking verwendet. Ausserdem wurde eine Datenbank von "Suberone"-Strukturen erstellt, welche solche "Suberone", von denen bereits Hemmwerte bekannt sind, sowie solche, mit denen man mögliche verschiedene Bindemodi untersuchen könnte, beinhaltet. Diese Datenbank wurde mit Hilfe der Dockingprogramme FlexX, Flexidock, GLIDE und eHITS in die verschiedenen inzwischen vorliegenden Kristallstrukturen gedockt.

Zusammen mit den Daten, die bei Studien mit GRID erstellt wurden, konnte dadurch nur ein möglicher Bindemodus ermittelt werden. Mit Hilfe einer Kristallstruktur einer p38 MAP Kinase mit einer "Suberone"-Struktur konnte der durch die Modeling Studien vorgeschlagene Bindemodus inzwischen bestätigt werden.

3. Introduction

3.1. Proteins

3.1.1. Basics

Proteins are composed of amino acid which contain two functional groups: the amino group (NH2) and the carboxyl group (COOH), which are connected via the alpha carbon (α-C) atom. Normally amino acids exist as "Zwitterions", where the amino group is protonated and the carboxylic group is in its carboxylate form. The side chains can be classified into three major groups: charged polar, uncharged polar or nonpolar. The charged polar side chains can be positively (Lysine, Arginine and Histidine) or negatively charged (Aspartate and Glutamate). The uncharged polar side chains have hydroxyl (Serine and Threonine), phenolic (Tyrosine), amide (Asparagine and Glutamine) or thiol groups (Cysteine). Nonpolar side chain residues differ in shape and size. Glycine is the smallest, followed by Alanine, Valine, Leucine and Isoleucine. Methionine has a thiol ether side chain, while Phenylalanine and Tryptophane are aromatic. Finally Proline has a cyclic pyrrolidine side group.
The geometry of the side chains is determined by the torsion angles of the bonds coming from the atoms of the side chains. The carbons of the side chain are called β-C, γ-C and δ-C. The residues Glycine, Alanine and Proline do not have torsion angles, because in case of the Glycine there is only a hydrogen, Alanine just has a methyl group as side chain, while the Proline side chain is forming a ring. Due to this the side chains can not be regarded as flexible. The amino acids in a protein are polymerized via the peptide bond which is created through the elimination of water. A protein is made of more than 35 residues connected via the peptide bond. A protein's primary structure is the sequence of the residues in a polypeptide chain. The residue with a free amino group is called the N-terminus, while the residue with a free carboxylate group is called the C-terminus. The backbone of a protein just consists of the atoms of the peptide bond. The conformation of the backbone is described by the torsion angles around the α-C-N (measured in ϕ) and the α-C-C (measured in ψ) bond. These angles are both defined as 180°, when the polypeptide chain is in its fully extended conformation and

increases clockwise when viewed from the α-C. Therefore the conformational freedom of the backbone and the torsions are sterically constrained. Rotation around the α-C-N and the α-C-C bonds to form certain combinations of ϕ and ψ angles may cause the amide hydrogen, the carbonyl oxygen, or the substituents of α-C of adjacent residues to collide.
The interactions between different backbone residues create the secondary structure of a protein. There are two immediately recognizable secondary structures: α-helix and β-sheet. In the α-helix every ninth C=O backbone residue points along the N-H group of the fourth residue. This results in a strong H-bond. The side chains project away from the helix. In β-sheets H-bonds occur between neighbouring polypeptide chains. The β-sheet can be divided into two varieties. In the antiparallel β-sheet the neighbouring chains run into opposite directions, while in the parallel sheet they run in the same direction. There are often combinations of parallel and antiparallel β-sheets. Many proteins surfaces contain variations of the secondary structure. α-helices and β-sheets can be joined by stretches, which abruptly change direction, the so-called loops. Loops play important roles in substrate recognition. Various other motifs can act as binding sites. The rearrangement of several motifs folded into two or more global clusters are called domains. Binding sites for natural substrates or small molecule inhibitors are often located between two domains. So the substrate is bound by groups from both domains. This allows flexible interactions between protein and substrate.
The tertiary structure describes the three-dimensional folding of the secondary structure and specifies the position of the side chains. Proteins which consist of more than one polypeptide chain, associate their subunits in a specific geometry; the quarternary structure (figure 3.1)[5].

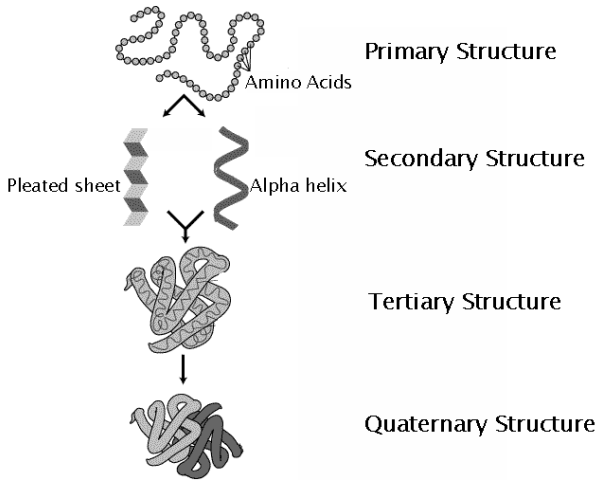

Figure 3.1.: Protein structure, picture taken from www.contexo.info

3.1.2. Determining Protein Structure

X-ray crystallography or nuclear magnetic resonance (NMR) can be used to obtain a three-dimensional picture of a protein. For this study only protein structure models which were obtained by X-ray crystallography were used.

3.1.2.1. X-ray crystallography

The first step is the production of crystals which is the rate-limiting step in the determination of structures. The crystallization process has to produce crystals, that are large enough and diffract sufficiently [6]. Then X-rays can make up an image of a molecule, because its wavelength is comparable to covalent bond distances. When a crystal of a protein is exposed to a parallel beam of X-rays, the atoms in the molecule scatter the X-rays, with the scattered rays reinforcing each other. This results in a diffraction pattern, which is recorded. The intensities of the diffraction maxima are used to calculate a three-dimensional image of the protein. The X-rays only interact with the electrons and not with the atomic nuclei. The outcome is an electron density map (figure 3.2).

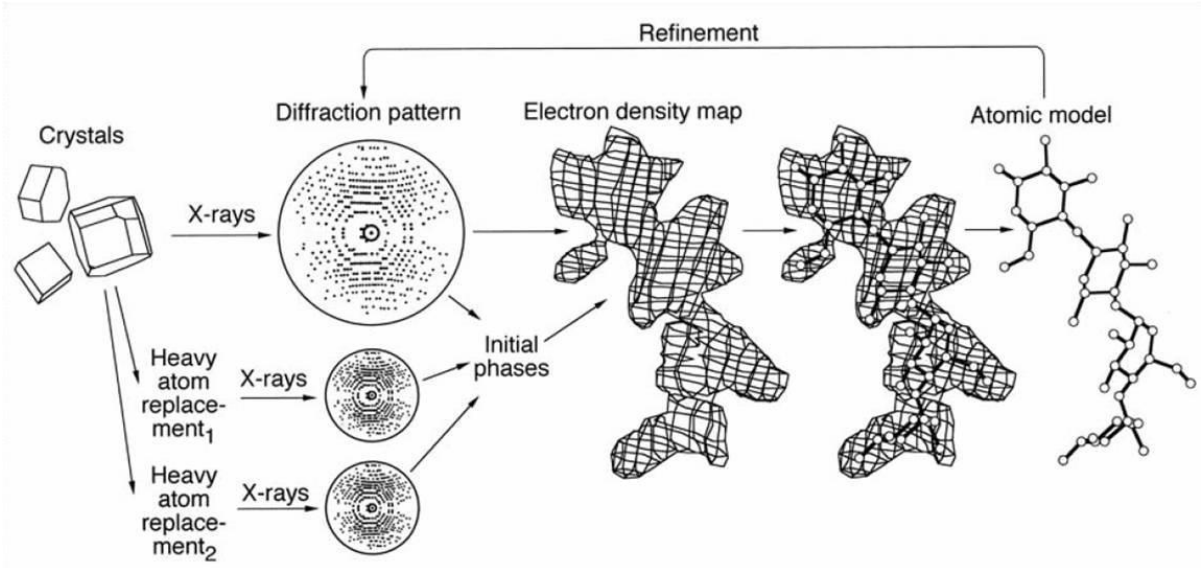

Figure 3.2.: X-ray crystallography

Hydrogens are invisible, because they only have one electron. All of the protein crystals contain water molecules, yielding to a disorder of the residues by a few Angström (Å). This requires a good resolution up to at most 2,5 Å. On the other hand the hydration of the protein reproduces the native conformation similar to that in cells. In the electron density map only the backbone

atoms can be clearly traced. To deduce the position of the side chains, the sequence has to be fitted on the electron density map [5].

3.1.2.2. NMR

Nuclear magnetic resonance (NMR) studies magnetic nuclei by aligning them with an applied constant magnetic field and perturbing this alignment using an alternating electric field, those fields being orthogonal. NMR spectroscopy handles the resulting response to the perturbing magnetic field. Therefore it can be used to obtain physical, chemical, electronic and structural information about molecules due to the chemical shift and Zeeman effect on the resonant frequencies of the nuclei. It can provide detailed information on the topology, dynamics and three-dimensional structure of molecules in solution. Commonly measured nuclei are hydrogen-1 and carbon-13, along with nuclei from isotopes of many other elements (e.g. ^{15}N, ^{14}N, ^{19}F, ^{31}P, ^{17}O, ^{29}Si, ^{10}B, ^{11}B, ^{23}Na, ^{35}Cl, ^{195}Pt). Since the mid-1980s NMR allows the determination of three-dimensional structures of proteins in aqueous solution. These measurements yield the inter-atomic distances between specific protons that are smaller than 5 Angstrom in a protein of known sequence. Nuclear Overhauser effect spectroscopy (NOESY) or correlated spectroscopy (COSY) can determine the inter-proton distances. Together with known geometric constraints (e.g. van der Waals radii) these distances are used to calculate a three-dimensional structure model. This structure can not be regarded as unique, because of the imprecision of the above inter-proton distances. A NMR structure is therefore a representative sample of structures that are consistent with the constraints. Another NMR technique is Transverse relaxation optimized spectroscopy (TROSY) which is principally used for large proteins, because the magnetization results in a shorter transverse relaxation times (T2). Therefore there is less time to detect a signal [7]. Attenuated T2 relaxation by mutual cancellation of dipole-dipole coupling and chemical shift anisotropy indicates an avenue to NMR structures of very large biological macromolecules in solution. TROSY selects the component for which the different relaxation mechanisms have almost canceled, leading to a single, sharp peak in the spectrum. This significantly increases both spectral resolution and sensitivity. In the end the NMR structures are in the most favourable cases comparable to that of an X-ray structure with a resolution of 2-2,5 Angström (Å). Therefore, NMR methods provide a mutual crosschecking with X-ray techniques and allow the determination of proteins which fail to crystallize [5].

3.1.2.3. Protein Kinases

Protein kinases play a crucial role in many signal transduction pathways and therefore are very important in biological processes such as cell growth, metabolism, differentiation and apoptosis. The development of small molecule inhibitors is a promising approach against many diseases caused by a kinase malfunction. Glivec® was the first kinase small inhibitor on the market for the treatment of cancer. Other therapeutic targets connected to kinase malfunctions are Psoriasis, Chronic Inflammatory Bowel Disease (CIDB) including ulcerative colitis and Crohn's disease, Rheumatoide Arthritis (RA) or Alzheimer's Disease. All therapeutic approaches so far targeting the diseases above are unsatisfying, whether due to their side effects (COX inhibitors) or high costs for the health insurance companies (figure 3.3).

Figure 3.3.: Rheumatoide Arthritis; picture taken from http://www.orthoteers.com

The Humane Genome Project identified over 518 genes which translate about 2500 protein kinases [8]. Based on the catalytic specificity, they can be divided into those specific for Tyr, for Thr/Ser and for both. This brought up the question, if there even can be any small molecule inhibitors which measure up to the demands in regard to selectivity and specificity. The crystallization of the first kinases identified the ATP-binding pocket as a suitable part of the protein kinases for drug design. For all kinases bind ATP (Adenosintriphosphate) to separate a phosphate of ATP to pass it to the next substrate for activation. In all kinases the ATP cave is highly conserved and is situated between the two domains. The hinge region which connects two domains allows donor-acceptor hydrogen-bonding, while the other parts invite rather hydrophobic/van der Waals interactions. Figure 3.4 shows the ATP binding site.

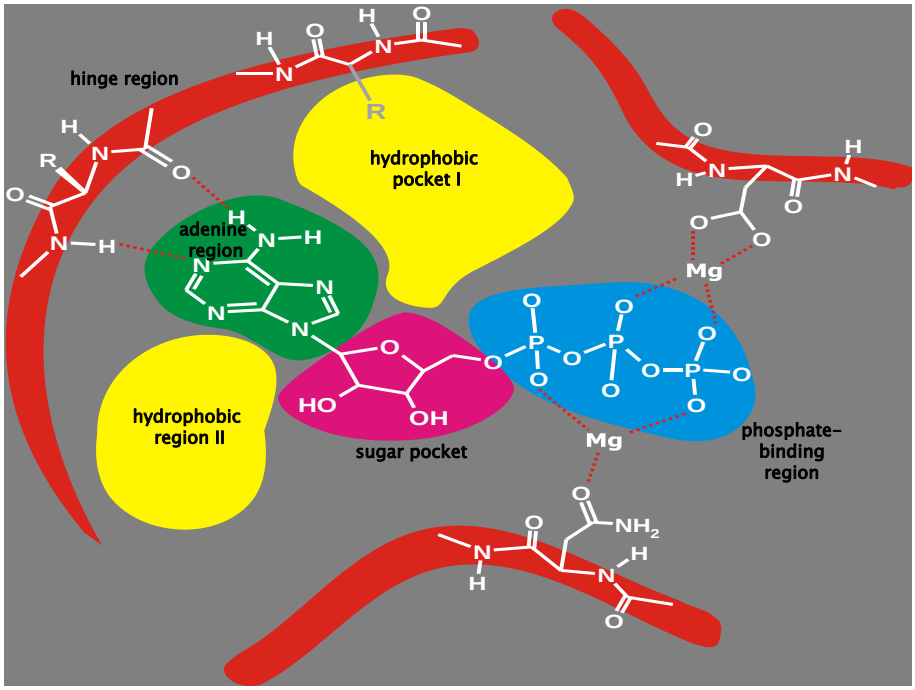

Figure 3.4.: ATP-binding site of protein kinases

In the adenine region ATP forms two H-bonds with the hinge region which connects the N- and C-terminal domain. Many recently developed small molecule inhibitors form one or more H-bonds to the hinge region of their target kinase as well. The hydrophilic sugar pocket is also the target of some research [9]. ATP's triphosphate group binds next to the sugar pocket in the so-called phosphate-binding region and is considered to be a less important region to target. The two hydrophobic regions are not occupied by ATP. The hydrophobic pocket `I` plays an important role to achieve selectivity. The gate keeper residue which also presents the beginning of the hinge region on the left side of the hydrophobic pocket `I` determines the width of the entrance to this pocket (see next section for further explanations). Many researchers try to gain selectivity and to improve solubility by adding substrates that occupy the hydrophobic region `II`. It is more a slot and is opened to solvent[10].

3.2. The p38 MAP kinase

The p38 MAP kinase belongs to the family of mitogen-activated protein kinases (MAPK). Those belong to the Serine/Threonine protein kinases, which play important roles in the cellular response to different signals (figure 3.5).

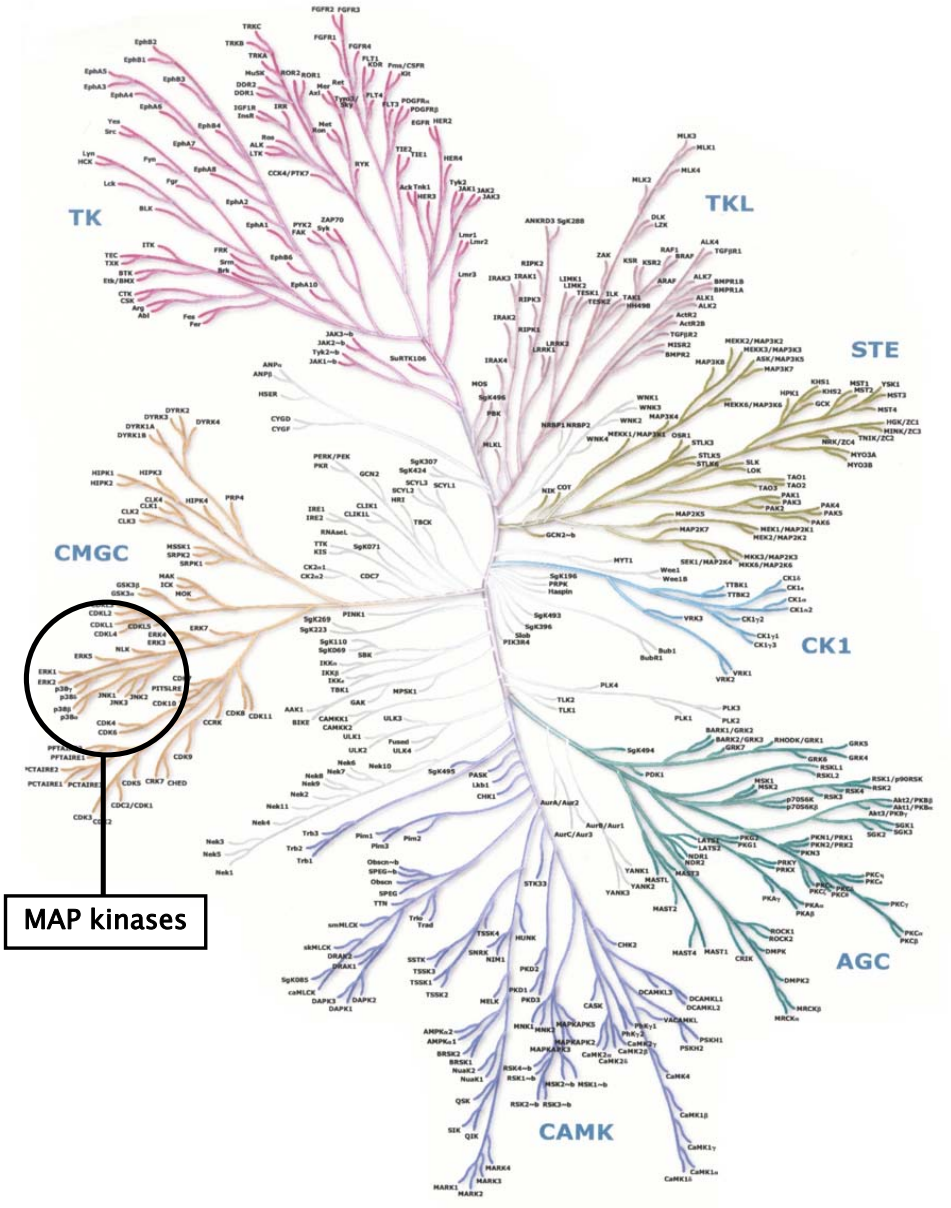

Figure 3.5.: The Human Kinome Project, picture taken from www.kinase.com/human/kinome

Cell growth, differentiation and apoptosis are regulated by extracellular signals. These signals are transmitted to the inside of the cells, where signaling complexes are assembled for integration and processing, and lead to a response. MAP kinases, which integrate and process various extracellular signals, are primary compounds of the intracellular signaling circuitry. The MAP kinases mitogen-activated protein kinase kinase kinase (MAPKKK), mitogen-activated protein kinase kinase (MAPKK) and MAP kinase create the MAP kinase cascade. In this cascade three MAP kinase pathways have been described. The three kinases in mammalian cells are extracellular signal-regulated kinase (ERK), c-JUN N-terminal kinase (JNK) and p38 MAP kinase, which are to 65% identical, but differ in their sequences and the size of the activation loop, as well as in their activation in response to different stimuli. Each MAP kinase is characterized by the substrate it phosphorylates and by its activators. Those MAPK subfamilies have different isoforms, which often have different functions. The p38 MAP kinase α isoform which is the best characterized and perhaps most physiologically relevant kinase is involved in the inflammatory process. The splice variants β, γ and δ have 60% identity to α and are expressed in different more local tissues, whereas α is ubiquitously expressed. Until now little is known about their function. All of these kinases are activated by dual phosphorylation of a Thr-X-Tyr motif.
The p38 MAP kinase consists of two domains, a N-terminal domain with 135 residues and a C-terminal domain of 225 residues. The N-terminus contains β-sheets, whereas the C-terminus is largely helical. The active site is located at the junction between the two domains. The domains are connected via the above mentioned hinge region [11]. The hinge region consists in the case of the p38α MAP kinase of the following residues:

- Thr106, His107, Leu108, Met109, Gly110, Ala111 and Asp112

The N-terminal domain creates the upper part of the binding pocket for ATP, while the C-terminal domain creates the loop, the catalytic base, the magnesium binding site (phosphate-binding region) and the underground of the ATP binding pocket. The phosphate anchor, which is composed of:

- Gly31, Ser32, Gly33, Ala34, Tyr35 and Gly36

and is therefore also called the Gly-rich loop (or Gly-X-Gly-X-X-Gly) which is highly mobile. The phosphorylation loop, which is also highly mobile, consists of 14 residues:

- Gly170, Leu171, Ala172, Arg173, His174, Thr175, Asp176, Asp177, Glu178, Met179, Thr180, Gly181, Tyr182 and Val183

The p38 MAP kinase is dual-phosphorylated on Thr180 and Tyr182. In between lies Gly181. Another important residue is Thr106 (hydrophobic pocket I), the so-called gatekeeper. The residues in this position of the hinge region determines the size of the entrance of the hydrophobic pocket I and differ in the other isoforms and MAPKs. Other differences occur concerning Gly110 (hinge region) [12] and Gly181 (phosphorylation loop). The hydrophobic pocket I is constituted of the residues:

- Ala51, Lys53, Leu75, Ile84, Leu86, Leu104 and Thr106

whereas the hydrophobic region II consists of the following resides:

- Val30, Leu108, Met109, Gly110, Ala111, Asp112, Ala157 and Leu167

The phosphate binding region is created by the residues Arg67, Arg79, Arg149, Arg173, Arg186 and Arg189. Figure 3.6 shows the three-dimensional structure model of the p38α MAP kinase.

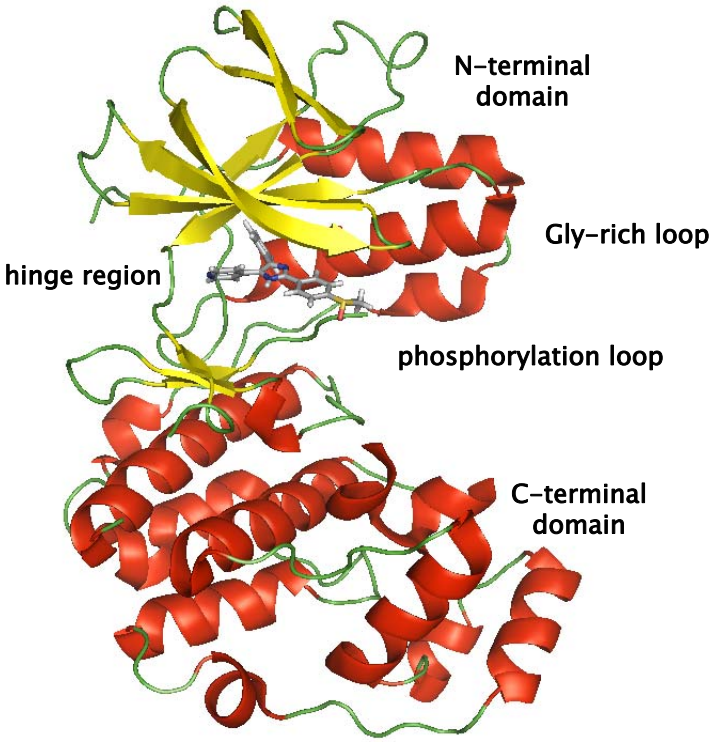

Figure 3.6.: Structure of the p38α MAP kinase, PDB 2EWA [1]

3.2.1. The p38 MAP kinase pathway

The p38 MAP kinase responds especially to environmental stress, including mechanical exposure, UV-light, heat, osmotic shock and proinflammatory cytokines. The activation by MAPKK, which in turn is phosphorylated by MAPKKK leads to the activation of p38 MAP kinase. MAPKK3, MAPKK4 and MAPKK6 phosphorylate and therefore activate p38 MAP kinase. Recently a MAPKK-independent mechanism by transforming growth factor-β-activated protein kinase (TAK1) binding protein 1 (TAB1) was described. The dephosphorylation by various protein phosphatases regulates the activity of p38 MAP kinase. The activated p38 MAP kinase phosphorylates and thus activates MAPK-activated protein kinase 2 (MAPKAPK2) in response to chemical stress and thus plays an important role in the regulation of cytokine expression. MAPKAPK2 regulates the production of Interleukin-6 (IL-6) and Tumor necrosis factor-α (TNF-α) via messenger RNA turnover during transcription and protein translation. Furthermore the p38 MAP kinase phosphorylates transcription factors such as ATF-2, which is responsible for the production of mRNAs coding for the inflammatory cytokines IL-1β and TNF-α. In addition the p38 MAP kinase controls the translation by phosphorylating an mRNA suppressor protein (cytokine binding protein) and through interaction with p90rsk/S6 at a ribosomal level (figure 3.7) [13].

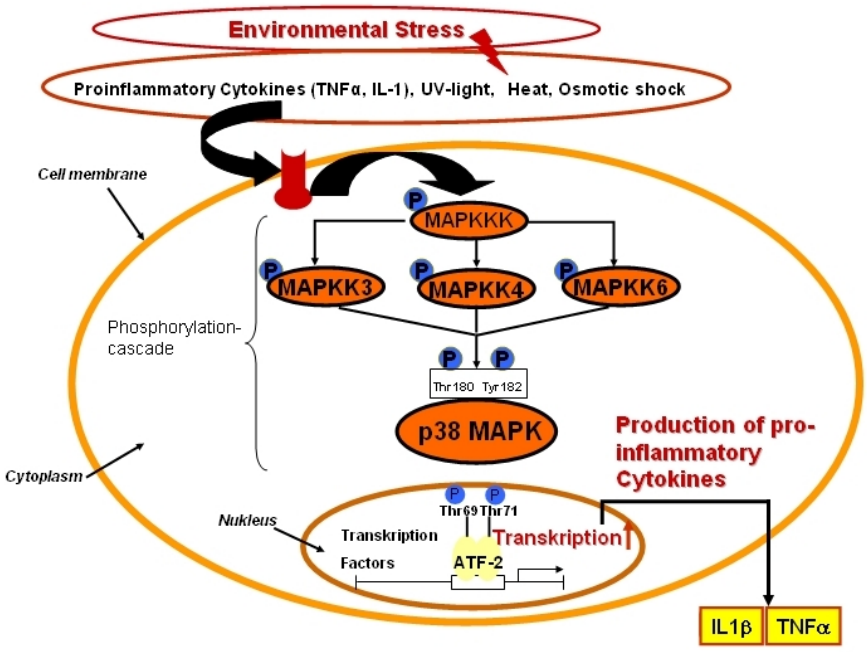

Figure 3.7.: p38 MAPK pathway

3.2.2. Inhibition of the p38 MAP kinase

The involvement of the p38 MAP kinase disclosed the search for selective p38 MAP kinase inhibitors. As there are over 2000 kinases in human cells, the small molecule inhibitors have to be selective for this special kinase. This is possible because the active sites of the kinases differ in a small amount. All kinases bind ATP and it's binding region is subdivided into six regions. The hinge region connects the N-terminal with the C-terminal domain. Here, the adenine part of ATP creates two H-bonds with the NH of Met109 and the amide C=O of Gly110. The adenine binding region is created of the side chains of the N-terminal domain above and the C-terminal domain below of adenine. In the sugar region the ribose is anchored over H-bonds with the C-terminal domain. With the support of two magnesium ions the phosphate groups are bound to the phosphate binding region. In addition to these hydrophilic regions the active site is created by two hydrophobic regions. These regions are not occupied by ATP. The key residue on case of the p38 MAP kinase is Thr106. The dimension of the its side chain defines the enlargement of the region. The other MAP kinases have bigger residues in this position. Many p38 MAP kinase inhibitors have a fluoro-phenyl to fit selectively in this region. That is why the hydrophobic pocket `I` is also called the selectivity pocket. The hydrophobic region `II` is more a groove, while the hydrophobic pocket `I` is deeply buried. Many small molecule inhibitors have substituents to fit in that region. But occupying this pocket does not increase selectivity, but helps to anchor the inhibitor in the active site, which may improve affinity [11]. Gly110 is a another specific residue of p38α MAP kinase. The selectivity of quinazolinones and pyridol-pyrimidines results from a glycine in position 110, e.g. [14].

3.2.3. p38 MAP kinase as a target in the treatment of inflammatory diseases

Although a variety of drugs is available for the treatment of inflammatory diseases, the therapy is still unsatisfying. Many of the used drugs just work as analgetics (e.g. COX inhibitors) and have just low or unspecific effects on the inflammation.
An alternative are the Biologicals such as the chimeric anti-TNF-α monoclonal antibody Infliximab or Adalimumab a recombinant human IgG_1 monoclonal antibody which bind TNF-α. Certolizumab pegol or CDP870 is a monoclonal humanized anti-TNF-α antibody Fab' fragment linked chemically to polyethyleneglycol. The IL-1 receptor antagonist Anakinra decrease the effects of IL-1. IL-1 and TNF-α are the most important inflammatory cytokines in stimulating the cascade of inflammation via the production of Prostaglandin E2 (PGE2), matrix

metalloproteinases and adhesive molecules. Unfortunately their high price and difficult production in addition to their need of parenterally administration prevent the Biologicals from being optimal drugs. So there is still a need for orally available small molecules, which decrease both IL-1 and TNF-α production at the same time [15], [16]. Feige *et al.* [17] showed that targeting both IL-1β and TNFα exhibits in a synergistic capacity. Lately, Wijbrandts *et al.* published that there are some patients who do not clinically respond to TNF-α blockade. Recent studies have suggested that individuals predisposed to high TNF production could show worse responses to anti-TNF-α therapy, while other studies propose exactly the opposite. It can be assumed, however, that a patient's baseline cytokine profile affects responding from non-responding. Another explanation may be that other inflammatory mediators are responsible for pathogenetic subsets of RA. That implies the need for point of action somewhere in the pre-TNF-α level, because the therapeutic effect can not be predicted. Thus p38α MAP kinase is responsible for the TNF-α and IL-1β production, it is a reasonable approach to inhibit the cytokine production rather at their starting point [18].

3.2.4. X-ray crystal structures of the p38α MAP kinase; DFG-IN Binders

3.2.4.1. DFG motif

The DFG motif is composed of Asp168, Phe169 and Gly170 in case of the p38α MAP kinase. This stretch of three amino acids is a widely conserved feature among the protein kinase superfamily. Asp168 coordinates a magnesium ion for catalysis, thus is thought to be critical for the activity of the hydrolysis of ATP. For the binding of the class of diarylurea inhibitors the DFG loop undergoes a structurally dynamic response to create an otherwise hidden cavity [3]. The hydrophobic pocket DFG-OUT is composed of Arg67, Arg70, Glu71, Leu74, Leu75 (upper part), Ile166, Leu167, Asp168, Ile141, Ile146, Ile147 and His148 (bottom). This conformation is called the DFG-OUT conformation. Phe169 shifts from a buried position to a solvent exposed position. It was also discovered during dynamic simulations and NMR studies. This supported the idea of the existence of a dynamic equilibrium between DFG-IN and DFG-OUT conformations of apo-p38α MAP kinase ([1], [19]). Vogtherr *et al.* even demonstrated that the inhibitor SB203580 can bind during both conformations. Lately, Bukhtiyarova *et al.* ([20]) studied the role of Phe169 in p38α MAP kinase. They suggest it is mainly important for catalytic stability. They discovered a new p38α DFG-OUT conformation which they termed α-DFG-OUT to reflect the α-helix-like conformation of Asp168 which also allows the entrance

to the Phe169 cavity mentioned above. In contrast the PDB entries 2EWA and 1KV1 ([3] had observed a rather β-sheet-like conformation of Asp168. The values of the torsion angles ϕ and ψ of Asp168 determine most of the local conformational differences between DFG-IN and DFG-OUT. Figure 3.8 visualizes the DFG-IN and DFG-OUT conformations.

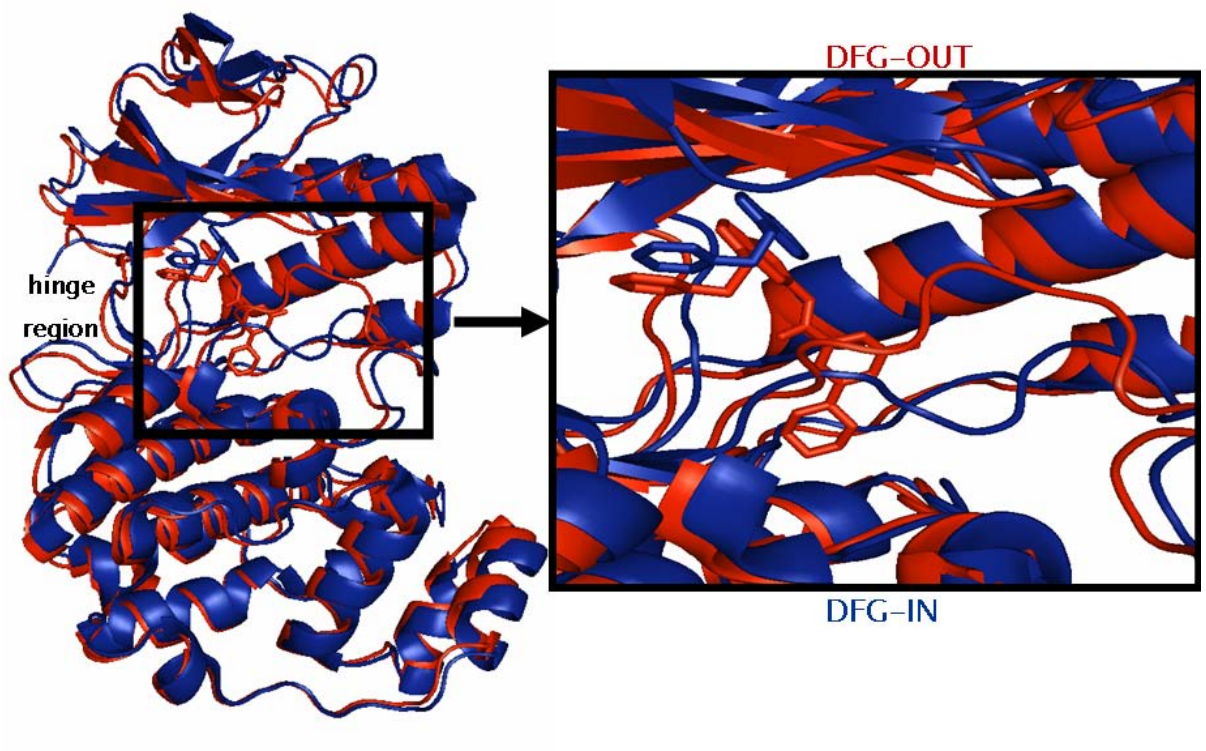

Figure 3.8.: Ligand L12 bound to p38α MAP kinasein DFG-IN conformation (PDB 1W84 coloured in blue) and ligand LI2 bound to p38α MAP kinasein DFG-OUT conformation (PDB 1WBS coloured in red); the DFG-OUT loop is situated above the DFG-IN loop

Bukhtiyarova *et al.* suggest that based on thermal stabilities and their structures that the α-DFG-OUT state is allowed, but less energetically favourable than the DFG-IN. It may be a intersection to the β-DFG-OUT state upon binding a diarylurea inhibitor. Taken together, the position of Phe169 seems to have influence for structural activity and structural dynamics, rather than for structural stability. Maybe the occurrence of different states represent a mechanism for conformational auto-inhibition.

3.2.4.2. PDB 1W84

3-(2-(4-pyridyl)ethyl)indole (PDB 1W84, IC_{50} 35 μmol) (figure 3.9) was optimized by using X-ray crystallographic screening.

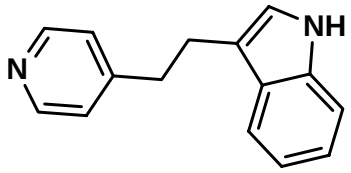

Figure 3.9.: Ligand of PDB 1W84

The inhibitor of PDB 1W84 binds to the ATP binding site between the N- and C-terminal domains of the p38 MAP kinase and forms an H-bond with the backbone -NH of Met109 (hinge region), while the hydrophobic pocket I contains the 3-indolyl group which forms contacts with the side chain of Lys53. In addition the indolyl NH acts as an H-bond donor to the backbone carbonyl of Ala51. PDB 1W84 was the first inhibitor which binds with both rings (the indole) within the hydrophobic pocket I [4].

3.2.4.3. PDB 1OZ1

In this publication of this X-ray crystal structure a native unphosphorylated p38 MAP kinase was solved with (3-(4-fluoro-phenyl)-2-pyridin-4-yl-1H-pyrrolo[3,2-B]pyridin-1-ol)(figure 3.10).

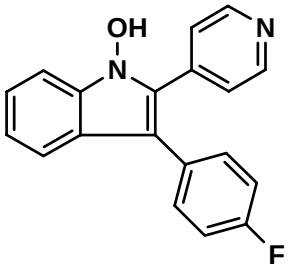

Figure 3.10.: Ligand of PDB 1OZ1

The 4-pyridyl moiety creates an H-bond with backbone -NH of Met109, the 4-fluoro-phenyl group fills the hydrophobic pocket I and the nitrogen of the central imidazol ring forms an additional H-bond with the terminal nitrogen of Lys53. This may be required for the regioselective positioning of the pyridyl and the fluoro-phenyl group. The 4-azaindole binds to the α- and β-isoforms (gatekeeper residue Thr106) to both the activated and inactivated form. Other gatekeeper residues for example a larger Met106 in γ and δ isoforms prevents the 4-fluorophenyl group to get access to the hydrophobic pocket I [21].

3.2.4.4. PDB 2GTN

The ligand in the X-ray crystal structure of PDB 2GTN is a C-2 tri-subsituted purine based inhibitor of the p38α MAP kinase. The author's efforts started with a co-crystal structure of a precursor of the ligand in PDB 2GTN, when they first studied the binding mode of this series. An inactive S180A and Y182F mutant of murine p38α MAP kinase was taken for SAR studies. The 2-fluoro-substituent lies in the hydrophobic pocket `I`, whereas the di-fluoro-phenyl lies in hydrophobic region `II` . A water molecule mediates an interaction between the NH of position C-8 with Lys53. The N-1 of the purine ring forms an H-bond with the backbone -NH of Met109. To establish this interaction the hinge region has to pass through a rearrangement. A so-called "flip" can be observed; the carboxyl of Gly110 turns away from the inside of the ATP binding pocket, whereas the backbone NH turns towards the inhibitor. This torsional flip allows an additional H-bond between the ligand's ether oxygen and NH Gly110 in case of the ligand of 2GTN. The replacement of the N-9 ethyl with an isopropyl led to the present ligand in PDB 2GTN with an IC_{50} of 4nM (figure 3.11).

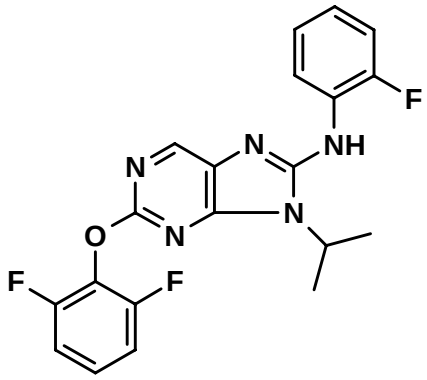

Figure 3.11.: Ligand of PDB 2GTN

3.2.4.5. PDB 2GFS

Compound RO3201195 of a series of 5-Amino-N-phenyl-1H-pyrazol-4-yl-3-phenylmethanones shows a H-bond between the exocyclic amin with the side chain hydroxyl of Thr106 and with the backbone oxygen of His107 in addition to a H-bond between the backbone HN of Met109 and the benzoyl oxygen of the inhibitor. The interaction between the inhibitor and Thr106 controls the high selectivity, because Thr106 is a rare residue at this position amongst the kinases, as for the MAP kinases it is just present in the α and β isoforms of the p38 MAP kinases. In the other two isoforms and all JNKs Methionine occupies this position,

whereas in ERK1 and ERK2 Gln and in ERK3 Phe, respectively [12]. Compound 63 [5-Amino-1-(4-fluorophenyl)-1H-pyrazol-4-yl]-(2(S)- 3-dihydroxy-propyl)methanone has a IC_{50} value of 0,7+0,1µM (p38 α MAP kinase) and is selective apart from p38α and β MAP kinase (IC_{50} 0,05µM), GAK (IC_{50}0,59µM) and PDGFRβ (IC_{50}0,61µM) (figure 3.12).

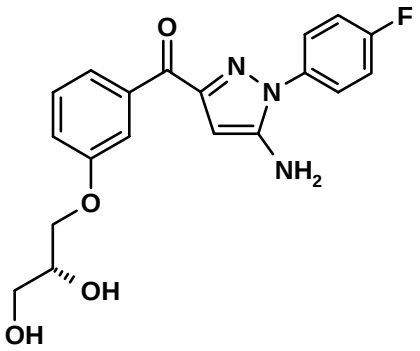

Figure 3.12.: Ligand of PDB 2GFS (compound 63)

3.2.4.6. PDB 2I0H

Some known compounds [22] have shown a unique binding mode, where the hinge region residues Met109 and Gly110 perform a "flip" to be able to form two H-bonds with a ligand. In other kinases the residues linked to Met109 have larger side chains which prevent the "flip". The first requirement to create this flip is that the ligand has to contain a carbonyl oxygen as an anchor point. Secondly, the hydrophobic pocket I has to be occupied by an aryl substituent, in this case bound via an amide linker to the 6-oxo-pyridazin scaffold. The occupation of the hydrophobic region II enhances potency and allows the variation of physical properties, because of its position in the front towards the solvent. 2-3-[(2-chloro-4-fluoro-phenyl)-[1-(2-chlorophenyl)-6-oxo-pyridazin-3-yl]amino]propyl]isoindole-1,3-dione comes up to the described requirements. SAR studies point to the importance of the carbonyl function (to maintain a high dipole moment). The authors suggest that the introduction of a neighbouring nitrogen negatively influences a dipole induced "flip" and lowers the stability of that state. The isoindole-1,3-dione optimal linked by a propyl did not create the expected H-bond to Asp168, but enabled a Π-Π stacking with Tyr35 of the Gly-rich loop. The IC_{50} values for p38α MAP kinase and p38β MAP kinase add up to 9nM and 20nM respectively. The ligand and it's analogues did show any significant activity against p38γ MAP kinase, p38δ MAP kinase, JNKs or ERKs. Figure 3.13 shows the ligand of PDB 2I0H.

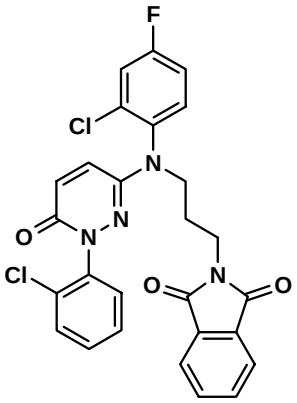

Figure 3.13.: Ligand of PDB 2I0H

3.2.4.7. PDB 2QD9

Following the Scios concept [23] where the introduction of methyl groups on the piperidine scaffold should prevent conformational mobility to increase potency, a series of imidazol[1,5-a]pyrazines was synthesized. Here a ring constraint between a benyzlmethylene and a proximal piperidine ring prevents conformational mobility. A second reason was to bury the arylgroup into the hydrophobic pocket I and simultaneously increase the possibility of an H-bond between Lys53 and nitrogen of the introduced ring. To improve the SAR data, an oxalamide side chain was introduced which effectively improved potency. The ligand of PDB 2QD9 was chosen for X-ray co-crystallographic studies with unphosphorylated p38α MAP kinase (figure 3.14).

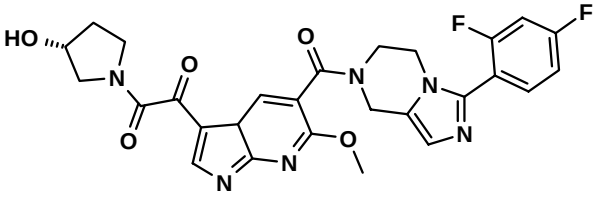

Figure 3.14.: Ligand of PDB 2QD9

The ligand's central amide carbonyl forms two H-bonds with the backbone NH of Met109 and Gly110. The imidazol nitrogen performs a water mediated H-bond with Lys53 and Asp168. The hydrophobic pocket I is occupied by the 2,4-difluorophenyl group. The oxalamide side chain lies between Val30 (Gly-rich loop) and the hinge region with no H-bonds. It's value lies in the improvement of binding affinity by the reduction of the network of bounded water molecules, the authors assume.

3.2.5. X-ray crystal structures of the p38 MAP kinase; DFG-OUT Binders

3.2.5.1. PDB 1W82 and PDB 1WBS

Before the binding of this class of urea inhibitors (PDB 1W82 (N-[(3Z)-5-tert-butyl-2-phenyl-1,2-dihydro-3H-pyrazol-3-ylidene]-N'-(4-chlorophenyl)urea) and PDB 1WBS (3-fluoro-5-morpholin-4-yl-N-[3-(2-pyridin-4-ylethyl)-1H-indol-5-yl]benzamide) in figure 3.15) a significant conformational rearrangement of the phosphorylation loop has to forego to open up a hydrophobic pocket, the so-called hydrophobic pocket DFG-OUT.

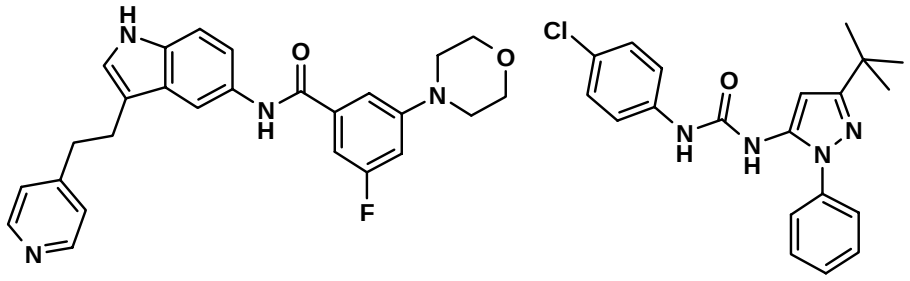

Figure 3.15.: Ligand of 1WBS (left) and ligand of 1W82 (right)

Phe169 (F) changes its postion in a range of 10Å. The ligand of 1W82 (IC_{50} 196nM) was found during the first case study of Gill *et al.*, while obtaining the ligand of 1W84. In their second case study they focused their efforts on indole-based compounds to bind in the DFG-OUT conformation and succeeded with the ligand of 1WBS (IC_{50} 630nM). Like with other DFG-OUT binders ([3], [14]) the amide forms H-bonds to Asp168 and Glu71, which is possible because of the formation of the polar channel through the movement of Phe169. This polar binding channel formed by Asp168 and Glu71 reaches from the ATP binding site to the hydrophobic pocket DFG-OUT. One oxygen of the side chain of Glu71 forms two H-bonds to each nitrogen of the urea group, while the backbone NH of Asp168 creates an H-bond with the oxygen of the urea group. The t-butyl group is situated in the hydrophobic pocket DFG-OUT. The hydrophobic pocket I is occupied by the indole, while the nitrogen of the pyridine interacts with Met109. The morpholino group occupies the hydrophobic pocket DFG-OUT. Altogether, the achieved X-ray crystal structures of this series (PDB codes 1Wx) are of very good quality.

3.2.6. DFG-IN and DFG-OUT

3.2.6.1. PDB 2EWA

The aim of the author's research was to study the role of different DFG conformations, which was observed in many kinase complexes. As X-ray structures are static and just show snapshots of a momentary state, the DFG movement from DFG-IN to DFG-OUT requires kinetic studies. NMR therefore can complement these studies to characterize an inhibitor. The authors studied the DFG-IN and DFG-OUT equilibrium of p38 MAP kinase with five well-characterized ligands (two DFG-IN and three DFG-OUT binders). 2EWA was obtained by X-ray crystallography with p38 MAP kinase and SB203580 (figure 3.16).

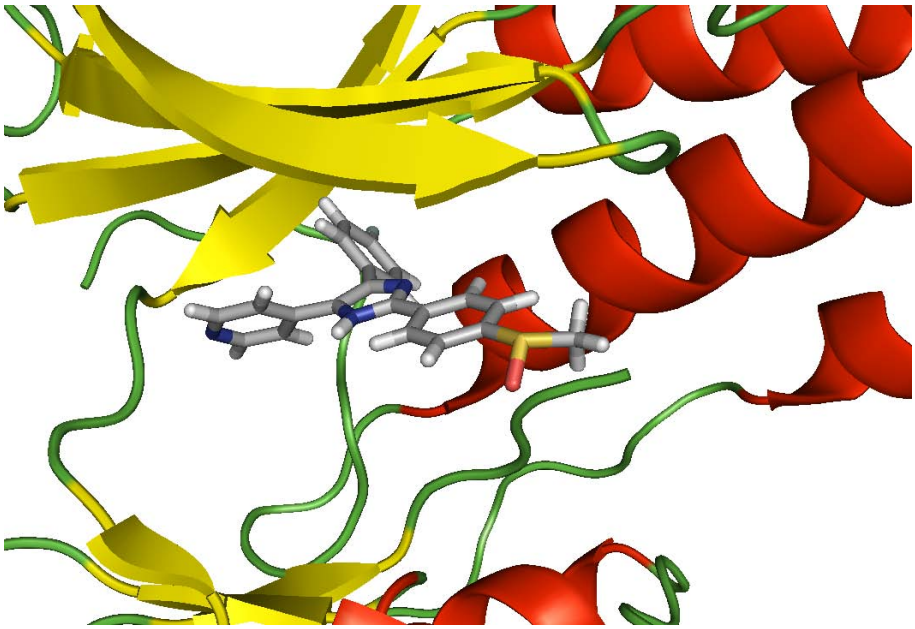

Figure 3.16.: SB203580 in PDB 2EWA

The pyridine forms an H-bond with Met109, whereas the nitrogen of the imidazol forms an H-bond with Lys53 and the fluoro-phenyl occupies the hydrophobic pocket I. The DFG-IN ligands bind to the DFG-IN conformation which was observed before in PDB code 1A9U [24]. Awkwardly, the NMR assignment is just to 79% complete for the N-terminal domain, while the C-terminal domain notably the DFG motif is unassigned. The missing signal can be explained by the mobility of the DFG loop during activation. To study the loop they used the 13 N-Phe-labeled p38 MAP kinase phenylalanine residues. Apart from one they all appeared in a $^{1}H,^{15}H$ TROSY spectrum. The missing one therefore is Phe169 which flows in case of no present ligand or a DFG-IN binder such as SB203580. In the presence of a DFG-OUT ligand the DFG

loop movement is restrained, resulting in the appearance of a thirteenth signal. Thus these ligands do not interfere with the DFG loop and are uninvolved with the activation. DFG-OUT binders block both the activity and the activation because they hinder the natural movement of the DFG loop. Taken together a new approach to characterize new structures as DFG-IN or DFG-OUT binders was introduced. [1]

3.2.7. X-ray crystal structures without a ligand

3.2.7.1. PDB 2FSO

The authors produced several intrinsically active D176A p38α MAP kinase mutants which reveal local alterations in the L16 loop region. This conformational change to enhance activation seems to be similar to the one which occurs in the natural activation. The mutants are in a constant active state and maintain all biochemical and pharmacological properties of an active p38α MAP kinase. The L16 loop, normally stabilized by a hydrophobic core, is a natural element maintaining the low basal activity of p38 MAP kinase (figure 3.17).

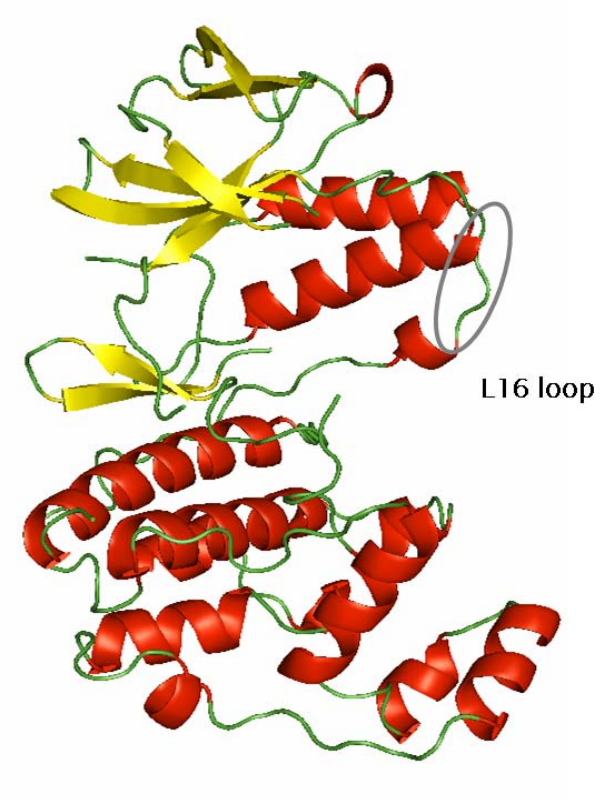

Figure 3.17.: L16 loop in PDB 2FSO

Moreover, they suggested that the conformation of L16 loop in the p38α wild-type maintains its basal activity [25]. Canagarajah *et al.* [26] and Zhang *et al.* [27] had observed this change in ERK2 and Bellon *et al.* [28] in p38γ MAP kinase before. In PDB 2FSO the L16 loop residue Glu328 forms a salt-bridge with Arg70, which interacts with the phosphorylated Thr180 upon activation [28]. Both Arg70 and Glu328 are conserved in the MAP kinase family.

3.2.7.2. PDB 2PKJ

In this paper the authors studied the role of Phe169 in a p38 MAP kinase. They produced five p38αMAP kinase DFG motif mutants and compared them to the wild-type especially examining *in vitro* phosphorylation by MKK6, activity towards ATF2 and thermal stability. 2PKJ is a F169A (Phenylalanine to Alanine) mutant. This mutation showed decreased thermal stability of p38αMAP kinase (1,3°), while the phosphorylation loop occurs in the DFG-IN conformation. In an *in vitro* kinase assay, using GST-ATF2 as substrate in the presence of ATP, F169A was dually phosphorylated at Thr180 and Tyr182, but its enzymatic activity was reduced in comparison to the wild-type. The other mutants showed different conformations and properties, but were not chosen for the docking studies. Through the mutation originated DAG conformation is similar to the DFG conformation in the wild-type, although the mutant suffers from a loss of almost all side chain surface area, and a small change in ϕ and ψ angles of Asp168 related to the shift in the positions of Asp168 atoms. PDB 2PKJ was chosen because its good quality according to the quality standards.

3.3. JNK

The c-Jun terminal kinases are also members of the MAP kinase family and therefore, regulate signal transduction in response to environmental stress. The focus of this work will just spot on the JNK3 isoform which is selectively expressed in the brain and to a lesser extend in the heart and the testis, whereas the other isoforms JNK 1 and 2 are widely expressed. The amino acid sequence identity is greater than 90%, with more than 98% homology within the ATP-binding site. The exchangement of Leu144 in JNK3 for Ile106 in JNK1, may along with different lobe orientations, contribute to selektivity approaches among the JNK family [2], [29]. The hinge regions contains the residues:

- Met146, Glu147, Leu148, Met149, Asp150, Ala151, Asn152

The hydrophobic pocket `I` is composed of:

- Val78, Ala91, Lys92, Lys93, Met115, Ile124, Ile126, Leu144, Val145, Met146 (gate keeper), Leu206

whereas the hydrophobic region `II` is composed of:

- Ile70, Ile148, Asp150, Ala151, Asn152, Gln155, Val196.

The Gly-rich loop contains the residues:

- Gly71, Ser72, Gly73, Ala74, Gln75, Gly76, Ile77, Val78

The phosphorylation loop is designed of the residues:

- Leu206, Asp207, Phe208, Gly209, Leu210, Ala211, Arg212, Thr213, Ala214, Gly215, Thr216 , Ser217, Phe218, Met219, Met220 , Thr221, Pro222, Tyr223, Val224, Val225, Thr226

The p38 MAP kinase and JNK3 share 51% sequence identity. Six residues differ in the ATP binding site. p38 MAP kinase can accommodate lager ligands, because its gate keeper residue (Thr106) is smaller than in JNK3 (Met146). Figure 3.18 shows the structure of JNK3.

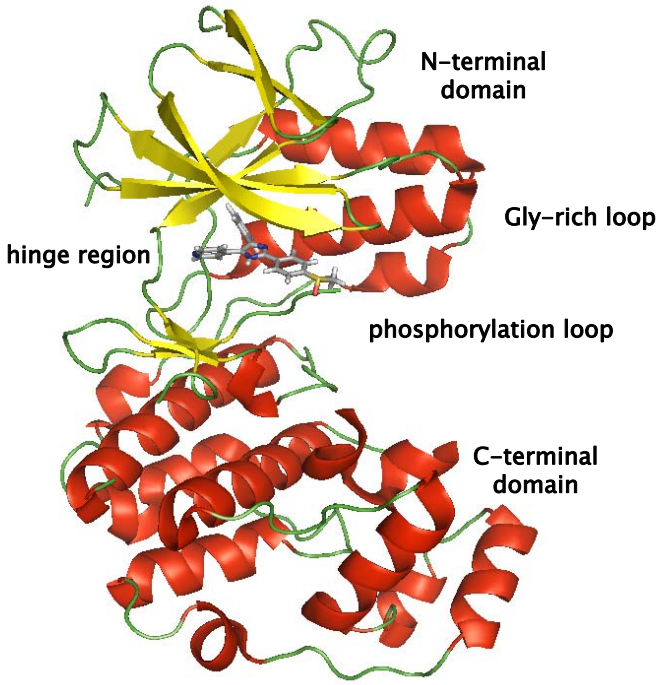

Figure 3.18.: Structure of the JNK3, PDB 2B1P [2]

3.3.1. The JNK pathway

The JNK pathway mediates beta amyloid processing, Tau phosphorylation, neuronal apoptosis and mediation of neurotoxicity, consequently the diseases caused by JNK3 include neurodegeneration, RA, inflammatory disorders, cancer and diabetes. In mammalian systems the intracellular signaling controls cellular proliferation, differentiation, development, inflammatory response and apoptosis. MAP kinases belong to these signaling proteins. One of these signalling pathways is controlled by c-Jun NH_2-terminal kinases (JNKs). It is activated by Cytokines and environmental stress. These stimuli activate the MAP3Ks (MAPKKK) for example transforming growth factor-β activated kinase-1 (TAK1) or Toll-like receptors (TLR-3, TLR-4,TLR-9), which then activate the MAP2K (MAPKK) isoforms MKK4 and MKK7 via phosphorylation. In turn these phosphorylate and activate JNK. The activation requires dual phosphorylation of the phosphorylation loop residues Thr183 and Tyr185. A major target of JNK is activator protein-1 (AP-1). The resulting phosphorylation of c-Jun on Ser63 and Ser73 results in the acquisition of enhanced transcription of AP-1. If the Serines are not activated the c-Jun is degraded by another pathway. The MAPK phosphatase (MKP) deactivates the JNK pathway. The JNKs signal transduction can be carried out by protein-protein interactions or scaffold proteins (JNK-interacting proteins (JIPs)). The inhibition of the JNK pathway can therefore be multiple accessed with small molecule inhibitors. SP-600125 was reported as a selective inhibitor of JNK1, JNK2 and JNK3 [30] and provides a first potential therapy approach for RA (figure 3.19).

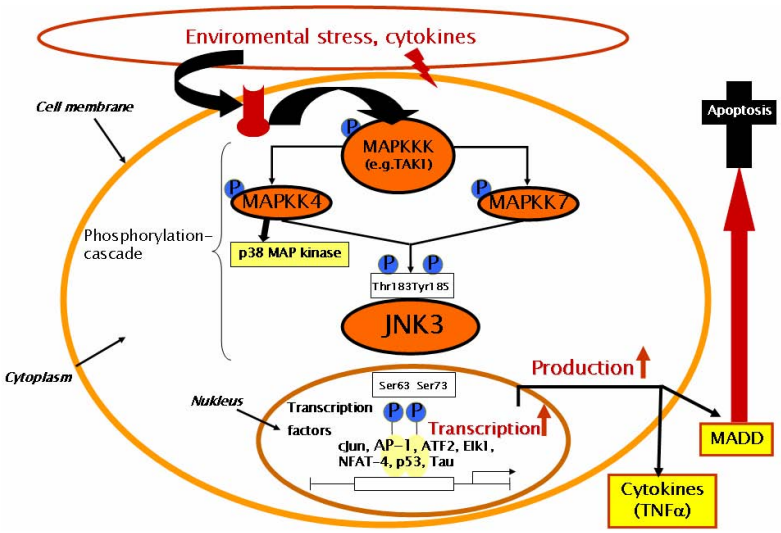

Figure 3.19.: JNK pathway

3.3.2. Inhibition of JNK

In 2001 Celgene discovered SP600125 (figure 3.20) as a small molecule inhibitor for autoimmune, anti-inflammatory and neurodegenerative diseases [31].

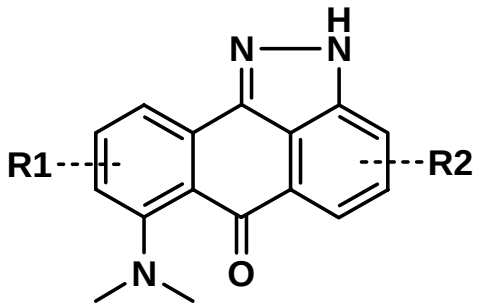

Figure 3.20.: First reported selective JNK small molecule inhibitor SP600125

It showed an IC_{50} of 110nM for JNK1 and JNK2, and 150nM for JNK3. The selectivity of this compound is still not fully figured out yet. Over the years several other companies introduced different kinds of compound selective for JNK2 and JNK3 or just JNK1 or JNK3 against stroke, neurodegenerative and inflammatory diseases, asthma and cancer [31]. Xie *et al.* [32] first obtained a crystal structure of unphosphorylated JNK3 with a ATP analogue (adenylylimidodiphosphate). It revealed that JNK3 has a typical kinase fold, with the ATP binding site between the N- and C-terminal domains. The N-terminal domain is composed of the residues 45-149 and 379-400, and is set up mostly of β-strands. It contains the Gly-rich loop. The C-terminal domain is composed of the residues 150-374 and includes the phosphorylation lip with the two phosphorylation sites Thr221 and Tyr223 and is mainly α-helical. Pro222 is situated between the two phosphorylation sites in the case of JNK3. The loop is two residues longer than in p38 MAP kinase. The ATP binding site has a larger residue as the "gatekeeper" (Met146) than p38α MAP kinase (Thr106) implying a possible approach for selectivity against p38α MAP kinase by introducing large substituents to the p38α MAP kinase scaffolds to address the hydrophobic pocket `I`. Met149 of the JNK3 hinge region corresponds to Met109 of p38α MAP kinase. The other often addressed residue in p38α MAP kinase Lys53 corresponds to Lys93 in JNK3 and guides the other side of the entrance (the right side) of the hydrophobic pocket `I` .

3.3.3. Ligands of JNK3

3.3.3.1. PDB 1PMN and PDB 1PMQ

The authors created a total of four crystal structures of JNK3 in complex with different compounds. The chosen ligands in PDB 1PMN (N-cyclopropyl-4-[5-(3,4-dichlorophenyl)-2-(1-methylpiperidin-4-yl)-3-propyl-imidazol-4-yl]pyrimidin-2-amine) and PDB 1PMQ (N-cyclohexyl-4-[5-(3,4-dichlorophenyl)-2-piperidin-4-yl-3-propyl-imidazol-4-yl]pyrimidin-2-amine) are not selective for JNK3 (IC_{50} 7,1 nM and 1,6 nM respectively)(see figure 3.21).

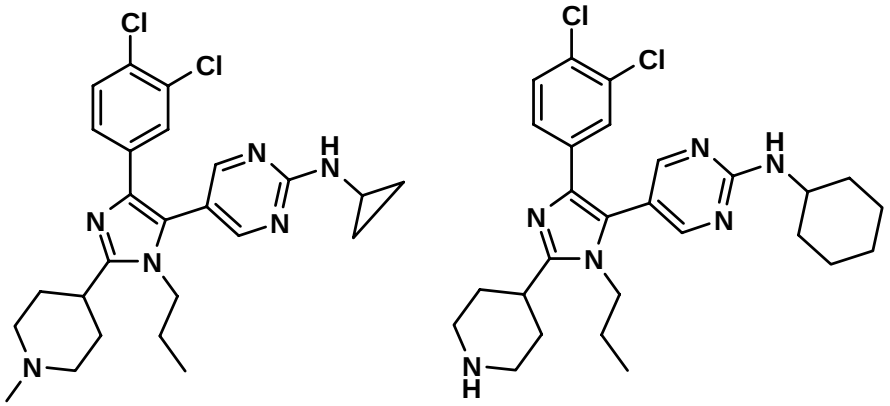

Figure 3.21.: Left: ligand of PDB 1PMN, right: ligand of PDB 1PMQ

The higher potency of the ligand in PDB 1PMQ is apparently due to the enhanced hydrophobic interactions of the cyclohexyl ring. That p38 MAP kinase is also inhibited with IC_{50} values of 0,2 nM and 4,0 nM respectively, but not ERK, makes these ligands unsuitable as therapeutic agents. Both inhibitors keep H-bonds with the nitrogen and oxygen atoms of Met149 in the hinge region, while the di-chloro-phenyl moiety lies in the hydrophobic pocket `I`. The piperidine ring occupies the phosphate binding area and is very much solvent exposed. The more potent compound allows more contacts with the hydrophobic region `II` due to the replacement of the cyclopropyl ring with a cyclohexylring [33].

3.3.3.2. PDB 2B1P

In this crystal structure the ligand is a 3-(4-pyridyl)indazole derivate. The scaffold was found through HTS. The 6-anilino group was added to occupy selectively the hydrophobic pocket `I`. The binding mode of this series was proved by X-ray crystallography, revealing, in addition to the hydrophobic interactions within the hydrophobic pocket `I`, two H-bonds with the indazole

nitrogens of the ligand with the backbone amino groups of the hinge region residues Met149 and Glu147 and a water mediated H-bond between Lys93 and the anilino NH of the ligand (figure 3.22).

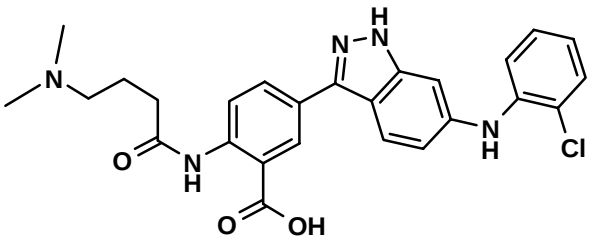

Figure 3.22.: Ligand of PDB 2B1P

They achieved selectivity amongst other kinases apart from p38α MAP kinase. To prevent this unintentional inhibition the 5-(4-dimethylaminobutanoylamino)benzoic acid derivate was synthesized to address two residues (the 3-carboxylic acid-Asn152 and the 3-amide with long chain bearing a basic amine-Asp150) on different sides of the hydrophobic region `II` , which differ in p38α MAP kinase. [2]

3.3.3.3. PDB 2O0U

The JNK3 inhibitory activity of the scaffold of N-[3-cyano-6-(3-piperidin-1-ylpropanoyl)-5,7-dihydro-4H-thieno[5,4-c]pyridin-2-yl]naphthalene-1-carboxamide was found in a binding assay (figure 3.23).

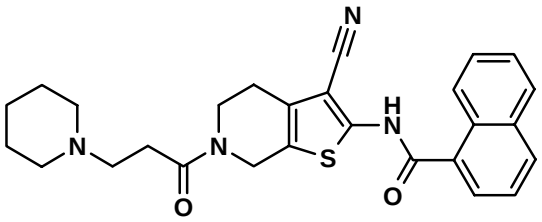

Figure 3.23.: Ligand of 2O0U

It shows pIC_{50} ([34]) values of 5,3 for JNK2 and 5,5 for JNK3 over JNK1 and the other members of the MAPK family. The only residue that differs between JNK3 and JNK2 is Met115 which corresponds to Leu77 in the latter. The obtained X-ray crystal structure reveals that the napthyl substituent lies in hydrophobic pocket `I`, while the piperidine of the 6-amide occupies the hydrophobic region `II` and the solvent exposed front. Met149's backbone -NH forms an H-bond with the 3-cyano substituent. Angell *et al.* also observed an H-bond between

the amide nitrogen to the sulfur of Met146. They suggest that this interaction contributes to the observed selectivity profile.The amide oxygen creates a water mediated H-bond to Lys93.

3.4. Ottosen et al.

In 2003 Ottosen *et al.* (LEO Pharma, Denmark) [35] reported the synthesis and SAR of a series of 4-aminobenzophenones as inhibitors of the p38 MAP kinase. They used molecular modeling to rationalize their SAR approach and suggested the following binding mode (see next page figure 3.24) The carbonyl oxygen forms an H-bond with the NH of Met109, whereas the ring A is situated in the hydrophobic pocket I and the aminophenyl (ring C) forms $\Pi - \Pi$ stacking interactions with Tyr35. Compound 45 inhibits the TNF-α production and the IL-1β production with IC_{50} of 6 and 14 nM. The increased activity is supposed to be created by the two lipophilic ortho substituents which force the benzophenone system to an energetically favourable conformation. Modeling suggested that the ketone bridge is hindered in its rotation. A variety of substitutions instead of a amino group at the ring C is accepted if possible. Only a nitro group is objectionable. The ketone group is essential; any reduced analogues were inactive. Alkylation at the secondary amino group which connects rings B and C is tolerated to a certain extent without any great loss of potency. The compounds did not inhibit the kinase activity of ERK1, ERK2 or JNK1 in a kinase assay. Compound 49 which has an additional p-bromide in ring C in comparison to compound 45 inhibited in a panel of 60 kinases only p38α MAP kinase, p38β MAP kinase and MKK6 at 1μM. The *in vivo* inflammatory effect of the compounds was proved in tests of acute and chronic murine model of skin inflammation. Energy analysis provides one possible explanation of the increased p38α MAP kinase activity of the ortho-substituted compounds. The conformational restriction results therefore in a lower loss of entropy upon protein binding and in the end to higher affinity (Menendez *et al.* [36]). Their docking studies confirmed the binding of the ketone to Met109. Since compounds without the secondary amino group have lower affinity, the amino group might form at least an H-bond with another residue inside of the ATP binding site. However, the docking in PDB 1A9U could not locate a possible binding partner. Although the position of the Gly-rich loop in PDB 1A9U does not imply anything, the flexibility of the Gly-rich loop might form a conformation which allows interactions with Tyr35.

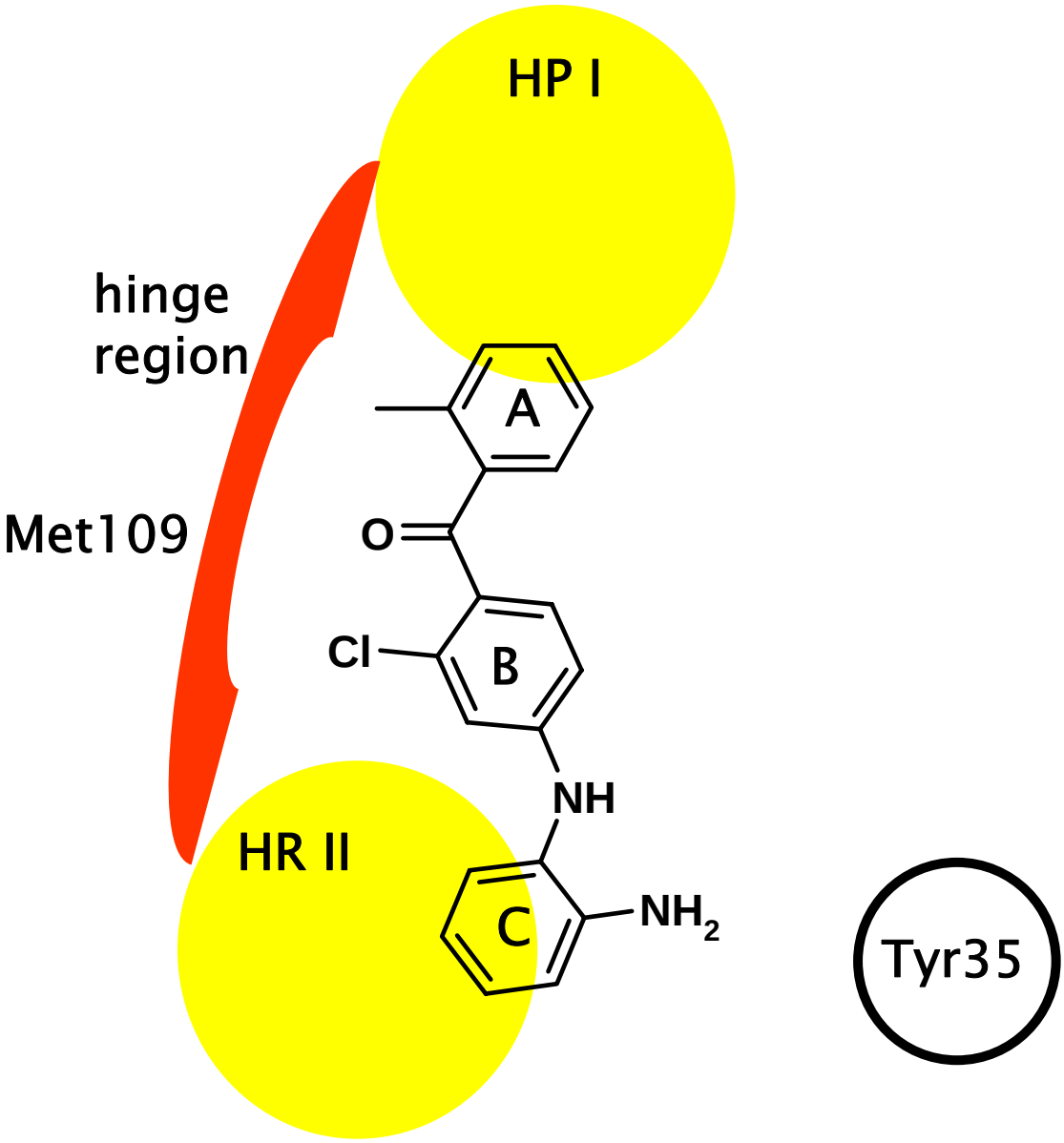

Figure 3.24.: Proposed binding mode of the Ottosen compound 45 in the ATP binding pocket of the p38α MAP kinase

3.5. Revesz et al.

The efforts to synthesize a p38 MAP kinase inhibitor first led to the identification of a pyrido[2,3-*d*]pyrimidine as a weak inhibitor [37]. The ring-opened analogues benzophenones or benzoylpyridines are much more potent (figure 3.25); benzophenones were slightly more potent.

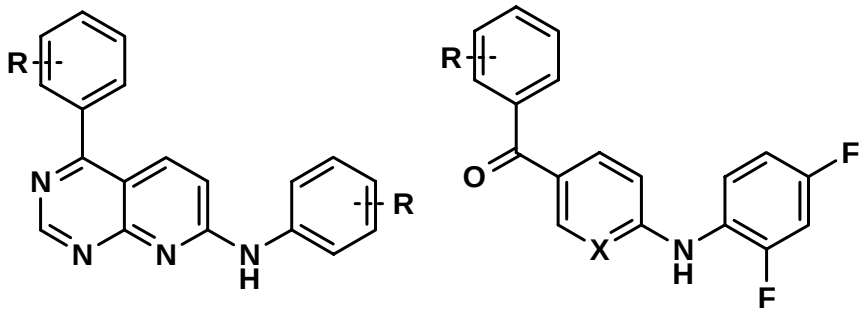

Figure 3.25.: Left: Revesz scaffold A, right: Revesz scaffold B

SAR studies demonstrated the necessity of the carbonyl oxygen, because any reduction led to inactive molecules. The authors propose a binding mode where the carbonyl oxygen forms an H-bond to the NH of Met109 and the difluorophenyl ring (ring C) occupies the hydrophobic pocket `I` . Ring A lies in the solvent accessible hydrophobic region `II`. Modeling suggests that the substituents on that ring for example a amino-dimethylpropynl lies near the DFG loop and may form an additional H-bond to Asp168. This proposed binding mode is opposed to that of the very similar compounds of Ottosen *et al.*, where the hydrophobic pocket `I` accommodates ring A instead of ring C in the case of Revesz *et al.* (see next page figure 3.26).

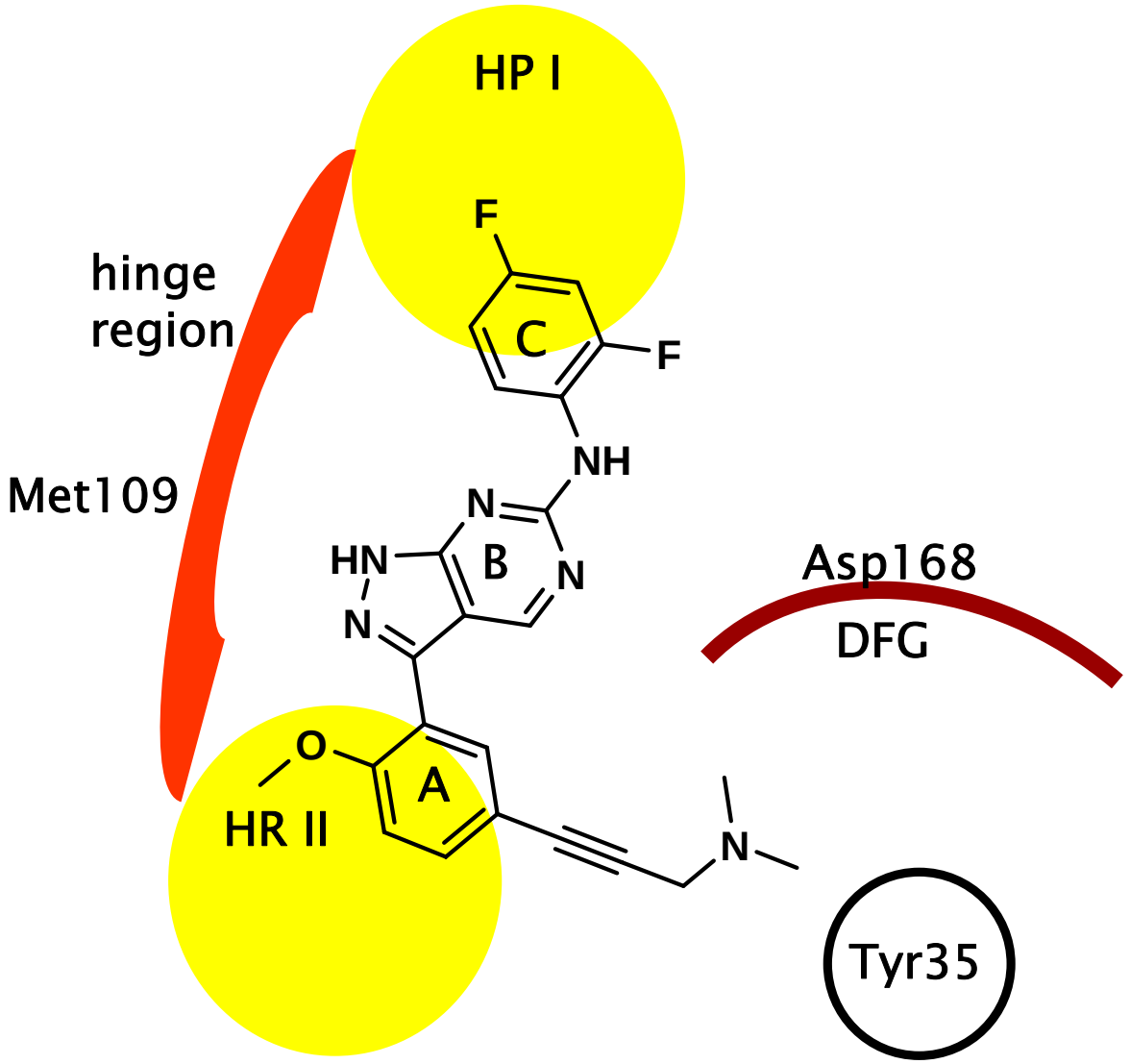

Figure 3.26.: Proposed binding mode of compound 6b, which is the most potent benzoylpyridine with an IC_{50} of 8 nM

This may be caused by the presence of the amino group encouraging the idea of an H-bond between the amino group an Asp168 or any other residue with electron acceptor properties. Further analysis disclosed that increased flexibility of the substituted side chain results in a loss in potency. An amine group at the end of any chain is preferred over an alcohol group. Otherwise the benzophenone analogue with a 1-methyl-4-hydroxy-4-vinylpiperidine in para position to the methoxy group at ring A was with an IC_{50} of 1 nM one the most potent compound in the series. The most potent compound with an IC_{50} of 0,7 nM is compound 19a; a benzoyl substituted benzimidazole (see figure 3.27 on the next page).

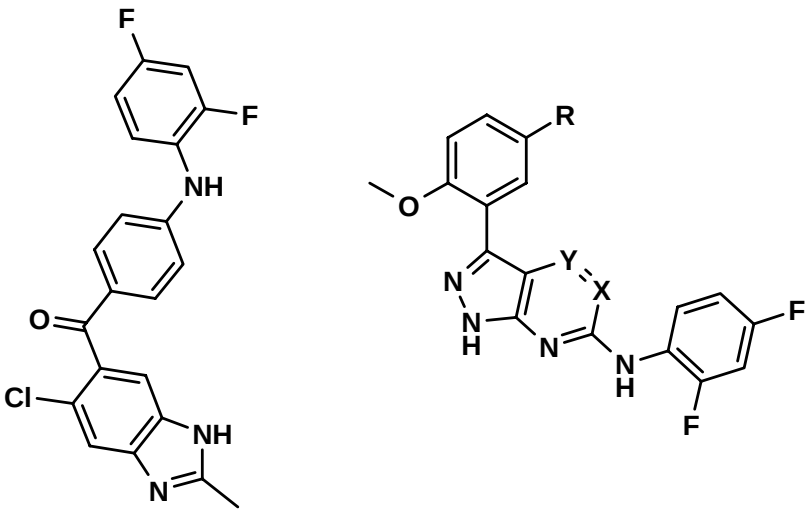

Figure 3.27.: Left: Revesz compound 19a, right: Revesz scaffold 3

Orally active compounds such as 6b and 19a were tested *in vivo* in the acute LPS induced TNFα release model and in the acute LPS/TNFα model and showed good potency. In 2005 Revesz *et al.* introduced another series of inhibitors of the p38 MAP kinase. This series also started with a modest pyrido[2,3-*d*]pyrimidine leading to the ring-opened analogue which was introduced in 2004. In this series further modifications led to pyrazolo[3,4-*b*]pyridines, pyrazolo[3,4-*d*]pyrimidines and pyrazolo[3,4-b]pyrazines. A 1,1-dimethylpropynylamino group was introduced to all three scaffolds to permit a comparison of their p38 MAP kinase inhibitory activity. Their potencies were very similar; the pyrazolo[3,4-b]pyridines slightly favoured. Further analysis supported the preference of rigid substituents as described in the publication of Revesz *et al.* a year before and points out the importance of the substitution of ring A. Two compounds of the pyrazolo[3,4-d]pyrimidines series with a secondary or ternary nitrogen (figure 3.28) on the next page inhibited the p38 MAP kinase at IC_{50} values of 0,6 and 0,9 nM respectively.

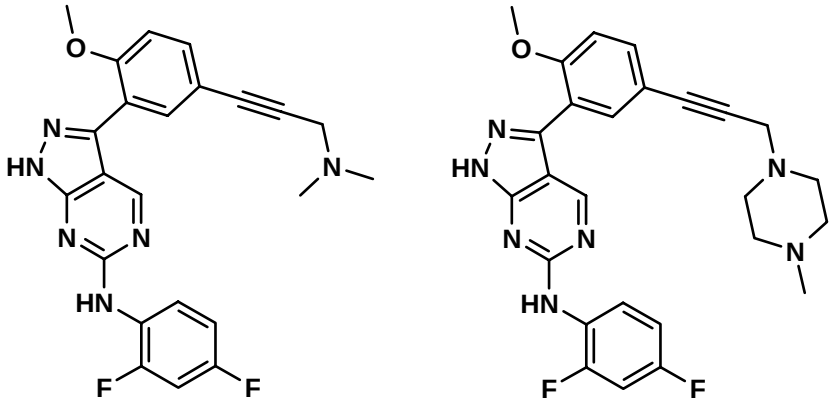

Figure 3.28.: Left: Revesz compound 18c, right: Revesz compound 18d

Beforehand mentioned interactions with Asp168 might be a possible explanation for the increased inhibitory. These series was also tested *in vivo* for oral efficiency. Some compounds showed less activity than against p38α MAP kinase, due to their inadequate pharmacological properties (e.g. half-life, plasma concentration, bioavailability). The three scaffolds were also tested against a panel of 13 kinases ($>$1000-100 fold) and for their ability to inhibit the cytochrome P450 isoenzymes (no adverse inhibition). The proposed binding mode of this series also includes an H-bond between the NH of Met109 in this case with the pyrazolo nitrogen and the difluorophenyl ring accommodates the hydrophobic pocket. A rigid, long enough substituent on ring A can form H-bonds to Asp168 (see next page figure 3.29).

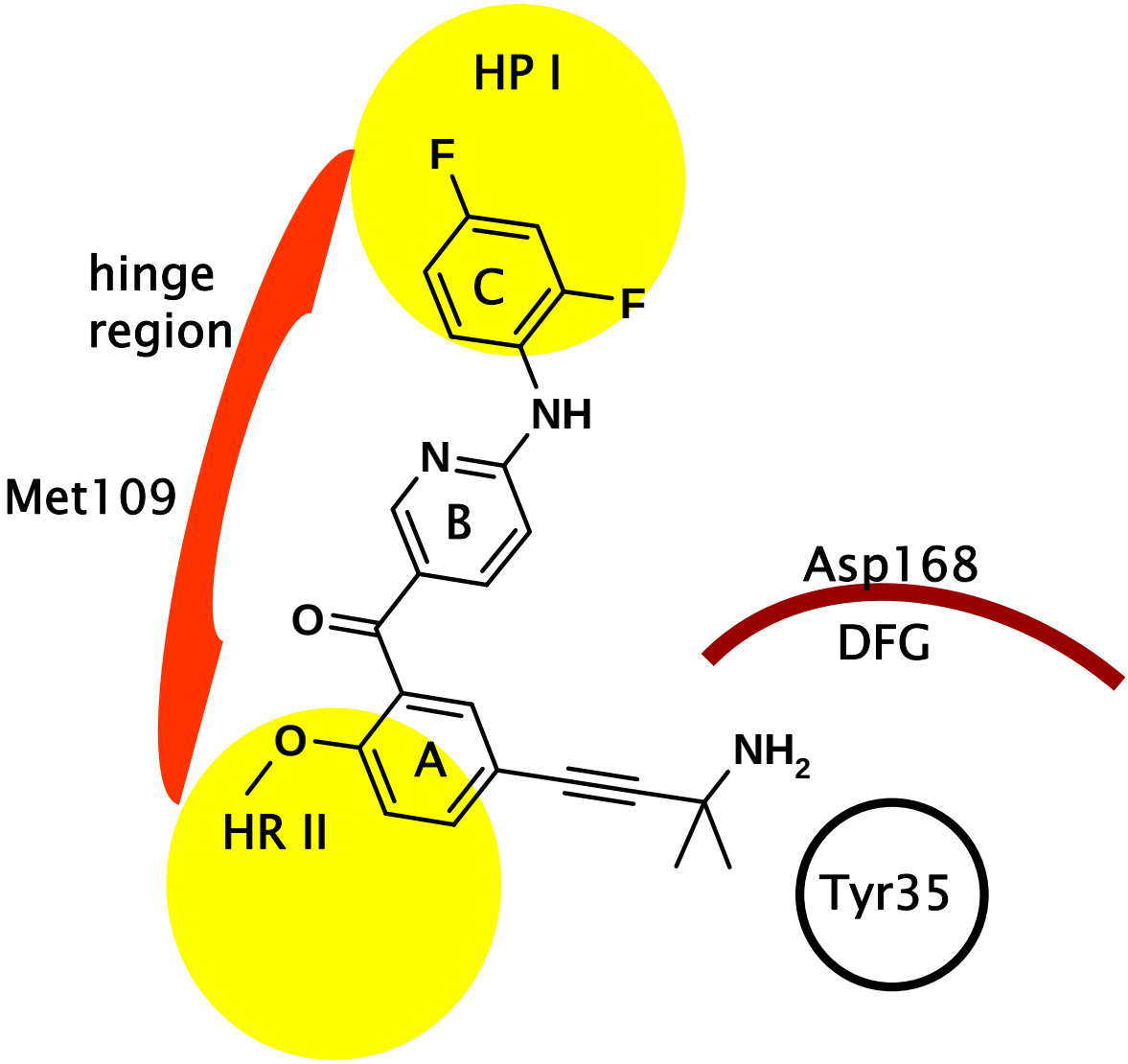

Figure 3.29.: Proposed binding mode of 18c

3.6. The Suberones

The concept of Ottosen *et al.* was the staring point of our in-house synthesis strategies. Ottosen and Revesz also belong to a new class of Linear Binders [38]. Vertex [39] introduced the first compound of the new class, in which a pyrimidopyridazine bicycle interacts with Met109. The bicycle is directly connected by a sulfur spacer to a phenyl ring that occupies the hydrophobic pocket `I`. These linear arranged parts are required for the basic interaction. The actual compound VX-745 has an additional 2,6-dichloro-phenyl substituent attached to the bicycle, which lies in hydrophobic region `II`. Several other compounds also followed this strategy ([40],[41]).
In our case the PhD thesis of R. Niess [42] and J. S. Hering [43] dealt with the synthesis of:

- 3-amino-6,11-dihydro-dibenzo[b,e]thiepin-11-ones
- N-substituted-3-amino-6,11-dihydro-dibenzo[b,e]oxepin-11-ones
- 2-amino-10,11-dihydro-dibenzo[a,d]cyclo-hepten-5-ones
- 2-amino-dibenzo[a,d] cyclo-hepten-5-ones.

The in-house term for the series is **Suberone** and for the general formula see figure 3.30 [44].

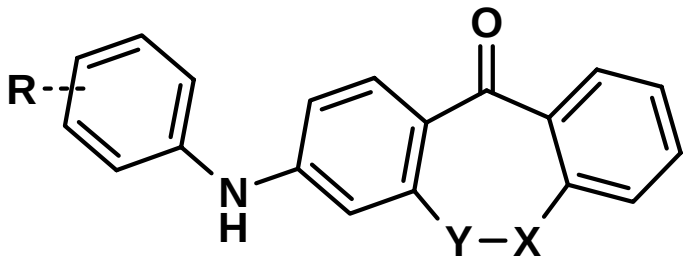

Figure 3.30.: Suberone scaffold: X=O,Y=CH_2; X=CH_2,Y=O; X=CH_2, Y=CH_2, X=CH, Y=CH; X=S, Y=CH_2

The idea of our concept was to restrict the conformational freedom by fixing the rings A and B by introducing condensed ring systems. Our new class of ligands are only build up of fragments that contribute directly to the binding. The Suberones are linear molecules (so-called Linear Binders). As kinases are very flexible per se, flexible ligands may support many induced fits, while a more rigid ligand, like a Suberone scaffold, may limit the number of these induced

fits and increase selectivity. Ethano-, etheno-, methylenoxy- and methylsulfanyl-subsituents were chosen as linkers for the ring systems to produce similar geometric and conformational properties in comparison to the benzophenones. The synthesis is described in Laufer *et al.* [44]. The compounds were tested in an isolated p38α MAP kinase assay described in Laufer *et al.* [45] and revealed the following SAR results. An ortho-substitution at ring C of the 2-amino-dibenzo[a,d]epines leads to potent inhibitors. Any isomeric structures ((8-amino-6,11-dihydro-dibenzo[*b,e*]oxepin-11-ones)) of the 3-amino-6,11-dihydro-dibenzo[b,e]oxepin-11-ones suffer from a so far unexplainable loss of potency. The position of the oxygen in the seven-membered ring seems to be of high importance. Less potency was also achieved by moving the amine to the meta- or para-position of ring C. A 2,4-diamino analogue also showed less potency. This suggests the participation of the amino-group in an H-bonding system. An introduction of the fluorine in the ortho-position in the presence of a para-substituents unexpectedly results in better inhibitory activity. Following this the introduction of a fluorine at the para-position of ring C resulted in a potent inhibitor. Choosing any bigger halogen resulted in increased inhibitory activity. The most potent compound was achieved by combining the insight of the amino and fluoride substitutions, resulting in JH31 with an IC_{50} of 38nM. First *in vivo* data showed promising results in agreement to CYP P450 inhibition. A binding mode analogue to the proposed to that of Ottosen *et al.* or Revesz *et al.* can be presumed.

4. Aim of the study

This study aims to find the binding mode of the Suberones mainly in the p38α MAP kinase. Some structures of the JNK3 are also included, because the Suberones inhibit this kinase as well. The Suberone belong to series of Linear Binders described in [38]. In this class the two essential rings (in this case A, B and C) are connected by spacer atoms (a carbonyl oxygen and an amine group). Therefore only the two rings and their substitutents form the required interactions; H-bond-network to the hinge region (to Met109; there called the "linker residue") and hydrophobic interactions with the hydrophobic pocket `I`. Whereas other ligands like the SB compounds ([46]) have a central scaffold that connects the all the substituents which interact with the hinge region and the hydrophobic pocket `I`. The Linear Binders represent a class of ligands with minimized linear located interaction points. The Suberone's structural similarity to the Ottosen and Revesz compounds (also Linear Binders) suggests, that the Suberone binding mode would be similar to theirs. Both groups propose that the carbonyl oxygen interacts with the hinge region, but they are contradictory on the position of the amino-phenol (ring C). Ottosen *et al.* believe that it will be situated in the hydrophobic region `II`, whereas Revesz *et al.* propose a location where it will be situated on the opposite site, in the hydrophobic pocket `I` to be precise (figure 4.1 on the next page). However none of them published a X-ray structure yet, so it is not possible to work with a PDB structure that includes one of these ligands.

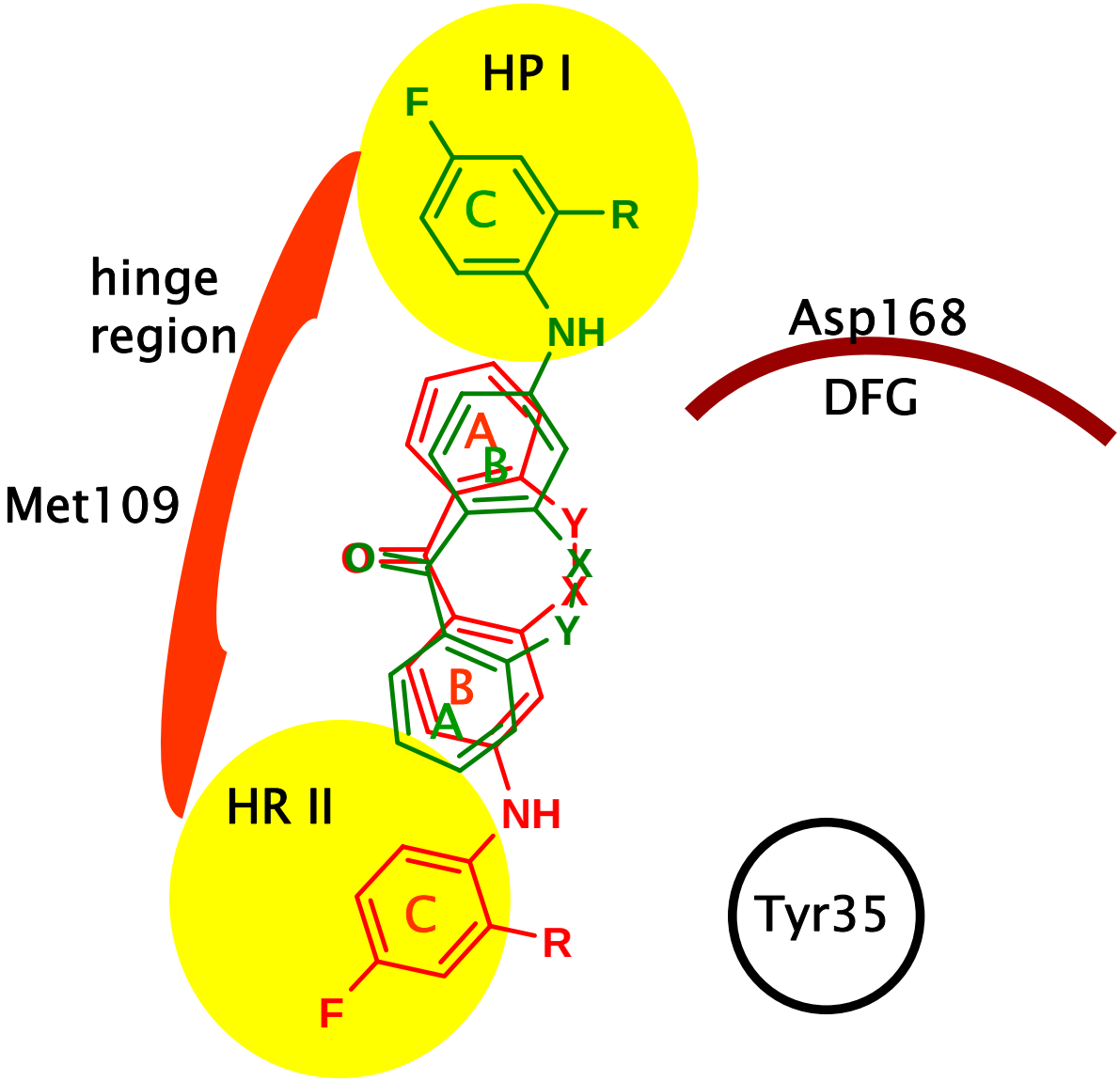

Figure 4.1.: Binding modes proposed by Ottosen *et al.* (in red) and Revesz *et al.* (in green)

There is a great number of available X-ray structures of different ligands of the p38α MAP kinase, but the compositions of these ligands are different, though some share the carbonyl oxygen , that binds to the hinge region. This study uses established methods of molecular modeling to get more information about the binding mode of the Suberones and tries to connect them to already obtained SAR data. The study is divided into three parts. First, a selection of usable PDB structures was chosen by several quality checks. This manageable number of p38α MAP kinase (and JNK3) models of different conformations is loaded in GRID afterwards. GRID is a molecular modeling programme, which calculates favourable positions of chosen probes (e.g carbonyl oxygen or -NH_2) in a PDB structure. Subsequent to this several docking studies are carried out (with FlexX, Flexidock, GLIDE and eHITS). For this two databank files are generated. The first one contains the ligands of the chosen PDB structures and is used for evaluating the docking programmes. The second databank file is composed of Suberone compounds which were already synthesized or were exclusively generated to answer special questions concerning docking issues. The poses suggested by the docking programmes together with such information as SAR data and GRID calculation will make up the base for a binding mode prediction for the Suberones. A X-ray crystallization attempt is also carried out in parallel, so that the results gained by the molecular modeling study can be checked and discussed. The general workflow of this study is presented in figure 4.2 on the next page.

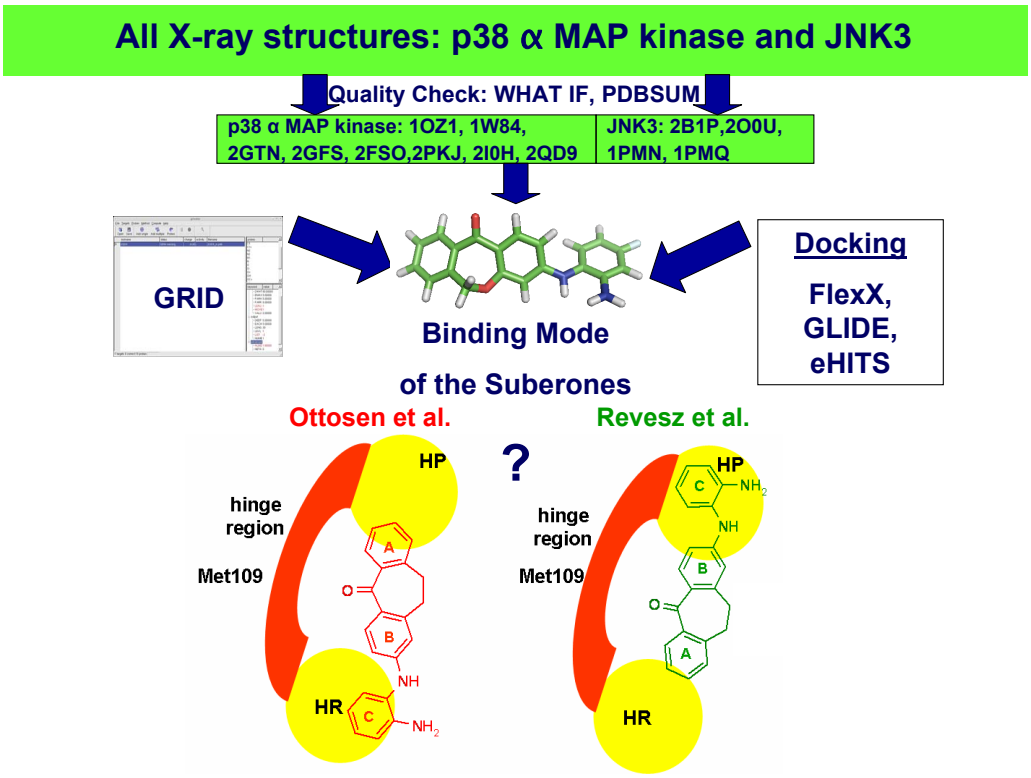

Figure 4.2.: Workflow: Aim of the study

5. Results

5.1. Validation of X-ray crystal structures: What is a good model?

Until November 2007 nine X-ray crystal structures of JNK3 (see Table 5.1) and 56 of p38α MAP kinase (see Table 5.2) have been deposited at the RCSB protein databank [47].

No.	PDB	Resolution in Å	Authors	Year
1	1PMN	2.20	Scapin *et al.* [33]	2003
2	1PMQ	2.20	Scapin *et al.* [33]	2003
3	1PMU	2.70	Scapin *et al.* [33]	2003
4	1PMV	2.50	Scapin *et al.* [33]	2003
5	2B1P	1.90	Swahn *et al.* [2]	2006
6	2EXC	2.75	Swahn *et al.* [2]	2006
7	2O0U	2.10	Angell *et al.* [29]	2007
8	2OK1	2.40	Aronov *et al.* [48]	2007
9	2P33	2.40	Alam *et al.* [49]	2007

Table 5.1.: PDB structures of JNK3 (Status: November 2007)

No.	PDB	Resolution in Å	Authors	Year
1	1A9U	2.50	Wang *et al.* [46]	1999
2	1BL6	2.50	Wang *et al.* [46]	1999
3	1BL7	2.50	Wang *et al.* [46]	1999
4	1BMK	2.40	Wang *et al.* [46]	1999
5	1DI9	2.60	Shewchuk *et al.* [50]	2000
6	1IAN	2.00	Tong *et al.* [51]	1998
7	1KV1	2.50	Pargellis *et al.* [3]	2002
8	1KV2	2.80	Pargellis *et al.* [3]	2002

9	1LEW	2.30	Chang *et al.* [52]	2002
10	1LEZ	2.30	Chang *et al.* [52]	2002
11	1M7Q	2.40	Stelmach *et al.* [41]	2002
12	1OUK	2.50	Fitzgerald *et al.* [53]	2003
13	1OUY	2.50	Fitzgerald *et al.* [53]	2003
14	1OVE	2.10	Fitzgerald *et al.* [53]	2003
15	1OZ1	2.10	Trejo *et al.* [21]	2003
16	1P38	2.10	Wang *et al.* [54]	1997
17	1R39	2.30	Patel *et al.* [6]	2004
18	1R3C	2.00	Patel *et al.* [6]	2004
19	1W7H	2.21	Hartshorn *et al.* [55]	2005
20	1W82	2.20	Gill *et al.* [4]	2005
21	1W83	2.50	Gill *et al.* [4]	2005
22	1W84	2.20	Gill *et al.* [4]	2005
23	1WBN	2.40	Gill *et al.* [4]	2005
24	1WBO	2.16	Hartshorn *et al.* [55]	2005
25	1WBS	1.80	Gill *et al.* [4]	2005
26	1WBT	2.00	Gill *et al.* [4]	2005
27	1WBV	2.00	Gill *et al.* [4]	2005
28	1WBW	2.41	Gill *et al.* [4]	2005
29	1WFC	2.3	Wilson *et al.* [56]	1997
30	1YQJ	2.00	Tamayo *et al.* [57]	2005
31	1YW2	2.01	Laughlin *et al.* [58]	2005
32	1YWR	1.95	Golebiowski *et al.* [59]	2005
33	1ZYJ	2.00	Michelotti *et al.* [60]	2005
34	1ZZ2	2.00	Michelotti *et al.* [60]	2005
35	1ZZL	2.00	McClure *et al.* [61]	2005
36	2BAJ	2.25	Sullivan *et al.* [14]	2005
37	2BAK	2.20	Sullivan *et al.* [14]	2005
38	2BAL	2.10	Sullivan *et al.* [14]	2005
39	2BAL	2.80	Sullivan *et al.* [14]	2005
40	2EWA	2.10	Vogtherr *et al.* [1]	2006
41	2FSL	1.70	Diskin *et al.* [62]	2007

42	2FSM	1.86	Diskin *et al.* [62]	2007
43	2FSO	1.83	Diskin *et al.* [62]	2007
44	2FST	1.45	Diskin *et al.* [62]	2007
45	2GFS	1.75	Goldstein *et al.* [63]	2006
46	2GHL	2.10	Brugel *et al.* [64]	2006
47	2GHM	2.35	Maier *et al.* [65]	2006
48	2GTM	1.90	Sabat *et al.* [66]	2006
49	2GTN	1.80	Sabat *et al.* [66]	2006
50	2I0H	2.00	Natarajan *et al.* [67]	2006
51	2PKJ	2.00	Bukhtiyarova *et al.* [20]	2007
52	2PTJ	2.20	Bukhtiyarova *et al.* [20]	2007
53	2PTO	2.30	Bukhtiyarova *et al.* [20]	2007
54	2PV5	2.10	Bukhtiyarova *et al.* [20]	2007
55	2PV8	2.20	Bukhtiyarova *et al.* [20]	2007
56	2QD9	1.70	Dhar *et al.* [68]	2007

Table 5.2.: PDB structures of the p38α MAP kinase (Status: November 2007)

The first step to gain inside of the binding mode of the Suberones was to choose a sample of structures in that bulk of available structures, because docking in all 65 structures would be too time consuming and would not be reasonable. The next step was to compare the available structures in respect to their quality. JNK3 was also chosen for the studies to examine the binding mode there as well, because JNK3 is also inhibited and there are enough structures available that are of good quality [42]. A structure should be regarded as a model, because it is just a hypothesis of a simplified representation of a molecule (a collection of coordinates representing the atoms). Kleywegt observed in this review [69] that errors in models based on crystallographic data is unavoidable. Since any subjective pitfalls of model building and refinement can be expelled (e.g. an unexperienced crystallographer) the possible types of error should be considered carefully. Several tools can be used to get an overview about the quality of a X-ray structure. Assessing the quality of a model is called validation. Validation needs to be done by both producers and users. It should always be considered that a model is gained through subjective interpretation of the experimental data. The first step for the user is to check the crystallographic data. The first clue of the quality a crystallographer offers the user is the resolution. A high resolution is obviously the most useful, represented

through small numbers. Models of high resolution have value of 2,5 or better. Altogether the model has to follow the concepts of chemical sense (bond lengths and angles, chirality, flat aromatic rings etc.), physical sense (favourable packing of the molecules in the crystal etc.), crystallographic sense (model agrees with the experimental data), statistical sense, protein-structural sense (good Ramachandran plot, usual main-chain and side-chain conformations) and biological sense (model explains activity, specificity, effect of mutations or inhibitors).

5.1.1. WHAT IF

WHAT IF identified the following PDB structures as good models for docking studies in comparison to other PDBs. The calculated results are shown in tables 5.3 and 5.4 on the next two pages.

In comparison to other PDB structures (for example PDB 1YWR which was used in the previous Diploma thesis [70] just because of its good resolution) those present in the tables above have better overall data. A closer look on the data was performed by checking the full output reports, identifying some "false" warnings or errors. Many warnings or errors did not occur anywhere near the ATP binding pocket or could be identified as irrelevant. For example all ligands appeared in the bond-distance check. The lower distances between special ligand atoms and residue atoms could be explained by the existence of possible H-bonds between them. Even the programme suggested this as a possible explanation. This is why the programme demands a closer look to the results. In the end the overall quality and the manual check identified the best X-ray crystal structures of p38α MAP kinase and JNK3. After the WHAT IF check all PDB structures underwent further quality tests.

	1W82	**1WBS**	**1W84**	**1OZ1**	**2GFS**	**2I0H**	**2QD9**
2nd generation packing quality	-0.774	-0.832	-0.762	-0.505	-0.204	-0.751	-0.674
Ramachandran plot appearance	-0.213	-0.191	0.310	0.017	-0.177	0.009	-1.148
χ-1/χ-2 rotamer normality	-0.419	-0.379	0.224	-0.651	0.867	-0.079	-1.963
Backbone conformation	*-3.294*	*-3.572*	*-3.573*	*3.515*	*-3.79*	-4.009	*-3.488*
Resolution	2.20	1.80	2.20	2.10	1.75	2.00	1.70
	-	-	-	-	-	-	-
Bond lengths	*0.552*	*0.411*	*0.629*	*0.659*	*0.376*	*0.493*	0.957
Bond angles	0.759	*0.624*	0.830	0.780	*0.601*	0.722	1.064
Omega angle restraints	1.047	0.950	1.092	1.034	0.989	*0.337*	1.123
Side chain planarity	*0.526*	*0.423*	*0.549*	0.738	*0.490*	*0.409*	1.358
Improper dihedral distribution	0.541	0.472	0.613	0.715	0.437	0.488	1.061
B-factor distribution	0.404	0.431	0.475	0.475	0.387	0.396	-
Inside/Outside distribution	1.046	1.032	1.040	1.033	1.030	1.040	1.025

Table 5.3.: Chosen PDB structures of the p38α MAP kinase and JNK3 after validation, first 5 values represent Structure Z-scores (positive is better than average) following represent RMS Z-scores (should be close to 1.0), part 1

	2GTN	**2FSO**	**2PKJ**	**1PMN**	**1PMQ**	**2B1P**	**2O0U**
2nd generation packing quality	-1.001	-0.333	-1.182	-1.063	-1.063	-0.487	-0.580
Ramachandran plot appearance	-0.756	0.649	-0.832	-1.663	-1.663	-0.833	-1.318
χ-1/χ-2 rotamer normality	-1.808	-0.488	-1.248	-1.223	-1.223	-0.544	-1.566
Backbone conformation	*-4.432*	*-3.270*	*-3.743*	*-4.971*	*-4.971*	*-5.225*	*-5.196*
Resolution	1.80	1.83	2.00	2.20	2.20	1.90	2.10
-	-	-	-	-	-	-	-
Bond lengths	0.817	0.689	*0.299*	0.481	0.481	*0.553*	0.714
Bond angles	0.925	0.823	*0.585*	0.707	0.707	0.689	0.868
Omega angle restraints	1.154	1.074	*0.500*	0.296	0.296	1.155	1.268
Side chain planarity	1.035	0.890	*3.251*	0.329	0.329	*0.609*	0.804
Improper dihedral distribution	0.889	0.720	0.480	0.470	0.470	0.542	0.741
B-factor distribution	0.528	0.595	0.611	0.497	0.497	0.418	0.508
Inside/Outside distribution	1.048	1.047	1.035	1.040	1.040	1.017	1.040

Table 5.4.: Chosen PDB structures of the p38α MAP kinase and JNK3 after validation, first 5 values represent Structure Z-scores (positive is better than average) following represent RMS Z-scores (should be close to 1.0), part 2

5.1.2. Experimental data check: R-value, ProSA, PDBSUM, Ramachandran plot

After this first validation with WHAT IF, all available models underwent further following quality checks.

5.1.2.1. R-Value

Apart from the resolution the R-Value also offers evidence of the quality of a model. The crystallographic R-value (or R-factor) is defined as: $\boxed{R=\frac{Sum\,|F(obs)-F(calc)|}{Sum\,F(obs)}}$. This R-factor is a measure of the level of disagreement between the (properly scaled) observed structure factors (F_{obs}) and calculated structure factors (F_{calc}). It is usually reported in %, i.e. a R-value of 0.18 is reported as 18%. This R-factor is distinct from the calculation of R_{merge} or R_{sym} values which are used to report the quality of the experimental diffraction data as the average discrepancy of multiple measurements of the same reflection. These R factors are based on diffraction intensities: $\boxed{R=\frac{Sum\,|I(obs(i))-I(mean)|}{Sum\,I(mean)}}$. The crystallographic R-factor is an attempt to report with a single number the degree to which a complex atomic model with four or more parameters per atom agrees with a large set of individual diffraction observations. Typically, thousands of atoms give rise to thousands of computed structure factors which are then compared to the observed structure factors to yield a single R-factor. This R-factor is not very sensitive to errors, especially in case of:

- low-resolution structures with a low observations-to-parameters ratios
- overall good structures with few localized errors
- structures with distorted geometry

Structures with a resolution at or better than 2.5 Å with R-factors below 25% tend to be largely correct [71]. The more recent advances in the field of macromolecular refinement has been the introduction of the free R-factor or R-free [72]. It is based on the statistical method called cross-validation. The free R-factor was introduced because it shows greatly reduced coupling to the target function used during minimization (the residual) than the R-factor. It measures the degree to which the atomic model predicts a subset of the observed diffraction data that has been omitted from the refinement. So instead of letting the minimizer refine against the complete dataset (all F_{obs}), a random subset (5-10%) of the dataset is set aside and labeled the free or test set. The remaining 90-95% of the dataset (working set) are used to form the target function for refinement and to compute the traditional crystallographic R-factor. The

free R-factor is commonly 2-8% higher than the regular R-factor. In table 5.7 all R-factors are displayed. PDB 2QD9 (0,252) slightly lies above 0.25 and PDB 2PKJ (0.280) is even higher. The other PDB structures fulfill the above mentioned expectations. In all cases the value of R-free is acceptable.
Another column of table 5.7 displays the number of water molecules in the crystal structure. A very low number is unusual. WHAT IF also includes a check of the positions of the water molecules. Water molecules are not visible in the X-ray structure and have to be positioned by the depositer anywhere he thinks it is wise. This subjective placement may not be the best objective.

5.1.2.2. ProSA

ProSA can reveal if the overall structure is correct and can identify faulty parts. Table 5.5 shows the ProSA calculations of the JNK3 models; the lower the Z-Score the better.

ProSA	Overall model quality	Z-Score
2B1P	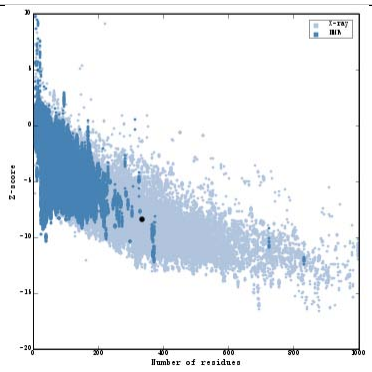	-8.32
2O0U	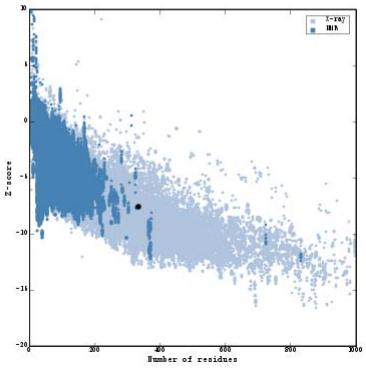	-7.57

1PMN	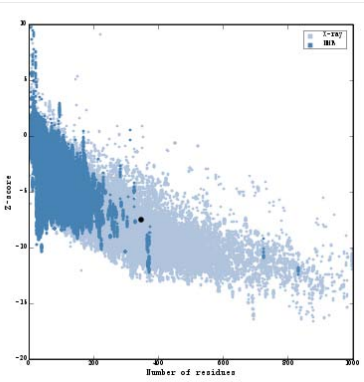	-7.43
1PMQ	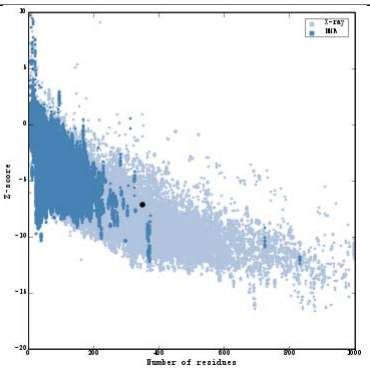	-7.12

Table 5.5.: Overall model quality of JNK3 models expressed by the Z-scores

The calculated values for the overall model quality range between -8.3 and -7.1. Altogether they are much better than those of p38α MAP kinase. The local model quality reveals high energy values for the phosphorylation loop regions. Their state seems to be energetically unfavourable according to this calculation. Table 5.6 on the next pages shows the values of the overall model quality calculated for p38α MAP kinase models.

ProSA	Overall model quality	Z-Score
1W84	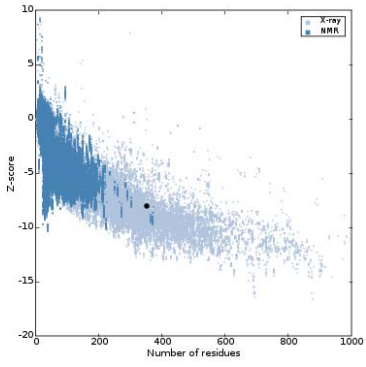	-8.02
1W82	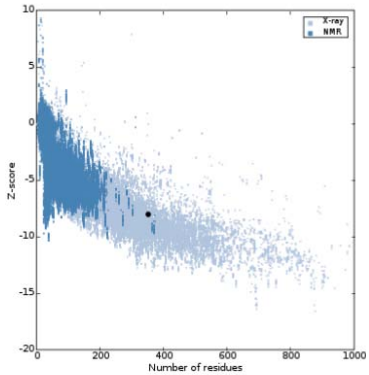	-7.98
1WBS	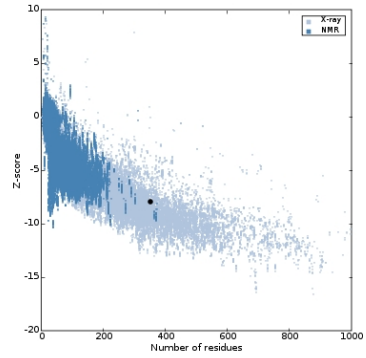	-7.92
2GFS	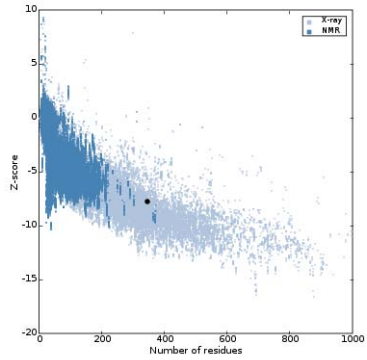	-7.75

2I0H	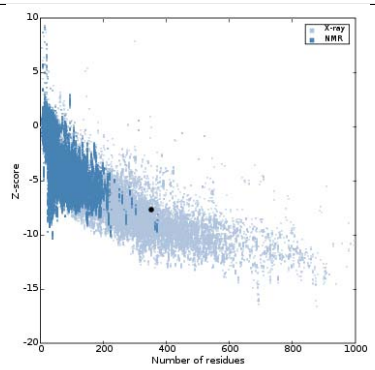	-7.64
1OZ1	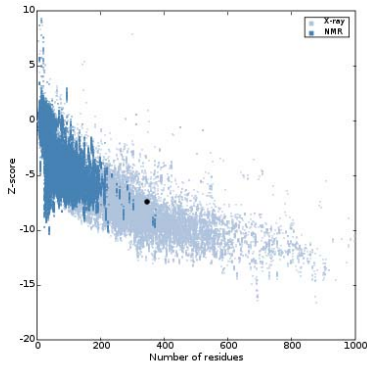	-7.37
2PKJ	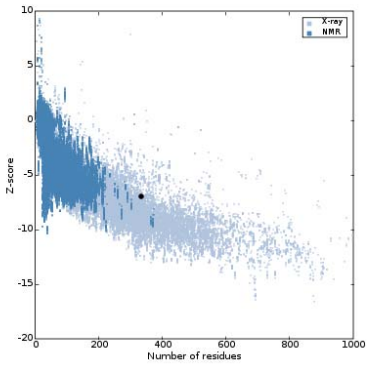	-6.93
2GTN	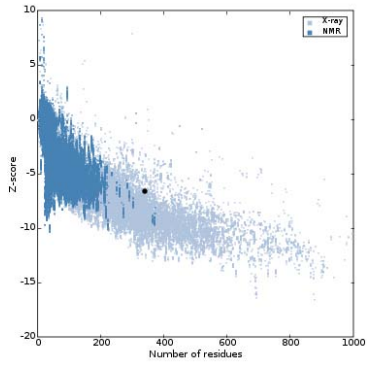	-6.55

2FSO	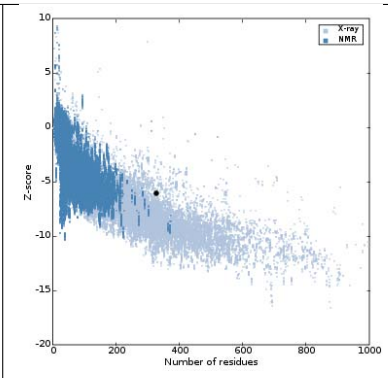	-6.00
2QD9	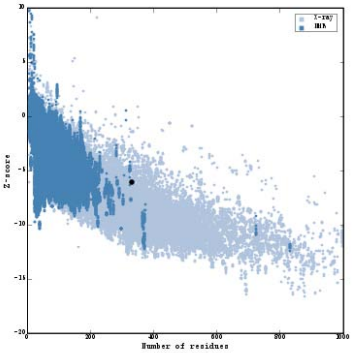	-5.99
1YWR	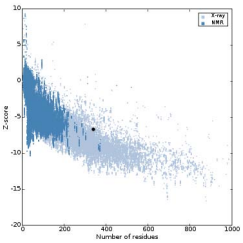	-6.65

Table 5.6.: Overall model quality of p38α MAP kinase models expressed by the Z-scores

All values are situated in the normal field; some in the middle (e.g. PDB 1W84), while others (e.g. PDB 2PKJ) are situated at the frame. The local model quality shows bad values in the sequence sector of the loop residues 210-220 (exemplified by figures of PDB 1OZ1 5.1 on the next page). PDB 1YWR [59] that was used in the Diploma thesis [70] has acceptable Z-scores as well.

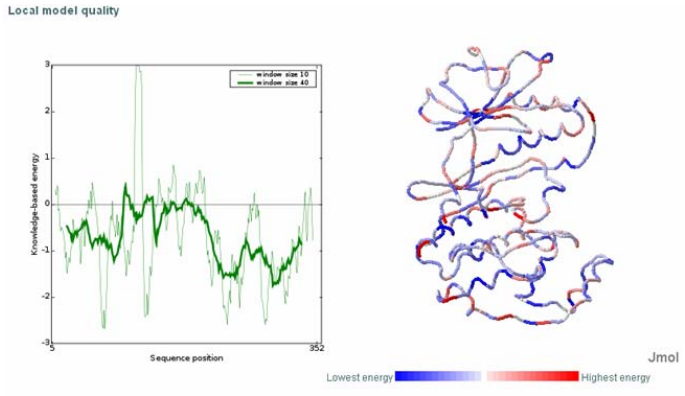

Figure 5.1.: Local model quality of PDB 1OZ1, red: areas of high energy, blue: areas of low energy

The folding of the phosphorylation loop arouses suspicion and should be therefore regarded with caution. Many loop regions have very high energy values, affecting adversely the overall model quality. Excluded PDB 1YWR, due to other validation tools, shows not the worst overall model quality here in comparison to others (PDB 2GTN). PDB 2QD9 has a very low overall model quality, because many residues in the loop sections have very high energy values (phosphorylation loop and Gly-rich loop (residues 30-38)). The pose of the phosphorylation loop of PDB 2GTN is highly unusual and was only seen in the PDB 2GTN model. It lies in the ATP binding pocket and may therefore cause heavy problems during the docking studies (Figure 5.2). Just like a missing loop may have a not-wanted influence on the docking.

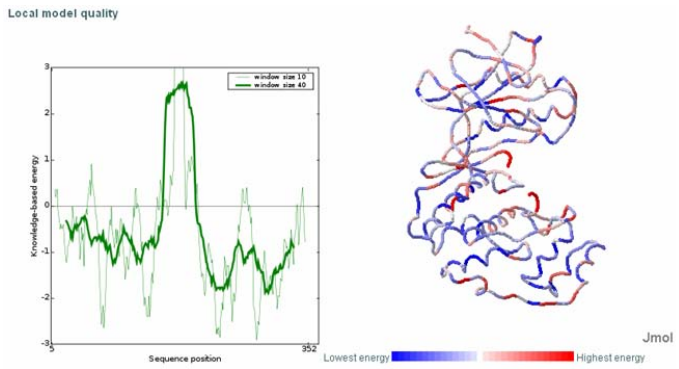

Figure 5.2.: Local model quality of PDB 2GTN, red: areas of high energy, blue: areas of low energy

The best values of p38α MAP kinase models were calculated for the PDB 1Wx series, supporting their usage in the study. The state of the phosphorylation loop seems to be energetically disadvantageous apart from the DFG-OUT states and PDB 1W84 (see figure 5.3).

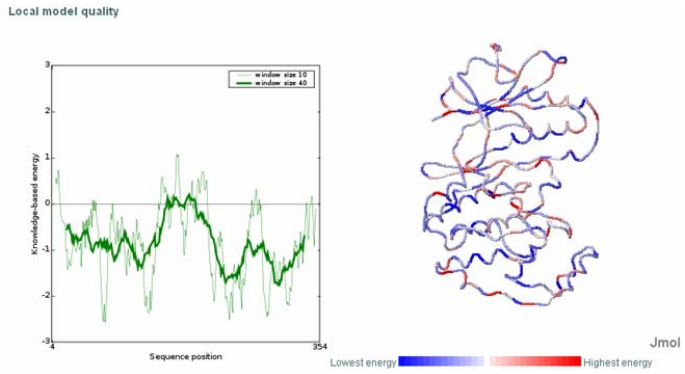

Figure 5.3.: Local model quality of PDB 1W84, red: areas of high energy, blue: areas of low energy

Surprisingly the local model quality of the DFG-OUT models have very low energy values in the phosphorylation loop section (Figure 5.4).

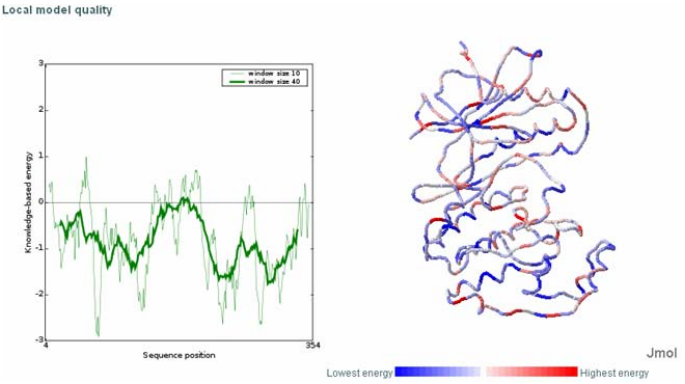

Figure 5.4.: Local model quality of PDB 1W82, red: areas of high energy, blue: areas of low energy

The state of the DFG-OUT conformation seems to be not unusual. Since just the beginning of the phosphorylation loop (residues 167-170) lies at the frame of the ATP binding pocket, the unfavourable energy state may not have influence on further modeling studies.

5.1.2.3. PDBSUM

PDBSUM [73] provides an at-a-glance overview of all PDB structures of the p38α MAP kinase and JNK3 in the Protein Data Bank (PDB). There is a link to the PROCHECK, where the Ramachandran plots in the next section come from.

5.1.2.4. Ramachandran Plot

The Ramachandran plot indicates allowed conformations of proteins. The conformation of the backbone of a residue is determined by three torsion angles, called ϕ(C[i-1]-N[i]-CA[i]-C[i]), ψ(N[i]-α-C[i]-C[i]-N[i+1]), and ω(α-C[i]-C[i]-N[i+1]-CA[i+1]) (figure 5.5 below).

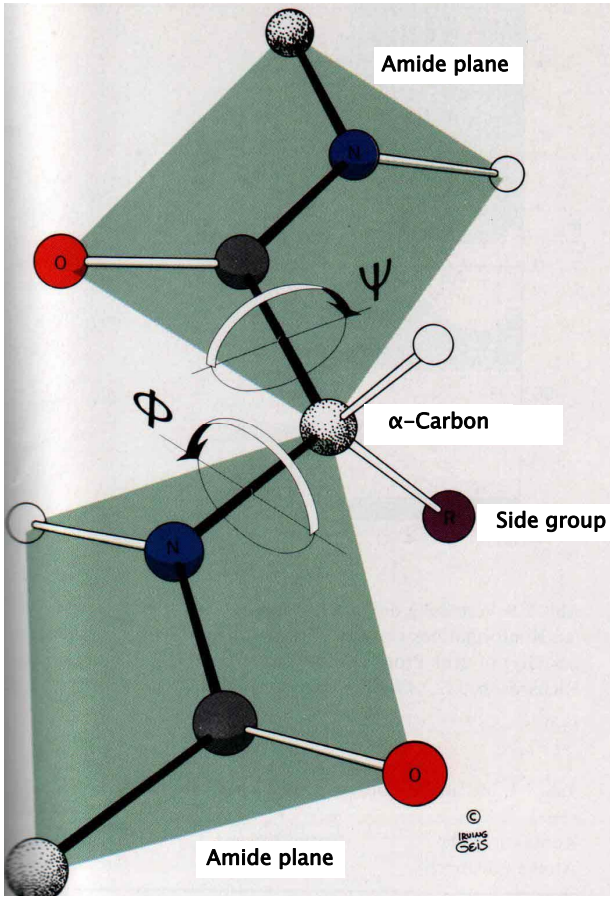

Figure 5.5.: Torsion angles of protein backbone

Proteins mainly are trans-peptides, so that the omega angle is restrained to values near 180°. Cis-peptides are rare and if they occur, the next residue is a Proline. The omega angle therefore offers little in the way of validation checks. Due to steric hindrance there are several clearly preferred combinations of ϕ and ψ values. The Ramachandran plot is therefore an useful indicator of model quality. Most areas of the Ramachandran plot represent forbidden conformations (coloured in white). Three regions are physically accessible to most residues. If the model was determined accurately, most of the angels fall in the so-called allowed regions (coloured in red, orange and yellow). Any residues which occur in the forbidden regions should not have adopted the observed conformations and would have required a check by the

crystallographer. The two residues Glycine and Proline are exceptions in that point. Proline is the most restricted residue and ϕ can only range around -6°, while the values of ϕ and ψ for Glycine, the only amino acid without any Cβ atom, cover a larger area on the Ramachandran plot. The Ramachandran Plot statistics of PROCHECK [74] demonstrate a easy overview (Check table 5.7). Good models have at least 90% (based on an analysis of 118 structures of resolution of at least 2.0 Å and R-factor no greater than 20.0) of their residues in most favoured regions. The G-factors provide a measure of how out-of-the-ordinary a property is. The overall average of the G-Factors should be above -0.5. A value below -1.0 is highly unusual. Below are shown the Ramachandran plots of the JNK3 models (Figures 5.6 and 5.7 on the next page).

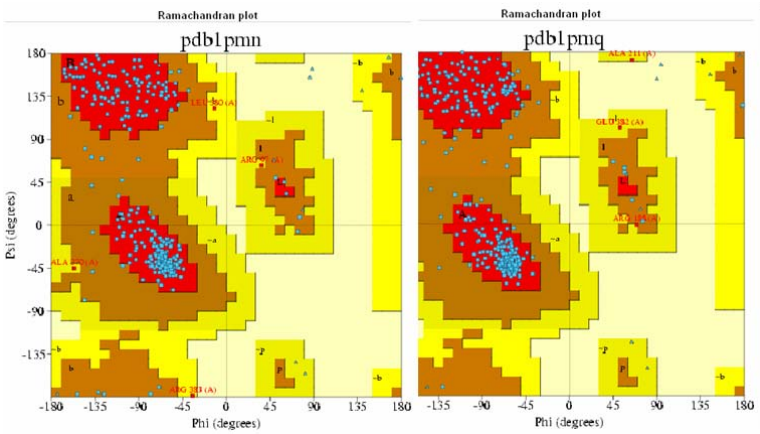

Figure 5.6.: Ramachandran plot of PDB 1PMN (left) and PDB 1PMQ (right) created by PROCHECK

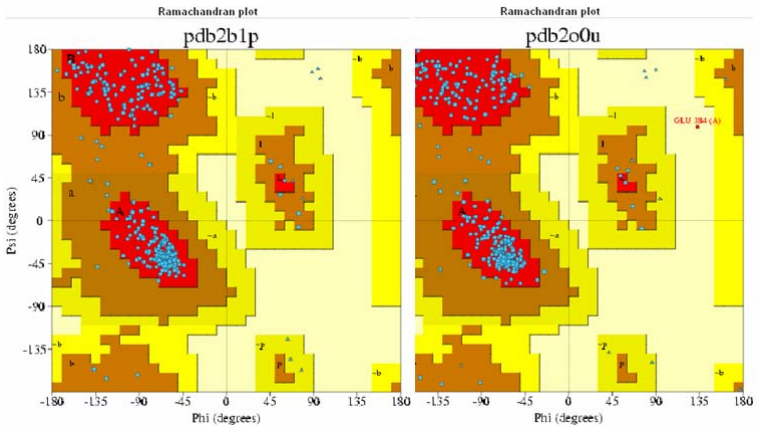

Figure 5.7.: Ramachandran plot of PDB 2B1P (left) and PDB 2O0U (right) created by PROCHECK

Apart from PDB 1PMQ all JNK3 models have over 90% of the residues in the the allowed regions (see also table 5.7). PDB 2O0U has one outlier (Glu384), what is of little importance, because it is outside of the interesting areas. The following two Ramachandran plots show the DFG-OUT p38α MAP kinase models (Figure 5.8).

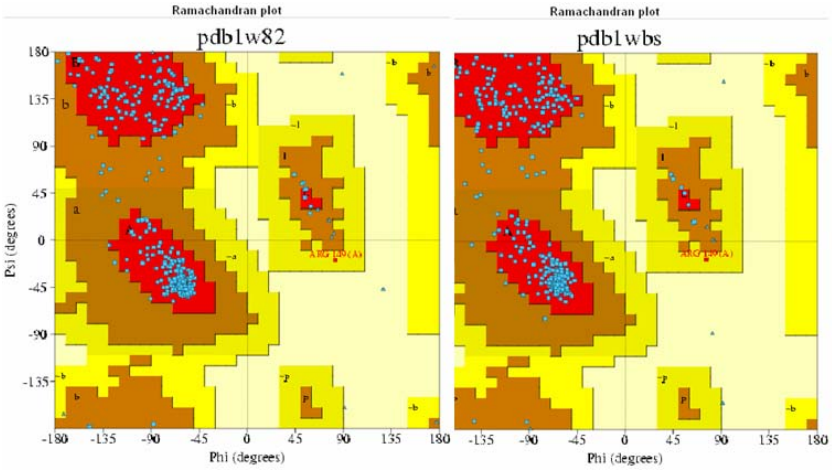

Figure 5.8.: Ramachandran plot of PDB 1W82 (left) and PDB 1WBS (right) created by PROCHECK

The two have no outliers and a very good score, see also table 5.7. Figures 5.9, 5.10 and 5.11 show the Ramachandran plots of the DFG-IN p38α MAP kinase models.

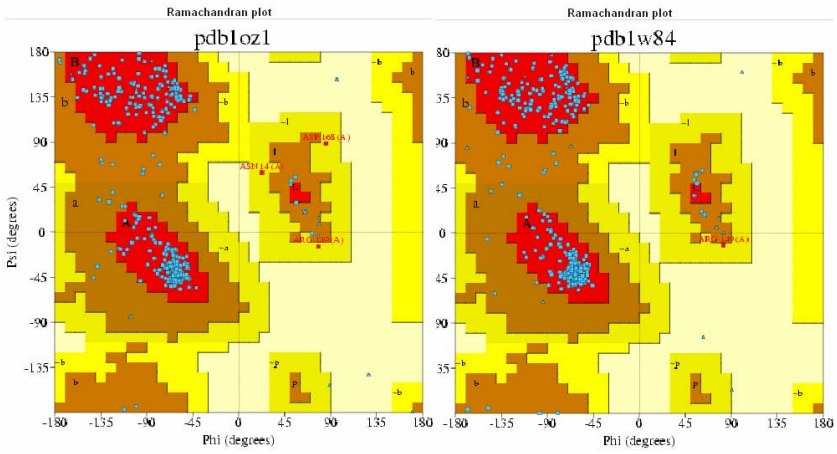

Figure 5.9.: Ramachandran plot of PDB 1OZ1 (left) and PDB 1W84 (right) created by PROCHECK

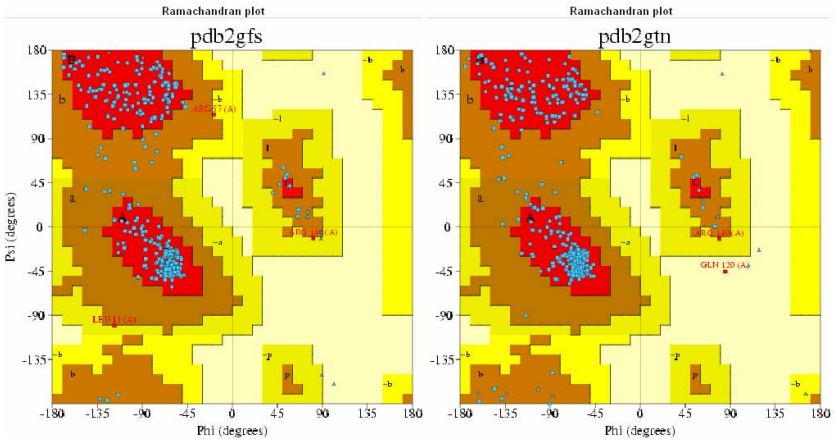

Figure 5.10.: Ramachandran plot of PDB 2GFS (left) and PDB 2GTN (right) created by PROCHECK

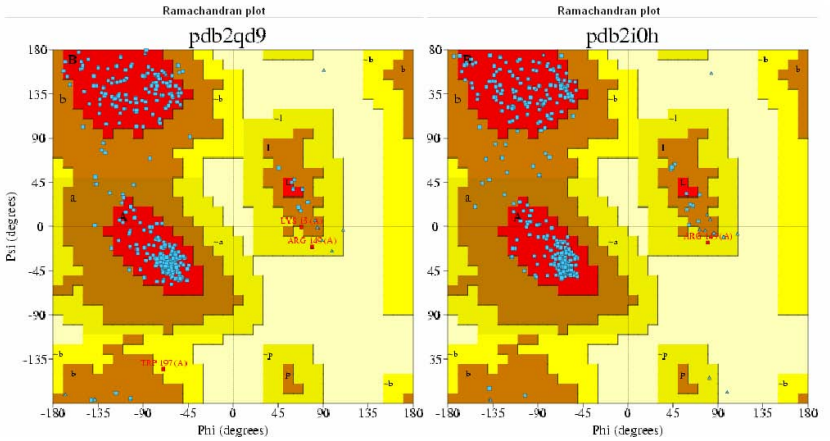

Figure 5.11.: Ramachandran plot of PDB 2QD9 (left) and PDB 2I0H (right) created by PROCHECK

The majority of the Ramachandran plots have no outliers and have over 90% of their residues in the favoured regions. Only PDB 2GTN has two outliers near the ATP binding site, but they are of little importance. PDB 2IOH has only 89.2% of its residues in the most favoured regions, but this small deviation can be overlooked. The Ramachandran plots of the DFG-IN p38α MAP kinase models without ligands are present in figure 5.12.

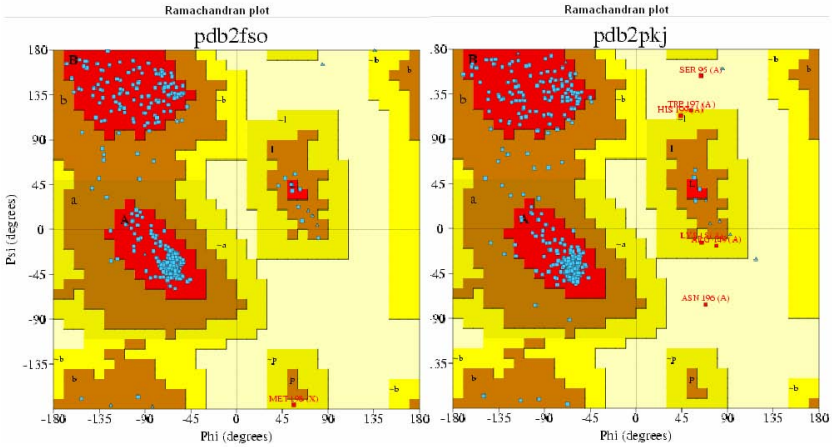

Figure 5.12.: Ramachandran plot of PDB 2FSO (left) and PDB 2PKJ (right) created by PROCHECK

PDB 2PKJ has below 90% of his residues in the favoured regions and several outliers (see also table 5.7). But it was neccessary to use another unliganded PDB apart from 2FSO, the deviations of PDB 2PKJ were accepted. PDB 2PKJ was still the best of its series and the deviations do not concern any important residues for this study. The in the diploma thesis used PDB 1YWR is of much less quality. It contains many outliers and only has 86,1% of its residues in the most favoured regions.

5.1.3. Chosen PDB structures

In the end the following PDB structures of JNK3: PDB 1PMQ, PDB 1PMN, PDB 2B1P, PDB 2O0U and p38α MAP kinase: PDB 1OZ1, PDB 1W82, PDB 1W84, PDB 1WBS, 2FSO, PDB 2GFS, PDB 2GTN, PDB 2I0H, PDB 2PKJ and PDB 2QD9 were chosen for the further analysis (see table 5.7).

PDB	Sequence	Mutation	Ligand	R-value	R-free	Waters	Rach in %	G-Factor
1OZ1	5-117, 121-352	-	FPH	0.204	0.251	201	90.3	0.08
1PMN	45-211, 217-371, 379-400	-	Q984-501	0.231	0.266	212	91.9	0.27
1PMQ	45-212, 217-374, 379-400	-	Q880-501	0.231	0.262	81	89.6	0.28
1W82	4-355	-	L10	0.174	0.235	1584	91.2	0.09
1W84	4-355	-	L12	0.182	0.238	576	92.1	0.03
1WBS	4-355	-	LI2	0.193	0.230	395	91.5	0.14
2B1P	46-210, 226-373, 376-400	-	AIZ501	0.220	0.267	206	92.2	0.09
2FSO	5-32, 36-114, 121-168, 184-354	D176A	-	0.177	0.224	460	91.0	0.08
2GFS	5-352	-	PQB	0.205	0.239	323	90.0	0.19
2GTN	5-172, 184-352	mouse	LIE301	0.203	0.248	221	90.1	-0.07
2I0H	4-352	-	Q222-400	0.180	0.228	455	89.2	0.31
2O0U	46-212, 218-363, 378-400	-	COM2000	0.225	0.283	164	90.8	-0.05
2PKJ	5-31, 36-172, 185-352	F169A	-	0.280	0.280	89	88.3	0.33
2QD9	5-117, 121-172, 186-352	-	LGF	0.252	0.282	139	90.8	-0.12

Table 5.7.: Chosen PDB structures of the p38 MAP kinase and JNK3 after validation with X-ray parameters and Rachmachandran plot values

This selection of models of good quality represent all the available conformations of the two kinases. JNK3 is just available in the DFG-IN conformation, while the models of p38α MAP kinases show the different conformations. PDB 1OZ1, PDB 1W84 and PDB 2GTN represent the DFG-IN conformation, whereas PDB 2GFS, PDB 2I0H and PDB 2QD9 also are DFG-IN representatives, but have a special conformation of the Gly-rich loop and/or the hinge region (PDB 2I0H). PDB 2GTN contains mouse p38α MAP kinase instead of human expressed in E.coli respectively. PDB 2FSO and PDB 2PKJ do not contain any ligand. PDB 1WBS and PDB 1W82 are models of the DFG-OUT conformation and make sure that the small possibility of the Suberones being DFG-OUT binders, is not overlooked. They were included after first in-progress reports during the crystallisation process, suggested the DFG-OUT pocket as a possible area for the binding of the Suberones.

5.1.4. Alignments by homology of the models

All PDB structures were aligned by homology with the Biopolymer⇒Compare Structures⇒Align by Homology panel of SYBYL to compare the differences. The four JNK3 models were aligned by homology on their C-α atoms (Figures 5.13, 5.14, 5.15 on the next pages).

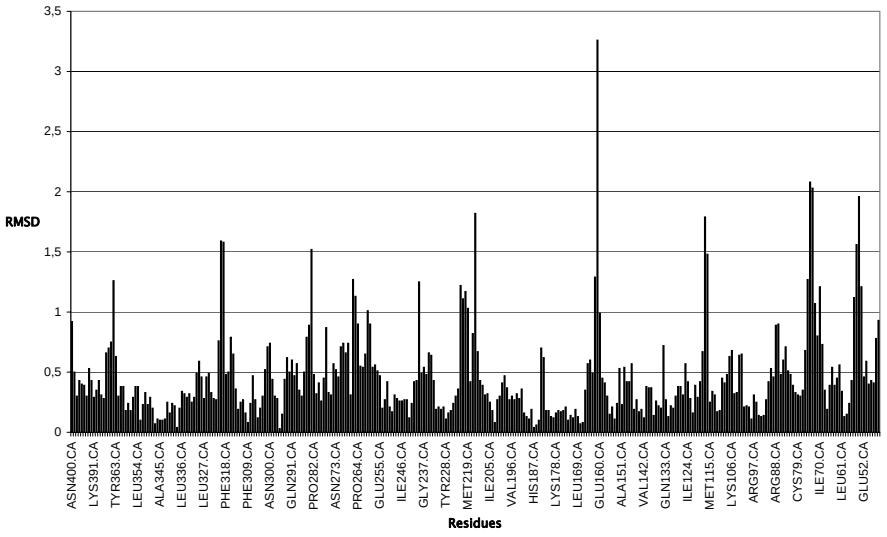

Figure 5.13.: Alignment of PDB 1PMQ, PDB 2O0U is fixed, RMSD 0.6043

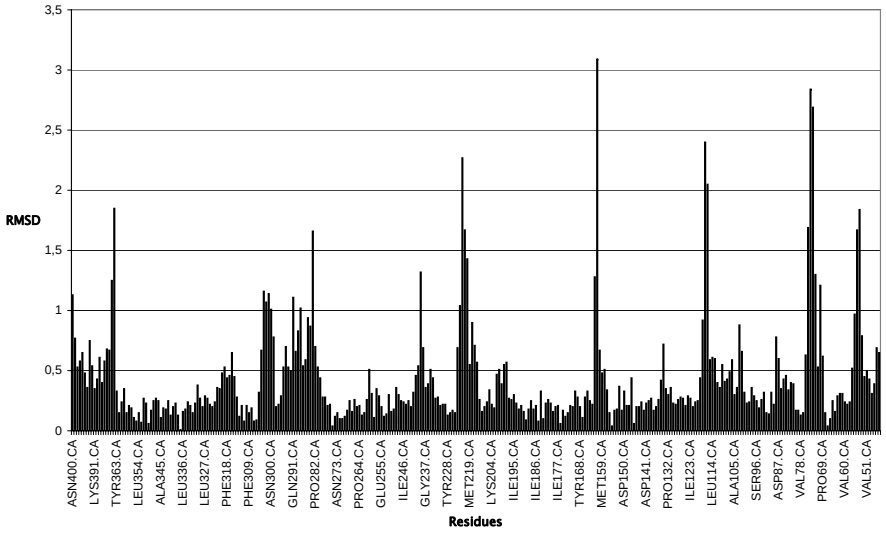

Figure 5.14.: Alignment of PDB 1PMN, PDB 2O0U is fixed, RMSD 0.5922

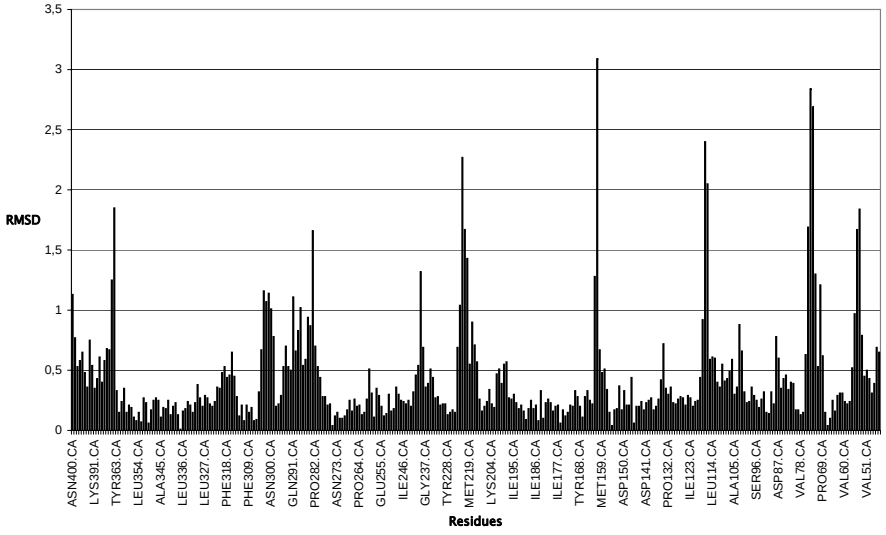

Figure 5.15.: Alignment of PDB 2B1P, PDB 2O0U is fixed, RMSD 0.6206

In all cases the relevant residues (residues of the ATP-binding site) are very similar; the Root mean square deviations (RMSDs) are below 1. The overall RMSDs are also below 1 and differ little. The four JNK3 models were also aligned by homology on all atoms (figures 5.17, 5.16, 5.18).

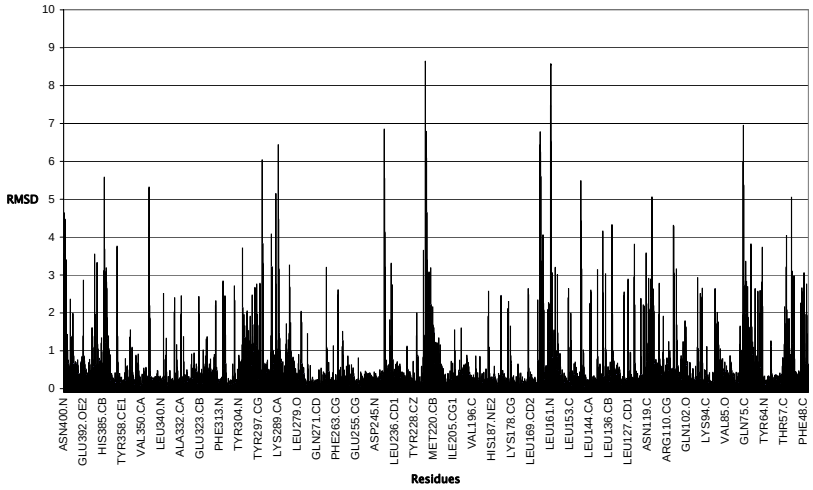

Figure 5.16.: Alignment of PDB 1PMN, PDB 2O0U is fixed, RMSD 1.1179

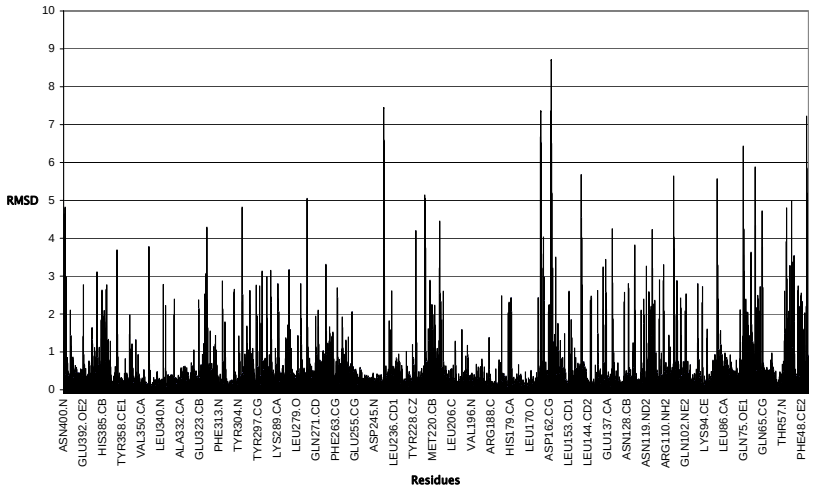

Figure 5.17.: Alignment of PDB 1PMQ, PDB 2O0U is fixed, RMSD 1.1158

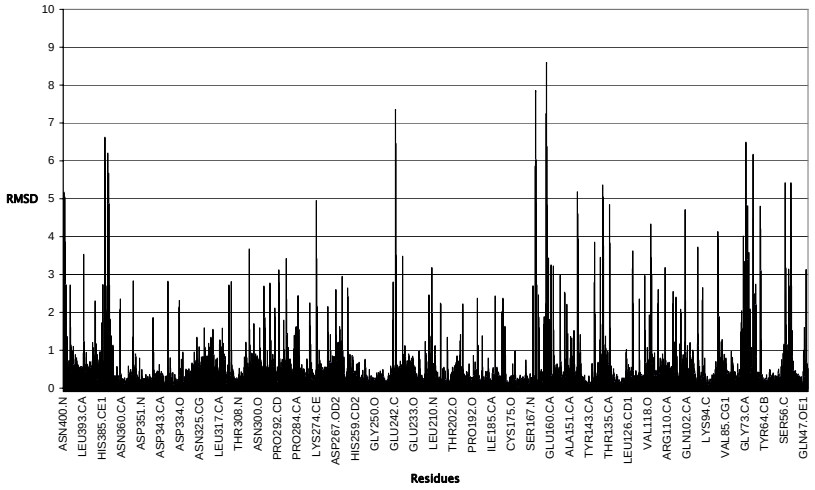

Figure 5.18.: Alignment of PDB 2B1P, PDB 2O0U is fixed, RMSD 1.0904

The RMSD values are higher, but that is due to the inclusion of the side chain atoms. Side chain conformations can differ among the protein models. The appearance of different side chain conformations is possible. But an unfortunate conformation may have influence on the docking, because during all dockings the model is treated as rigid. The concerning residues here is the side chain of Glu147 differs in PDB 2O0U in comparison to the others. The overall RMSD values are acceptable and all other important residues have a RMSD around 1. Figure 5.19 shows the alignment by the C-α atom of the four JNK3 PDB structures.

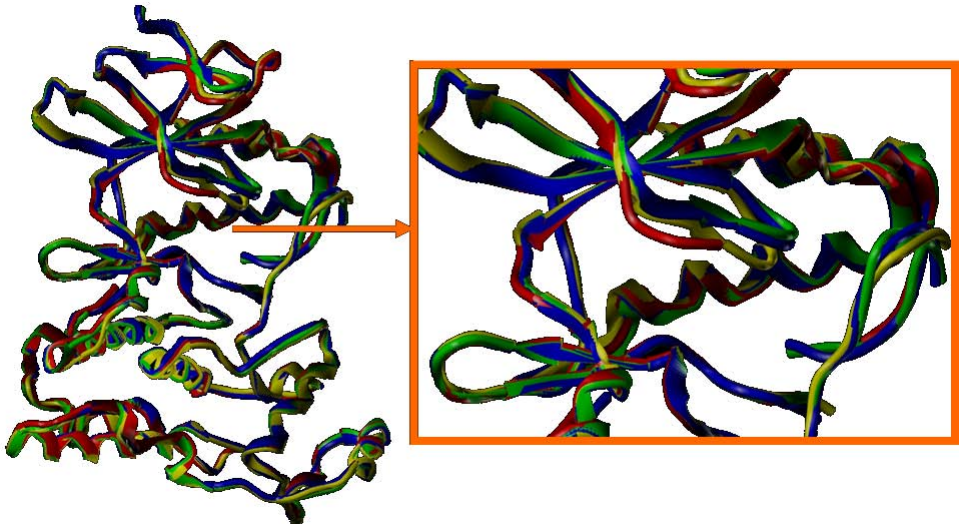

Figure 5.19.: Alignment of PDB 1PMN (green), PDB 1PMQ (blue) and PDB 2B1P (red); PDB 2O0U (yellow) is fixed

The chosen PDB structures of p38α MAP kinase were also aligned by homology. PDB 2PKJ

was fixed and all the other PDB structures were aligned on the PDB 2PKJ coordinates. The RMSDs of Lys53 are not presented, because the conformations do not differ significantly among the PDBs. Figure 5.20 visualizes the data of table 5.8. Unfortunately many atoms of the Gly-rich loop atoms are missing in several PDB structures. Still recognizable is that Gly31 ($\geq$5) and Gly36 ($\geq$2) have high RMSD values, especially in PDB 2I0H and PDB 2GFS. The other residues have lower RMSD values and do not differ among the PDB structures.

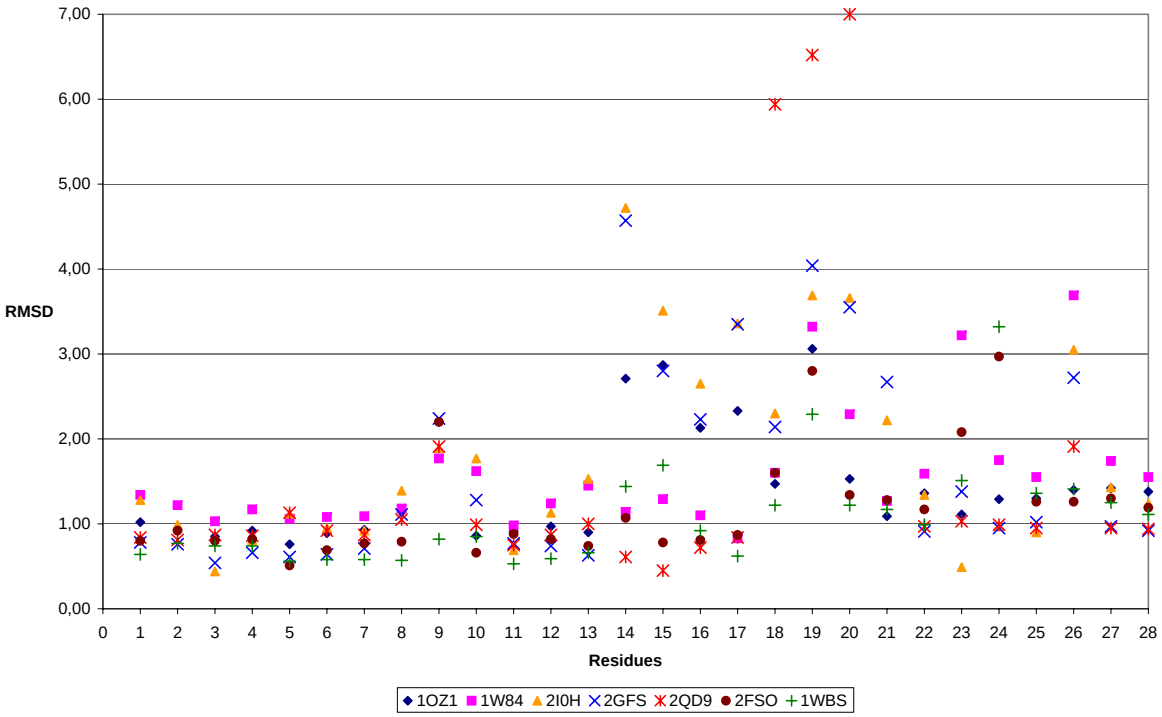

Figure 5.20.: Alignment the Gly-rich loop atoms of PDB 2PKJ to all other chosen PDBs of the p38α MAP kinase

No.	Residue	1OZ1	1W84	2I0H	2GFS	2QD9	2FSO	1WBS
1	VAL38 N	1.02	1.34	1.28	0.78	0.84	0.80	0.64
2	VAL38 CG2	0.93	1.22	0.99	0.76	0.81	0.92	0.77
3	VAL38 CG1	0.85	1.03	0.44	0.54	0.87	0.80	0.74
4	VAL38 CB	0.92	1.17	0.81	0.66	0.86	0.82	0.74
5	VAL38 O	0.76	1.06	1.12	0.61	1.13	0.51	0.56
6	VAL38 C	0.89	1.08	0.95	0.64	0.92	0.69	0.58
7	VAL38 CA	0.93	1.09	0.92	0.71	0.87	0.77	0.58
8	SER37 N	1.14	1.18	1.39	1.11	1.05	0.79	0.57

9	SER37 OG	2.20	1.77	1.89	2.24	1.91	2.20	0.82
10	SER37 CB	0.86	1.62	1.77	1.28	0.99	0.66	0.85
11	SER37 O	0.91	0.98	0.69	0.77	0.75	0.88	0.53
12	SER37 C	0.97	1.24	1.13	0.74	0.87	0.82	0.59
13	SER37 CA	0.90	1.45	1.53	0.63	1.00	0.74	0.66
14	GLY36 N	2.71	1.14	4.72	4.57	0.61	1.07	1.44
15	GLY36 O	2.87	1.29	3.51	2.80	0.45	0.78	1.69
16	GLY36 C	2.13	1.10	2.65	2.23	0.72	0.81	0.92
17	GLY36 CA	2.33	0.83	3.36	3.35	0.84	0.87	0.62
18	GLY31 N	1.47	1.60	2.30	2.14	5.94	1.60	1.22
19	GLY31 O	3.06	3.32	3.69	4.04	6.52	2.80	2.29
20	GLY31 C	1.53	2.29	3.66	3.55	7.00	1.34	1.22
21	GLY31 CA	1.09	1.27	2.22	2.67	7.01	1.28	1.17
22	VAL30 N	1.36	1.59	1.34	0.91	0.97	1.17	0.99
23	VAL30 CG2	1.11	3.22	0.49	1.38	1.03	2.08	1.51
24	VAL30 CG1	1.29	1.75	0.97	0.95	0.99	2.97	3.32
25	VAL30 CB	1.30	1.55	0.90	1.02	0.95	1.26	1.36
26	VAL30 O	1.40	3.69	3.05	2.72	1.91	1.26	1.41
27	VAL30 C	1.42	1.74	1.43	0.97	0.95	1.30	1.25
28	VAL30 CA	1.38	1.55	1.24	0.92	0.94	1.19	1.11
	Average	2.24	2.13	1.59	1.89	1.11	1.25	3.77

Table 5.8.: Data of the alignment of the Gly-rich loop atoms of PDB 2PKJ to all other chosen PDBs of the p38α MAP kinase

Figure 5.21 visualizes the data of table 5.9 (see the next pages). Noticeable are the high RMSD values of the PDB 1W84 and PDB 1OZ1. The side chains of Met109 in these structures differ greatly to that of the others. Here the side chain of Met109 extends to the ground of the ATP binding side, limiting the accessible space in front of the hinge region considerably. The side chain of PDB 1WBS also has high values, representing the changes which occur in the hinge region during the DFG-OUT conformation. The three PDB structures also step forward when taking a look at Gly110. Next to Met109 on the opposite side of Gly110, Leu108 does not show such high RMSD values. This may indicate that any "flip" in the hinge region happens exclusively at the residues Met109 and Gly110. The side chain of His107 also shows

different conformations, but thus it is not directed into the ATP binding pocket, it is of little consequence. Much more important is Thr106. The side chain's oxygen in the PDB 2GFS, PDB 2FSO and PDB 2I0H has another conformation (PDB 2QD9 with it's RMSD of 1 lies in the middle). The side chain of Asp112 in PDB 2GFS is the only one which is similar to PDB 2PKJ. All the other hinge region atoms are very similar.

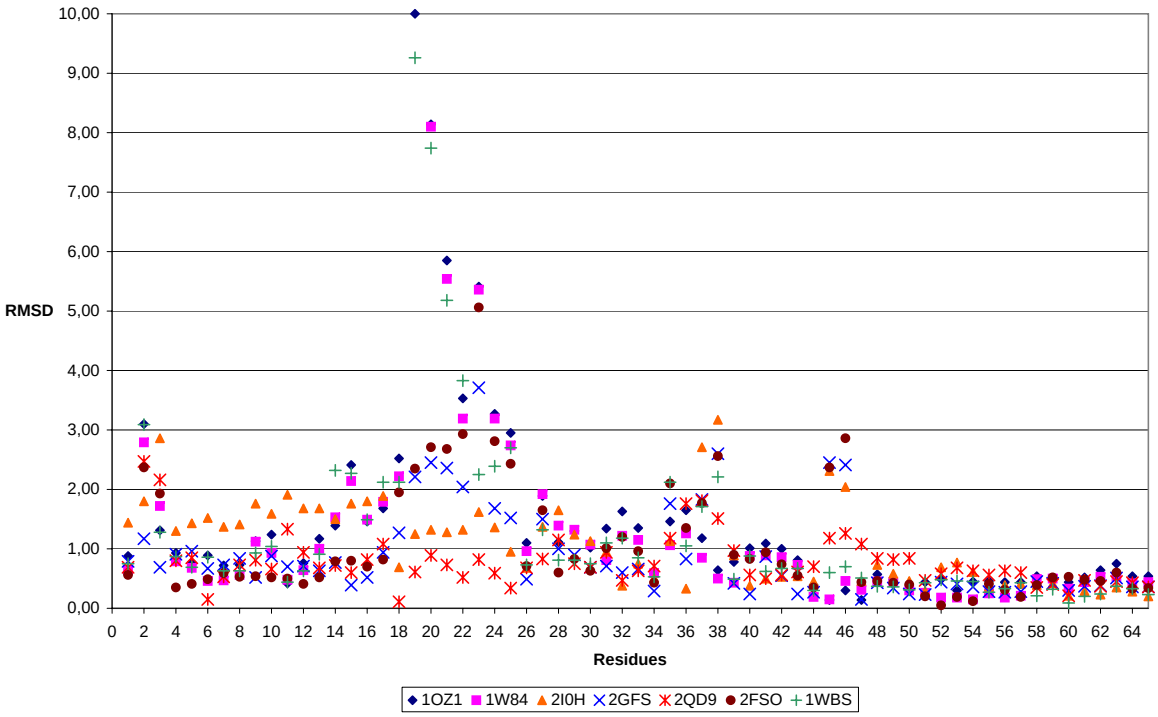

Figure 5.21.: Alignment the hinge region atoms of PDB 2PKJ to all other chosen PDBs of the p38α MAP kinase

No.	Residue	1OZ1	1W84	2I0H	2GFS	2QD9	2FSO	1WBS
1	ASP112 N	0.88	0.64	1.44	0.79	0.69	0.56	0.75
2	ASP112 OD1	3.10	2.79	1.80	1.17	2.47	2.37	3.09
3	ASP112 OD2	1.31	1.72	2.86	0.69	2.16	1.93	1.28
4	ASP112 CG	0.93	0.79	1.30	0.91	0.80	0.35	0.87
5	ASP112 CB	0.77	0.68	1.43	0.96	0.85	0.41	0.69
6	ASP112 O	0.89	0.46	1.52	0.67	0.15	0.49	0.86
7	ASP112 C	0.72	0.47	1.37	0.73	0.53	0.59	0.63
8	ASP112 CA	0.73	0.56	1.41	0.84	0.73	0.53	0.63
9	ALA111 N	1.13	1.12	1.76	0.52	0.81	0.54	0.93

10	ALA111 CB	1.24	0.93	1.59	0.88	0.66	0.52	1.04
11	ALA111 O	0.42	0.48	1.91	0.70	1.33	0.50	0.44
12	ALA111 C	0.76	0.64	1.68	0.71	0.94	0.41	0.63
13	ALA111 CA	1.17	1.00	1.68	0.63	0.68	0.52	0.91
14	GLY110 N	1.39	1.53	1.50	0.77	0.72	0.79	2.32
15	GLY110 O	2.41	2.14	1.76	0.39	0.60	0.80	2.27
16	GLY110 C	1.46	1.49	1.80	0.52	0.82	0.70	1.49
17	GLY110 CA	1.68	1.79	1.89	0.94	1.08	0.82	2.12
18	MET109 N	2.52	2.22	0.69	1.27	0.11	1.95	2.12
19	MET109 CE	10.00	10.04	1.25	2.21	0.61	2.35	9.26
20	MET109 SD	8.14	8.10	1.32	2.45	0.89	2.71	7.74
21	MET109 CG	5.85	5.54	1.28	2.36	0.73	2.68	5.18
22	MET109 CB	3.53	3.19	1.32	2.04	0.52	2.93	3.83
23	MET109 O	5.41	5.36	1.62	3.71	0.82	5.06	2.25
24	MET109 C	3.27	3.19	1.36	1.68	0.59	2.81	2.39
25	MET109 CA	2.95	2.74	0.95	1.52	0.34	2.43	2.70
26	LEU108 N	1.10	0.96	0.68	0.49	0.68	0.71	0.73
27	LEU108 CD1	1.89	1.92	1.37	1.50	0.83	1.65	1.32
28	LEU108 CD2	1.11	1.39	1.65	1.00	1.15	0.60	0.81
29	LEU108 CG	1.30	1.32	1.24	0.90	0.75	0.83	0.81
30	LEU108 CB	1.02	1.07	1.13	0.69	0.69	0.63	0.75
31	LEU108 O	1.34	0.81	0.95	0.71	0.94	1.01	1.10
32	LEU108 C	1.63	1.22	0.38	0.60	0.47	1.20	1.18
33	LEU108 CA	1.35	1.15	0.75	0.66	0.63	0.96	0.85
34	HIS107 N	0.59	0.59	0.51	0.29	0.71	0.43	0.53
35	HIS107 ND1	1.46	1.06	1.13	1.76	1.18	2.10	2.12
36	HIS107 CE1	1.65	1.26	0.33	0.83	1.76	1.35	1.05
37	HIS107 NE2	1.18	0.85	2.71	1.83	1.81	1.77	1.71
38	HIS107 CD2	0.64	0.50	3.17	2.60	1.51	2.56	2.21
39	HIS107 CG	0.78	0.43	0.89	0.42	0.97	0.90	0.49
40	HIS107 CB	1.01	0.88	0.38	0.24	0.56	0.83	0.88
41	HIS107 O	1.09	0.89	0.50	0.87	0.50	0.94	0.62
42	HIS107 C	1.00	0.86	0.53	0.55	0.56	0.74	0.67

43	HIS107 CA	0.81	0.73	0.54	0.24	0.61	0.55	0.67
44	THR106 N	0.39	0.19	0.45	0.27	0.70	0.35	0.30
45	THR106 CG2	0.14	0.15	2.31	2.45	1.18	2.37	0.60
46	THR106 OG1	0.30	0.46	2.04	2.41	1.26	2.86	0.70
47	THR106 CB	0.14	0.31	0.46	0.15	1.08	0.44	0.51
48	THR106 O	0.57	0.45	0.73	0.43	0.84	0.46	0.37
49	THR106 C	0.48	0.44	0.58	0.34	0.82	0.43	0.36
50	THR106 CA	0.32	0.30	0.46	0.24	0.84	0.40	0.31
51	VAL105 N	0.44	0.26	0.29	0.23	0.47	0.20	0.43
52	VAL105 CG2	0.49	0.18	0.69	0.44	0.58	0.05	0.48
53	VAL105 CG1	0.30	0.18	0.77	0.41	0.68	0.19	0.46
54	VAL105 CB	0.45	0.15	0.61	0.36	0.63	0.12	0.45
55	VAL105 O	0.46	0.25	0.36	0.28	0.56	0.41	0.27
56	VAL105 C	0.44	0.18	0.39	0.27	0.63	0.31	0.33
57	VAL105 CA	0.44	0.21	0.41	0.28	0.60	0.19	0.43
58	LEU104 N	0.54	0.49	0.39	0.45	0.35	0.39	0.21
59	LEU104 CD1	0.49	0.50	0.42	0.42	0.40	0.52	0.32
60	LEU104 CD2	0.44	0.33	0.21	0.30	0.21	0.53	0.09
61	LEU104 CG	0.52	0.44	0.29	0.37	0.47	0.48	0.20
62	LEU104 CB	0.64	0.53	0.23	0.38	0.37	0.46	0.24
63	LEU104 O	0.75	0.53	0.35	0.51	0.45	0.60	0.37
64	LEU104 C	0.54	0.42	0.28	0.36	0.43	0.33	0.33
65	LEU104 CA	0.54	0.44	0.20	0.36	0.36	0.34	0.23
	Average	1.44	1.31	1.08	0.89	0.78	1.05	1.27

Table 5.9.: Datatable: Alignment of the hinge region atoms of PDB 2PKJ to all other chosen PDBs of the p38α MAP kinase

Figure 5.22 visualizes the data of table 5.10 (see also the next pages). The DFG region is represented by Asp168 and Gly170, while Phe169 is unfortunately missing in some structures. Hence Leu167 was included, but does not show any notable differences among the PDB structures. PDB 1WBS certainly has very high RMSD values in that region. PDB 1W84 and PDB 1OZ1 have more moderate high values. PDB 2I0H has also high RMSD values at the position of Asp168. Altogether all RMSD values of the side chain of Asp168 are fairly high.

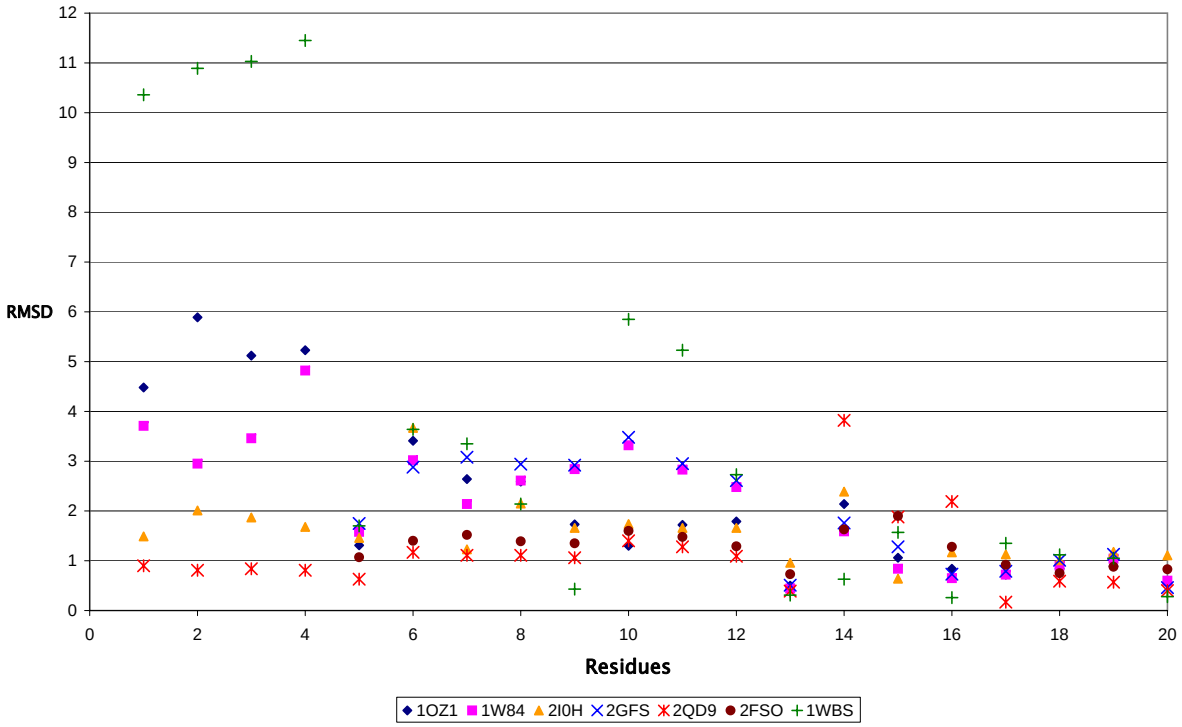

Figure 5.22.: Alignment the DFG atoms of PDB 2PKJ to all other chosen PDBs of the p38α MAP kinase

No	Residue	1OZ1	1W84	2I0H	2GFS	2QD9	2FSO	1WBS
1	GLY170 N	4.48	3.71	1.49	-	0.90	-	10.40
2	GLY170 O	5.89	2.95	2.01	-	0.81	-	10.90
3	GLY170 C	5.12	3.46	1.87	-	0.84	-	11.00
4	GLY170 CA	5.23	4.82	1.68	-	0.81	-	11.50
5	ASP168 N	1.31	1.58	1.46	1.75	0.63	1.07	1.70
6	ASP168 OD1	3.41	3.02	3.67	2.88	1.17	1.40	3.64
7	ASP168 OD2	2.64	2.14	1.23	3.08	1.11	1.52	3.35
8	ASP168 CG	2.59	2.61	2.15	2.94	1.11	1.39	2.14
9	ASP168 CB	1.73	2.84	1.66	2.92	1.06	1.35	0.43
10	ASP168 O	1.30	3.32	1.74	3.48	1.40	1.60	5.85
11	ASP168 C	1.72	2.83	1.66	2.95	1.28	1.48	5.23
12	ASP168 CA	1.79	2.48	1.66	2.61	1.09	1.29	2.73
13	LEU167 N	0.50	0.44	0.96	0.51	0.39	0.73	0.31

14	LEU167 CD1	2.14	1.59	2.39	1.76	3.82	1.63	0.63
15	LEU167 CD2	1.06	0.84	0.64	1.28	1.88	1.9	1.57
16	LEU167 CG	0.84	0.65	1.17	0.73	2.19	1.28	0.26
17	LEU167 CB	0.72	0.72	1.13	0.79	0.17	0.92	1.35
18	LEU167 O	0.84	0.9	1.01	1.01	0.59	0.75	1.12
19	LEU167 C	0.89	1.04	1.18	1.13	0.57	0.88	1.05
20	LEU167 CA	0.56	0.60	1.11	0.46	0.40	0.83	0.28
	Average	1.42	1.58	1.80	1.63	1.78	1.19	1.08

Table 5.10.: Data of the alignment of the hinge region atoms of PDB 2PKJ to all other chosen PDBs of the p38α MAP kinase

5.1.5. PDB 2GTN

As mentioned above the genetic source of the p38α MAP kinase of PDB 2GTN is of murine origin. However, the differences between PDB 2GTN and the other humane models are not significant.
Table 5.11 shows the RMSD values of PDB 2GTN in comparison with PDB 2I0H, PDB 1W84 and PDB 1OZ1. RMSD values lower than 3 Angström are acceptable.

PDB 2GTN	**PDB 2I0H**	**PDB 1OZ1**	**PDB 1W84**
Backbone atoms	2.0965	1.6844	1.7914
C-alpha atoms	2.0950	1.6765	1.7670
Side-chain atoms	2.7280	2.4183	2.5960
All Atoms	2.4372	2.0883	2.2347

Table 5.11.: RMSD values of all atoms of PDB 2GTN aligned by homology to all atoms of PDB 2I0H, PDB 1W84 and PDB 1OZ1

Figure 5.23 on the next page shows the detail of the RMSD values of all atoms of the hinge region (residues 104-112). The calculated RMSD values are acceptable. The highest RMSD values occur at the side chain atoms of Met109, what is of little matter, because they also vary in all the humane p38α MAP kinase models.

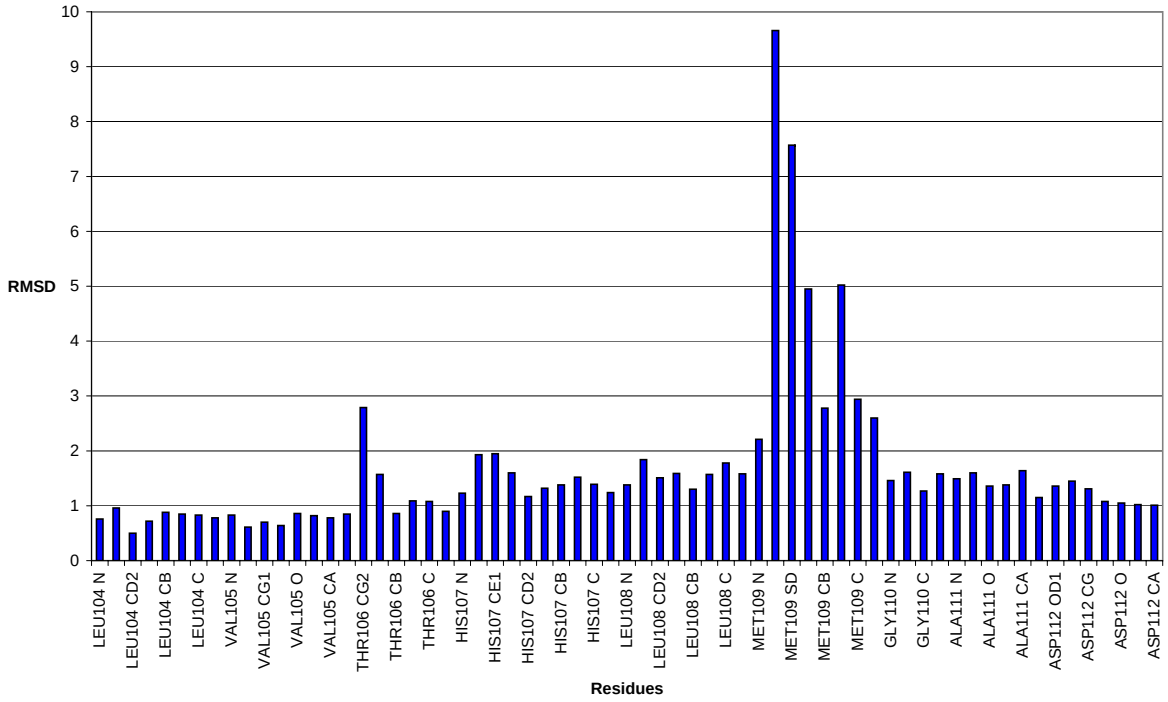

Figure 5.23.: Alignment by homology in SYBYL of PDB 1W84 to PDB 2GTN (fixed)

5.2. Creating databases for Docking

5.2.1. The ligands for the docking studies

Selected molecules according to Ottosen *et al.*, Revezs *et al.* and Suberone-scaffolds were built with SYBYL7.2 and minimized with MMFF94s. The database includes active (OTTO1-OTTO3 and REV1-REV8) and those with less activity (OTTO4 and REV9-10), so-called decoys. Suberone-scaffolds which were already tested (JH's and RN 's) were included, as well as newer ones (GA). The GA Suberones include both possible positions of the oxygen. The small Suberones (SK1-32) were built to examine the different position of a nitrogen in the rings. Later added SK and GA followed by three number represent the newest synthesized Suberones which were synthesized and tested recently. During the docking studies several other Suberones were built to test the first binding mode suggestions (MORE, MORE2). Some of these structures were exclusively built to check if the docking can find false positives (e.g. MO9min, MO10min, MO15min, MO16min); the decoys. All molecules were minimized under the conditions seen in figure 7.1 in Materials and Methods and therefore share the common ending -min. Conformations of molecules minimized in SYBYL7.2 are rarely distinguishable from to those determined by X-ray crystallography [75]. If the conformation is identical to

the conformation in a small molecule-protein complex is not clear. All compounds with their two-dimensional structures, energies, molecular weight and IC_{50} values can be found in the appendix tables A.2, A.3, A.4, A.5, A.6, A.7, A.8, A.9, A.10.

5.2.1.1. Ligands of the chosen PDB structures

The ligands of the chosen PDB structures of the p38α MAP kinase and JNK3 were extracted to a database. They were not minimized further, but were kept in the exact conformation that has been found in the X-ray structure. All ligands bind to p38α MAP kinase, apart from the ligand of PDB 2B1P, which is supposed to be only selective for JNK3 according to Swahn *et al.*. The other ligands should therefore show reasonable binding poses in the docking studies. For some ligands the author did not publish a selectivity profile. The ligand of PDB 2GFS is reported to be less active on JNK3, whereas the ligand of PDB 2I0H should not have any activity against JNK3 at all. PDB 2FSO and PDB 2PKJ contain no ligand. The energies and molecular weights were calculated with SYBYL and can be seen in table A.1 in the appendix.

5.2.2. Properties of the Compounds

The position of the oxygen in the 3- or 8-amino-6,11-dihydro-dibenzo[*b,e*]oxepin-11-ones suffer from an unexplainable loss of potency. A clue might be given from the properties. In SYBYL all distances and angles of the Suberones were determined with the "Measure" panel. All the distances and angles are displayed in tables A.11, A.12, A.13, A.14, A.15, A.16, A.17, A.19, A.18, A.20, A.21, A.22, A.23, A.24, A.25, A.26, A.27, A.28, A.29, A.30, A.31, A.32, A.33, A.34, A.35 in the appendix. Figure 5.24 (next page) describes where which measurements were carried out. In some cases no data could be collected, because the composition of the molecule was too different to the Suberone scaffold (e.g. the missing seven-membered ring in REV or OTTO compounds or the missing aminophenyl substituent of SK1-32). The θ and accordingly the ι account for the hydrogen which points on the direction of the viewer, if the amino-phenyl is on the right side.
Figure 5.25 on the next page represents the distances that occur in the Suberone database.

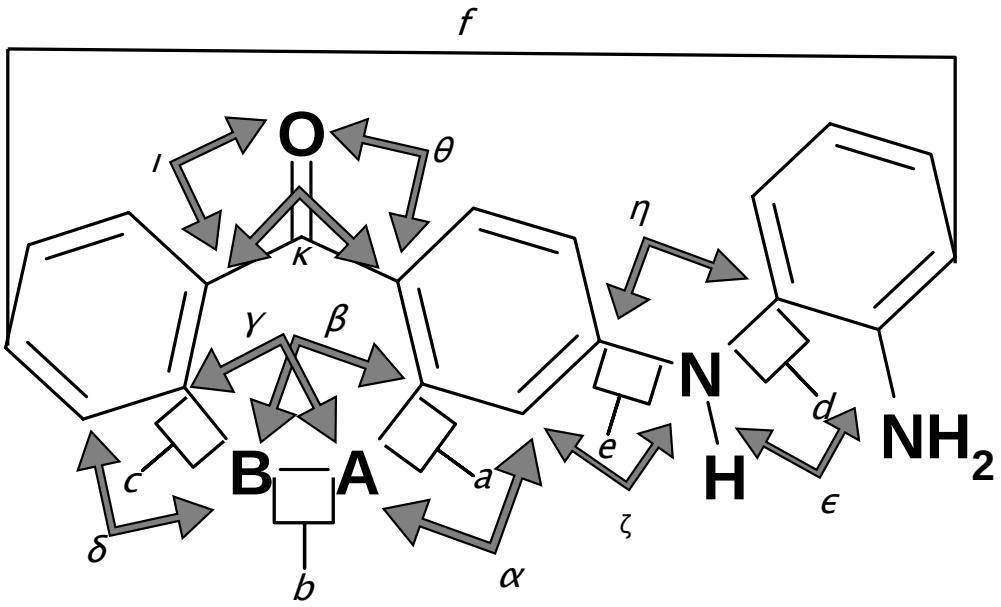

Figure 5.24.: Measurement of distances in Å (a-f) and angles in ° (α-κ), B=C and A=0 or B=O and A=C

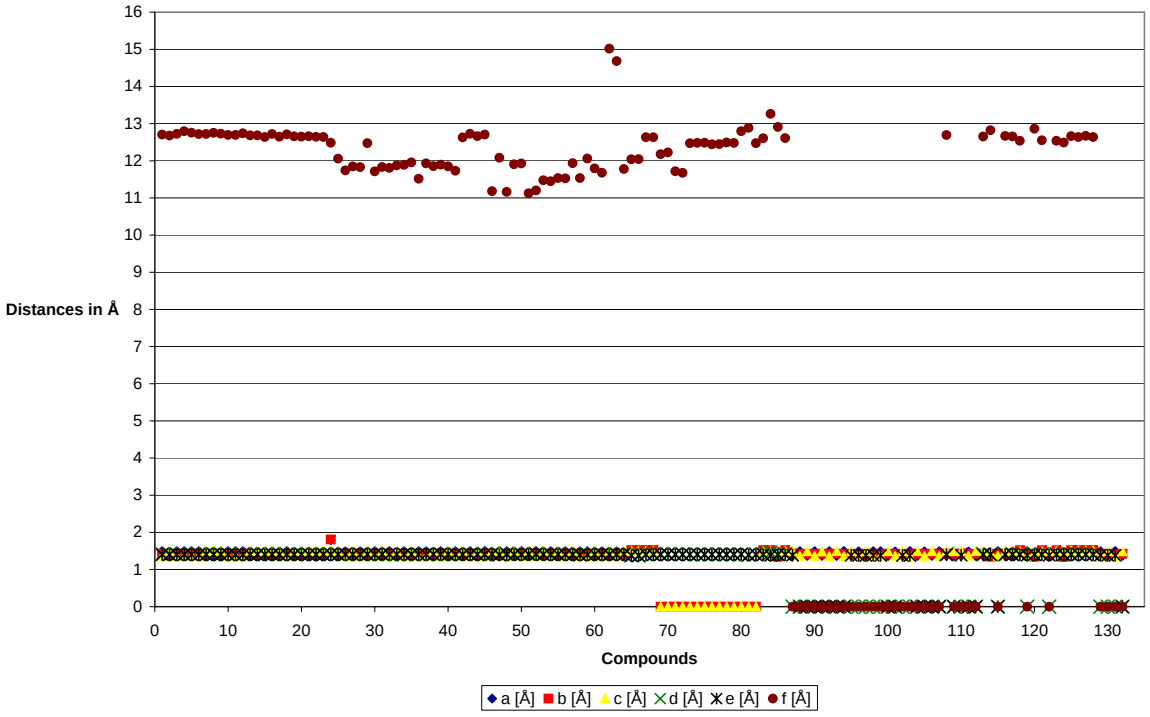

Figure 5.25.: Measurement of distances

The values of the distances **a**, **b** and **c** vary little. Just JH46min is an outlier, due to the sulphur in the seven-membered ring (orange square above at position 64). No differences between the GAmin and the JHmin molecules can be observed. In the MOREmin group MO1min, MO2min, MO25min-30min, and MO39min and MO40min stand out as outliers, in comparison to the other MOREmin compounds, but differ little from the GAmin or JHmin compounds. MO7min and MO8min are above all others, due to their additional fused ring. The OTTOmin compounds 1 and 2 are a little shorter than 3 and 4. The same occurs in the case of REV1min-6min, which are shorter than REV7min and REV8min. RN14min and RN14amin have longer distances from one end to the other than RN13amin and RN15min. The SK with three identification numbers differ little. For SK1-SK32 no measurement was possible. Figure 5.26 visualizes the first six values of the angles.

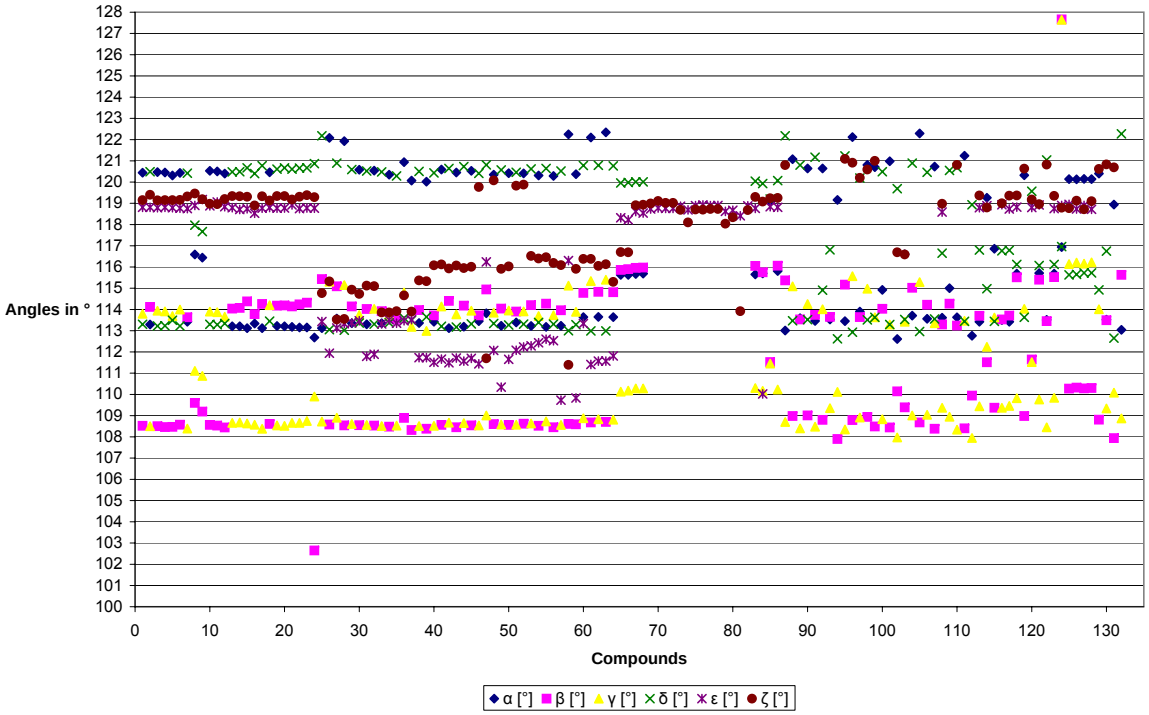

Figure 5.26.: Measurement of the angles in ° (α-ς)

The molecules of the GAmin group do not show any conspicuousness. Only GA16min and GA17min are outliers. Their values of ϵ and ς are very similar. The other angles differ in some degrees to their constitution. The JHmin compounds are nearly indistinguishable from GA5min-GA9min or GA425min, GA430min or GA553min. The first three angles of the MOREmin compounds differ little from the GAmin and JHmin's, but the following angles show great differences. This can be explained by e.g. the substituents above the amino-phenyl

group, which force different conformations. The ϵ and ς values of the OTTOmin and REVmin compounds are also very similar to those of JHmin and GAmin. The other angles could not be determined due to the composition of the OTTOmin and REVmin compounds. Compounds of the RNmin series have similar values there. The angles differ from the JHmin and GAmin series, notably having higher values for α-γ and values a little lower for δ. In the series of the small SKmins many variations occur. Any SKmin molecules with the three numbers (e.g. SK318min) follow in some degree the examples of the JHmin and GAmin series again once again. Figure 5.27 shows the second part of the angles.

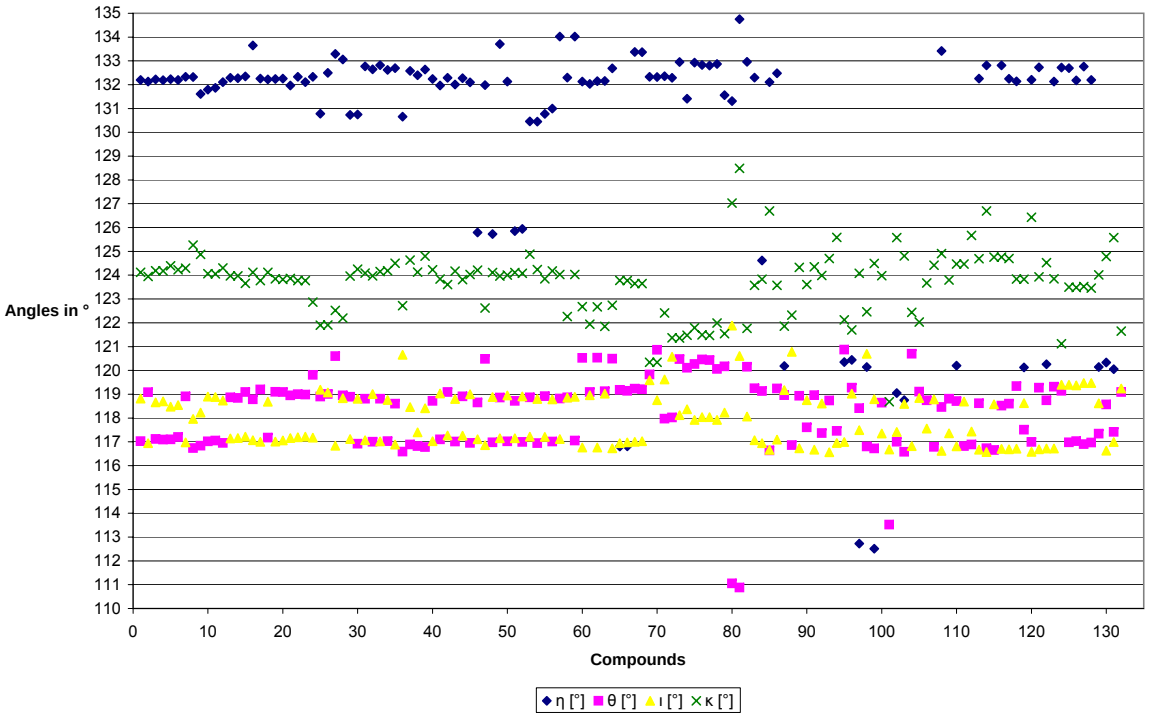

Figure 5.27.: Measurement of the angles in ° (η-κ)

The values of the η angles are in general very similar (above 130°). Only in some cases they stick out, e.g. MO29min or MO30min, which rings B and C are bounded by a ternary amine instead of a secondary; or RN14min which rings are bound via an ethylamine instead of a methylamine. All the other θ values take up around 120°. Only REV7min, REV8min and SK22min are outliers. For ι nothing significantly occurs. All GAmin, JHmin and MOmin compounds have very similar κ values. Only JH46min, MO1min, MO2min, MO3min and MO4min-MO12min lie below the others. The OTTOmin and REVmin compounds have also very similar κ values. Outliers are here OTTO3min, REV7min and REV8min. In case of the RN series RN14amin lies above the others of that series. In the SKmin series more variations

of the κ values can be observed. SK316min, SK345min and SK362min lie a little above the other three-numbered SKmins. The compounds of figure 5.28 were selected to to take a more accurate look at the the different scaffolds.

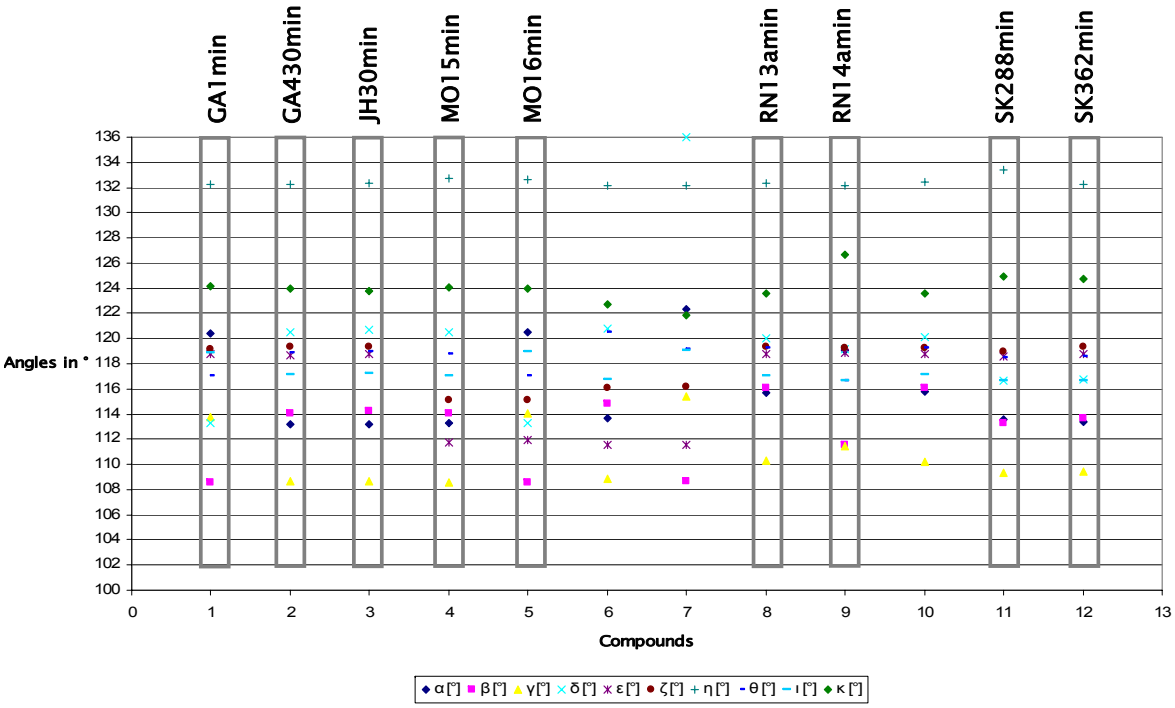

Figure 5.28.: Angles of selected compounds GA1min, GA430min, JH30min, MO15min, MO16min, RN13amin, RN14amin, SK288min, SK362min

The differences that emerge of the oxygen position in GA1min (bad inhibition) in comparison that in JHmin or GA430min (very good inhibition) is striking. All angles of active compounds rather have a similar arrangements or order. MO15min is very similar, but has a lower ϵ than e.g. GA430min. It's isomer MO16min with the alternative oxygen position in the seven-membered ring is very similar to GA1min. RN14amin represents an outlier which differs greatly, but has shown activity against p38α MAP kinase in biologicals tests. SK288min is less active than SK362min in the test and varies a little in the arrangements of the angle values. By this diagram the following order of the angle values can be proposed to create active compounds (from top to bottom):

- η
- κ
- δ

- ϵ or ς or θ
- ι
- β
- α
- γ

5.3. GRID

The following PDB structures were loaded in GREATER. The calculated GRIN charges are displayed in table 5.12.

PDB	GRIN Charge	PDB	GRIN Charge
PDB 1PMN	-1.16	PDB 1W84	-9.08
PDB 1PMQ	-1.04	PDB 1OZ1	-9.00
PDB 2B1P	-1.00	PDB 2GFS	-8.00
PDB 1WBS	-8.89	PDB 2GTN	-5.00
PDB 1W82	-9.08	PDB 2I0H	-9.96
PDB 2PKJ	-3.63	PDB 2QD9	-6.00

Table 5.12.: Calculated GRIN charges

While loading the PDB structures all of them received GRIN warnings, because they had missing atoms e.g somewhere at the N- or C-terminal domain and the hydrogens could not be added. However these warnings can be overlooked, because no atoms in the ATP binding site were concerned, using the "accept all errors" button. The probes which were chosen to calculate the Molecular Interaction Fields (MIF) can be divided into two groups. Probes which can be found in the Suberones (such as carbonyl or amine) and probes to proof the reliability of the GRID calculations. For example the phosphate groups were chosen to check if GRID finds MIF where the phosphate groups of ATP would be originally situated. Water probes were found in all PDB structures everywhere near hydrophilic residues. The probes are display in table 7.1 in Materials and Methods. For a better overview they were divided into groups as follows:

- DRY, C3 : hydrophobic interactions
- N2, N:, N1:, N2: : nitrogen probes

- O, O::, OC=, OH : oxygen probes
- STH : sulphur
- F : fluoride
- PO4, PO4H : phosphate
- MG+2, AR.COO-, AR.CONH2 : others

The probes in the others group were not permanently calculated. The sulfur probe was exclusively chosen, because of JH46 which contains a sulphur in the seven-membered ring. If any highlights occurred within the groups they will be discussed in particular. The usefulness of the programme was positively tested among other studies (e.g. [76]). Only the MIFs with the lowest energies for the probes (the more negative the better) are described below. The regions what are used for describing the positions of the MIF below correspond to the naming according to [10] in the introduction. In the PDB JNK3 structures of PDB 1PMN, PDB 1PMQ and PDB 2B1P GRID calculated the following MIFs:

- hydrophobic interactions in hydrophobic pocket `I` and hydrophobic region `II` and hydrophobic pocket DFG-OUT (only PDB 2B1P)
- nitrogen probes around Asn152 and next to the hinge region inside of the ATP pocket
- oxygen probes next to hinge region in hydrophobic region `II`, next to Lys93, Asn152 (OC= only in PDB 2B1P)
- sulphur in hydrophobic pocket `I` and hydrophobic region `II`
- fluoride in hydrophobic pocket `I` (only PDB 1PMN)
- others: magnesium next to hydrophobic region `II` (sugar pocket), aromatic probes situated exactly where the aromatic parts of the ligand of PDB 2B1P are

The results of the MIF calculation vary. In some cases (the magnesium or the hydrophobic interactions) the calculation are comprehensible, but in other cases they are surprising. No MIF was found e.g. for the fluoride in hydrophobic pocket `I` in PDB 1PMQ and PDB 1B1P. For the DFG-OUT p38α MAP kinase PDB structures PDB 1W82 and PDB 1W84 the following MIFs were calculated:

- hydrophobic interactions in hydrophobic pocket I, hydrophobic region II and hydrophobic pocket DFG-OUT, and between the the Gly-rich loop and the DFG residues
- nitrogen probes next to Glu71, Met109, Asp112, Asp168 and Phe169
- carbonyl oxygen exactly at the position of the oxygen of the ureayl part of the ligand
- sulphur in hydrophobic pocket I, hydrophobic region II and hydrophobic pocket DFG-OUT
- fluoride in hydrophobic pocket I (only PDB 1WBS), hydrophobic pocket DFG-OUT and between the the Gly-rich loop and the DFG residues (only PDB 1WBS)
- phosphate in the ATP binding pocket and between Glu71 and the Gly-rich loop

Many results here are very good, e.g. the exact position of the oxygen and the hydrophobic interactions. Again the fluoride calculations were unexpected. The phosphate calculation revealed, that the phosphate may not be able to bind in the so-called phosphate binding region during the DFG-OUT conformation.
The MIF calculations for the p38α MAP kinase PDB structures yielded in the following results:

- hydrophobic interactions in hydrophobic pocket I, hydrophobic region II and sometimes along the hinge region (PDB 2QD9, PDB 2PKJ) or between Lys53 and Tyr35 (2IOH)
- nitrogen probes chiefly near Asp112 and Asp168, and sometimes near Tyr35 (PDB 1W84), near Lys53 (PDB 2I0H) or between both (PDB 2GFS)
- oxygen probes next to the hinge region, Thr106 (PDB 2GFS), chiefly Met109 (PDB 1W84) and/or Gly110 (both PDB 2QD9)
- sulphur in hydrophobic pocket I and hydrophobic region II or in some cases next to hinge region (Thr106 in 2FSO, Met109 in PDB 1OZ1, Met109/Gly110 in PDB 2QD9 and Asp112 in PDB 2PKJ)
- fluoride in hydrophobic pocket I and/or near Asp112 (hydrophobic region II), in front of Asp168 (2FSO) and between Tyr35 and Lys53 (PDB 1W84)
- phosphate in the phosphate binding region (PDB 2PKJ, PDB 2QD9)
- others: magnesium in the phosphate binding region, the aromatic carboxyl next to Met109/Gly110 and the aromatic amine next to Asp168 and His107 (PDB 2QD9)

The oxygen calculations on one hand found perfect posed MIF near Met109/Gly110 in PDB 2QD9 (figure 5.29), but on the other hand in case of PDB 2I0H only in the sugar pocket.

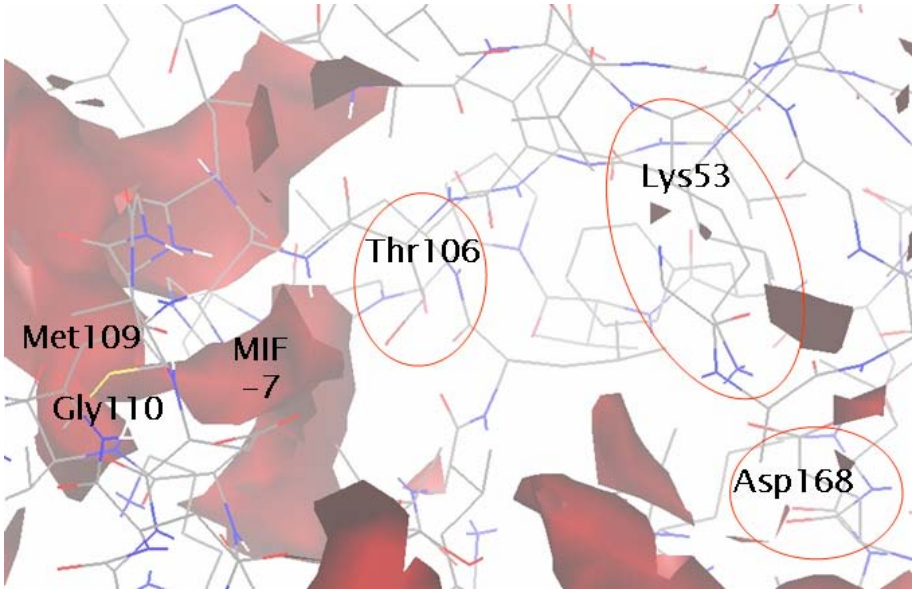

Figure 5.29.: GRID: Calculated MIF of oxygen probe in PDB 2QD9

Many nitrogen positions were situated next to Asp168 or Asp112 as expected. But the results varied and no prediction can be made which is the more likely position of the amine. Both results tend to both proposed binding modes and therefore can not help at all in this case. In figure 5.30 (next page) it can be assumed that the position near Asp168 is more likely, because the field is much more bigger than that of Asp112. When examining even more negative ranges, only the field around Asp168 remains.

The results for fluoride and sulphur were also not ideal. The hydrophobic pocket `I` was obviously identified by the hydrophobic probes and the fluoride probe as an area of hydrophobic interaction. As a surprise came the identification of another hydrophobic area between Tyr35 and Lys53. The phosphate probes were placed in the phosphate binding regions in many cases but sometimes next to the hinge region (PDB 2QD9). Figure 5.31 visualizes the position of the phosphate probe in PDB 2QD9.

Also the magnesium showed unusual positions, e.g. next to Asp112 (PDB 2PKJ). The multi-atom aromatic probes showed good positions, even suggesting that an aromatic amine is more likely next to Asp168 than next to Asp112. In the end there are a few hints that a carbonyl is very likely around Met109, as some X-ray crystal structures proofed before (PDB 2QD9). That ring C of the Suberones is more likely to bind in the hydrophobic pocket `I` and its amine substituents may form interactions with Asp168 is still very unsecure.

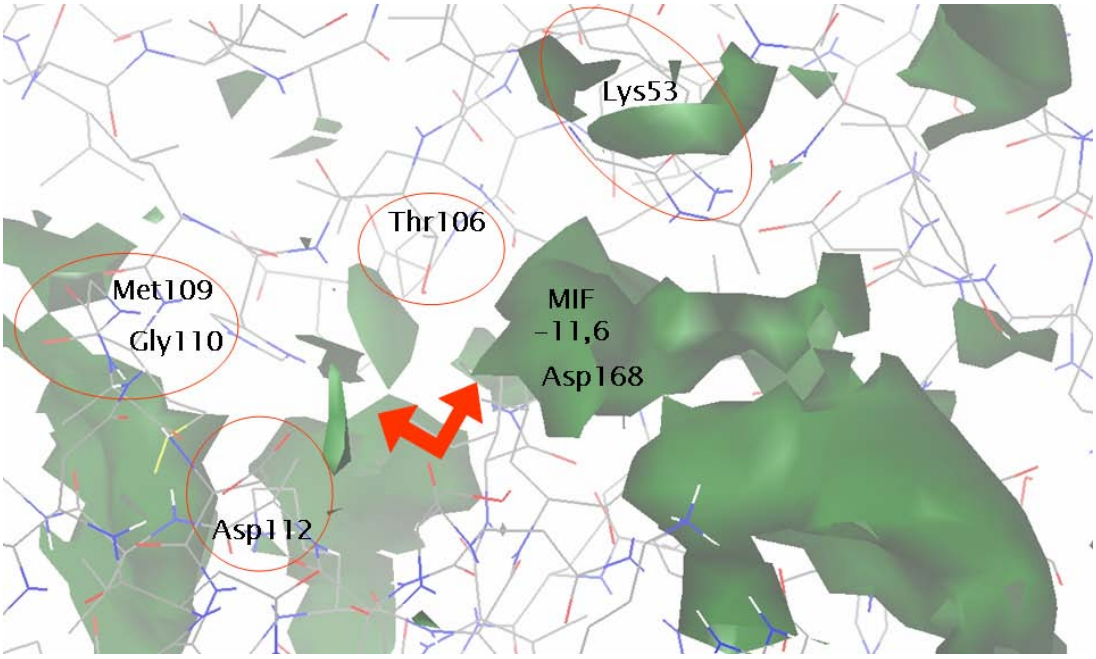

Figure 5.30.: GRID: Calculated MIF of amine probe in PDB 2QD9

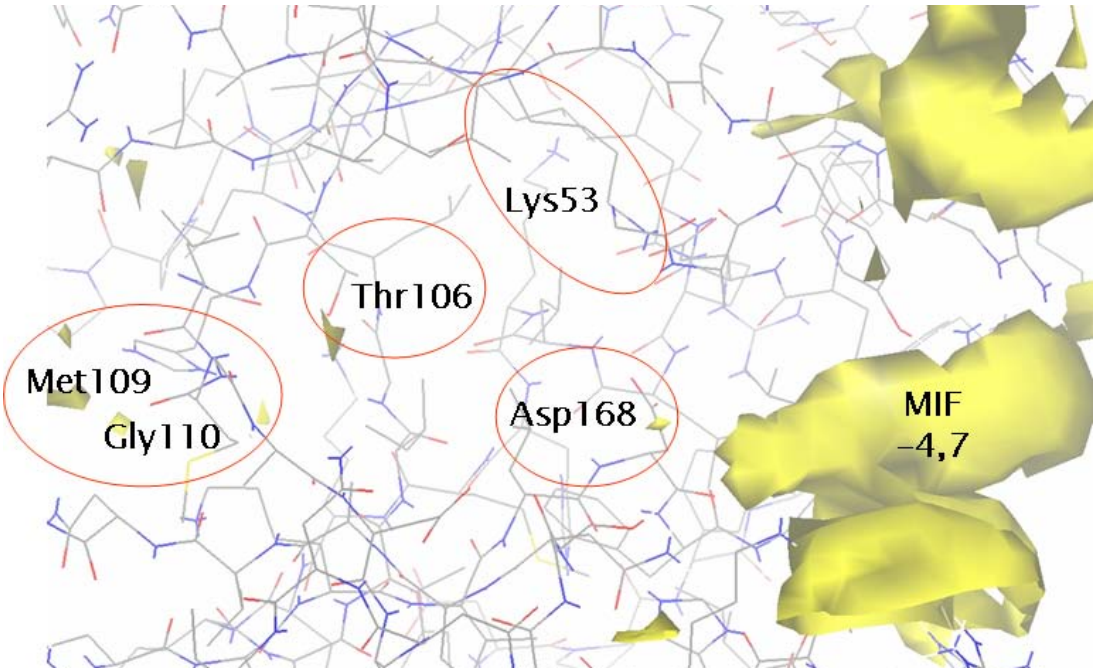

Figure 5.31.: GRID: Calculated MIF of phosphate probe in PDB 2QD9

5.4. Docking

The docking studies are used to predict the binding orientation or pose of a ligand in a protein receptor [77]; in this case the Suberones in p38α MAP kinase. Re-docking and cross-docking methods were used, before the actual docking of the Suberones. During re-docking the ligand of a PDB structure is extracted and the docking programme is challenged to pose the ligand as closely as possible to its experimental structure [78]. In this study cross-docking included docking of ligands of the p38α MAP kinase and ligands of JNK3 into the PDB structures PDB 1PMN, PDB 1PMQ, PDB 2B1P and PDB 2O0U (JNK3) and PDB 1W84, PDB 1OZ1, PDB 2GTN, PDB 2GFS, PDB 2FSO, PDB 2PKJ, PDB 2QD9, PDB 1WBS and PDB 1W82 (different conformations of p38α MAP kinase). This is the real challenge for a docking programme: to dock a ligand into a structure with which it was not crystallized [79]. The re-dockings were not carried out independently, thus the ligand database included all ligands of the PDBs. Several conformations of the p38α MAP kinase could be used, whereas the PDB structures of the JNK3 are very similar among one another. Many papers (e.g. [80, 81, 82]) deal with pose prediction and the finding of active in a set of compounds (termed Virtual Screening (VS)). The sorting of active and inactive was not part of this study; it might be a task for further studies. Cole *et al.* describe in their review [83] the difficulties of pose-prediction. The measurement they introduce critically is the RMSD [84], which needs visual inspection, for it is just a geometric measure between two poses, so it only compares the atomic positions. Such accurately examination was not invested here. The usage of the docking programmes was examined before. Several programmes were used to strengthen the proposed docking poses in the end. The chosen docking programmes work with different algorithms. Choosing enough residues to cover the whole of the binding sites ensures that the correct ligand-protein-interactions are found. Water molecules are also a great uncertainty. The exclusion from the docking, which is sometimes necessary, because the algorithm can not cope with them, may result in wrong docking poses. This is very likely in case the ligand is bound to the protein via water molecules. The quality check to choose the best models was necessary to make sure that possible docking failures are not the result of a inapplicable docking algorithm. For example some docking programmes are influenced by the molecular weight [85]. These programmes favour compounds with a higher molecular weight, because they have more atoms that interact with the target molecule and this increase the interaction energy. This may also have influence on pose-prediction. Another often described is the inadequacy of docking programmes to cope with ligand-induced changes in the protein conformation (induced-fit), which is highlighted by several cross-docking studies [83].

5.4.1. FlexX

All PDB files were examined in SYBYL7.2 with the protein preparation tool, to identify bond orders or clashes and to add hydrogens. The appearance of any inadequacies fortunately did not concern any residues of the binding sites. Thus the ligand and if present any crystallization artefacts (such as sulphate) were extracted. For the dockings the native PDB structures were used, because any inadequacies outside of the binding pocket were irrelevant for the docking. The re-docking studies of the preceding diploma thesis demonstrated that FlexX is not as applicable for the p38α MAP kinase as Flexidock. However for this study it was still used, because docking of large databases is very easy with FlexX [70].

5.4.1.1. Re-docking

More re-docking studies following the diploma thesis had been carried out with more PDB structures (data not shown). It showed that FlexX should be able to propose suitable binding poses. For further evaluation cross-docking studies were executed (see next chapter). The ligand database for cross-docking also included the native ligands of the used PDB structures, so another re-docking is also included in the cross-docking studies.

5.4.1.2. Cross-docking

The first cross-dockings were carried out with the JNK3 models (apart from PDB 2O0U which was lately published). FlexX put the three JNK3 inhibitors on the first three ranks (AIZ501, Q880-501, Q984-501) in the PDB 1PMN docking. The majority of the poses were alike the poses in their native crystal structure (apart from 5 outliers out of 50 poses). The p38α MAP kinase inhibitors appeared in the the order PQB1, LIE301, Q222-400, L12 and FPH. Just in case of LIE301, L12 and FPH some (5-10) poses were relatively similar to the pose of their native structures. The rest was posed rather insignificantly. The ranking of the three JNK3 inhibitors was alike in PDB 1PMQ, but the poses for the first ranked AIZ501 were not even similar to the native pose. However the poses of Q880-501 and Q984-501 were very much alike. PQB1, Q222-400, LIE301, FPH and L12 on the next ranks were slightly different to PDB 1PMN, but FPH was the only one which pose was comprehensible.
PDB 2B1P own native ligand was rank on one and its posed was very similar to the one in PDB 2B1P. The second rank was occupied by PQB1 and its pose was also very alike its native X-ray structure (PDB 2GFS). The rest of the ligands (in the order LIE301, Q880-501, Q984-501, L12, Q222-400 and L12) had no acceptable poses, some of them were even posed

outside of the ATP binding pocket.
PDB 1OZ1's cross-docking yielded to AIZ501 on the first rank with many alike poses out of the fifty possible poses. This also applied for FPH (the native ligand of PDB 1OZ1), Q880-501, Q222-400 and L12. Therefore LIE301 and PQB1's poses at the bottom ranks were very unrealistic (no traceable interactions).
Most of the PDB 1W84's cross-docking results did yield to reasonable poses. Only Q984-501 (rank 2) was posed alike in its PDB structure (PDB 1PMN). Some poses of FPH (rank 3) and L12 (rank 7 and the native ligand of PDB 1W84) were acceptable. All other poses were outside if the ATP binding site or positioned without any interactions (rank one AIZ501, rank 4 PQB1, rank 5 LIE301, rank 6 Q222-400 and rank 8 Q880-501).
AIZ501 also appeared on the first rank in the cross-docking to PDB 2GFS. Its binding pose was alike the one in PDB 2B1P, although this ligand is supposed to be selective for JNK3. For second ranked PQB1 half as much good and non-acceptable poses were found. Q22-400 was next, but was not posed suitable (most outside of the ATP binding site), as was next FPH. LIE301 binding pose was found in some solutions, but in the majority of the poses it was not. With L12 it was the same. Between them was Q880-501 posed mainly outside of the ATP binding site, as was Q984-501 on the last rank.
AIZ501 was only on the second rank in the PDB 2GTN cross-docking and its pose was all the time about-faced. PDB 2GTN own native ligand was situated on the first rank alike the X-ray structure in the majority of the solutions. All the other ligands were posed outside of the ATP binding pocket. Very few were posed in the inside and if the poses were unacceptable. The order was PQB1, FPH, LIE301, Q222-400, L12, Q984-501 and Q880-501. AIZ501 was then again on the first rank when docked in PDB 2I0H. LIE301's pose on the next rank was also in many solutions much alike in (PDB 2GTN). With the next ranked ligands Q880-501, Q222-400, FPH, PQB1, L12 and Q984-501 it was not as good. Only very few poses could be considered a little similar to their native poses. The rest was posed unacceptable.
For the last cross-docking COM2000 the native ligand of PDB 2O0U was included in the docking database. AIZ501 was on the first rank alike in PDB 2B1P. The majority of the poses of Q984-501 on the next rank were also acceptable. However, for the rest of the ligands no suitable poses were found (PQB1, FPH, Q880-501, LIE301, COM2000, L12 and Q222-400).

Because some in-between results from the crystallization team hinted that the Suberones might bind in the DFG-OUT conformation, subsequently DFG-OUT cross-dockings were executed with PDB 1W82 and PDB 1WBS. The following DFG-OUT ligands were chosen (figure 5.32 on the next page).

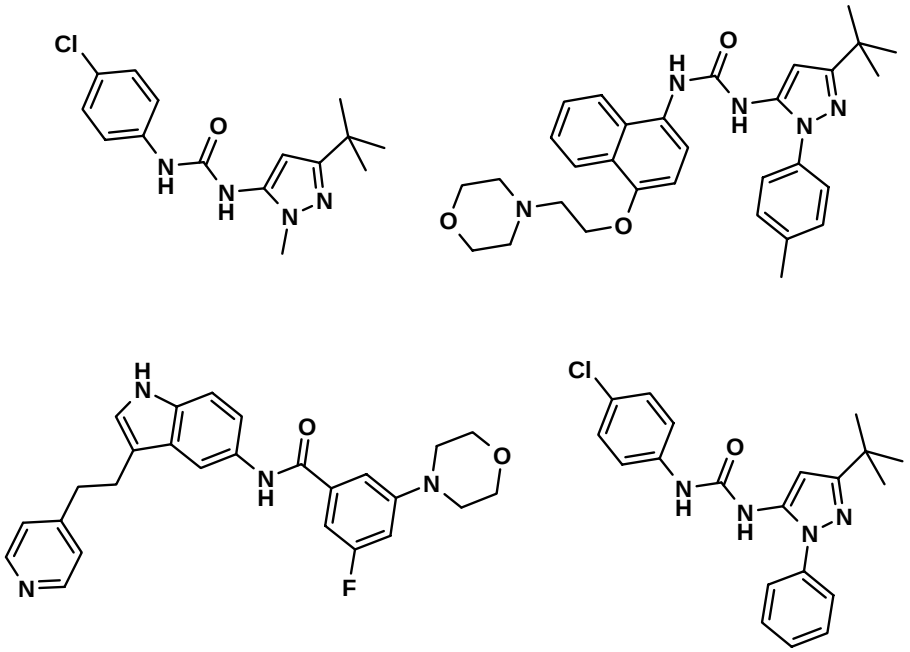

Figure 5.32.: Ligands (from left: BMU (PDB 1KV1 [3]), B96 (PDB 1KV2 [3]), LI2 (PDB 1WBS [4]), L10 (PDB 1W82 [4])

The ligands were taken out of the PDB structures, the atom types checked, modified when necessary and saved in a separate file. All ligands were docked in PDB 1W82 and PDB 1WBS. In both cases very good poses were found for LI2 (PDB 1WBS). Only the position of the morpholino substituent varied slightly. The four ligands appeared on the same ranks in both PDB structures. But just in case of PDB 1W82 some poses of L10 were correctly docked (approximately 50%). In most cases for all the other ligands not even poses inside of the binding site were found.
In the end the cross-docking results were not very promising. The outcome can not be connected to any ligand properties or IC_{50} values, because they are too inhomogeneous and irreproducible. However, FlexX was used for the docking of the Suberone database.

5.4.1.3. Docking of the Suberones

The first dockings were carried out for PDB 1PMN and PDB 1PMQ. In both cases REV6min was on the first rank. The poses were alike: the carbonyl oxygen pointed to the hinge region and the amino-phenol was in the hydrophobic region II. Second ranked was REV4min, also in both cases. REV4min of PDB 1PMN took up the binding pose, whereas REV4min of PDB

1PMQ lay across the ATP binding pocket. In PDB 1PMN next ranked REV9min's carbonyl oxygen had an H-bond to backbone -NH of Met149 and its amino-phenol in the hydrophobic pocket I (see figure 5.33) and an additional H-bond to the backbone oxygen of Asp150.

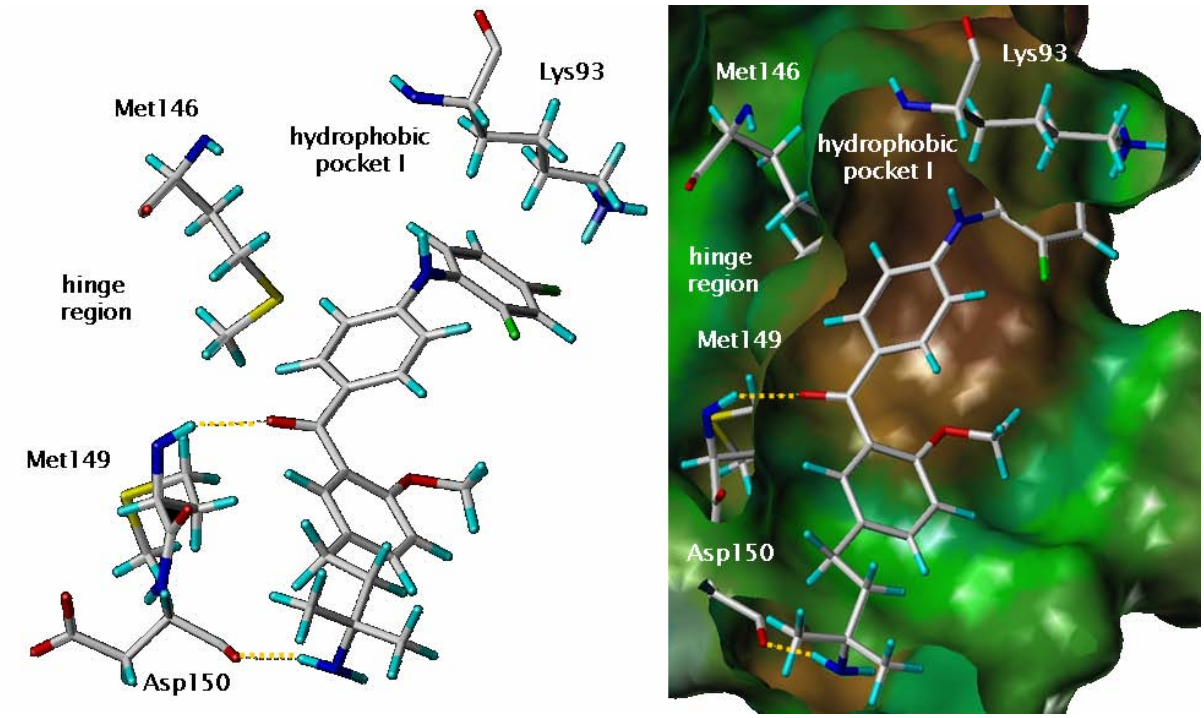

Figure 5.33.: Docking of PDB 1PMN, pose of REV9min, left: stick representation, right: MOLCAD surface representation

From now on different Suberone compounds appeared in the rankings. In case of PDB 1PMN next were more REV compounds (REV3min, REV5min) which took up the observed pose alike the other REV compounds. GA7min's carbonyl oxygen pointed to Lys93, whereas the amino-phenol was situated in the hydrophobic region II. This pose was also chosen by all the following GA compounds (and most of the RN compounds). The REV and OTTO compounds were posed alike the poses of rank one. An outlier was OTTO4min which took up a pose alike REV9min. All JH compounds were posed around Lys93 (rather like shielding it). RN15min's carbonyl oxygen pointed to the hinge region and formed H-bonds to the backbone atoms of Met149 and Asp150, whereas the amino-phenol lay in the hydrophobic region II. This binding pose would be correspond to the binding mode proposed by Ottosen *et al.* (see figure 5.34 on the next page).

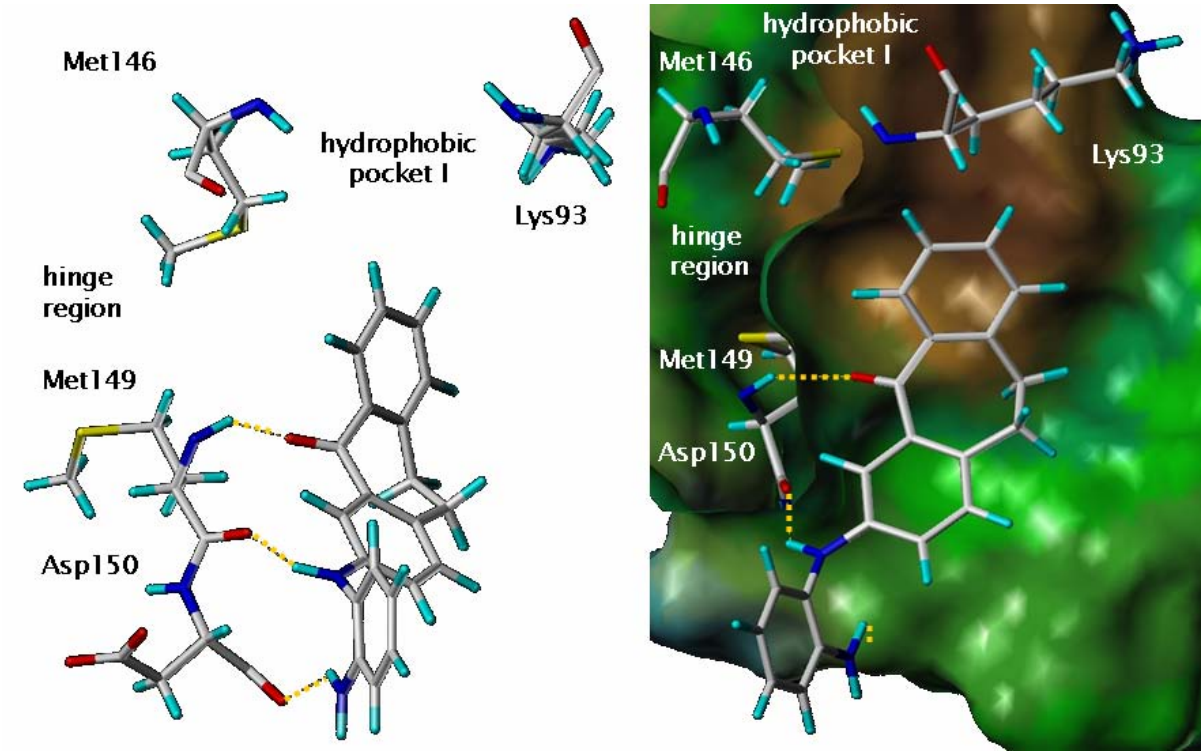

Figure 5.34.: Docking of PDB 1PMN, pose of RN15min, left: stick representation, right: MOLCAD surface representation

The first SK compound that appeared was SK10min, posed alike the GAmin compounds. The last ranks were exclusively reserved for the SK compounds. The further docking results of PDB 1PMQ were marked by many poses which lay across the ATP binding pocket, what seemed not very likely, because they had no interaction sites. The GA compounds took up their pose alike in PDB 1PMN, just like RN15min. The REV compounds appeared much later in the ranking and took up also this rather unlikely poses. The SK compounds followed their precursor poses, if they were even positioned in the ATP binding site at all. The results of this docking were rather useless. The docking results of PDB 2B1P were focused on the side chain -NH_2 of Gln155. Most of the carbonyl oxygen of the Suberone compounds pointed and formed H-bonds to that residue. The position of the amino-phenol varied, either it was positioned in front of the hydrophobic pocket I or it was solvant exposed left above the hinge region. Likely poses were rare. REV7min and REV2min were one of the few exceptions. Their pose was similar to that proposed by Revesz *et al.*. However many other rather unlikely poses occurred. For example GA15min, which carbonyl oxygen pointed to the hinge region, but without any H-bonds to it, whereas the ether oxygen of the seven-membered ring formed one to the side chain -NH_2 of Gln155. Additionally the pyridazin nitrogens interacted with the

side chain nitrogen of Lys93. The SK compounds took up the pose which allowed interactions with Gln155 and again could only be found at the bottom of the ranking. PDB 2O0U results also focused on Gln155 as a possible interaction partner for the Suberone compounds. Many unlikely poses occurred as presented in figure 5.35.

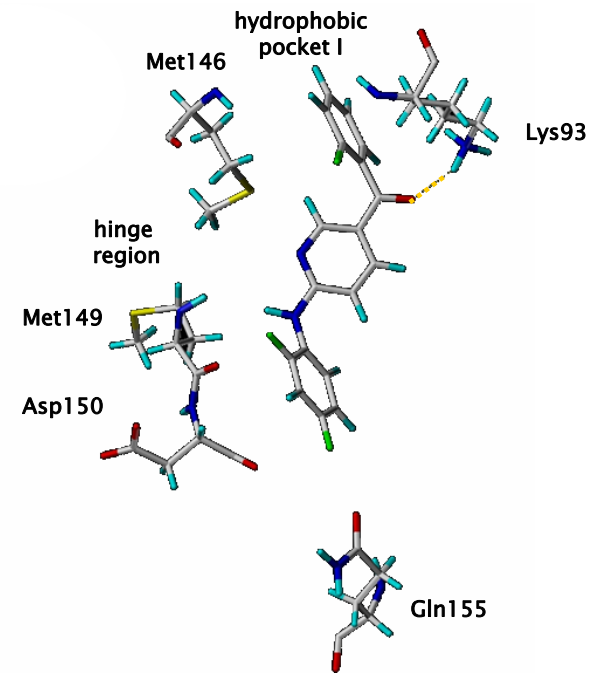

Figure 5.35.: Docking of PDB 2O0U, pose of REV10min in stick representation

REV10min is pictured, which carbonyl oxygen formed an H-bond to Lys93; also never observed before. Few acceptable poses were obtained. An example is shown in figure 5.36.

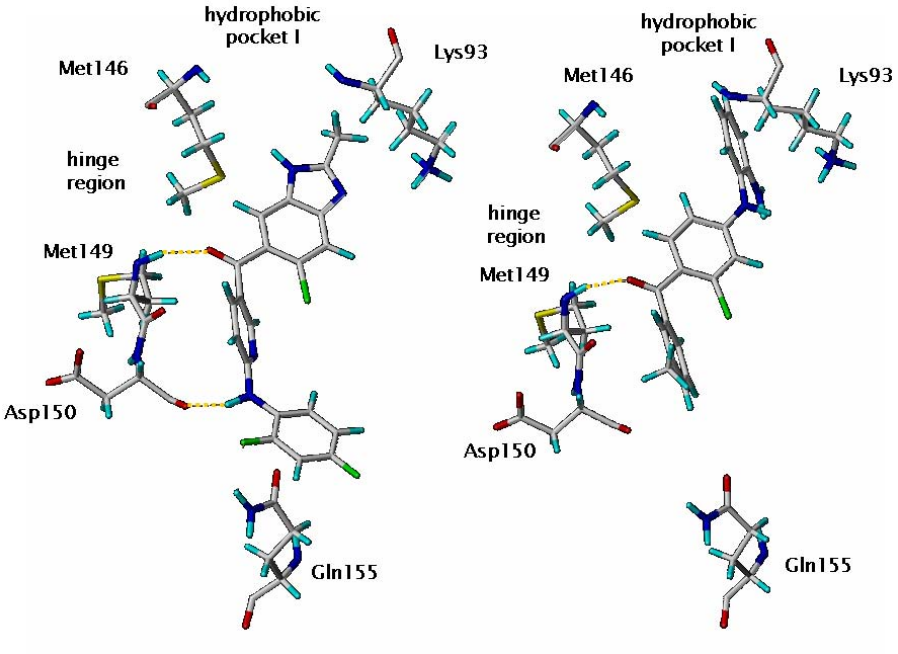

Figure 5.36.: Docking of PDB 2O0U, left: pose of REV6min in stick representation, right: pose of OTTO4min in stick representation

REV6min's carbonyl oxygen formed an H-bond to the backbone -NH of of Met149 and the -NH to the backbone oxygen of Asp150. However, this binding pose conflicts with the proposed binding mode of Revesz *et al.*. Right pictured OTTO4min in contrast supported it again. The ranking or any other properties could not be connect to any docking results. So, in the end docking to the JNK3 models could not give any new insights which binding mode of the Suberones is the most probable.

The first dockings to the p38α MAP kinase were carried out with PDB 1W84. GA11min was on the first rank. The amino-phenol lay in front of the hydrophobic pocket I and both the -NH and -NH_2 formed H-bonds to the side chain oxygens of Asp168. The carbonyl oxygen pointed to the Gly-rich loop and had two H-bonds to the backbone -NH of Tyr35 and Gly36. GA10min on the next rank lay outside of the ATP binding pocket (between Lys53 and Tyr35). OTTO4min on rank three took up the binding pose of GA11min again, as did the following compounds. The two poses that had appeared on the first rank dominated the ranking and were also observed for the RNmin and REVmin compounds. GA14min was different, but the backbone -NH of Tyr35 and Gly36 also were the main binding partners (in this case with the nitrogens of the pyridazin ring). The rest of GA14min lay across the entrance of the ATP binding pocket. JH31min's pose (alike all other JH compounds) was also posed in front of

the entrance of the ATP binding site. The lower a compound appeared the more unlikely its pose. RN15min's carbonyl oxygen had an H-bond with the side chain hydroxyl group of Tyr35, whereas the amino-phenol lay in front of Lys53. The SK compounds which of course appeared at the bottom of the ranking took up the first observed pose (figure 5.37).

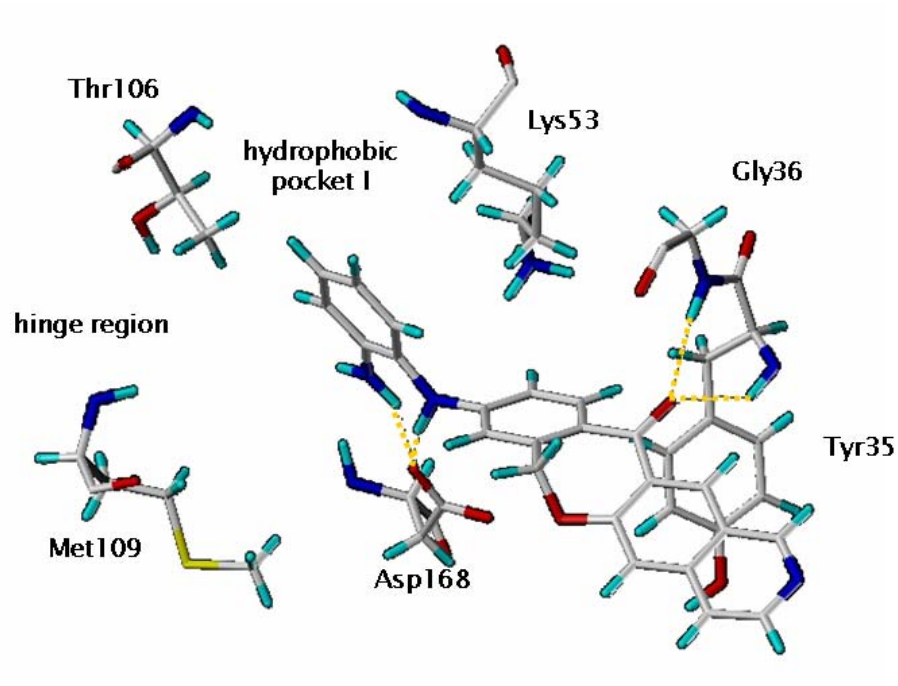

Figure 5.37.: Docking of PDB 1W84, pose of GA11min, left: stick representation, right: MOLCAD surface representation

This docking was dominated by Gly-rich interactions. The observed binding poses can not be regarded as very likely, because the loop is such a high mobile region, that its position in this X-ray structure can not be treated as certain.

Docking to PDB 1OZ1 yielded to REV6min on the first rank. The pose was similar to the pose proposed by Ottosen *et al.*. The amino-phenol lay in hydrophobic region II and the -NH formed an H-bond to the backbone oxygen of Met109 and the nitrogen of the pyridin formed another one to the backbone -NH of Met109. The sp^2 nitrogen of the imidazol subsituent formed a third H-bond to the backbone -NH of Asp168. The carbonyl oxygen pointed to back of the ceiling of the ATP binding pocket. The pose is visualized in figure 5.38.

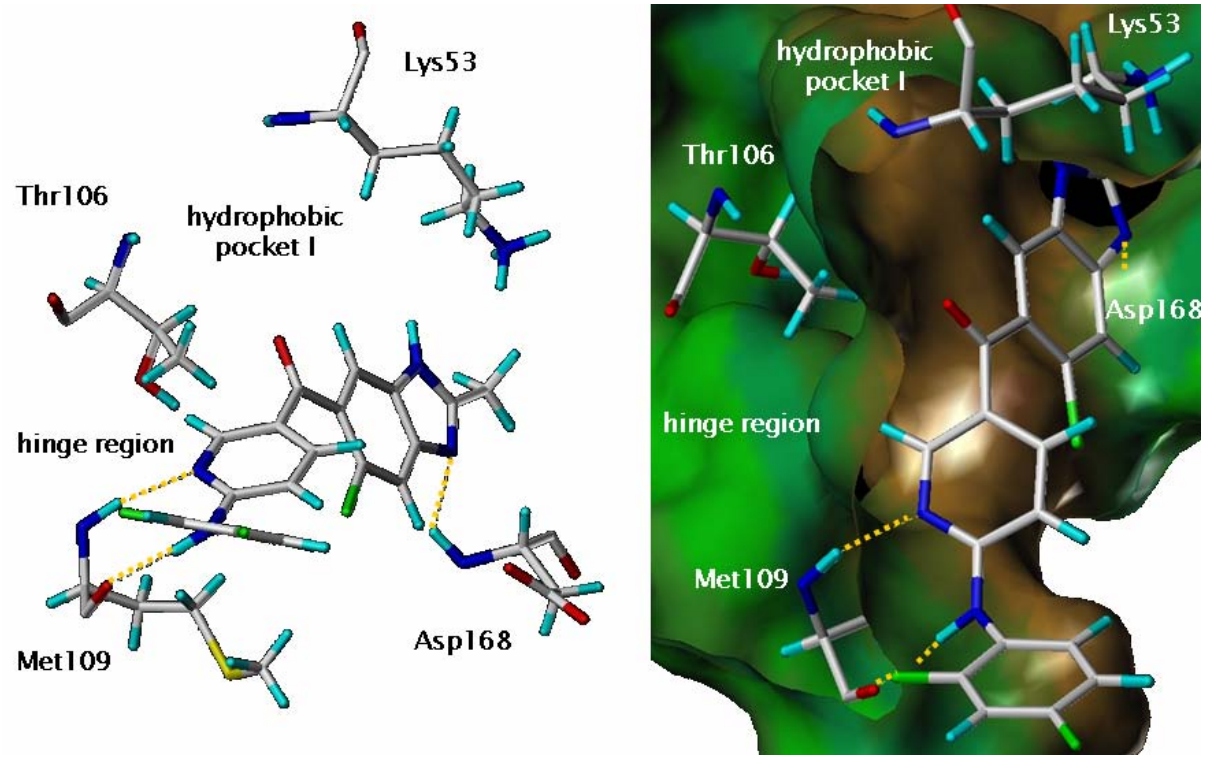

Figure 5.38.: Docking of PDB 1OZ1, pose of REV6min, left: stick representation, right: in MOLCAD surface representation

GA4min on rank 3 was posed as proposed by Revesz *et al.*. The carbonyl oxygen formed an H-bond to Met109 and the amino-phenol was situated in the hydrophobic pocket I. Though the position is not optimal. The -NH interacted with a side chain oxygen of Asp168 (figure 5.39).

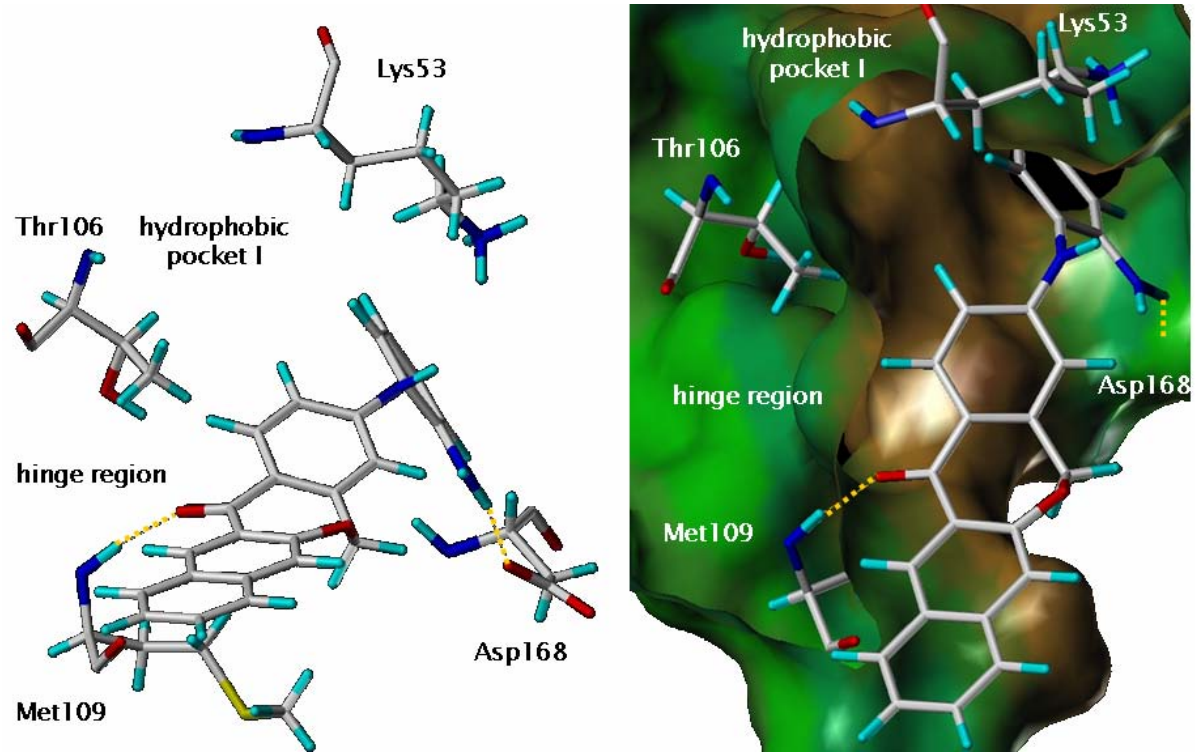

Figure 5.39.: Docking of PDB 1OZ1, pose of GA4min, left: stick representation, right: in MOLCAD surface representation

The following compounds took up either the pose of the first or of the third rank. Only the OTTO compounds were positioned differently, where the carbonyl oxygen was situated in the hydrophobic pocket I. This docking again showed that both binding poses of Ottosen *et al.* and Revesz *et al.* are possible, but none was preferred and no connection between the composition of the Suberone compounds (e.g. the position of the oxygen of the seven-membered ring) could be identified.

In the PDB 2GFS docking REV6min was on rank one again, however this time the carbonyl oxygen formed an H-bond to Thr106. The subsituents were posed alike PDB 1OZ1, but formed several additional H-bonds to the hinge region (-NH and -NH_2 to the backbone oxygen of Met109 and -NH_2 to the backbone oxygen of Gly110 (pose of OTTO1min see figure 5.40) on the next page).

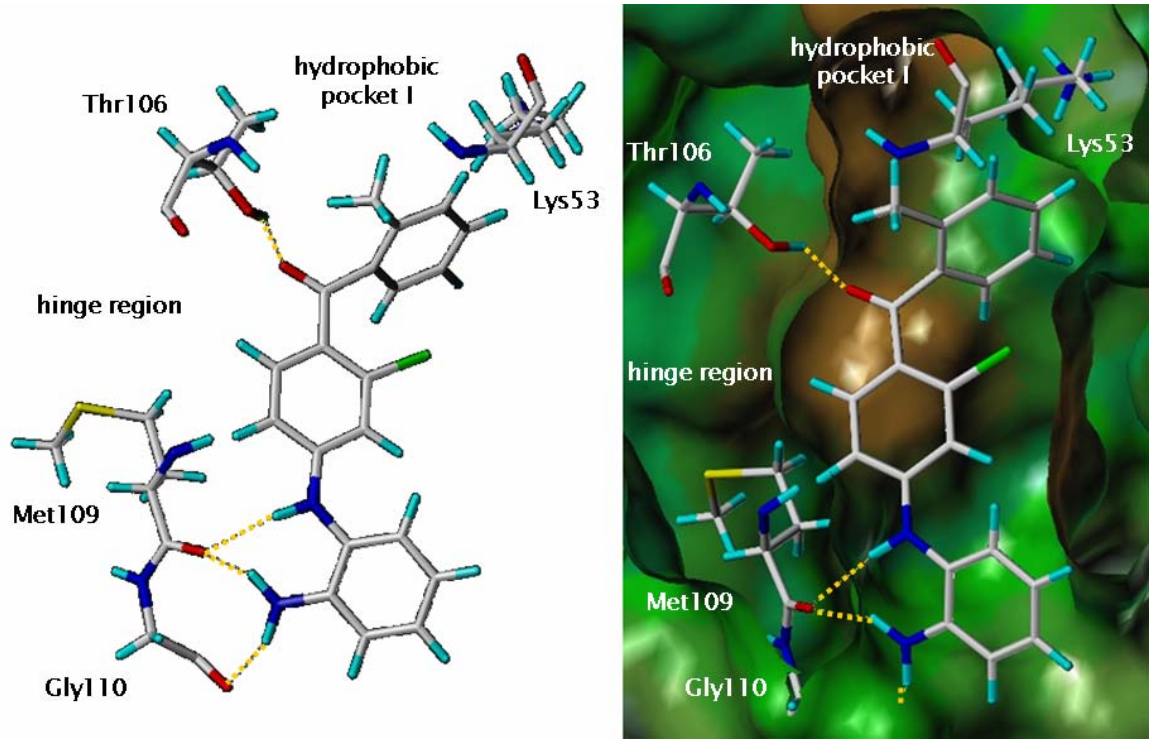

Figure 5.40.: Docking of PDB 2GFS, pose of OTTO1min, left: stick representation, right: in MOLCAD surface representation

The carbonyl oxygen of GA7min on rank 5 again pointed to Met109, while the amino-phenol was situated in hydrophobic region `II` (figure 5.41).

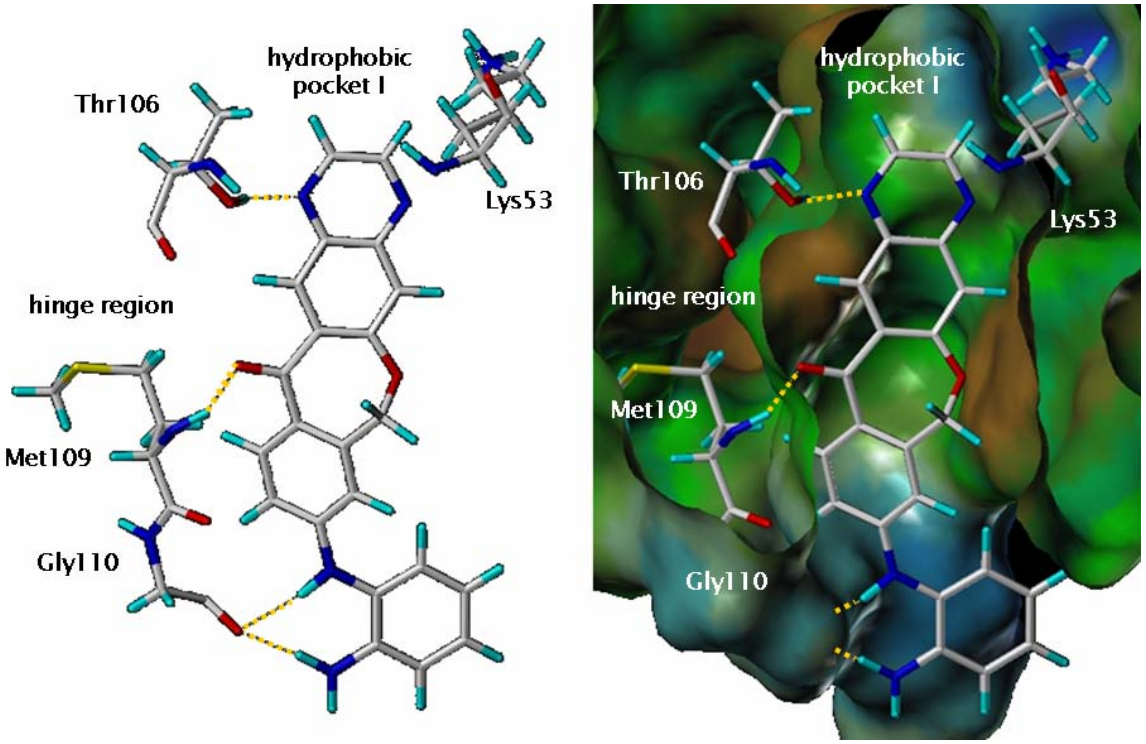

Figure 5.41.: Docking of PDB 2GFS, pose of GA7min, left: stick representation, right: in MOLCAD surface representation

The amino-groups formed two H-bonds to the backbone oxygen of Gly110 and one nitrogen of the pyrazin formed an additional H-bond to the side chain hydroxy group of Thr106. Most of the compounds had their carbonyl oxygen directed to Thr106 and their amino-phenol in the hydrophobic region II. Some few AD compounds had their carbonyl oxygen about-faced to the hinge region, but these were just few exceptions. The SK compounds appeared again on later ranks.

PDB 2GTN was modified before it was used. The phosphorylation loop lies partially in the ATP binding pocket (parallel to the hinge region). First dockings yielded in very bad results. FlexX could not find any poses, because the residues and the ligand atoms constantly clashed. For further usage it was decided to delete the residues that extend to the ATP binding pocket; so Phe169-Ala172 were removed. The position of Asp168 is unusual in PDB 2GTN. It is situated in the back of the hydrophobic pocket I, whereas in all the other PDB structures it is if at all present a little right below of Lys53. Altogether the position of the phosphorylation loop has to be treated with care. In the following docking all OTTO compounds appeared in a row (OTTO1min, OTTO4min, OTTO2min and OTTO3min) and all shared the same binding mode. The carbonyl oxygen had two H-bonds to the backbone -NH of Met109 and to the

backbone -NH of Gly110. The amino-phenol was situated in the hydrophobic pocket I and its -NH_2 formed an H-bond to the side chain oxygen of Asp168 (see figure 5.42).

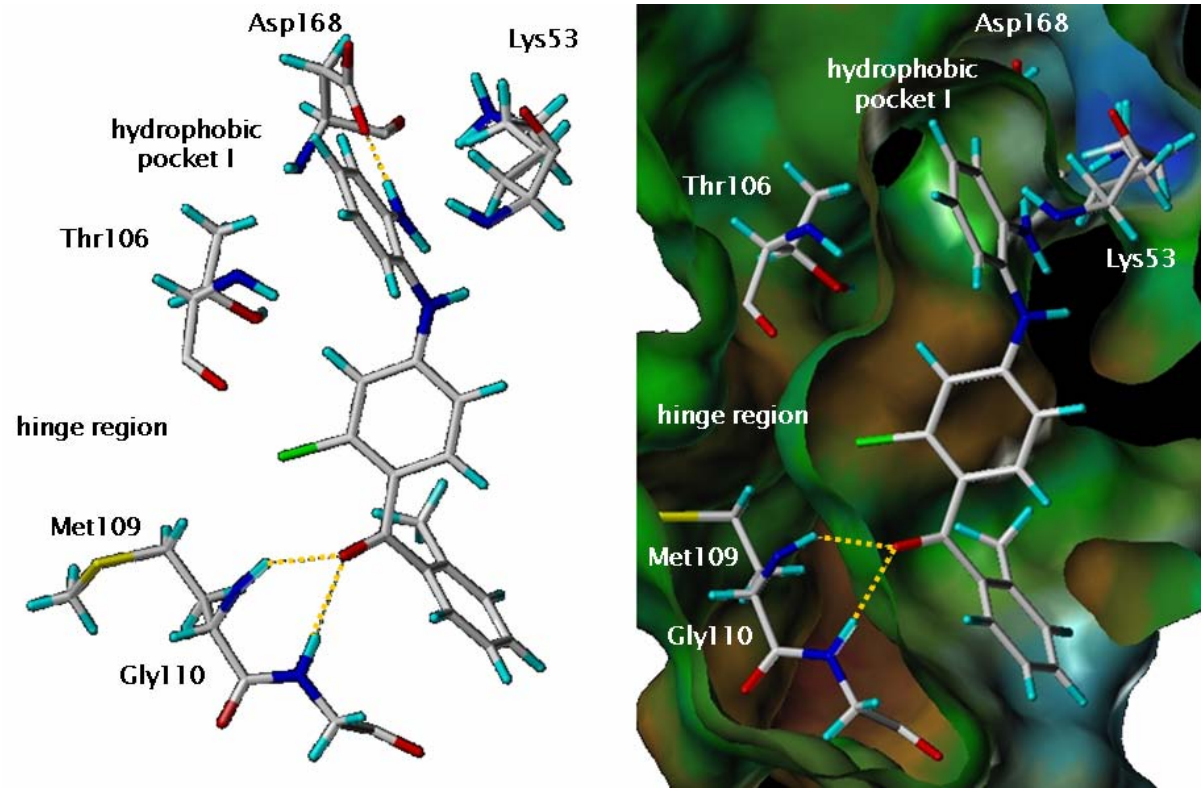

Figure 5.42.: Docking of PDB 2GTN-modified (without Phe169-Ala172), pose of OTTO1min, left: stick representation, right: in MOLCAD surface representation

Most of the database compounds took up the same binding pose, but sometimes only an H-bond to either Met109 or Gly110. Only a few outliers appeared (most of them later in the ranking), for example GA6min, GA7min or the RN compounds. The amino-phenol was situated in the hydrophobic region II or the pose was across the entrance of the ATP binding pocket. JH126min was posed alike but had no H-bonds to the hinge region. Again all SK compounds appeared at the bottom with their carbonyl oxygen pointing to the hinge region and their amine subsituent situated in the hydrophobic region II.

In the PDB 2I0H docking GA15min was on rank one. It lay across the ATP binding site and the nitrogens of the pyridazin formed two H-bonds to the backbone -NH of Met109 and Gly110. Meanwhile the amines of the amino-phenol interacted with the side chain oxygens of Asp168. Second ranked was again REV6min. The amino-phenol was situated in the hydrophobic pocket I and the pyridine interacted with the side chain of Thr106. The sp^3 hybridized

nitrogen of the imidazol formed an H-bond with the backbone oxygens of Gly110, whereas the carbonyl oxygen formed two H-bonds to the backbone -NH of Met109 and Gly110 (figure 5.43).

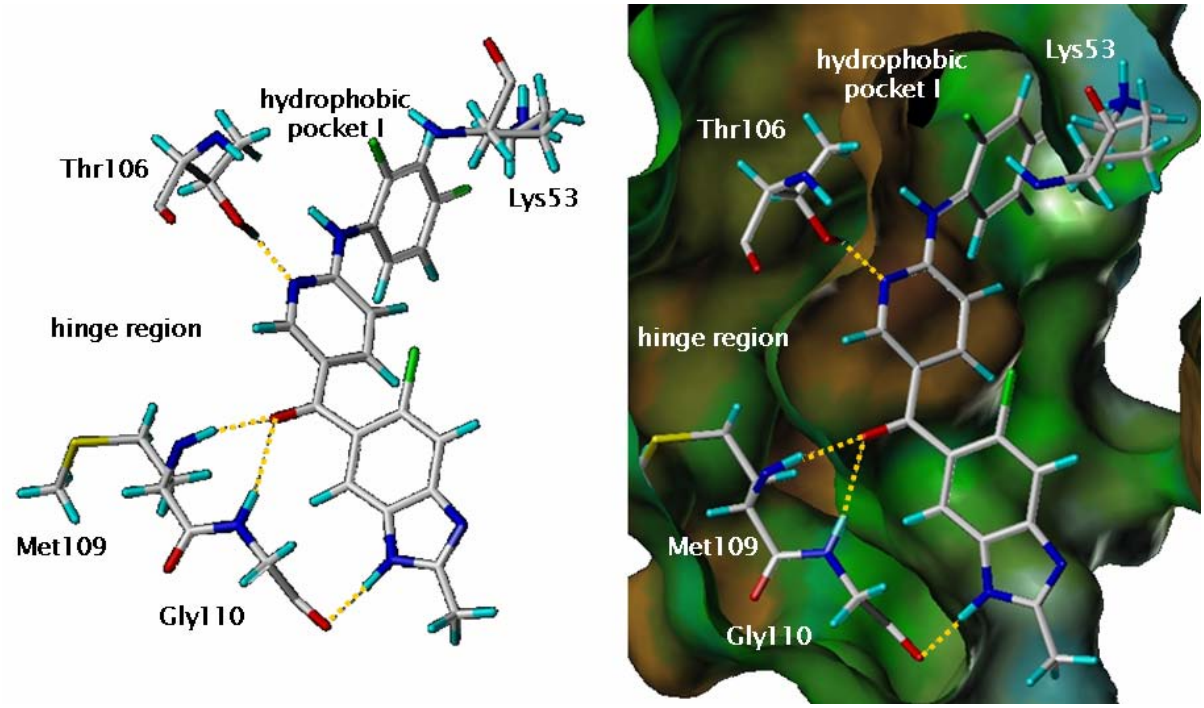

Figure 5.43.: Docking of PDB 2I0H , pose of REV6min, left: stick representation, right: in MOLCAD surface representation

Apart from REV2min all REV compounds had the same binding mode, as had OTTO2min and OTTO3min. The GAmin compounds were found across in the entrance of the ATP binding pocket. The SKmin compound's carbonyl oxygen also interacted with both Met109 and Gly110. However the amino-phenol was situated in the hydrophobic region II and the -NH formed an H-bond to a side chain oxygen of Asp112 at the end of the hinge region as always found at the bottom of the ranking. The docking to PDB 2I0H supported the binding mode proposed by Ottosen *et al.*.

The docking to PDB 2FSO which does not contain a ligand put REV6min on the first rank. Its carbonyl oxygen formed an H-bond to Thr106 alike in PDB 2GFS. Only the pose of the benzyl-imidazol varied. In PDB 2FSO parts of the Gly-rich loop are missing. So the benzyl-imidazol has enough free space to lie in front of Lys53. From there it formed two additional H-bonds; the sp^3 nitrogen to the side chain oxygens of Asp168 and the sp^2 nitrogen to the side chain of Lys53. This pose was often took up the other REVmin compounds. Many GAmin,

OTTOmin and RNmin compounds on the following ranks were even positioned outside of the binding pocket. The amino-phenol groups of the compounds were mainly situated in the hydrophobic region II. JH30min's carbonyl oxygen formed an H-bond to the hydyoxy group of Thr106 and the -NH and -NH_2 formed H-bonds to Glu71, which is situated behind Lys53 and normally forms a salt-bridge with it. All the SKmin compounds, again ranked at the bottom, formed H-bonds to the hinge region (Met109 mainly). The absence of parts of the Gly-rich loop seem to have a negative influence on the docking results.
Subsequent the MORE database was generated and added to Suberone database. Several of the MORE compounds were exclusively build to fail in the docking attempts (e.g. MO15min). An additional phenyl substituent may help to decide if one or the other proposed binding mode is more likely. The proposed binding mode of Revesz *et al.* would not allow the a phenyl substituent in that position, whereas an additional amino substituent may form additional H-bonds (e.g. to Thr106). However PDB 2QD9 was the only PDB structure, where the MORE compounds were included. For the so far practical PDB structures PDB 2I0H and PDB 2GTN they were carried out later exclusively with the MORE compounds. FlexX positioned in both cases some of the MORE compounds which had to fail the docking (MO9min, MO10min, MO15min, MO16min, MO19min, MO20min, MO21min and MO22min) with the added phenyl/benzyl rings outside of the ATP binding pocket. The main pose was the one according to Ottosen *et al.*, or with the carbonyl oxygen about faced of the hinge region or complete outside of the ATP binding pocket. Nevertheless no connection to the MORE compound's compositions or properties could be found. The poses seemed to be accidental. Some poses of FlexX were extremely bad. Figure 5.44 shows two poses the left in PDB 2GTN and right in PDB 2I0H, which can not be realistic at all.

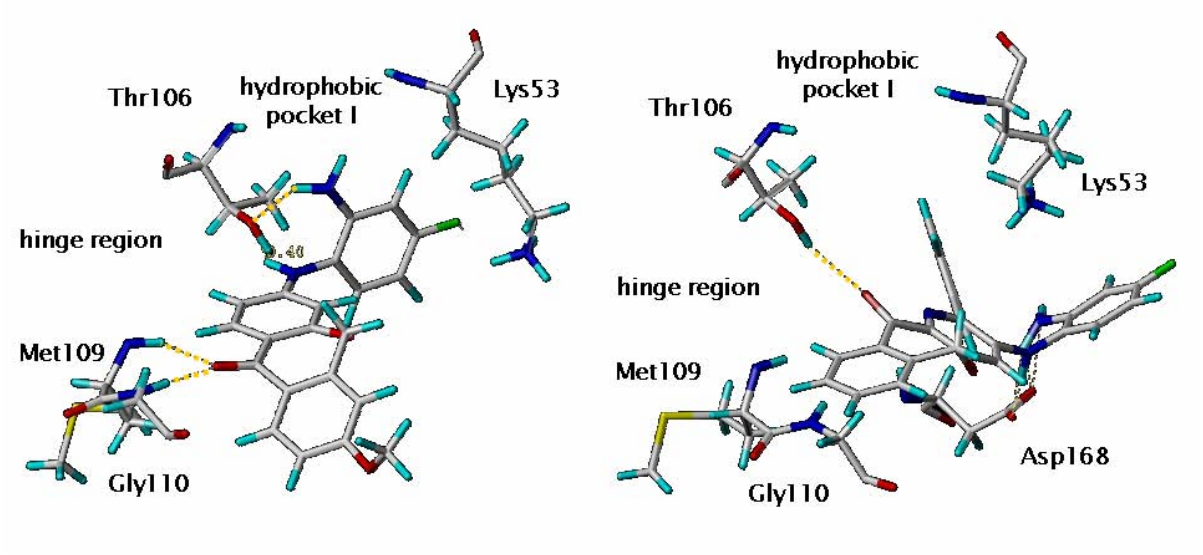

Figure 5.44.: Docking of the MORE database to PDB 2GTN (left stick representation) and PDB 2I0H (right stick representation). The distance between Thr106 and the amine of MO25min (0.4 Å) and the way MO9min is posed are unrealistic.

Docking the Suberone database to PDB 2QD9 yielded to OTTO2min on the first rank. Its pose was characterised through three H-bonds. Two between the carbonyl oxygen and the backbone -NH of Met109 and Gly110 and the third was formed between the -NH_2 and the backbone oxygen of Leu104. The amino-phenol was situated in the hydrophobic pocket `I`, so that this pose comes up to the proposed binding mode of Revesz *et al.* (see figure 5.45 on the next page).

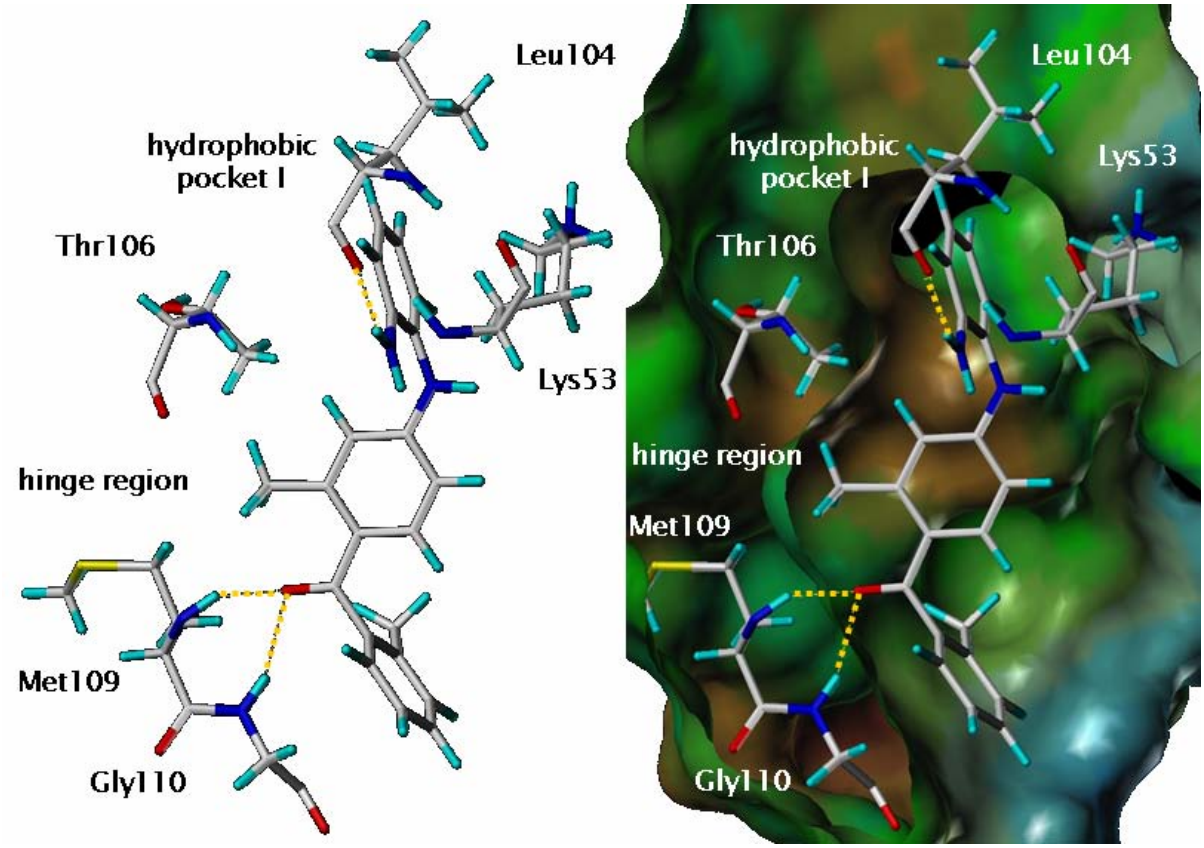

Figure 5.45.: Docking to PDB 2QD9, pose of OTTO2min, left: stick representation, right: MOLCAD surface representation

Many of the following compounds (e.g. REV6min, REV1min, OTTO3min, OTTO4min) until rank 15 took up this pose. The rest of the poses were dominated by the pose according to Ottosen *et al.*. Only now and then some compounds were posed alike the pose proposed by Revesz *et al.*. As was RN14min (see figure 5.46 on the next page), where the carbonyl oxygen formed an H-bond to the backbone -NH of Met109 and the amino-phenol in the hydrophobic pocket I was anchored there with an H-bond between -NH_2 and the backbone oxygen of Ala51.

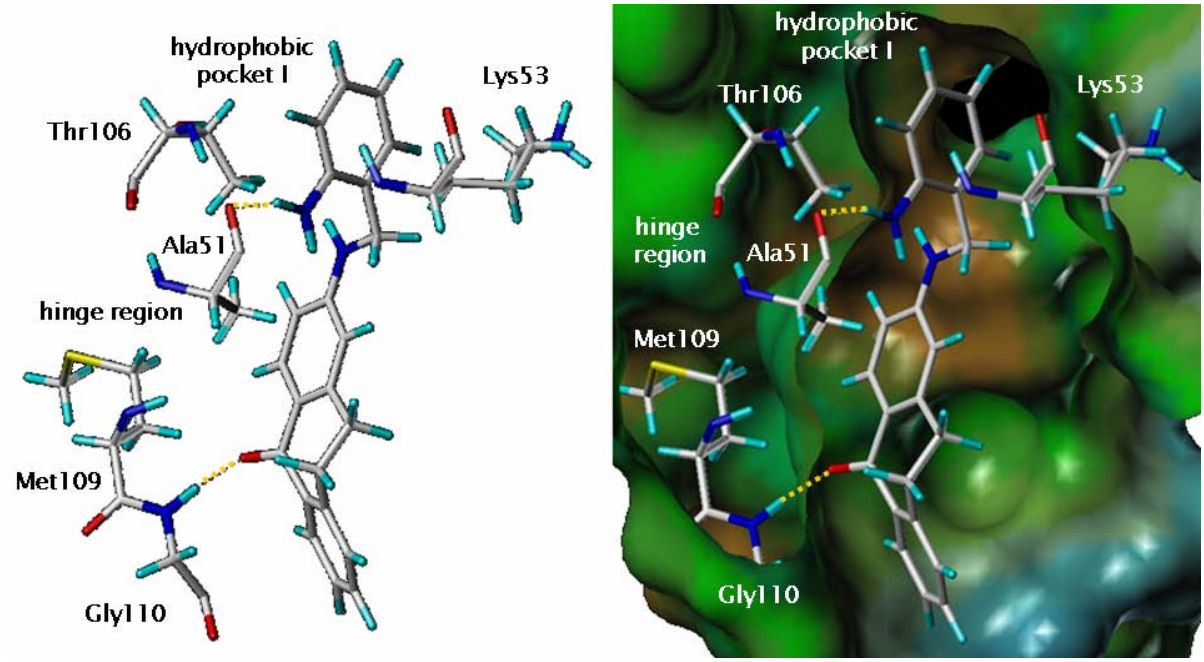

Figure 5.46.: Docking to PDB 2QD9, pose of RN14min, left: stick representation, right: MOLCAD surface representation

Docking of the Suberones into PDB 1W82 ranked MO11min first, but was posed outside of the binding pocket, alike MO17min on the next rank. Next was OTTO3min, where the -NH_2 and NH of the amino-phenol formed H-bonds to the side chain oxygen of Glu71. The carbonyl oxygen interacted with side chain of Arg70 and the methoxy oxygen was supposed to form H-bonds to the side chain of Arg67 (figure 5.47).

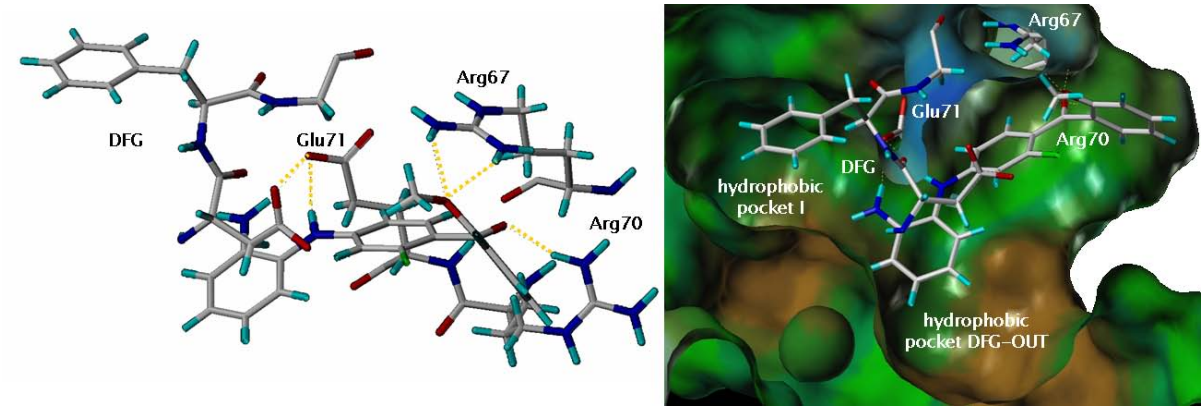

Figure 5.47.: Docking of PDB 1W82, pose of OTTO3min, left: stick representation, right: MOLCAD surface representation

Next ranked REV10min took up the Glu71-H-bond-interaction, whereas the -NH formed an H-bond to Asp168, which is situated on the opposite side of Glu71. The sp^3 thiazol nitrogen of REV7min on rank six formed an H-bond to Arg70, whereas the methoxy oxygen formed one to the side chain of Arg67. All the others compounds took up the two binding modes of OTTO3min (e.g. MO38min, GA13min, MO4min) or REV10min (e.g. MO19min, MO27min, MO21min, MO35min, MO22min, MO4min, MO15min, MO32min, REV9min, MO31min, REV1min, JH31min). The second pose appeared less often, though. The pose seems comprehensible. However, the preference of some MO compounds for the second pose cannot be explained. The last ranks were all lined up by SK compounds.
REV6min was ranked first on the docking studies with PDB 1WBS. The thiazol was situated next to the hinge region and formed an H-bond with Met109. No part of the molecule was situated the DFG-OUT binding site. The amino-phenol was situated in the hydrophobic pocket I, neither was next ranked REV10min. The di-fluoro-phenyl was situated in the hydrophobic pocket DFG-OUT. The pyridine nitrogen had an H-bond with the backbone nitrogen of Asp168. The chloro-phenyl occupied the hydrophobic pocket I. REV5min on the third rank detained also only the ATP binding pocket. The di-fluoro-phenyl occupied hydrophobic pocket I, the carbonyl oxygen formed two H-bonds to the hinge region (the backbone -NH of Met109 and Gly110) and the benzyl-thiazol occupied hydrophobic region II. This is clearly the binding mode according to Revesz *et al.*. and even in the DFG-OUT conformation (figure 5.48).

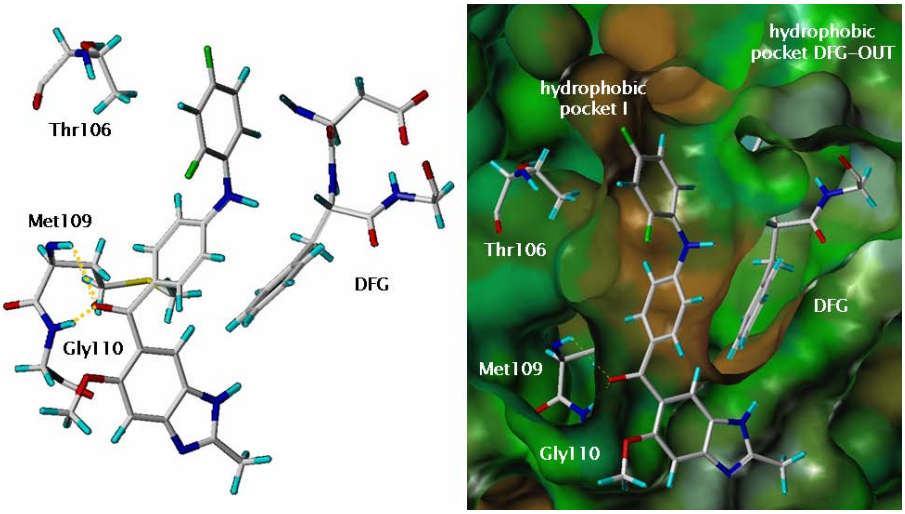

Figure 5.48.: Docking of PDB 1WBS, pose of REV5min, left stick: representation, right: MOLCAD surface representation

REV4min and REV3min took up the same binding mode. Many other compounds had one of the two binding modes alike in PDB 1W82 (OTTO1min, GA7min, RN14amin). Noticeable

was that the majority of the GA compounds were docked outside of the ATP binding site. In the end the REV5min-alike poses were outstanding and the poses which were obtained with PDB 1W82 were found as well. But more unusual poses appeared. The docking yielded to the result that the Suberones may also bind in the DFG-OUT conformation.

The docking with FlexX was not capable to determin which of the binding poses (Ottosen or Revesz *et al.*) would work for the Suberones. Above that many poses FlexX suggested, did not seem correct. As described above FlexX has problems to treat ligands of small molecular weight alike ligands with a high molecular weight. This was shown that the SK compounds were always found at the bottom of the ranking.

5.4.2. Flexidock

Flexidock's main failure is the inability to dock large databases. In the diploma thesis [70] it was identified to deliver good re-docking results for X-ray crystallographic structures of the p38α MAP kinase. For the further studies is was simply not useful, because all Suberones had to be positioned manually, which would have required a lot of time. Therefore Flexidock was just applied to check mainly FlexX results. Proposed good or bad poses were used as input for Flexidock to check if Flexidock agrees or disagrees to the proposed binding mode. For example the dockings to PDB 2I0H, PDB 2GTN, PDB 2QD9 resulted in very acceptable binding modes. They were saved and docked with Flexidock, which confirmed the good poses. The DFG-OUT FlexX docking of PDB 1W82 identified a pose (type OTTO3min) as very potential. The coordinates of the docking result of RN14amin were saved and transfered to Flexidock. The Flexidock dockings (with the parameters described in Materials and Methods) confirmed the pose as comprehensible.

5.4.3. GLIDE

Due to the cooperation with the Wilhelm Schickard Institute for Computer Science, Div. for Simulation of Biological Systems, University of Tuebingen is was possible to work with GLIDE (Schrödinger). All the databases which were created in SYBYL7.2 were used. All parameters and pre-docking-preparations of the GLIDE dockings are described in Materials and Methods. Before using GLIDE it was evaluated by re-docking and cross-docking studies. The focus on the binding pose in any JNK3 models was neglected in the GLIDE docking study due to in-between results of the crystallization team that the Suberones might bind in the DFG-

OUT conformation. So the docking was more concentrated on the different conformations of exclusively the p38α MAP kinase. Any further studies may include dockings to JNK3 models.

5.4.3.1. Re-docking

The re-docking was not carried out separately, it was included in the cross-docking studies. However two ligand databases were generated, one which is the original SYBYL7.2 and a Maestro-LigPrep-database. The last one contained more conformations of the nine ligands from the start. It was generated to find out, if more ligand conformations (in the LigPrep-database) yield to better poses. Additionally the differences between docking with contraints or not as well as the two screening modes (SP or XP) were compared and tested for their applicability.

5.4.3.2. Cross-docking

Thus the number of possible poses was set to 50, the ligand's first appearance in the ranking will be described or if any specialties arose. It occurred that the first appearance resulted in good/similar poses and others later ranked were less similar. The first cross-docking was carried out with PDB 1OZ1 (SP mode). AIZ501 was on rank one. But its binding mode was not similar to the native in PDB 2B1P, except for the chloro-phenol which was situated in hydrophobic pocket I. The next ligand that appeared was PDB 1OZ1 own ligand FPH (rank 7) and was very much posed alike. Next ranked was Q222-400 (rank 20) and its pose was similar to PDB 2I0H. This also applied for L12 (PDB 1W84) on rank 24. The next ligand that appeared in the ranking was PQB1 on rank 50; its pose also very similar to that in PDB 2GFS. The other ligands were situated on ranks above 100 (132: COM2000 (PDB 2O0U), 238: Q880-501 (PDB 1PMQ), 259: LIE301 (PDB 2GTN) and 337: Q984-501 (PDB 1PMN)) and their poses were very unlike to their native poses.
For the next docking studies the XP mode was used. FPH was here on rank one and very similar posed, followed by also good poses for AIZ501 (rank 3), Q984-501 (rank 6), Q222-400 (rank 7) and L12 (rank 8). The poses for Q880-501 (rank 15), COM2000 (rank 21) and PQB1 (rank 23) seemed not correct then again. However the calculations were even more time consuming (70 minutes for 9 ligands).
The docking of the LigPrep database (SP mode) resulted in a slightly different ranking (AIZ501, FPH, Q222-400, L12, Q984-501, Q880-501, PQB1, COM2000, LIE301). For AIZ501, FPH, L12, Q984-501 and Q880-501 good docking poses were found. The docking was much more time consuming, however. The same docking in the XP mode resulted

in the following ranking: FPH (rank one), Q984-501 (rank 3), COM2000 (rank 22), AIZ501 (rank 23), L12 (rank 26), Q222-400 (rank 31), Q880-501 (rank 41), LIE301 (rank 43) and PQB1 (rank 51), where all proposed binding poses were acceptable.
The next docking was carried out with the contraints (con) option in the SP mode. It yielded in the following ranking: AIZ501 (rank one), FPH (rank 6), Q222-400 (rank 10), PQB1 (rank 11), L12 (rank 14), COM2000 (rank 66), LIE301 (rank 92) and Q984-501 (rank 260). From including L12 on the poses were not good, while Q880-501 was not even ranked at all. Docking the database in the XP mode scored FPH hightest, followed by AIZ501 (rank 3), Q880-501 (rank 4), L12 (rank 10), Q222-400 (rank 12), COM2000 (rank 20), PQB1 (rank 23) and LIE301 (rank 35). The last three poses were not alike those of their X-ray crystal structures.
The docking in the SP mode of the LigPrep database yielded to the following ranking (with constraints) : FPH (rank one), Q222-400 (rank 5), AIZ501 (rank 6), L12 (rank 7), Q984-501 (rank 9), Q880-501 (rank 14), COM2000 (rank 22), PQB1 (rank 47) and LIE301 (rank 236). The last two ligand's poses were not good. Starting the same docking in the XP modes led to a modified ranking: Q984-501 (rank one), FPH (rank 2), Q222-400 (rank 6), L12 (rank 20), Q880-501 (rank 35), LIE301 (rank 30), AIZ501 (rank 37), COM2000 (rank 39) and PQB1 (rank 47). All binding poses were similar to those observed in the PDB structures.
In the end the native ligand FPH was found in a similar pose on the first two ranks at least. Reasonable poses for AIZ501 were also surprisingly found as for all ligands. LIE301 was always situated at the bottom of the ranking, but even there some good poses were found, but only when the XP mode was used. The LigPrep database was not superior to to the normal database, even worse especially looking at the calculation time. XP was a little superior to SP, but also is much more time consuming. When docking a large database the time, that is needed, is a huge factor. Perfect results, but generated with more time consuming methods, are less worthwhile than only good results with less time consuming methods. The use of SYBYL7.2 generated databases for docking studies in the SP mode so seems be a good compromise for finding the correct binding mode of the Suberones.
Another evalution was carried out with PDB 2B1P. The appearance of the ligands in the ranking during the different modes can be seen in table 5.13.

ranked	**Ligands-SP-glide**	**Ligands-XP-glide**	**con-Ligands-SP-glide**	**con-Ligands-XP-glide**
1.	AIZ501	AIZ501	AIZ501	AIZ501
2.	COM2000	COM2000	COM2000	Q880
3.	Q880-501	Q880	Q880	Q984-501
4.	PQB1	PQB1	PQB1	FPH
5	FPH	FPH	FPH	LIE301
6.	Q222-400	Q222-400	Q222-400	COM2000
7.	Q984-501	Q984-501	Q984-501	Q222-400
8.	L12	L12	L12	L12
9.	LIE301	LIE301	LIE301	PQB1
ranked	**LigPrep-SP-glide**	**LigPrep-XP-glide**	**con-LigPrep-SP-glide**	**con-LigPrep-XP-glide**
1.	AIZ501	Q880	AIZ501	Q880
2.	PQB1	Q984-501	PQB1	Q984-501
3.	Q880	LIE301	COM2000	AIZ501
4.	COM2000	Q222-400	Q880	Q222-400
5.	Q984-501	PQB1	LIE301	PQB1
6.	LIE301	AIZ501	Q984-501	COM2000
7.	FPH	COM2000	FPH	FPH
8.	L12	FPH	L12	L12
9.	Q222-400	L12	Q222-400	LIE301

Table 5.13.: GLIDE evaluation with PDB 2B1P

All the dockings found very good poses with high scores for the JNK3 inhibitors (Q984-501, Q880-501 and AIZ501). However, GLIDE had some problems with the posing of COM2000. Its interactions were not often found. No difference between the quality of the SP and XP modes could be observed. When the normal ligand database was used in the SP mode GLIDE found reasonable poses for most of the other compounds, apart from LIE301. Good poses for that ligand were hardly found. When the LigPrep database was used, the results for the JNK3 inhibitors became even more accurate, whereas good poses for the other ligands were found to a less extent.
So far it seemed that docking with normal databases in the SP mode are useful for finding the correct binding mode for the Suberones. The next part will present the results of the Suberone docking.

5.4.3.3. Docking of the Suberones

The first docking was carried out with PDB 1OZ1, where RN14min was ranked first. The carbonyl oxygen pointed to the hinge region, but without any H-bonds, whereas the amino-phenol was situated in the hydrophobic pocket `I`. The -NH formed an H-bond to the backbone oxygen of Ala51. The MOmin compounds like MO40min (rank 30) which had in some cases their amino-phenol in the hydrophobic region `II` as well (MO37min rank 24, MO2min rank 40). Other MO compounds followed the pose on rank one (MO27min on rank 20). On rank 19 GA17min even was posed in this manner. It had appeared first on rank 6 with another, even stranger pose (amino-phenol in the hydrophobic pocket `I`, whereas the oxygen of the seven-membered ring pointed to the hinge region and the hydroxy groups of the substituents had H-bonds with Met109 and Gly110). The SK compounds appeared very early in the ranking (SK9min rank 14) and their carbonyl pointed to Lys53. JH30min was on rank 35 and its analogue JH126min was on rank 42 and their oxygen in the seven-membered ring were supposed to form an H-bond with Lys53. However, an H-bond with a ether oxygen which is situated between two aromatic rings is very unlikely. In the end the docking studies with PDB 1OZ1 were not very successful, because they did not clearly prefer any pose.
The next docking was carried out with PDB 2GFS. REV9min was situated on rank one. Its amino-phenol lay in the hydrophobic pocket `I` and the -NH_2 formed H-bonds to the backbone oxygen of Ala51. The carbonyl oxygen group formed an H-bond to the hinge region and interacted with the backbone -NH of Met109. OTTO3min and REV5min on the next ranks also took up the pose of rank one, apparently forming H-bonds with their carbonyl oxygen to the backbone -NH of of Met109. All the compounds that followed (exclusively REVmin

compounds) took up the observed binding poses. The first change happened with OTTO4min on rank 15. While the carbonyl oxygen maintained the H-bond to Met109, this time the -NH_2 formed an H-bond to the side chain oxygen of Asp168 instead of Ala51. The amino-phenol remained in the hydrophobic pocket I. The next rank was occupied by MO3min. Here the carbonyl oxygen pointed to the free space between Lys53 and Tyr35 (approximately the DFG loop). The amino-phenol was still situated in the hydrophobic pocket I and the backbone oxygen Ala51 formed an H-bond to -NH_2. The rest of the ranking was ruled by the binding pose of rank one (or rank 4 when regarding the carbonyl oxygen) e.g. MO13min (rank 18) and MO1min (rank 26). The binding mode of rank 15 also appeared several times (REV2min on rank 20 and OTTO1min on rank 31). In some cases no H-bond between the oxygen and the hinge region was observed (RN14min rank 42). REV9min on rank 40 showed a special binding pose. The carbonyl oxygen still pointed to the hinge region, whereas the amino-phenol occupied the hydrophobic pocket I and the amine substituent formed an additional H-bond to the backbone oxygen of Gly31 (part of the Gly-rich loop). The Revesz and Ottosen compounds were often found in the top 100. On rank 70 GA17min appeared and was posed alike rank 4. It again was ranked on 103, where the hydroxy group formed additional H-bonds to the hydroxy group of Tyr35 (also Gly-rich loop). JH126min (rank 89) and GA6min (rank 105) took up the binding pose of rank one, but their carbonyl oxygen rather pointed below the hinge region and therefore did not form any H-bonds. The SK compounds only appeared above rank 200. The poses on the ranks above 50 became more and more useless. But taken together the poses obtained with PDB 2GFS strongly hinted at the pose according to Revesz *et al.*.

The modified PDB 2GTN (with the deleted residues Phe169-Ala172) was used for the dockings. OTTO1min was on the first rank. The carbonyl oxygen formed to H-bonds to backbone -NH of Met109 and Gly110, whereas the amino-phenol was situated in the hydrophobic pocket I and the -NH_2 formed an H-bond with the side chain amines with Asp168. OTTO2min was next and posed alike. REV3min occupied the next rank and also took up the pose. Fifth ranked GA17min's binding pose was alike, but the H-bonds to the hinge region were missing. Instead the two hydrogens of the -NH_2 formed in the hydrophobic pocket I two H-bonds to the backbone oxygens of Ala51 and Leu104. Besides its hydroxy subsitutents formed two additional H-bonds. One to the backbone oxygen of Val30 (beginning of the Gly-rich loop) and the other to the side chain oxygen of Asp112 (at the end of the hinge region). Figure 5.49 shows the observed binding mode.

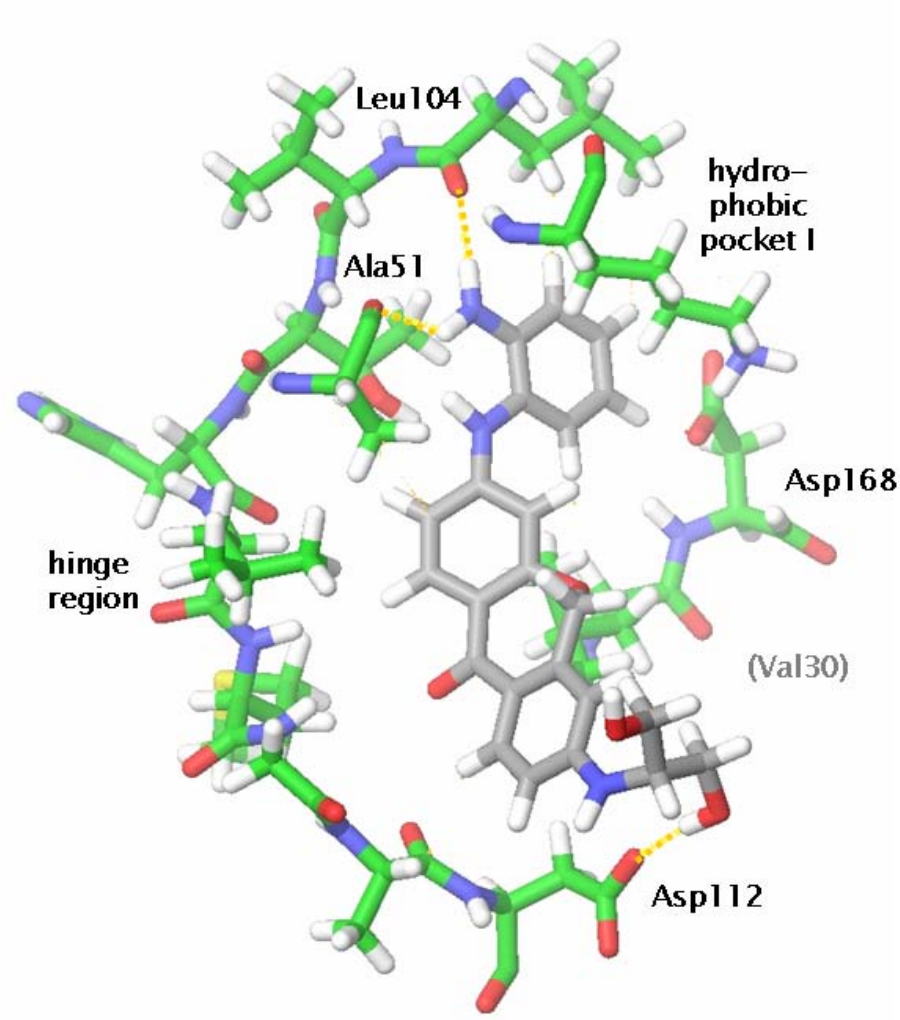

Figure 5.49.: Docking to PDB 2GTN (green stick representation): GA17min; rank 5; (grey stick representation), Val30 was left out to ensure a clear view, its position is represented by the label

The following compounds all took up the pose. Sometimes they formed two H-bonds to the hinge region (REV2min), or only one to Met109 or Gly110 or only pointed to the hinge region, but had no H-bonds at all. From rank 14 on more unusual poses appeared. For example JH126min's carbonyl oxygen pointed to Lys53 (as did RN13amin, JH46min, MO3min, MO4min, MO13min).The first SK compound appeared on rank 37, but its pose was negligible, as those SK compounds that followed. Altogether it could be observed that the amino-phenol was preferably posed in the hydrophobic pocket I (so alike Revesz *et al.*), whereas the pose of the carbonyl oxygen and its H-bonds varied more.

Apart from one outlier all compounds of the Suberone database on the first 100 ranks had

the same binding pose when docked in PDB 2I0H. MO4min on rank 65 had its carbonyl oxygen pointed to Lys53, whereas all other compounds pointed with their carbonyl oxygen to the hinge region. The first compounds formed H-bonds to Met109 and Gly110 (OTTO2min, OTTO1min and OTTO3min). OTTO4min (rank 22) formed an H-bond to backbone -NH of Gly110. All amino-phenol of the compounds were situated in the hydrophobic pocket `I`. The amino-phenol on rank 44 was situated in hydrophobic region `II`. Several different H-bonds of the aminogroups of the amino-phenol were found in the hydrophobic pocket `I`, e.g. with the backbone oxygen of Ala51, with the backbone oxygen of Leu104 or with both or with none of them. So this docking also supports the binding mode proposed by Revesz *et al.*.
The GLIDE docking to PDB 2QD9 was carried out twice. Once with the normal database and an extra docking with the then newly generated SG compounds. The first docking study yielded to the REV compounds on the top ranks. REV9min was first and its carbonyl oxygen formed two H-bonds to the backbone -NH of Met109 and Gly110 and the amino-phenol in the hydrophobic pocket `I`. The -NH_2 substituent formed an additional H-bond to the backbone oxygen of Gly110. Until rank 44 all compounds were conformations of the REV compounds apart from REV7min which did not appear at all. Rank 44 was occupied by SK510min which took up the pose of the REV compounds, but only formed an H-bond to the backbone -NH of Gly110. Both poses are displayed in figure 5.50.

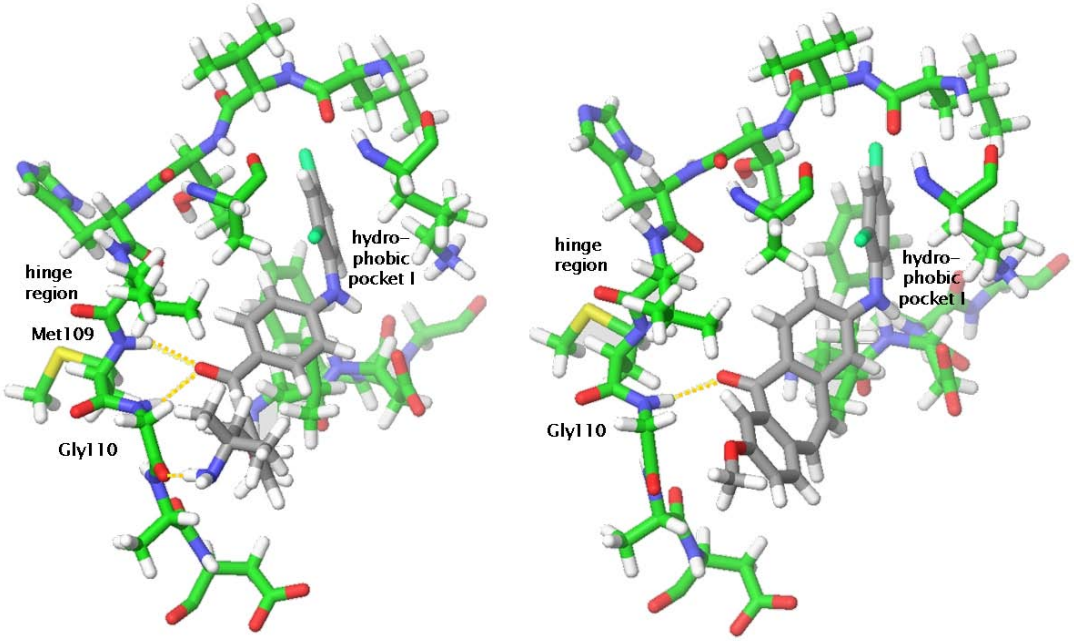

Figure 5.50.: Docking to PDB 2QD9 (green stick representation): left REV1min; rank one; (grey stick representation), right SK510min; rank 44 (grey stick representation)

From then on more Suberones (not only REV compounds) appeared with similar poses (rank one-44) appeared. An outlier was SK468 which lay across the ATP binding pocket in front of the entrance. The OTTO compounds were primary ranked from rank 109 on. All poses until the rank 160 were rather good and took up the poses alike the first ranks. Normaly there was at least one H-bond either to Met109 and /or Gly110. And the amino-phenol was positioned in the hydrophobic pocket I. There also the additional H-bonds to e.g. the backbone oxygen of Leu104 appeared now and then. An extra docking of only the SGmin compounds yielded to SK510min on the first rank. The pose was alike the one on rank 44 in the previous docking. Next was SK318min, but had no H-bonds to the hinge region. Apart from SK288min all SG compounds took up the pose, just varied in the formation of the H-bonds (Met109 and/or Gly110 or no H-bond). Unlike the rest SK288min's amino-phenol was in the hydrophobic region II, and its carbonyl oxygen pointed to Lys53. The appearance of the SG compounds was as follows: SK510min, SK318min, SK539min, SK558min, SK345min, SK468min, SK568min, SK508min, SK541min, SK383min, GA430min, SK362min, SK316min, SK288min, GA425min, SK436min and GA553min. The ranking could not be connected with the binding affinity (if IC_{50} values existed, see also appendix). However, the results strongly support the binding mode proposed by Revesz *et al.*.

The docking of PDB 1W84 yielded in REV3min on the first rank. Its amino-phenol was situated in the hydrophobic pocket I, but the pose of the carbonyl oxygen was unusual. It pointed to the ceiling of the ATP binding pocket and did not form any H-bonds (figure 5.51).

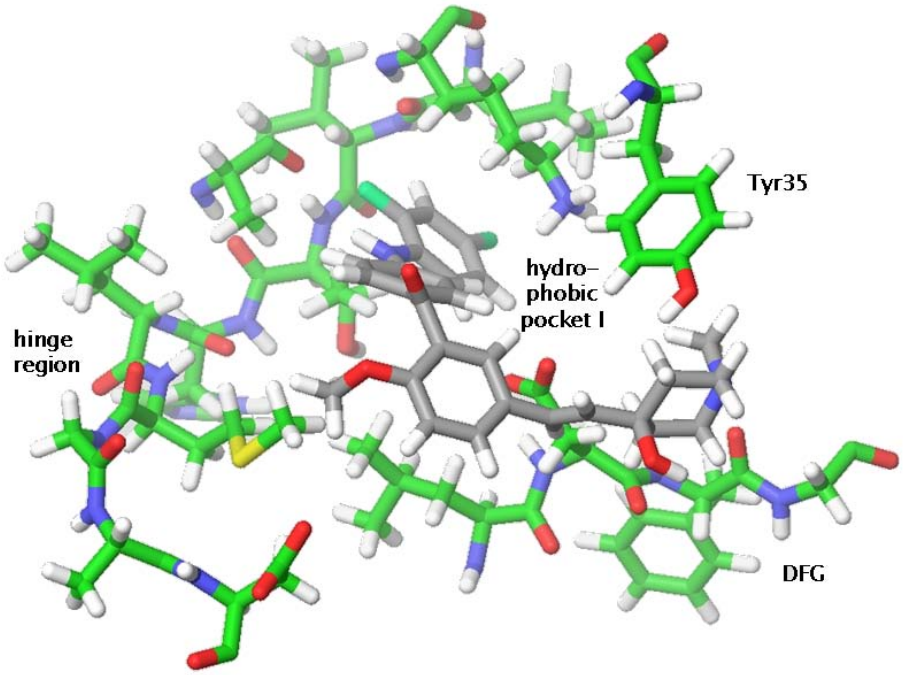

Figure 5.51.: Docking to PDB 1W84 (green stick representation): REV3min; rank one; (grey stick representation)

SK345min appeared on rank 2 (in this docking the SGmin compounds were already added to the Suberone database). Its carbonyl oxygen pointed to the hinge region, but no H-bonds could be formed. SK318min pose on the next rank was partly posed outside of the ATP binding site. The next compounds (SK508min, SK362min and SK468min) were posed alike rank one. MO23min's pose (rank 7) was very unusual; the ether oxygen of the seven-membered ring formed an H-bond to Lys53 and the amino-phenol lay across in front of Tyr35. An unlikely pose is demonstrated in figure 5.52.

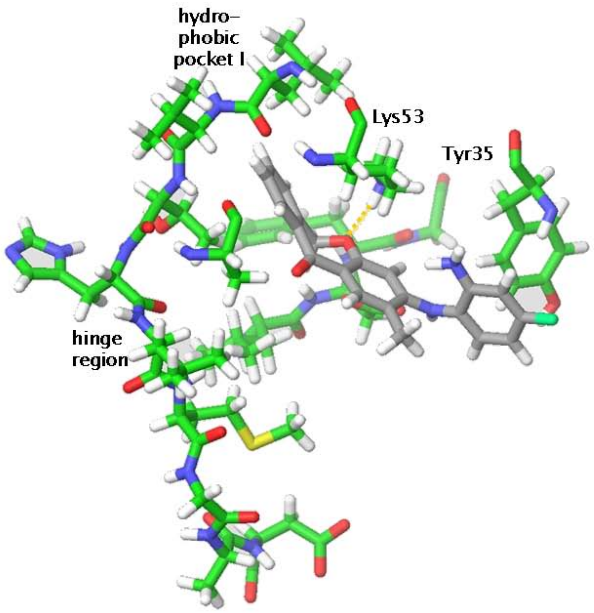

Figure 5.52.: Docking to PDB 1W84 (green stick representation): MO23min; rank 7; (grey stick representation)

Many of the following poses were in fact not as unlikely as those of rank 7 and 9. While they kept their amino-phenol in the hydrophobic pocket I, the rest of the molecule lay across the binding pocket as well. No interactions between the carbonyl oxygen and the hinge region were found. This docking was rather unsuccessful, because the poses were unlikely.
In PDB 2PKJ, one of the two unliganded PDB structures, RN14amin was put on rank one. Its carbonyl oxygen pointed to the hinge region, but without any H-bonds. The amino-phenol was situated in hydrophobic pocket I and the -NH_2 formed H-bonds to the backbone oxygen of Ala51. OTTO1min was next and its pose alike, but it formed an H-bond to backbone -NH of Met109. The -NH_2's H-bond partner this time was the backbone oxygen of Leu104. Third ranked GA17min's amino-phenol was situated in hydrophobic region II (and the -NH_2 formed an H-bond with Gly110), whereas the hydroxy substituents lay in the hydrophobic pocket I and formed H-bonds to Asp168. This pose was very unlikely. GA1min's carbonyl oxygen on rank 5 pointed to Lys53, but still had its amino-phenol in the hydrophobic pocket I. Another conformation of GA17min appeared in the exact pose on rank 9. The majority of the results was posed alike the first rank, the only other alternative pose which occurred was the one alike GA1min or OTTO1min (MO18min, MO28min, MO24min, GA2min, MO40min, another conformation of RN14amin (rank 41) and MO12min) for the first 50 ranks. The SK compounds appeared in this docking very late (rank 372, SK26min). Altogether the poses

were very homologue and also hinted to the binding mode according to Revesz *et al.*.
PDB 2FSO's dockings came to the same result, if regarding the actual poses. But here the first 50 ranks included no OTTOmin or REVmin compounds, but even there their poses took up the two often poses that occurred most. The SK compounds were also only found on later ranks. GA17min's amino-phenol on the second rank was anchored by an H-bond to Asp168 in the hydrophobic pocket I, but its carbonyl oxygen pointed to Lys53. The hydroxy-groups of the substituent had H-bonds to Gly110 and Asp112 (figure 5.53).

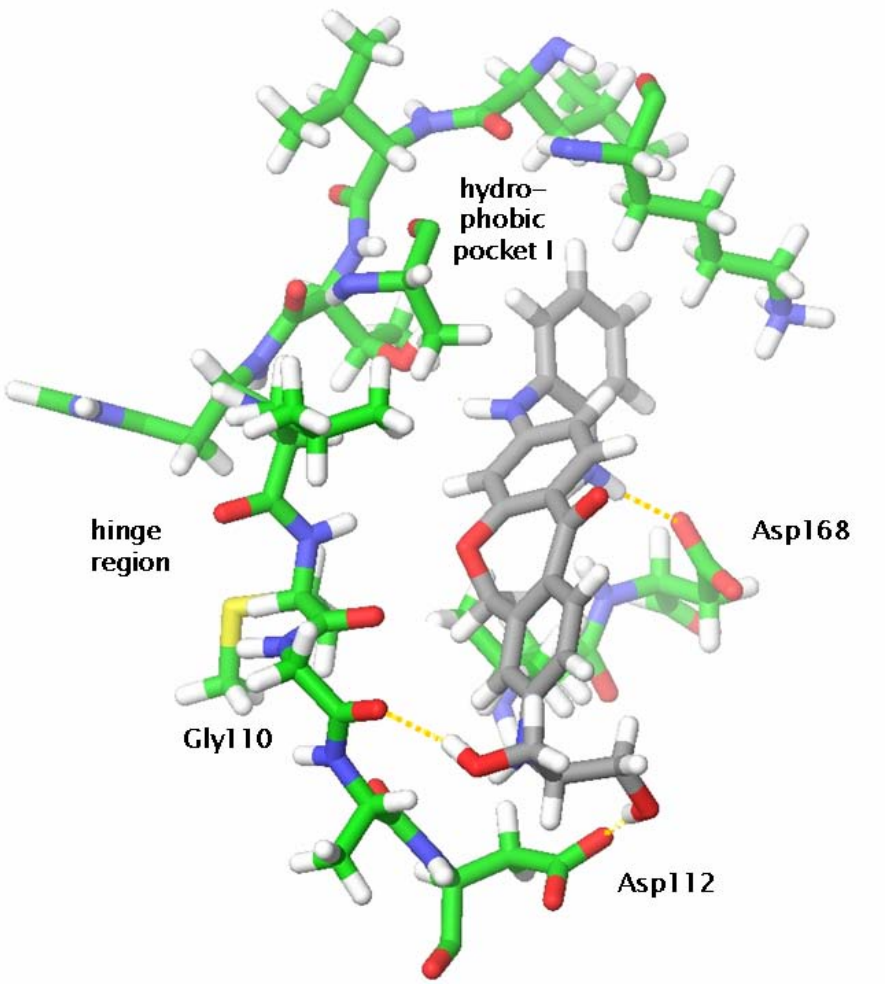

Figure 5.53.: Docking to 2FSO (green stick representation): GA17min; rank 2; (grey stick representation)

Many of the GA compounds had the same pose and even once a conformation of RN14amin. Other compounds were situated with the amino-phenol in the hydrophobic pocket I anchored with the H-bond to Ala51 and the carbonyl oxygen connected to Met109 with an additional H-bond , but sometimes chose Asp168's side chain oxygen instead of Ala51's backbone oxygen as an H-bond binding partner or alternatively Gly110 instead of Met109 or both at the same time. Taken together docking to 2FSO also supports that the Suberones rather bind to the p38α MAP kinase in the manner proposed by Revesz *et al.*.

PDB 1W82 (DFG-OUT conformation) first rank was occupied by OTTO1min. The carbonyl oxygen formed an H-bond with Met109 and the amino-phenol lay in the hydrophobic pocket I. The other OTTO compounds followed this example on later ranks. In case of OTTO3min the -NH_2 was also anchored in hydrophobic pocket I by an additional H-bond with Ala51. The other compounds were all posed alike the poses FlexX had suggested. The -NH_2 and NH of the amino-phenol formed H-bonds to the side chain oxygen of Glu71 or Asp168. However the carbonyl oxygen had no interactions. The SK compounds appeared very early in the ranking (rank 41 SK23min), but also without any H-bonds. On rank 46 MO4min was posed again in the ATP binding pocket alike OTTO3min.

MO39min was on the first rank in the PDB 1WBS (also DFG-OUT conformation) docking. The pose was also alike the OTTO3min in PDB 1W82. But even with fewer H-bonds. OTTO1min (rank 9) had the first of a small number of outliers. The carbonyl oxygen pointed to Lys53, whereas the amino-phenol was directed to the hydrophobic pocket DFG-OUT and the -NH formed an H-bond to a side chain oxygen of Glu71. The next ranks (e.g. REV1min) took up the pose. Another conspicuity was situated on rank 16, where SK26min's pose was across the ATP binding pocket. Many other SK compounds on the next ranks, but their poses were as unusual as the first one. In the end the pose that allowed H-bonds between the -NH_2 to Glu71 or Asp168 was the preferred one. So alike FlexX GLIDE suggests that the Suberones may also bind during the DFG-OUT conformation.

Further studies were carried in the XP mode and with contraints. The data is not presented here. However the results did not alter much from the SP/without constraints studies, but took much more calculation time. The results of the SP dockings were able to consider the binding mode according to Revesz *et al.* as the more probable binding pose. Taken together Glide docked the Suberones in very many acceptable poses, so it seems that it is more applicable for the p38α MAP kinase and a more reliable docking programme in comparison to FlexX. Further docking was carried out next with eHITS to hopefully find more proof for the GLIDE results.

5.4.4. eHITS

5.4.4.1. Defining the docking options

With PDB 1OZ1 and PDB 1W84 the first re-dockings were carried out to decide if the accurate or standard option produces results of different quality. Any fast docking is preferred over an accurate if no loss of the quality of the poses can be observed. The standard option was chosen, because it resulted in more similar results (17 of 32 instead of 7 of 32 in case of PDB 1OZ1) and altogether just three proposed binding modes of which two were nonsense (to four of which three were unacceptable (PDB 1OZ1)) occurred. For PDB 1W84 only two poses were proposed; the standard option resulting in more similar poses. The removal of the existing water molecules of the PDB structures resulted in both PDB structures in more worse poses. With eHITS it was apparent that low RMSD values refer to the right pose. Very similar poses had RMSD values between 0,5000 and 1,0000 while any other positions had obviously higher RMSD values (4,500 or more). The first good poses had high scores and therefore appeared among the first ranks, but could also to be found in higher ranks (32 poses were calculated).

5.4.4.2. Re-docking

After choosing the right options more re-docking were carried out. The re-dockings in PDB 2GFS were worse in comparison to those done before. Overall the RMSD values were higher and the binding modes varied considerably to the one in the X-ray structure. In general the calculated orientations were very similar, but in many cases the position was shifted (e.g. fluorophenyl not buried in the inside of hydrophobic pocket `I`, but rather in front of it).
Re-docking of PDB 2GTN resulted in very many similar poses with low RMSD values. In case of PDB 2GTN is was of no consequence if water molecules were present or not. Docking first PDB 2I0H led to some difficulties, because two ligands are present in the X-ray crystal structure. To enable an eHITS docking one of the ligands of the ATP binding pocket had to be removed. The re-docking yielded in different results as mentioned before. Similar poses were rare and were ranked lower than other totally unacceptable poses. Here the removal of the water molecules resulted in more similar poses. But the RMSD values were higher (above 1,600 at least). PDB 2QD9 was also tested. Most of the binding poses were very similar to the crystallized. The RMSD values are a little bit higher (most of them above 1), but that comes from the size of the ligand with more large substitutents. The pose per se is correct, but small variations in the substituents result in higher RMSD values in comparison to smaller ligands (e.g. PDB 1W84). Completely wrong poses occurred rarely.

To test eHITS on the re-docking of DFG-OUT conformations PDB 1WBS was chosen. The poses here were also very similar, unveiled by the low RMSD values of 0,500-3,600 at most. Small variations of the morpholine substituent yielded to RMSD values around 3. Figure 5.54 shows two re-docking results (PDB 1W84 (left) and PDB 1WBS (right)).

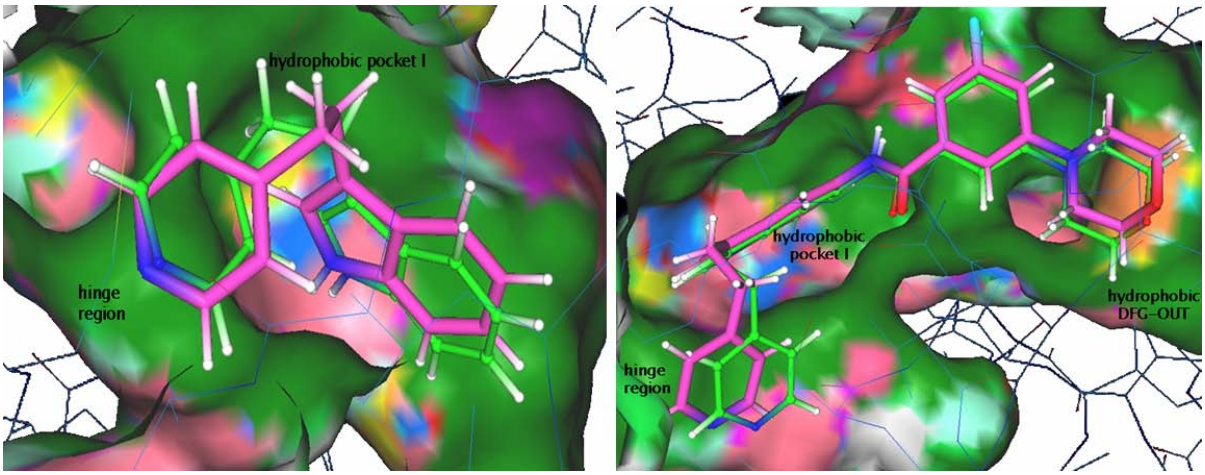

Figure 5.54.: Left re-docking of ligand L12 (pink stick representation) of PDB 1W84, rank 9(green stick representation) and right re-docking PDB 1WBS, native ligand pose (pink stick representation) and docked ligand pose (green stick representation)

5.4.4.3. Cross-docking

During the cross-dockings eHITS does not calculate any RMSD values anymore. The poses are judged visually and compared to the pose in their own X-ray crystal structure. If no reasonable pose is expected, eHITS would hopefully not be able to find a pose at all. The first cross-dockings included the refined water molecules. L12 the ligand of PDB 1W84 was found on rank one in a very similar pose to the X-ray crystal structure and shared the same interactions (pyridine-Met109, and indole in the hydrophobic pocket I). But altogether eHITS only found poses for three other ligands (LIE301 (PDB 2GTN), FPH (PDB 1OZ1) and PQB1(PDB 2GFS)) which were positioned very unusual (not the expected H-bonds or even H-bonds at all). For the next docking all water molecules were deleted. Here all ligands were docked and they were all posed in the ATP binding site. Surprisingly the original ligand of PDB 1W84 was only on rank 6. On the first rank was Q984-501 (PDB 1PMN), followed by Q880-501 (PDB 1PMQ). Their poses were very similar to the poses in their JNK3 X-ray structures. Positioned on the next ranks were FPH (PDB 1OZ1), Q222-400 (PDB 2I0H) and LIE301 (PDB 2GTN),

which are also very closely posed in comparison to their X-ray crystal structures. For PQB1 (PDB 2GFS) it is all the same. On the last ranks AIZ501 (PDB 2B1P) and COM2000 (PDB 2O0U) are located. Their poses are unusual, what goes along with their selectivity for JNK3 against p38α MAP kinase.

2FSO was also provided with SB203580, as mentioned before to ensure that eHITS finds the ATP binding site. The cross-docking placed Q984-501(PDB 1PMN) on the first rank, but the pose was unusual. The hydrophobic pocket `I` accommodated the cyclo-propyl-substituent, whereas the di-chloro-phenyl was positioned in the hydrophobic region `II`. On the second rank FPH is situated also differently, as well as LIE301 which is about-faced, Q222-400 (totally different as well), L12 and Q880-501 (outside of the ATP binding site). The seventh rank is occupied by PQB1 which position is also not similar to the native position in the X-ray structure. This also applies for COM2000 and AIZ501. For them it is not unexpected however, because they should not be able to bind in regard to their selectivity profile.

In case of PDB 2GFS LIE301 was on the first rank and its pose was very similar to that of the native structure. The second rank was occupied by COM2000 which pose was also very alike. PQB1's position on the third rank was less alike its crystal structure, followed by AIZ501 which was again very much alike. In contrast to AIZ501 the five remaining ligands had very unusual poses. The cross-docking of PDB 2GTN also set LIE301 on the first rank, but the pose was about-faced from the crystal structure. Second ranked was Q222-400, but also in a different orientation. PDB 1OZ1's FPH on the third rank was posed alike its crystal structure, whereas next ranked Q880-501 was not. On rank five AIZ501 is situated very much alike its pose in JNK3. JNK3 structure PDB 1PMN's ligand Q984-501, however, was posed very dissimilar to native pose. On the last three ranks L12, PQB1 and COM2000 were situated. None of their prosposed poses was similar to those of their crystal structures.

In case of PDB 2I0H ligand LIE301 was ranked best. Its pose was very similar. Second ranked Q880-501's position was about-faced to its observed in JNK3. PDB 2I0H own ligand Q222-400 was ranked third best and in a very similar pose. COM2000's naphtylene on the fourth rank positioned in hydrophobic pocket `I` like in its crystal structure, but the rest of the ligand was posed unusual. Next ranked FPH's pose was also similar in regard to the substituent in hydrophobic pocket `I`, but the pose of the rest of the molecule was twisted. The same applies to Q984-501, followed by PQB1, L12 and the last ranked AIZ501.

The last cross-docking studies were carried out with PDB 2QD9. Q222-400 was best ranked and its pose was alike the one in its crystal structure. Second ranked LIE301 was about-faced, as well as Q984-501 on rank three. Fourth scored COM2000's pose was very similar to its

observed in PDB 2O0U, only the piperidin substituent is slightly different. Next ligand PQB1 was also very much alike, just like L12. On the seventh rank Q880-501 was situated, but not very good posed. Eighth ranked FPH was very good posed again. The pose of AIZ501 on the last tank was also very similar to that in its X-ray crystal structure.
The cross-docking studies showed that eHITS is able to find the right poses, but the user has to check the results carefully, because there may be false results in between. In the end eHITS seems to be as applicable for the docking studies as the other programmes. Figure 5.55 shows a result of the cross-docking study of PDB 2QD9.

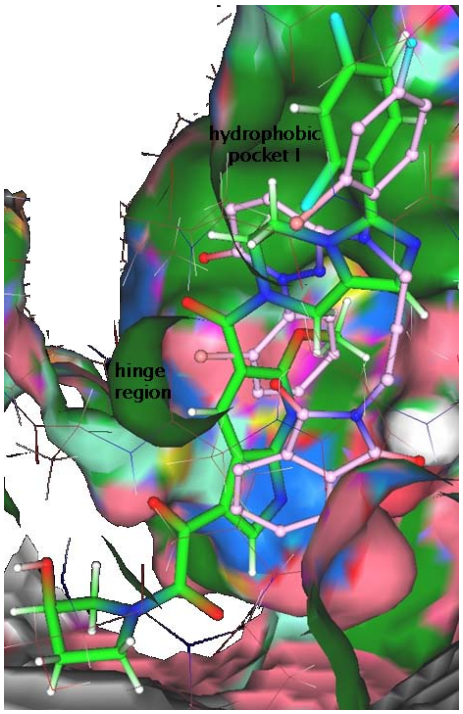

Figure 5.55.: Cross-docking study: ligand LIE301 (pink stick representation) of PDB 2GTN in PDB 2QD9 (ligand LGF in green stick representation), rank 2

5.4.4.4. Docking of the Suberones

The first docking was carried out with PDB 2IOH (options standard accurancy, no water molecules). On the first rank was REV8min in an orientation according to Ottosen *et al.*. The sp^2nitrogen of the pyrazol formed an H-bond to Thr106's side chain oxygen. The amino-phenol lies to the right of hydrophobic region `II`. The second rank was occupied with REV4min. Its pose refers to the Revesz *et al.* binding mode. The carbonyl oxygens form two H-bonds to the

backbone nitrogens of Met109 (distance 2,6187 Å) and Gly110 (distance 1,9603 Å) and the amino-phenol lies in the hydrophobic pocket I (figure 5.56).

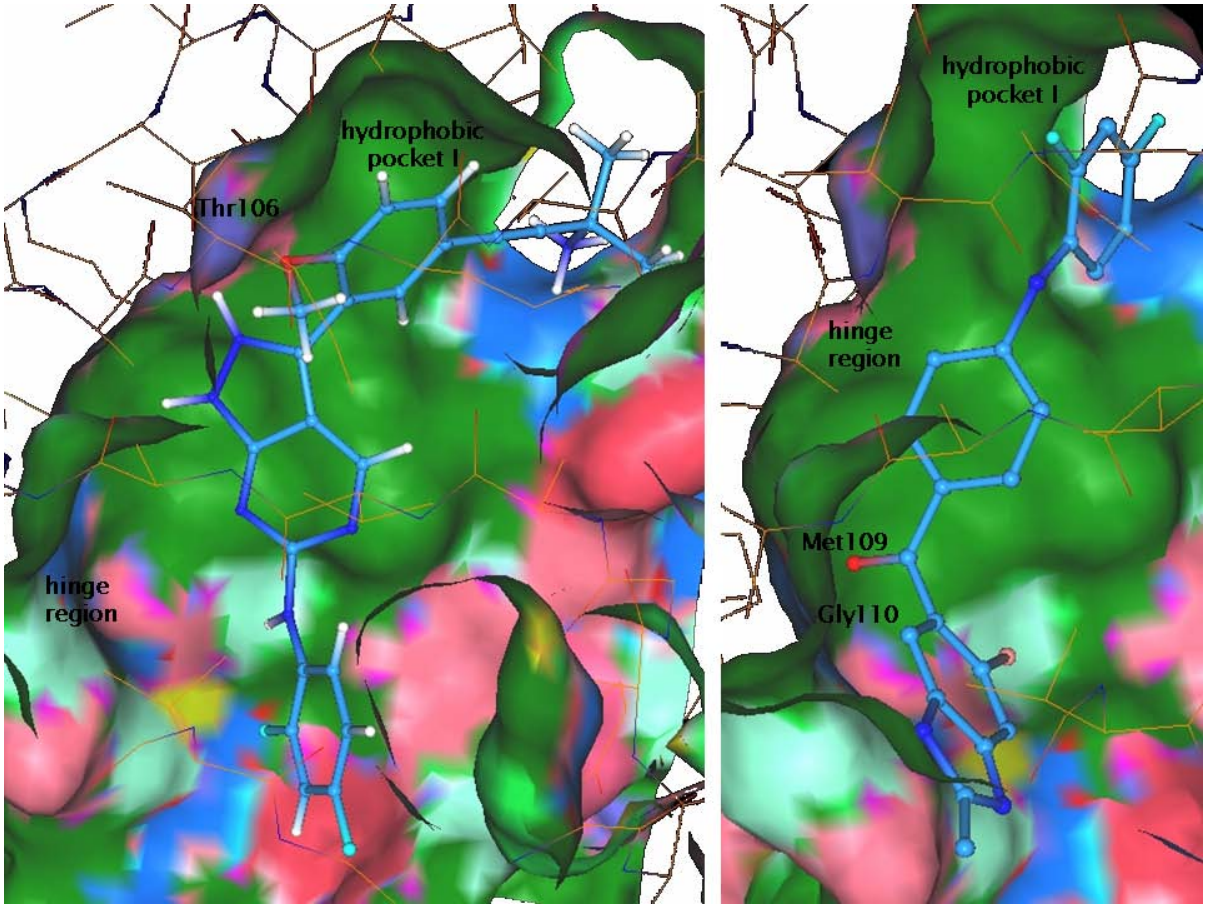

Figure 5.56.: Docking to PDB 2I0H: left proposed pose of REV8min rank one and right proposed pose of REV4min rank 2 (no hydrogens were added for this representation)

REV10min (rank 3) formed again the H-bonds to the backbone nitrogens of Met109 (distance 2,2435 Å) and Gly110 (distance 1,8263 Å) and additionally the pyridine nitrogen to the side chain oxygen of Thr106 (distance 3,0814 Å) (these three H-bonds also occur with Q22-400, the native ligand). Next ranked REV1min formed then again only two H-bonds to the backbone nitrogens of Met109 and Gly110 (distance 2,4370 Å and 1,8540 Å respectively). However, in both cases the amino-phenol was situated in the hydrophobic pocket I. Next compound which stepped out was on rank 11 (MO15min). The amino nitrogen formed an H-bond with the side chain oxygen of Thr106 (distance 2,8647 Å). The amino phenol was situated in the hydrophobic pocket I, but the carbonyl oxygene was far away from the hinge region, although it still pointed to it. The additional phenol substituent should have prevented any posing, but it was posed surprisingly anyway (figure 5.57).

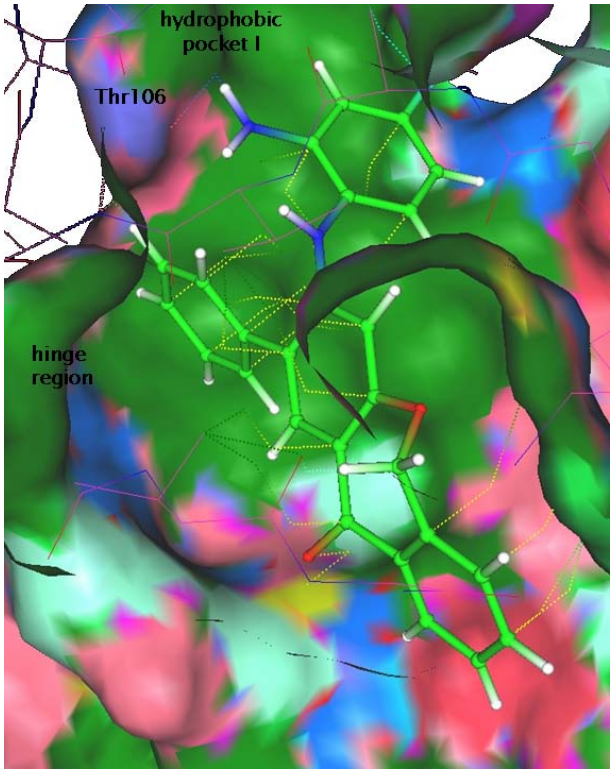

Figure 5.57.: Docking to PDB 2I0H: proposed pose of Mo15min rank 11

On the next rank was OTTO1min. The carbonyl oxygen formed two H-bonds to the backbone -NH of Met109 (distance 2,2789 Å) and Gly110 (distance 1,6181 Å) and an additional H-bond between the nitrogen of the amine to the backbone oxygen of Leu104 (distance 1,9050 Å). The amino-phenol occupied the hydrophobic pocket `I` and binds therefore according to the Revesz *et al.* binding mode. Next eHITS ranked MO10min and MO16min. This time opposed to the similar compound MO15min on rank 11 their pose was very unusual as it would have been expected, due to their composition. Many other MO compounds were ranked subsequently, but their carbonyl oxgen was about-faced and pointed rather to Lys53 instead of the hinge region, whereas the amino-phenol was situated in the hydrophobic region `II`. Sometimes the carbonyl oxygen even pointed to the hinge region, but formed no H-bonds to it and had the amino-phenol situated in the hydrophobic region `II` (MO33min on rank 18). An exception was MO29min on rank 19, where the oxygen pointed again to the hinge region. RN15min's (rank 21) binding pose also followed the unusual binding poses of the MO compounds. The higher the rank the more unusual poses appeared. OTTO2min appeared on rank 27, had its amino-phenol situated this time in the hydrophobic region `II`. The carbonyl oxygen pointed to the hinge region, but was too far away posed to form any H-bonds. The REVmin compound's

poses remained traceable. GA16min was ranked on the 37th place; the oxygen only pointed to the hinge region, whereas the amino-phenol was situated in hydrophobic region II, while its amine formed an H-bond to the side chain oxygen of Asp112 (atom OD2, distance 2,0318 Å). JH31min's oxygen (rank 46) pointed again rather to Lys53, while keeping the amino-phenol in the hydrophobic pocket I, where the amine formed an H-bond to the backbone oxygen of Leu104 (distance 1,5072 Å). This pose and the one of OTTO1min are demonstrated in figure 5.58.

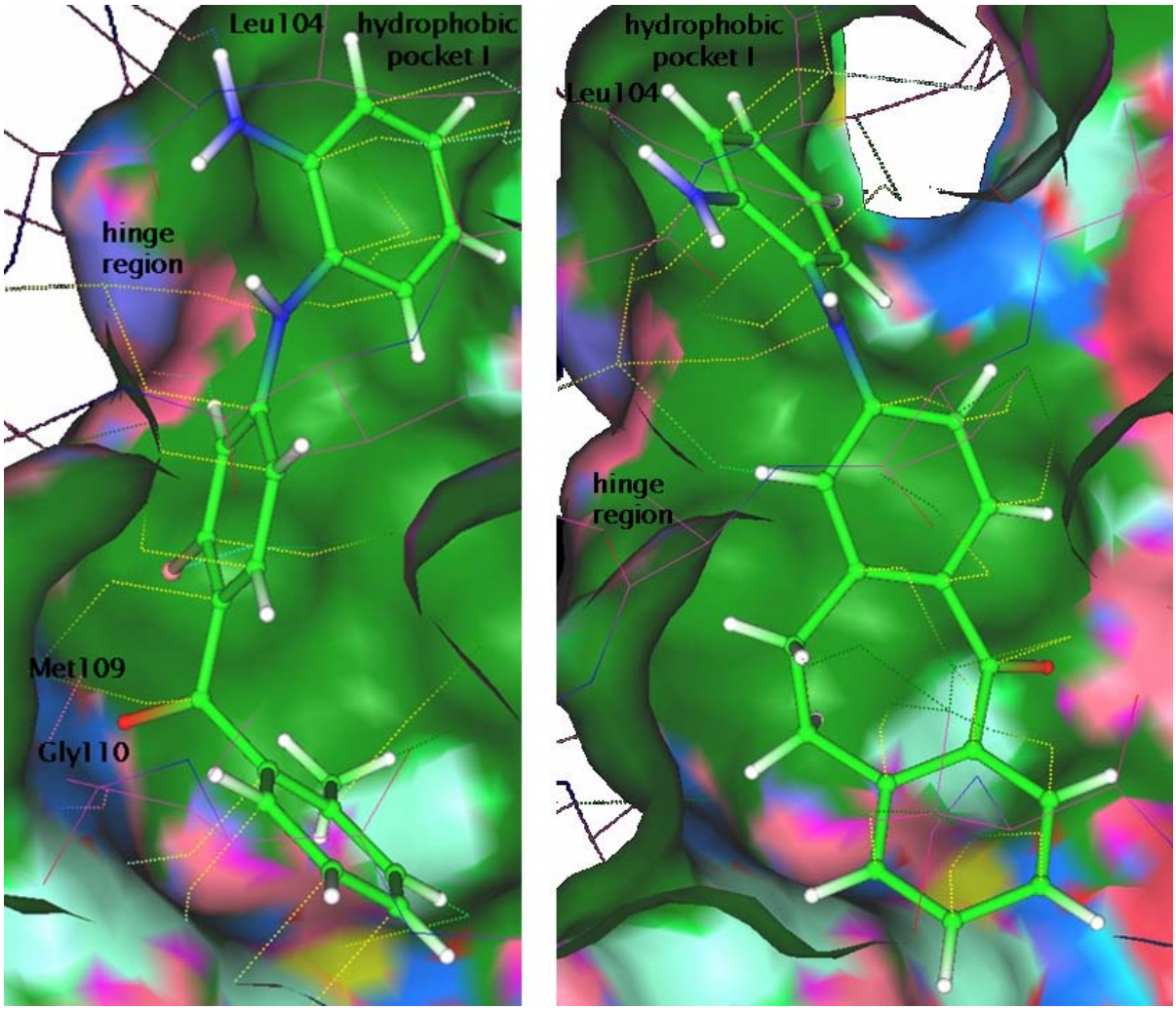

Figure 5.58.: Docking to PDB 2I0H: left proposed pose of OTTO1min rank 12 and right proposed pose of JH31min rank 81

The first SK compound appeared on rank 103 (SK29min), but not comprehensible posed. GA17min (rank 137 and 148) poses were acceptable. In both cases the carbonyl oxygen formed two H-bonds to the backbone nitrogens of Gly110 (distances 3,0354 Å and 2,4073 Å

respectively) and Ala111 (distances 2,4759 Å and 2,1366 Å respectively) (figure 5.59).

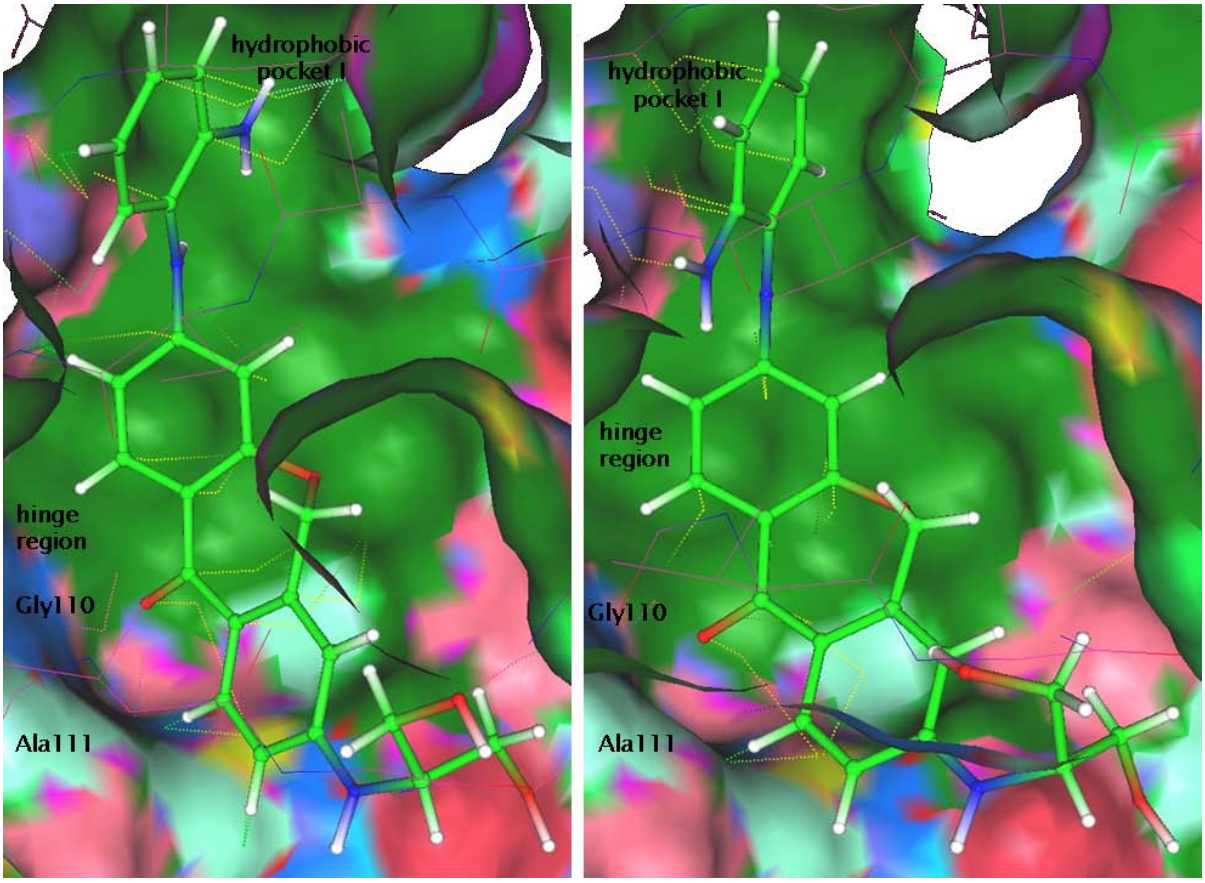

Figure 5.59.: Docking of the Suberones in PDB 2I0H: proposed pose of GA17min rank 137 (left) and rank 148 (right)

PDB 2GTN' first rank was occupied by MO35min which pose was alike JH31min in PDB 2I0H (the carbonyl oxygens points to Lys53 instead of the hinge region, while keeping he amino-phenol in the hydrophobic pocket `I`). The next ranked ligands shared this pose. MO37min's amino-phenol (rank 8) was situated in hydrophobic pocket `I` and its -NH_2 formed two H-bonds; one to the backbone oxygen of Phe169 (distance 2,1882 Å) and another to the side chain oxygen of Asp168 (distance 1,4197 Å). REV9min is on rank 12 and the carbonyl oxygens formed an H-bond to backbone -NH of Gly110 (distance 2,5406 Å) and the -NH_2 of the substitent to the backbone oxygen of Gly110 (distance 2,0254 Å) (figure 5.60).

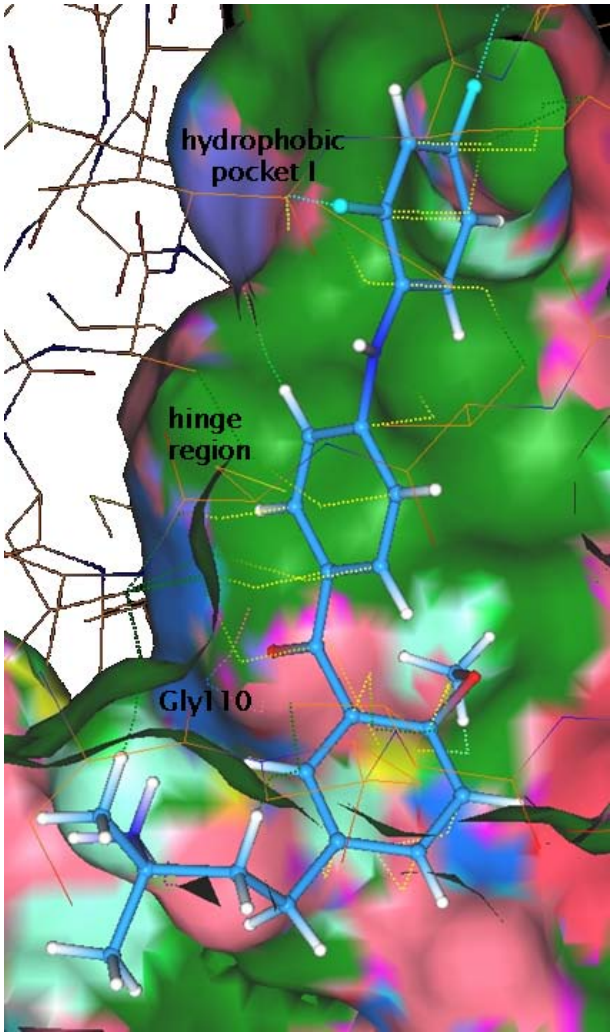

Figure 5.60.: Docking of the Suberones in PDB 2GTN: proposed pose of REV9min rank 12

Most of the following compounds pointed with their carbonyl oxygen to Lys53, whereas the amino-phenol was situated in the hydrophobic pocket I. RN15min (rank 16) had its carbonyl oxygen to the hinge region, but without any H-bonds. The amines in hydrophobic pocket I had two H-bonds to the side chain oxygen of Asp168 (distance 2,8234 Å) and to the Glu71 (distance 2,3819 Å) in the meantime. The OTTO compounds (OTTO3min (rank 37) and OTTO1min (rank 41)) were posed according to the Revesz *et al.* binding mode; on rank 43 RN13amin as well. Poses on the following ranks resulted in less good or acceptable poses. The first SK compound was on rank 100 (SK12min), JH30min was unusual posed on rank 55, whereas a good pose of GA17min was on rank 101. Altogether the eHITS docking to PDB 2GTN supported the theory that the amino-phenol would occupy the hydrophobic pocket I rather than hydrophobic region II (so alike Revesz *et al.*). Several H-bonds of the amines

were discovered, but the carbonyl position was often unusual (no pointing to the hinge region, but in the other direction).
Docking the Suberones to PDB 2QD9 resulted in MO38min on the first rank. The amino-phenol was in hydrophobic pocket `I`, whereas the carbonyl oxygen pointed to the hinge region, but there no H-bond interactions were found. Analogue MO36min was on rank 2 and took up the same pose. Many of the following compounds were about faced. They maintained the amino-phenol position in hydrophobic pocket `I`, while sometimes forming an H-bond to the backbone -NH of Met109 with the amino-phenol in the hydrophobic pocket `I`. Very few were posed about-faced alike this with the carbonyl oxygen pointing to Lys53 (MO35min). In the first twenty ranks almost exclusively MOmin compounds could be found. OTTO21min on rank 21 was posed according to the Revesz *et al.* proposed binding mode. It formed three H-bonds: the carbonyl oxygen to the backbone nitrogen of Met109 (distance 2,1560 Å) and Gly110 (distance 1,7916 Å) and the -NH_2 to the backbone oxygen of Leu104 (distance 1,8317 Å). Two ranks later JH46min was positioned alike, but with only an H-bond to the backbone nitrogen of hinge region residue Met109 (distance 3,0168 Å). eHITS offered two additional H-bonds between the -NH_2 and the backbone oxygens of Ala51 and/or Leu104 (distances 2,2977 Å and 1,5705 Å). The carbonyl oxygen of GA14min on the next rank pointed again to Lys53, also RN15min on rank 28. REV4min on rank 37 shares the same hinge regions interaction like GA17min of PDB 2I0H (Gly110 2,1685 Å and Ala111 2,0904 Å). Figure 5.61 shows the proposed binding poses of REV9min and REV4min.

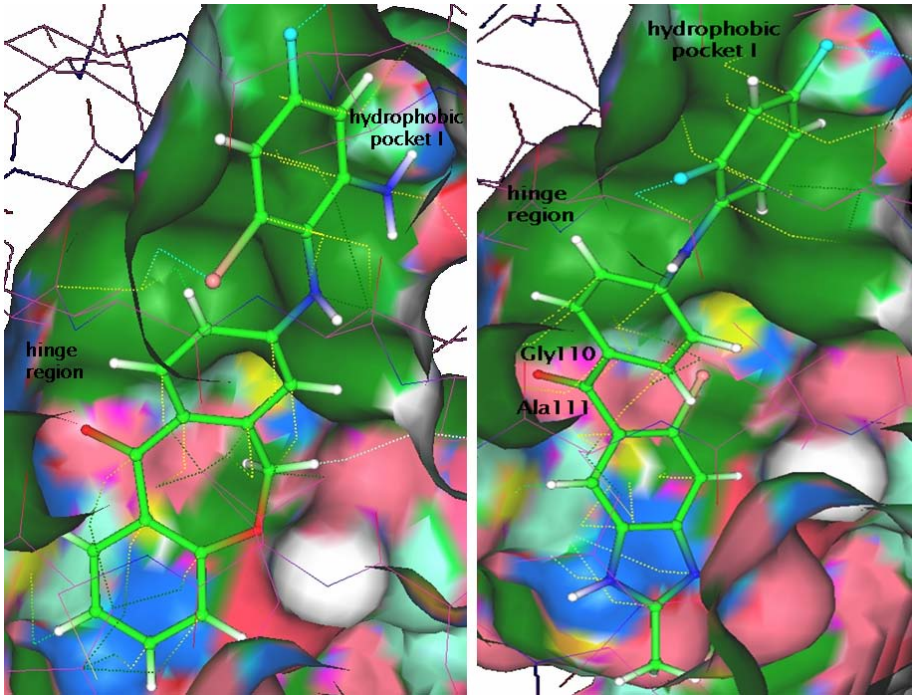

Figure 5.61.: Docking to PDB 2QD9: left proposed pose of REV9min rank one and right proposed pose of REV4min rank 37

In the following poses the Suberone's carbonyl oxygen mostly pointed to Lys53, or if not it did not form any H-bonds to the hinge region atoms. The first SK compound was found on rank 115 (SK9min), but the oxygen pointed again to Lys53.
This docking study strengthens that the amino-phenol is situated in the hydrophobic pocket I (Revesz binding mode). It also introduced a new binding partner to anchor the amino-phenol there (Ala51). Thus, the SG compounds were added later to a separate database, they were exclusively docked in PDB 2QD9, because it had shown very good docking results. The first rank was occupied with SK568min. The hydrophobic pocket I accommodated the amino-phenol, but the oxygen pointed to Lys53 instead to the hinge region. Next ranked GA425min's also had its amino-phenol in hydrophobic pocket I, while forming two H-bonds to the hinge region.The backbone nitrogens of Met109 and Gly110 had each an H-bond with the carbonyl oxygen (distances 2,2036 Å and 1,9980 Å). Figure 5.62 on the next page illustrates the proposed binding mode.

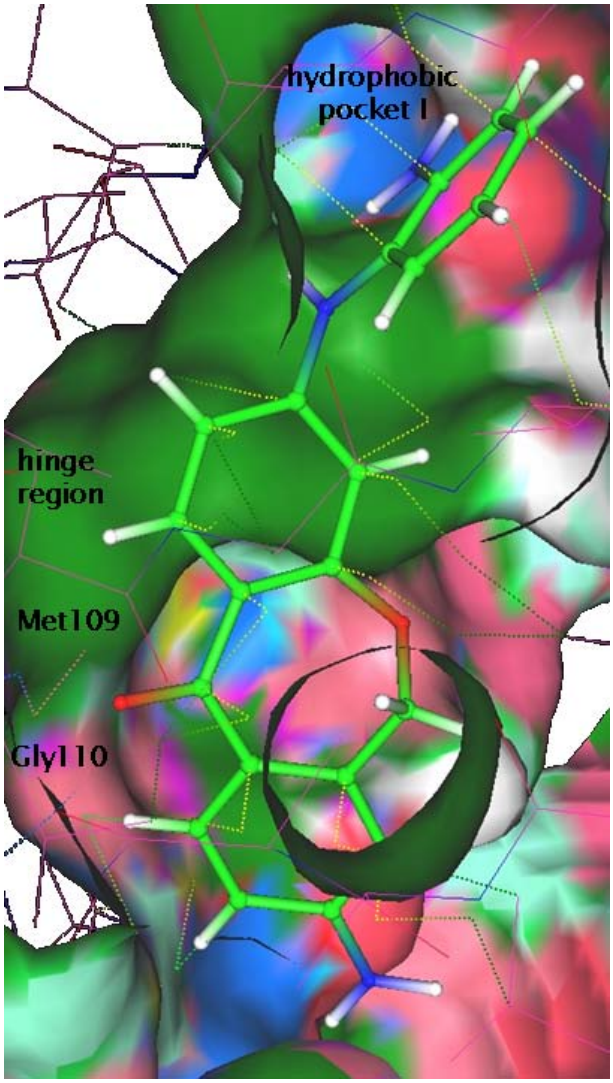

Figure 5.62.: Docking to PDB 2QD9: proposed pose of GA425min rank 2

Third ranked SK539min was similar posed, but did not form any H-bonds. The following ranks followed the poses which had been found on the first three ranks: rank one (SK383min, GA553min, SK318min, SK468min), rank 2 (SK316min, SK288min) and rank 3 (SK541min, SK558min). On the ranks 13-17 eHITS calculated for GA430min, SK508min, SK436min, SK345min and SK362min the same pose. The amino-phenol was situated in the hydrophobic pocket I, and the carbonyl oxygen pointed approximately to the DFG area. No correlation between IC_{50}, rank or composition could be observed.

PDB 1W84's first rank was occupied by MO15min, but its pose was according to Ottosen *et al.*, placing the amino-phenol to hydrophobic region II. The carbonyl oxygen pointed to Lys53. Besides MO15min was built to fail in the docking studies, because of the large substituent next

to the amino-phenol. MO38min on rank 4 is the only one until rank 13 where the carbonyl oxygen pointed to the hinge region and had its amino-phenol in the hydrophobic pocket I, but did not form any H-bonds. MO38min pops up three time during the eHITS docking studies (rank one PDB 2QD9 and later (278SLS)), although it has the wrong position of the oxygen in the seven-membered ring. Its pose was hardly obtained by docking the suberones in PDB 1W84 (exceptions MO36min (rank 21), MO35min and MO7min (rank 25-rank 26)). The other compounds (GA, JH, OTTO or REV) have their amino-phenol in the hydrophobic region II and/or their carbonyl oxygen pointing to Lys53. On rank 87 the first SK compound was situated (SK9min), but with no comprehensible pose.
Altogether two poses appeared. In case of pose one the compounds were situated outside of the ATP binding pocket and did not have any H-bonds. Or their amino-phenol was situated in the hydrophobic pocket I, while the carbonyl oxygen pointed to Lys53 or the amino-phenol was situated in the hydrophobic region II instead. PDB 2FSO yielded to very poor results (figure 5.63).

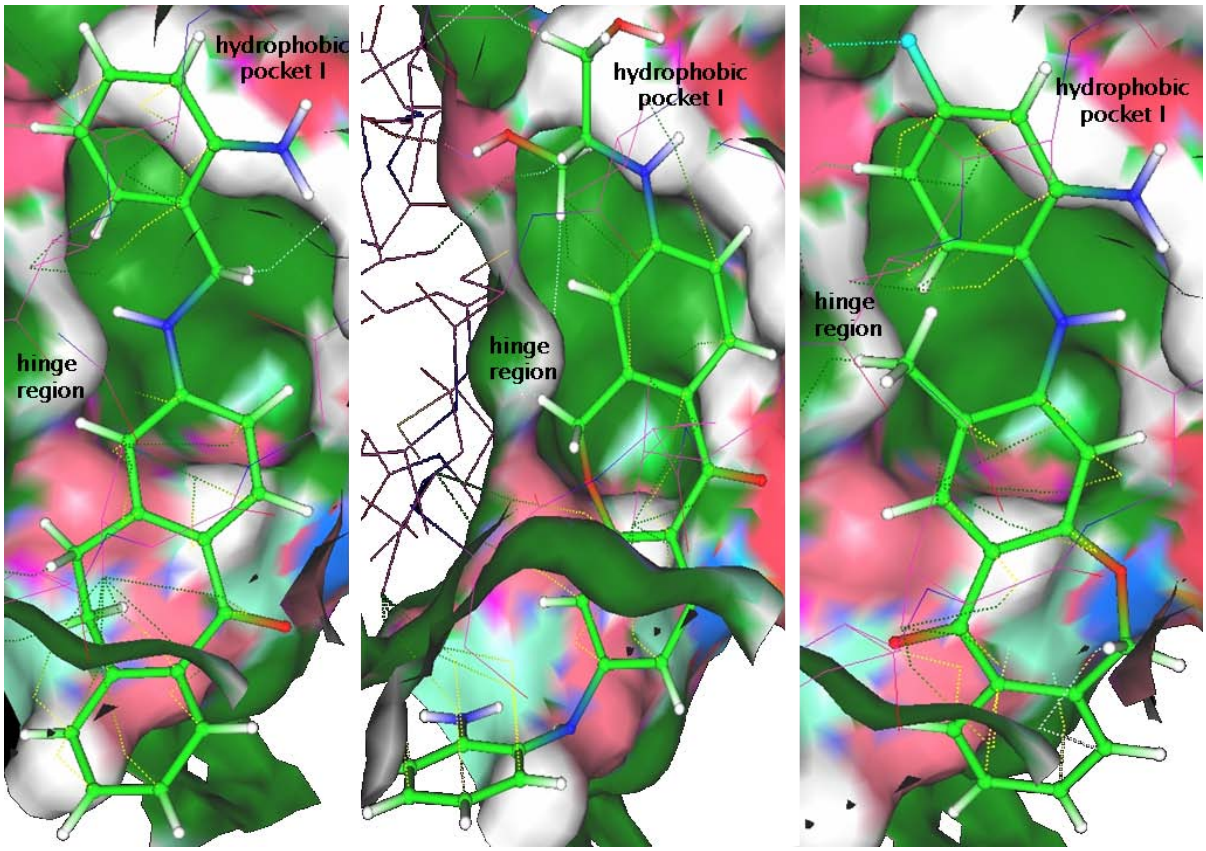

Figure 5.63.: Docking to PDB 2FSO yielded in very poor results, left RN14min, middle GA17min, right MO23min

The first rank in PDB 1WBS (DFG-OUT conformation), the X-ray structure of the DFG-OUT conformation, was REV6min. The pose is visualized in figure 5.64.

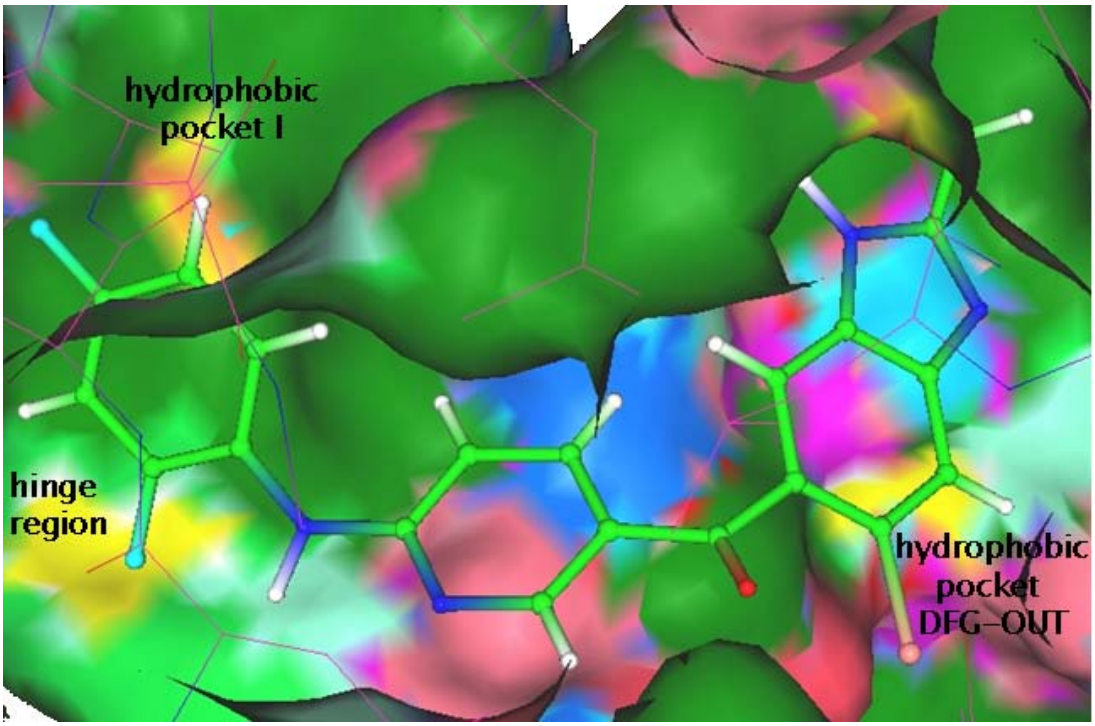

Figure 5.64.: Docking to PDB 1WBS, REV6min, rank one

The interaction file revealed only one H-bond interaction between the lone pair of the -NH linker atome of the amino-phenol and the -NH_{3+} of Lys53. The amino-phenol was situated in hydrophobic pocket `I`, while the carbonyl oxygen pointed to the DFG loop region, but formed no H-bond interactions. All the following poses of all left Suberone compounds were found as pictured below (figure 5.65).

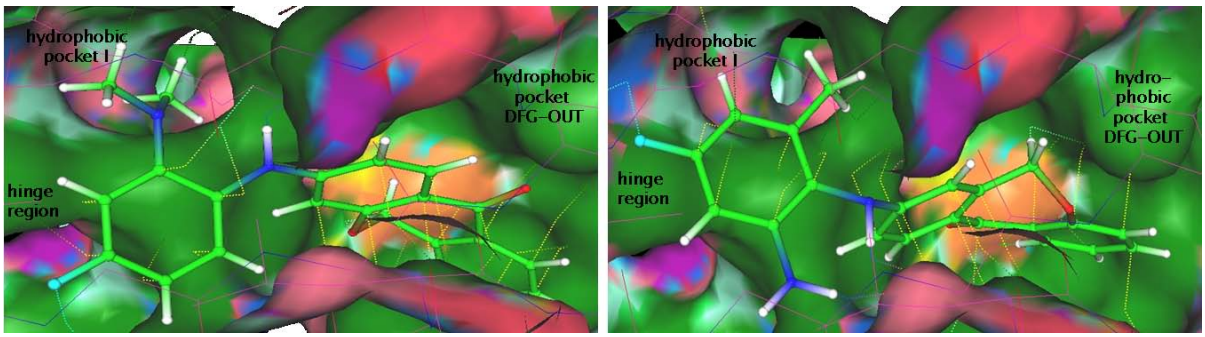

Figure 5.65.: Docking to PDB 1WBS, left docked binding poses are all alike MO39min (rank 7) and right MO36min (rank 8)

In both cases the amino-phenol was situated in front of the hydrophobic pocket I. Then either the Suberone were posed similar to MO39min, where the carbonyl oxygen pointed to DFG loop or similar to MO36min, where the carbonyl oxygen was about faced. Two additional H-bonds were found in these poses. The amine linker formed one to H-bond to the side chain oxygen of Glu71 (distance 2,6759 Å) and in case of MO36min the -NH_2 to the backbone oxygen of Asp168 (distance 2,2258 Å).
Neither of these poses seemed likely however and was supported by the results in the following section. But in the end eHITS supported the results GLIDE had given, so that the Suberones may rather take up the binding pose proposed by Revesz *et al.*.

5.5. X-ray crystal structure 278SLS

In cooperation with the biochemistry department (Prof. Stehle, J. Romir) a X-ray crystal structure was obtained with NR13a as ligand in September 2007. It revealed that the suspicions of the binding mode suggested by the docking studies are correct. The oxygen of NR13a binds to the hinge region residues Met109 (NH) and Gly110(NH) (distances 1,920Å and 2,063Å). For this the hinge region performed a "flip", so that the NH of Gly110 is able to form the H-bond. The amino-phenyl lies in the hydrophobic pocket I just as the docking studies and Revesz *et al.* had proposed (figure 5.66 on the next page).

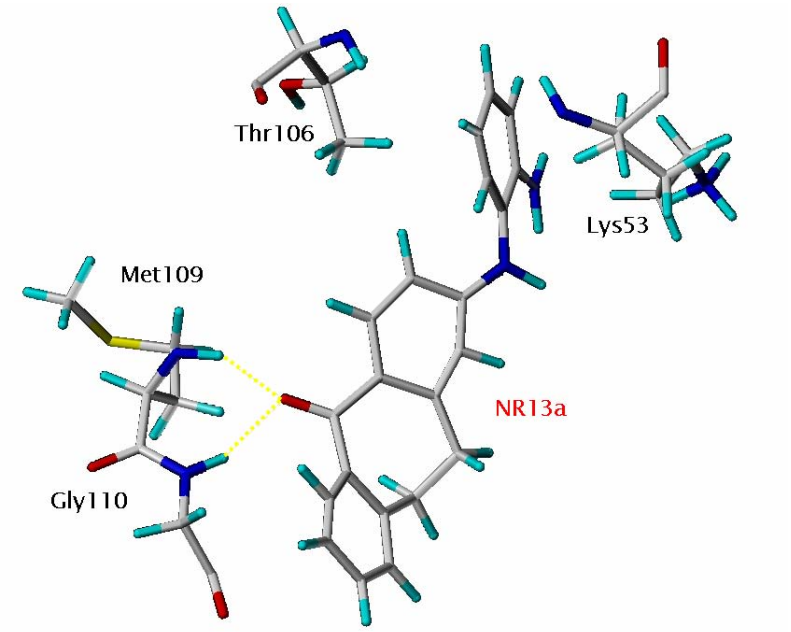

Figure 5.66.: Binding mode of NR13a in 278SLS, shot taken in SYBYL7.2

In the end the refined structure revealed two additional water mediated H-bonds.The H of the amine linker formed an H-bond over the oxygen of water1 with a hydrogen of Lys53, while the H of the amino-phenol formed over the oxygen of water2 an H-bond with the backbone NH of Asp168 (figure 5.67).

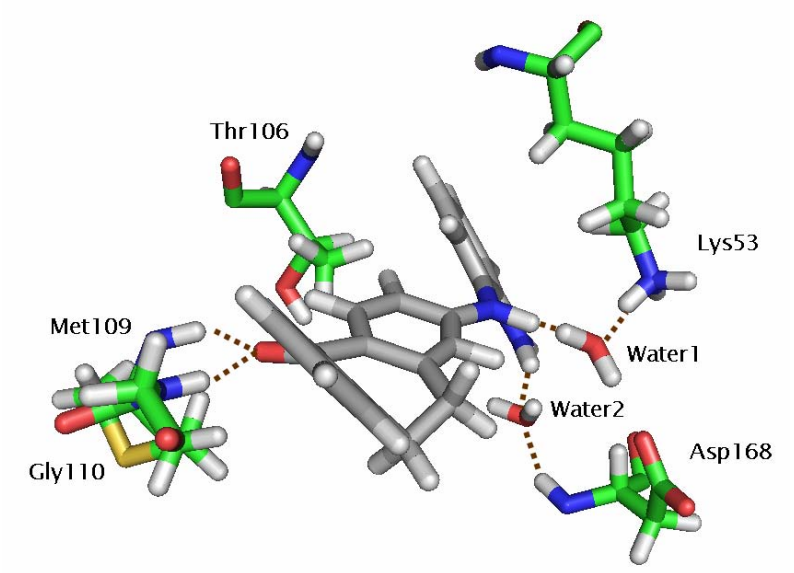

Figure 5.67.: Binding mode of NR13a in the refined 278SLS (now MK38), shot taken in GLIDE

The next step was to compare 278SLS with the chosen PDB structures to identify the differences. The alignments by homology may explain the problems which occurred in the docking studies (see table 5.14).

No.	All atoms	2FSO	2GFS	1OZ1	1W84	2I0H	2PKJ	1WBS	2GTN	2QD9
1	ASP112 N	1.61	0.71	1.99	1.56	0.44	1.24	1.97	0.63	0.82
2	ASP112 OD1	2.07	1.05	2.56	2.25	0.50	1.46	2.81	1.16	1.99
3	ASP112 OD2	1.44	3.21	2.00	1.76	0.68	3.13	1.92	0.99	1.53
4	ASP112 CG	1.45	1.19	2.04	1.68	0.54	1.27	2.09	0.73	1.34
5	ASP112 CB	1.48	0.91	1.84	1.49	0.51	1.26	1.88	0.76	1.11
6	ASP112 O	1.84	0.97	2.37	1.84	0.37	1.52	2.40	1.14	1.51
7	ASP112 C	1.50	0.77	1.87	1.50	0.39	1.27	1.91	0.73	0.97
8	ASP112 CA	1.55	0.74	1.83	1.44	0.39	1.25	1.87	0.70	0.90
9	ALA111 N	0.98	0.86	1.62	1.41	0.97	0.88	1.29	0.31	0.21
10	ALA111 CB	1.19	0.76	2.02	1.62	0.87	0.95	1.95	0.22	0.56
11	ALA111 O	0.90	0.91	1.41	1.23	0.77	1.24	1.61	0.22	0.21
12	ALA111 C	1.22	0.77	1.76	1.44	0.64	1.16	1.76	0.32	0.37
13	ALA111 CA	1.17	0.65	1.94	1.61	0.83	0.95	1.77	0.27	0.36
14	GLY110 N	0.55	1.04	1.15	1.30	1.12	0.46	1.87	0.25	0.34
15	GLY110 O	0.71	0.60	2.25	1.81	1.36	0.51	2.00	0.32	0.20
16	GLY110 C	0.70	0.86	1.31	1.18	1.25	0.64	1.11	0.23	0.22
17	GLY110 CA	0.50	1.27	1.39	1.47	1.43	0.57	1.63	0.20	0.53
18	MET109 N	1.82	1.23	2.44	2.12	0.59	0.29	2.02	0.27	0.24
19	MET109 CE	2.56	2.69	9.93	9.84	2.30	2.64	9.16	2.23	2.18
20	MET109 SD	1.91	1.72	7.07	7.03	1.05	1.34	6.54	0.97	1.11
21	MET109 CG	1.64	1.47	4.94	4.64	0.39	1.00	4.37	0.38	0.32
22	MET109 CB	2.02	1.28	2.69	2.37	0.52	0.86	2.94	0.50	0.38

23	MET109 O	4.54	3.25	4.92	4.87	1.18	0.59	1.75	0.31	0.30
24	MET109 C	2.32	1.32	2.86	2.78	0.97	0.46	1.93	0.26	0.19
25	MET109 CA	2.00	1.26	2.60	2.41	0.64	0.37	2.31	0.28	0.11
26	LEU108 N	1.52	1.11	1.88	1.53	0.41	1.00	1.44	0.24	0.36
27	LEU108 CD1	2.03	1.71	2.40	2.09	0.71	1.23	1.86	0.61	0.52
28	LEU108 CD2	1.49	1.42	2.10	1.69	0.65	1.58	1.61	0.69	0.43
29	LEU108 CG	1.44	0.96	1.82	1.42	0.46	1.28	1.61	0.90	0.89
30	LEU108 CB	1.61	1.29	2.01	1.63	0.50	1.40	1.65	0.66	0.72
31	LEU108 O	2.07	1.34	2.51	2.02	0.69	1.56	2.06	0.52	0.63
32	LEU108 C	1.83	1.27	2.35	1.97	0.58	0.78	1.90	0.19	0.33
33	LEU108 CA	1.68	1.21	2.09	1.71	0.49	1.02	1.61	0.33	0.43
34	HIS107 N	1.31	0.94	1.42	1.21	0.49	0.93	1.10	0.08	0.38
35	HIS107 ND1	3.00	2.68	1.55	1.28	2.10	1.07	3.00	1.56	0.58
36	HIS107 CE1	2.99	2.57	1.61	1.38	1.78	1.89	2.65	2.01	0.63
37	HIS107 NE2	1.72	1.25	1.78	1.56	1.38	2.01	1.44	1.94	0.61
38	HIS107 CD2	2.34	2.10	1.84	1.59	2.44	1.74	2.17	1.49	0.65
39	HIS107 CG	1.61	1.10	1.72	1.44	0.73	0.97	1.41	0.88	0.62
40	HIS107 CB	1.74	1.29	1.80	1.47	0.82	0.97	1.40	0.14	0.76
41	HIS107 O	1.63	1.39	1.77	1.36	0.66	0.90	1.18	0.26	0.58
42	HIS107 C	1.53	1.18	1.76	1.41	0.52	0.95	1.29	0.14	0.42
43	HIS107 CA	1.43	1.02	1.62	1.32	0.51	0.94	1.26	0.05	0.51
44	THR106 N	1.05	0.85	1.17	0.92	0.41	0.79	0.85	0.07	0.19
45	THR106 CG2	2.58	2.63	1.19	1.09	2.37	1.19	0.72	2.40	0.45

46	THR106 OG1	3.96	3.53	1.22	0.99	3.04	1.21	0.63	2.52	0.44
47	THR106 CB	1.42	1.13	1.18	0.95	0.68	1.08	0.65	0.09	0.41
48	THR106 O	1.24	0.79	1.35	1.17	0.17	0.83	1.13	0.18	0.16
49	THR106 C	1.26	0.87	1.33	1.12	0.35	0.88	1.05	0.02	0.17
50	THR106 CA	1.20	0.92	1.19	0.96	0.46	0.88	0.85	0.07	0.20
51	VAL105 N	0.70	0.71	0.97	0.81	0.37	0.57	0.69	0.08	0.20
52	VAL105 CG2	0.72	0.70	1.24	0.84	0.25	0.75	1.04	0.29	0.22
53	VAL105 CG1	0.56	0.62	0.89	0.77	0.23	0.65	0.99	0.17	0.08
54	VAL105 CB	0.71	0.72	1.12	0.83	0.25	0.70	0.96	0.18	0.14
55	VAL105 O	0.99	0.78	1.17	0.97	0.44	0.70	0.81	0.07	0.27
56	VAL105 C	0.94	0.81	1.16	0.91	0.39	0.73	0.84	0.06	0.19
57	VAL105 CA	0.82	0.79	1.12	0.89	0.36	0.69	0.88	0.09	0.15
58	LEU104 N	0.63	0.73	0.89	0.69	0.32	0.47	0.67	0.38	0.24
59	LEU104 CD1	0.82	0.79	0.86	0.78	0.61	0.45	0.77	0.61	0.59
60	LEU104 CD2	0.69	0.55	0.55	0.43	0.37	0.32	0.40	0.48	0.36
61	LEU104 CG	0.70	0.68	0.79	0.65	0.47	0.39	0.59	0.42	0.55
62	LEU104 CB	0.68	0.66	0.91	0.72	0.43	0.39	0.64	0.41	0.42
63	LEU104 O	0.83	0.81	1.11	0.86	0.42	0.66	1.04	0.37	0.51
64	LEU104 C	0.70	0.71	0.99	0.76	0.28	0.50	0.76	0.24	0.23
65	LEU104 CA	0.58	0.64	0.86	0.64	0.28	0.41	0.60	0.34	0.24
	Average	1.48	1.21	1.94	1.68	0.76	1.00	1.71	0.56	1.27

Table 5.14.: Alignment by homology of all hinge region atoms, 278SLS is fixed

The alignments reveal that only PDB 2I0H, PDB 2GTN and PDB 2QD9 share the observed "flip" of Met109 and Gly110 (atoms 14-25) in the hinge region which is required for the binding of the Suberones. Others like PDB 1W84 or PDB 1OZ1 do not include the required flip and therefore the dockings with those resulted in wrong docking poses. In figure 5.68 the differences can be observed. PDB 2GTN shares the flip with 278SLS, while the hinge region of PDB 1W84 does not perform a flip.

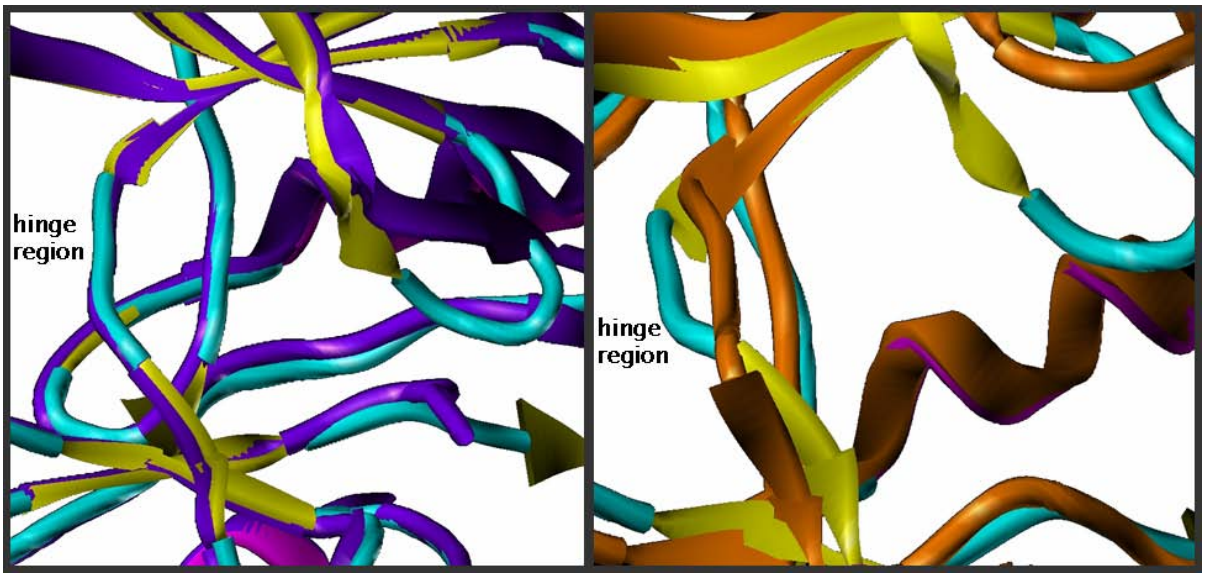

Figure 5.68.: Left: 278SLS (colored by atom) and PDB 2GTN (purple) aligned by homology; right: 278SLS (colored by atom) and PDB 1W84 (orange) aligned by homology, shots taken in SYBYL7.2

The loop regions, especially the Gly-rich loop, point at major differences. The real state can not be determined, because the electron density was very low in that regions and was only assumed by the depositer. The conformation of the backbone of Thr106 (atoms 44, 48, 49, 50) which limits the left side of the hydrophobic pocket I is not relevant for it does not take part in the flip, indicated by the fact that all PDB structures have very low RMSD values there. The position of the oxygen of the side chain (atom 46 (OG1)) on the other hand differs greatly. There are some PDB structures where the oxygen points into to the ATP binding pocket, in some cases also forming an H-bond with the ligand. Docking can therefore be influenced by the different conformations of the oxygen which can lead to wrong docking poses. That fact makes PDB 2QD9 the more similar PDB structure in comparison to PDB 2I0H and PDB 2GTN, where the oxygen points into the ATP binding pocket, when compared to 278SLS (figure 5.69).

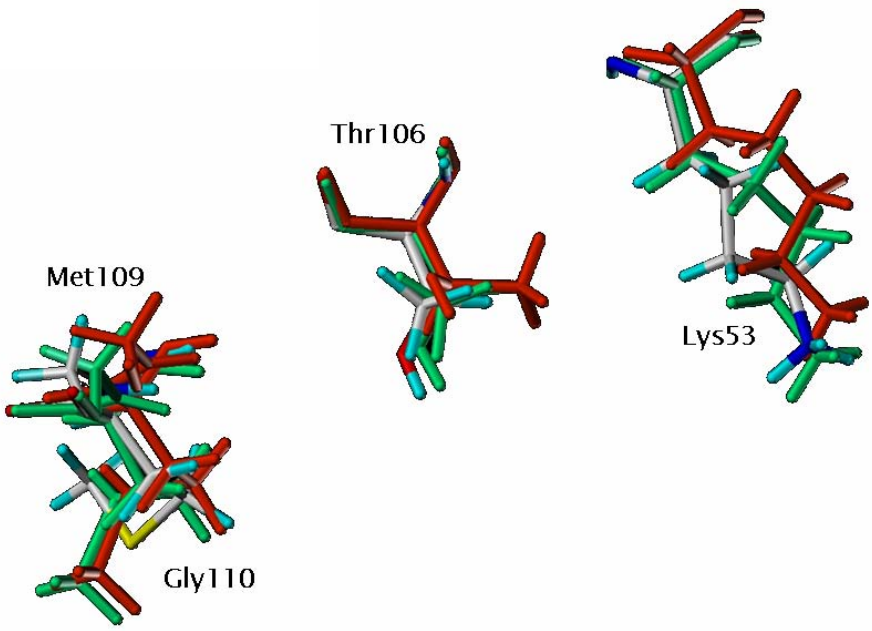

Figure 5.69.: Lys53, Thr106, Met109 and Gly110 of PDB 2I0H (red), PDB 2QD9 (green) and 278SLS (colored by atom) aligned by homology, shot taken in SYBYL7.2

Figure 5.70 shows the results of the alignment by homology in a diagram.

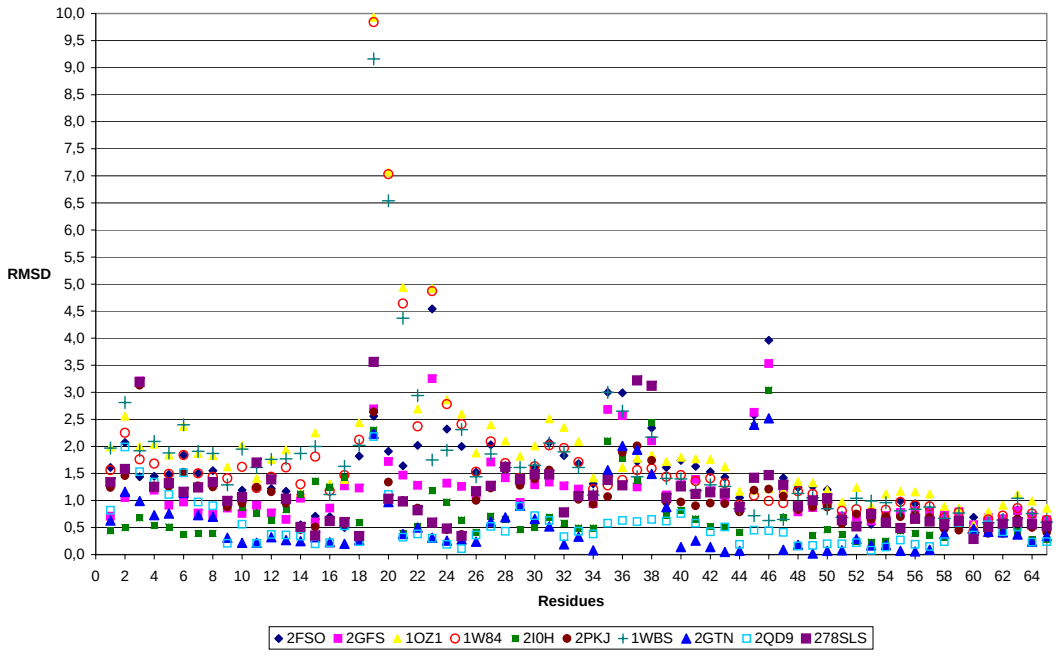

Figure 5.70.: Alignment by homology of all atoms of the hinge region, 278SLS is fixed

The conformation of Lys53 which lies on the other side of the hydrophobic pocket I does

not differ greatly among the models (see table 5.15). Therefore it has no influence on the docking. Table 5.15 on the next page also presents the differences between the chosen PDBs and 278SLS in the DFG area (in addition with Leu167).

No.	All	2FSO	2GFS	1OZ1	1W84	2I0H	2PKJ	1WBS	2GTN	2QD9
1	LYS53 N	1.21	1.05	1.28	1.17	0.46	0.75	1.00	0.27	0.28
2	LYS53 NZ	1.66	0.61	1.10	0.88	0.82	1.49	0.84	0.63	0.41
3	LYS53 CE	2.12	1.48	1.12	0.96	0.66	1.95	0.46	0.70	0.47
4	LYS53 CD	1.70	1.64	2.18	1.76	2.19	1.25	1.45	1.44	1.70
5	LYS53 CG	1.61	1.33	1.97	1.65	1.31	0.88	1.32	0.71	0.58
6	LYS53 CB	1.29	1.08	1.54	1.36	0.90	0.72	1.06	0.25	0.29
7	LYS53 O	1.07	0.97	1.34	0.94	0.46	0.59	0.76	0.18	0.14
8	LYS53 C	1.22	1.07	1.41	1.15	0.60	0.67	0.89	0.23	0.19
9	LYS53 CA	1.29	1.09	1.43	1.27	0.65	0.74	1.01	0.23	0.21
	Average	1.00	1.21	1.13	1.18	1.03	1.95	2.93	0.99	0.90
No.	**All**	**2FSO**	**2GFS**	**1OZ1**	**1W84**	**2I0H**	**2PKJ**	**1WBS**	**2GTN**	**2QD9**
1	GLY170 N	-	-	4.04	1.08	2.69	4.08	8.01	8.56	3.27
2	GLY170 O	-	-	4.25	1.99	1.95	3.77	8.85	12.01	3.15
3	GLY170 C	-	-	4.23	1.06	1.71	3.56	9.33	12.30	2.83
4	GLY170 CA	-	-	3.40	1.75	2.81	4.24	7.99	10.39	3.61
5	PHE169 N	-	2.55	2.50	2.43	2.46	-	6.86	4.22	2.77
6	PHE169 CD1	-	2.47	2.74	2.37	2.1	-	13.18	7.98	1.98
7	PHE169 CE1	-	1.92	1.89	1.79	2.74	-	14.55	8.46	2.49
8	PHE169 CZ	-	1.60	2.36	1.69	1.66	-	14.86	8.48	1.63
9	PHE169 CE2	-	2.95	3.01	2.96	2.32	-	14.20	7.97	2.59
10	PHE169 CD2	-	2.26	1.61	2.17	2.86	-	13.03	7.20	3.24
11	PHE169 CG	-	1.19	1.77	1.09	1.61	-	12.27	7.27	2.07

12	PHE169 CB	-	1.60	3.32	1.60	2.26	-	11.03	7.70	2.68
13	PHE169 O	-	3.37	6.84	3.52	4.18	-	10.25	8.58	4.59
14	PHE169 C	-	1.50	4.65	1.55	2.42	-	8.95	7.55	2.96
15	PHE169 CA	-	1.36	2.66	1.23	1.65	-	8.58	5.75	1.91
16	ASP168 N	1.58	2.11	1.97	2.03	1.01	1.59	2.33	1.42	1.15
17	ASP168 OD1	5.91	6.66	5.44	6.62	2.71	5.80	2.62	7.70	5.60
18	ASP168 OD2	4.04	5.40	3.85	4.04	2.8	2.98	1.88	5.38	3.35
19	ASP168 CG	3.83	5.01	3.56	4.59	1.92	3.49	1.42	5.64	3.42
20	ASP168 CB	1.94	3.32	1.92	3.29	1.01	1.83	1.77	4.03	1.73
21	ASP168 O	2.91	4.33	3.53	4.29	3.43	3.47	4.15	3.00	2.97
22	ASP168 C	2.15	2.72	2.01	2.68	1.93	2.72	4.56	2.04	1.86
23	ASP168 CA	1.25	2.12	1.71	2.08	0.53	1.82	2.52	1.61	1.00
24	LEU167 N	1.37	1.25	1.51	1.35	1.02	1.21	1.50	0.93	0.90
25	LEU167 CD1	2.98	2.39	4.07	3.91	2.08	3.28	3.60	2.15	1.03
26	LEU167 CD2	1.45	2.08	2.47	2.44	1.8	2.07	1.35	2.25	2.25
27	LEU167 CG	2.10	1.73	2.21	2.17	1.14	1.67	1.72	1.31	0.77
28	LEU167 CB	2.13	1.42	1.89	1.93	1.86	1.34	1.66	1.31	1.47
29	LEU167 O	1.25	0.95	1.38	1.28	1.02	1.70	1.56	1.44	1.11
30	LEU167 C	1.15	1.23	1.42	1.37	0.58	1.32	1.65	1.08	0.83
31	LEU167 CA	1.60	1.34	1.68	1.60	1.15	1.30	1.56	1.05	1.04
	Average	2.35	2.48	2.90	2.39	1.98	2.66	6.38	5.38	2.33

Table 5.15.: Alignment by homology of all DFG atoms, 278SLS is fixed

PDB 1WBS has the highest average RMSD obviously, because here the DFG is in the DFG-OUT conformation. PDB 2GTN has also a very high average RMSD. The loop in this PDB structure is very unusual, because it lies in the ATP pocket. The other PDB structures are very similar in the DFG region in comparison with 278SLS. The DFG region of 2IOH is the most similar one when compared to 278SLS. The highest calculated RMSD values occur at Phe169, however all conformations of Leu167 are rather the same. Asp168 which is directly situated next of Phe169 has surprisingly low RMSD values. The highest concern the side chain oxygens. At the backbone the nitrogen and the C-α atome have very low RSMD values. Therefore here another "flip" which concerns only a very local region can be observed. Figure 5.71 visualizes the alignment of the DFG atoms and Leu167.

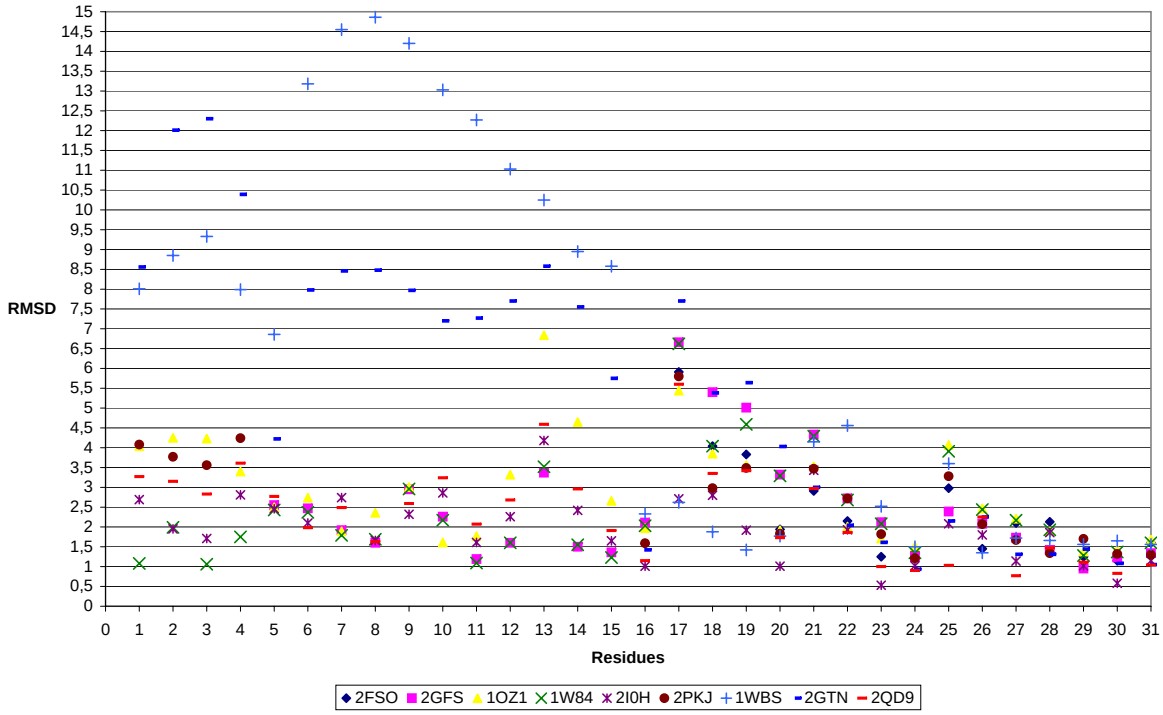

Figure 5.71.: Alignment by homology of all DFG atoms, 278SLS is fixed

Combining all facts so far PDB 2QD9 is the most similar to 278SLS, when regarding the hinge- and DFG region. The only remaining problem is the Gly-rich loop. If it's conformation in the X-ray crystal structure 278SLS is the real state, but might cause problems with further dockings. It may be therefore wise to use both, PDB 2QD9 together with 278SLS, for further dockings to judge any poses correctly and not be wrongly influenced by the Gly-rich loop.
The ligand of 278SLS can not be compared to the generated molecules in the database. The conformation of the ligand is as seen in figure 5.72 badly resolved. The state of ring B is

obviously unusual.

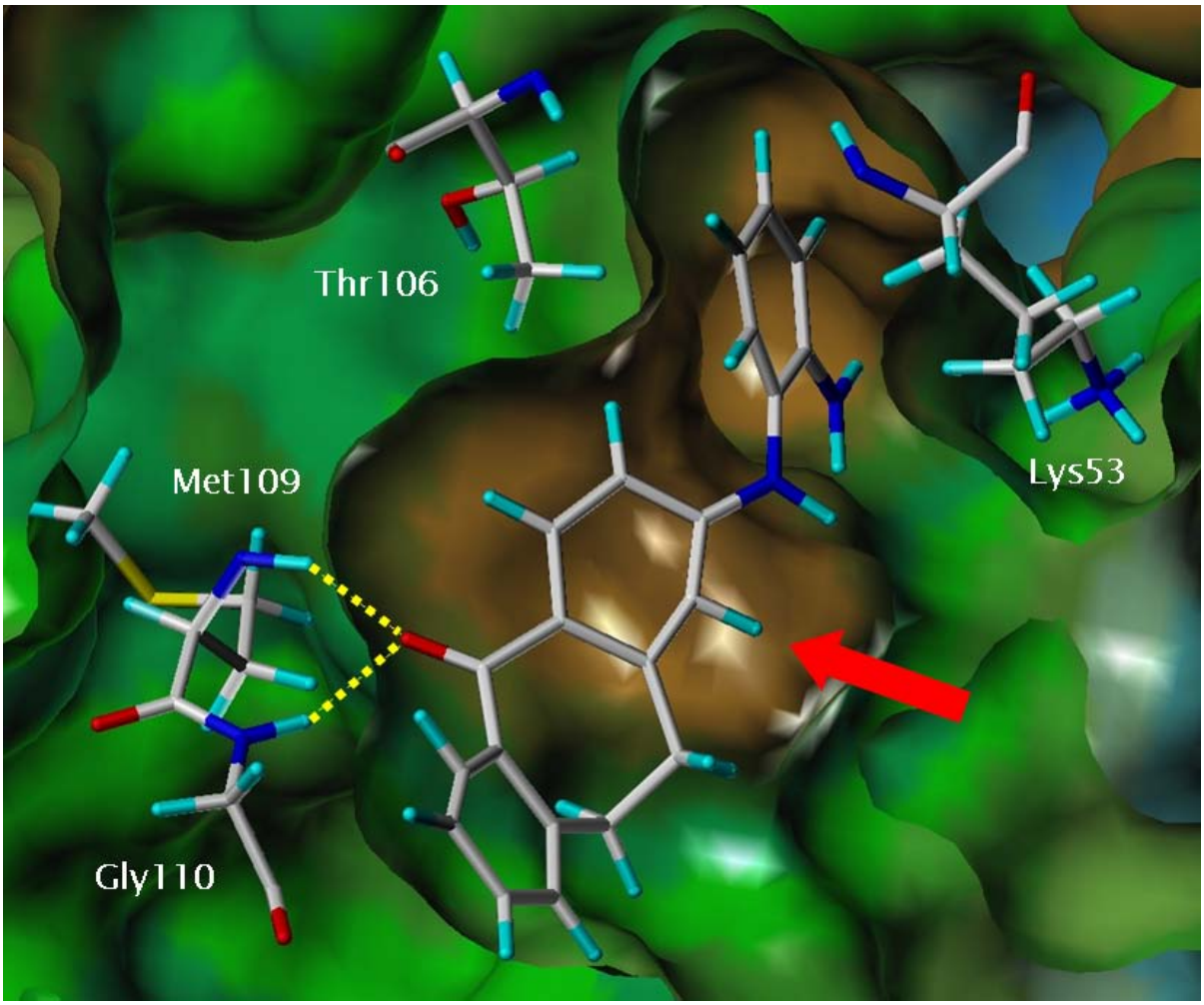

Figure 5.72.: 278SLS (MOLCAD surface representation) with ligand (stick representation), ring B marked with red arrow, shot taken in SYBYL7.2

In table 5.16 the WHAT IF report is presented. The values are not good. If this had been a published structure it would not have been chosen for the docking studies. The X-ray structure needs more refinement.

	278SLS
2nd generation packing quality	*-1.755*
Ramachandran plot appearance	*-2.779*
χ-1/χ-2 rotamer normality	*-3.207*
Backbone conformation	*-6.529*
Resolution	1.95

Bond lengths	*0.537*
Bond angles	*0.612*
Omega angle restraints	*1.449*
Side chain planarity	*0.249*
Improper dihedral distribution	0.521
B-factor distribution	0.349
Inside/Outside distribution	1.058

Table 5.16.: WHAT IF report of 278SLS; the first 5 values represent Structure Z-scores (positive is better than average) following represent RMS Z-scores (should be close to 1.0)

5.5.1. Docking studies with 278SLS

5.5.1.1. FlexX

FlexX was not used, because GLIDE and eHITS were found to be superior to FlexX. So Flexidock was not used either to check the FlexX results.

5.5.1.2. GLIDE

The complete Suberone database was docked to 278SLS. REV4min occupied the first rank. The carbonyl oxygen formed two H-bonds to Met109 and Gly110 (distance 2,001Å and 2,102 Å) and the hydrophobic pocket I accommodated the amino-phenol (figure 5.73 on the next page). The next ranks were also occupied by REV compounds (REV6min and REV5min) which took up then same pose. SK468min had its carbonyl oxygen pointed to the side chain hydroxyl group of Tyr35, whereas the nitrogen of the pyridine interacted with the backbone -NH of of Gly110 (figure 5.74). This pose occurred when a compound had the pyridine alike SK468min (e.g. SK383min (rank 74)). The other poses (most of them took up by REV compounds) were alike the one of rank one or alike rank 22 where SK510 was posed alike, but only formed an H-bond to Gly110 (see figure 5.75). On later ranks (from 200) some more irrelevant poses occurred, but until then most of the poses were very similar to the X-ray crystal structure.

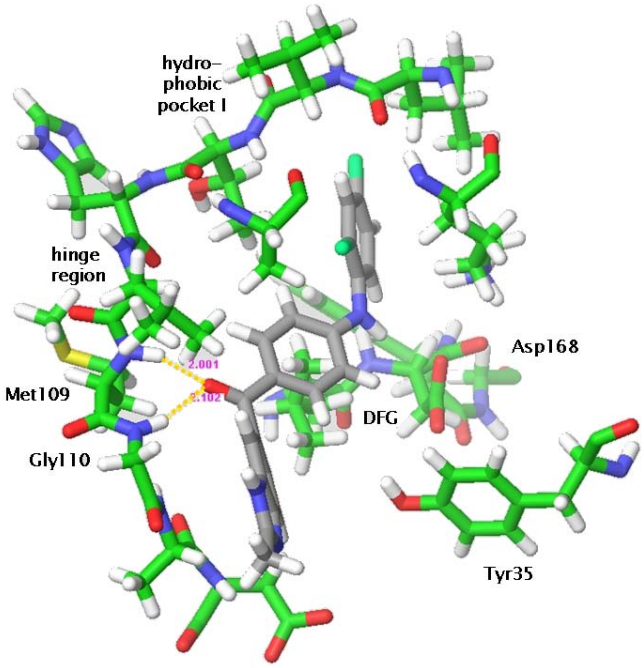

Figure 5.73.: Docking of 278SLS (green stick representation): REV4min; rank one (grey stick representation)

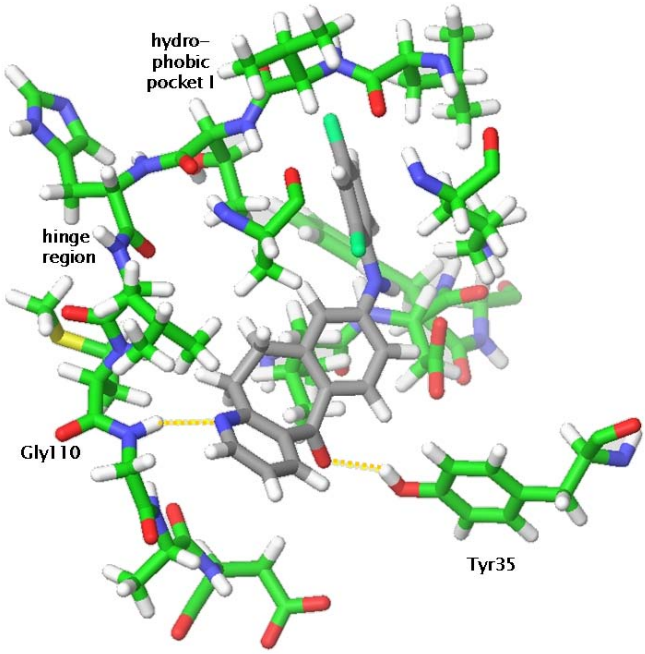

Figure 5.74.: Docking of 278SLS (green stick representation): REV4min; rank one (grey stick representation)

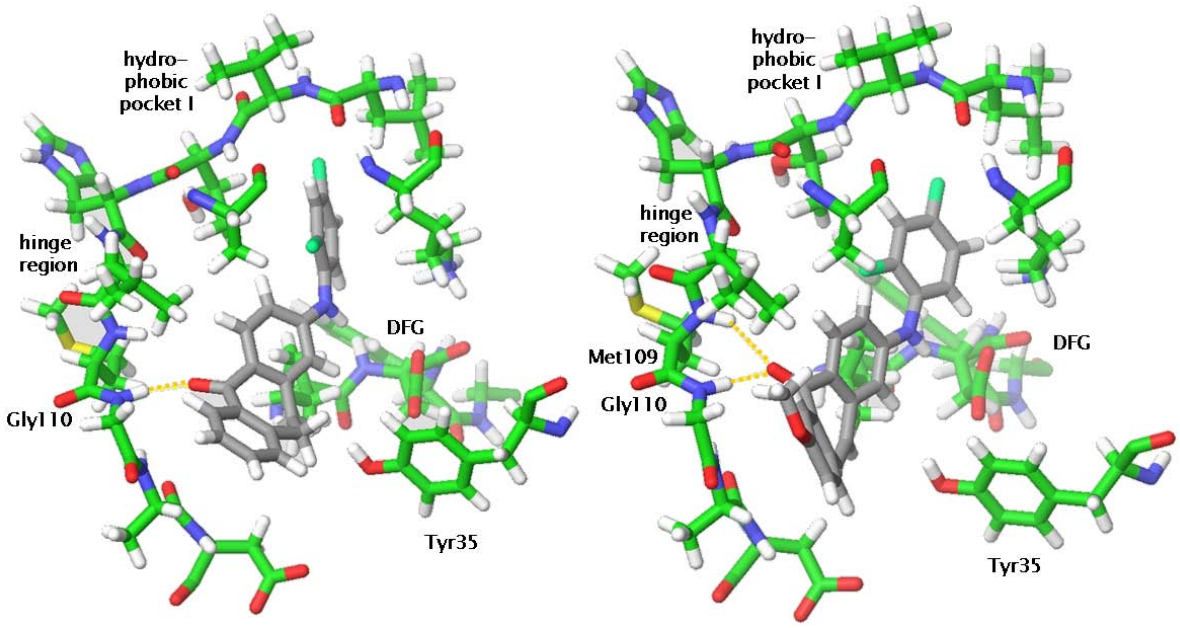

Figure 5.75.: Docking of 278SLS (green stick representation): left SK539min; rank 50 (grey stick representation), right SK508min; rank 77 (grey stick representation)

5.5.1.3. eHITS

Thus the ligand in 278SLS was so badly refined, as mentioned before, SYBYL7.2 was used to determine the correct atom types, e.g. that in the carbonyl C and O are sp^2 hybridised, so that the correct number of hydrogens is added. The modified ligand was saved in the PDB file. Two re-docking studies were started (water was kept), surprisingly disclosing that the modified PDB file resulted in less good poses; sometimes lacking H-bonds to the hinge region or even reversed. Figure 5.76 on the next page shows the differences between the re-dockings. It also demonstrates that eHITS is unable to recognize the oxygen as sp^2 hybridised.

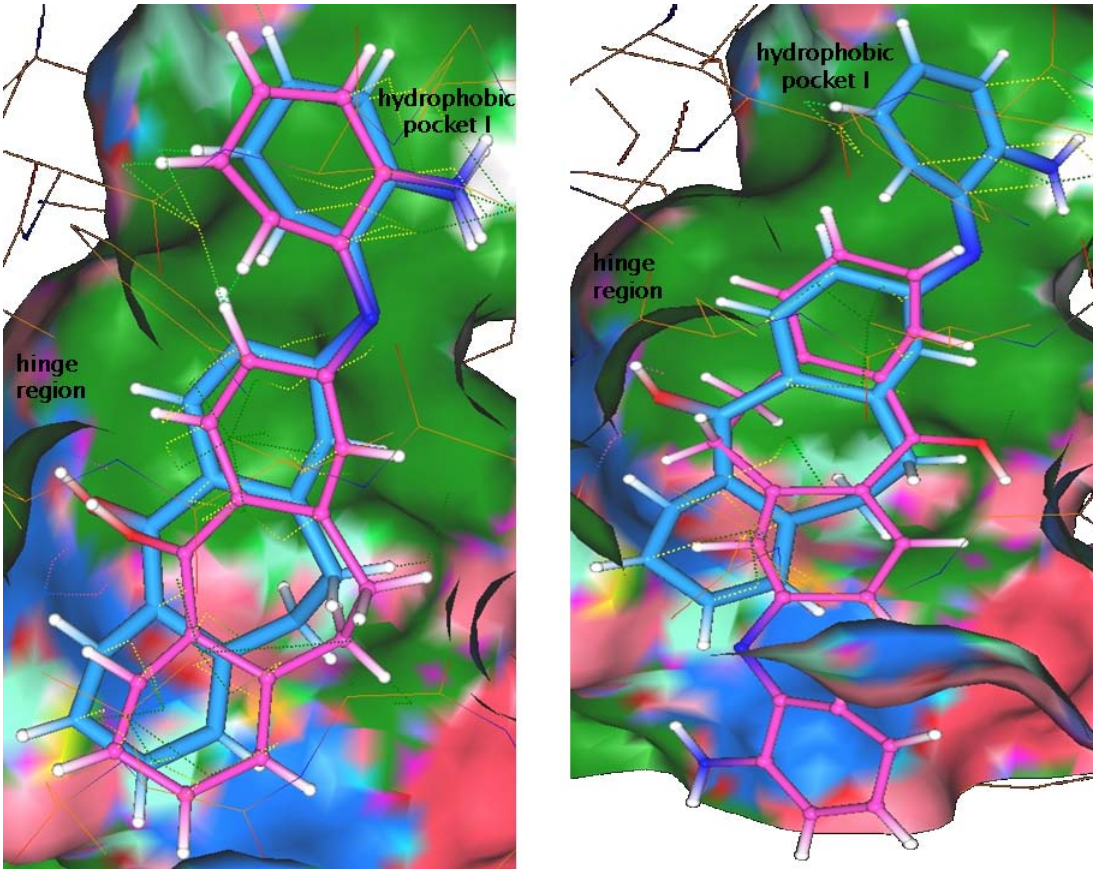

Figure 5.76.: Re-docking studies of 278SLS: docking result with unmodified ligand (left blue stick representation original ligand) and result with modified ligand (right pink stick representation docked ligand)

Docking of the Suberones placed MO38min on the first rank (just like the docking to PDB 2QD9). It had the oxygen of the seventh ring on the opposite side of the amino-phenol. But this time the interaction-file revealed two H-bonds of the carbonyl oxygen to the NH of Met109 and Gly110 and an additional between NH_2 and a side chain oxygen of Asp168 (figure 5.77 on the next page). The pose is in agreement with the proposed binding mode of Revesz *et al.*.

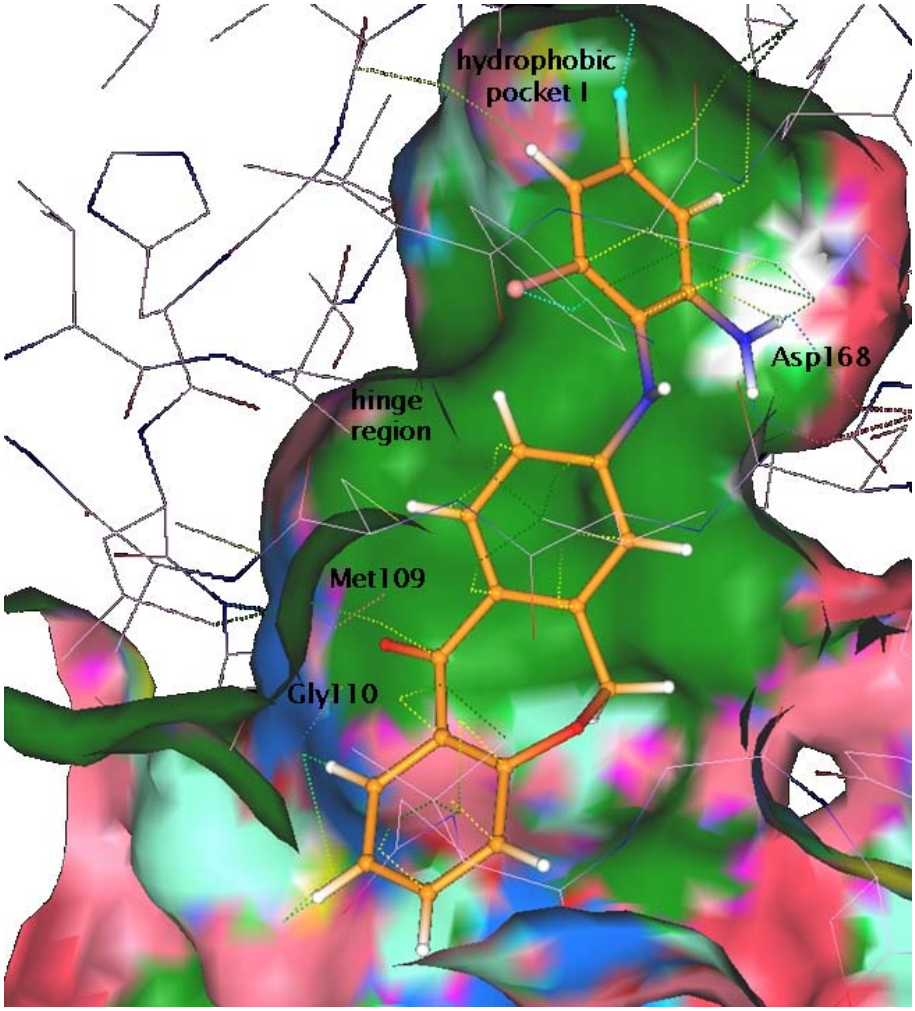

Figure 5.77.: Docking of the Suberones to 278SLS: MO38min (rank one) has three H-bonds; to Met109 distance: 2,9383Å to Gly110 distance: 2,3915Å and to Asp168 distance: 1,1317 Å

GA4min (rank 36) and GA11min (rank 64) formed two H-bonds to Met109 and Gly110. The two GA compounds have the oxygen of the seventh ring on the opposite side of the aminophenyl. Several other compounds had at least one H-bond to Met109 (e.g. GA13min (rank 43) and RN14amin (rank 48)) RN14amin is the SYBYL7.2 built ligand and very similar to the ligand of 278SLS (figure 5.78 on the next page). The two carbons of the seven-membered ring are only sp^2 hybridised in the case of RN14amin. Here it formed no additional H-bond to Asp168.

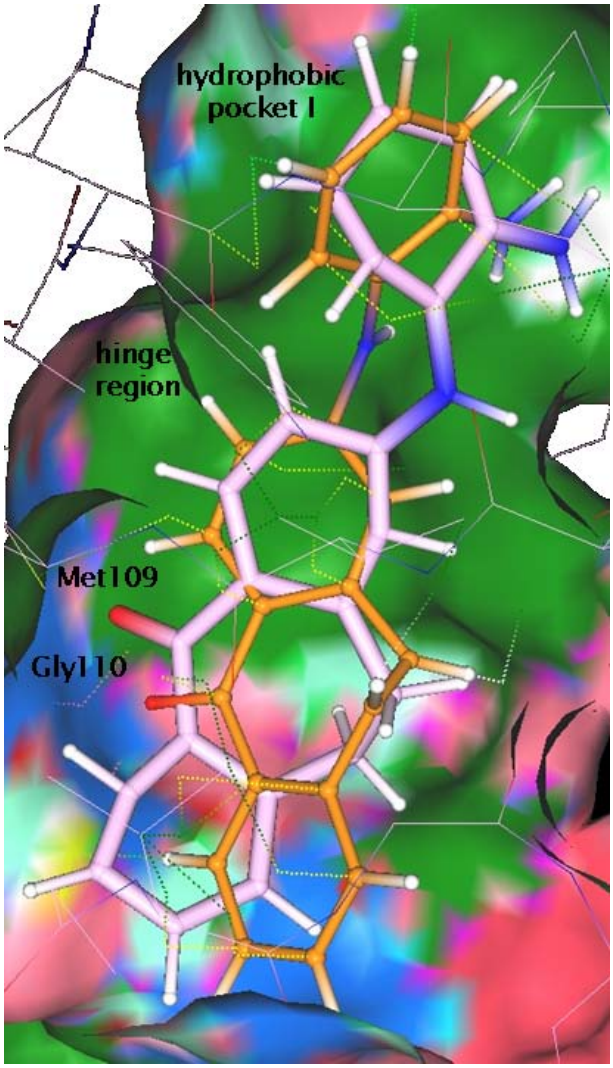

Figure 5.78.: Docking of the Suberones to 278SLS: RN14amin (orange stick representation, rank 48) has one H-bond to Gly110: distance 2,192Å, and the ligand of 278SLS (pink stick represenation)

All carbonyl oxygens of the other compounds did not form any H-bonds, but still pointed to the hinge region. However the majority of the carbonyl oxygens pointed to the opposite site of the hinge region. But all amino-phenyl substituents were situated in the hydrophobic pocket I.

Thus SG ligands were added later to the database, they were docked exclusively in PDB 2QD9 (see also section eHITS) and 278SLS. On the first rank SK541min was situated. The hydrophobic pocket I contained the amino-phenol substituent, but the carbonyl oxygen did not point to the hinge region, but rather to Lys53. A single H-bond interaction was found between the side chain oxygen of Asp168 and the -NH (distance 2,5408 Å). Second ranked

SK468min formed with its carbonyl oxygen an H-bond to Lys53 (distance 1,7600 Å), whereas the amino-phenol was situated in the hydrophobic region II. Figure 5.79 presents the two proposed binding poses.

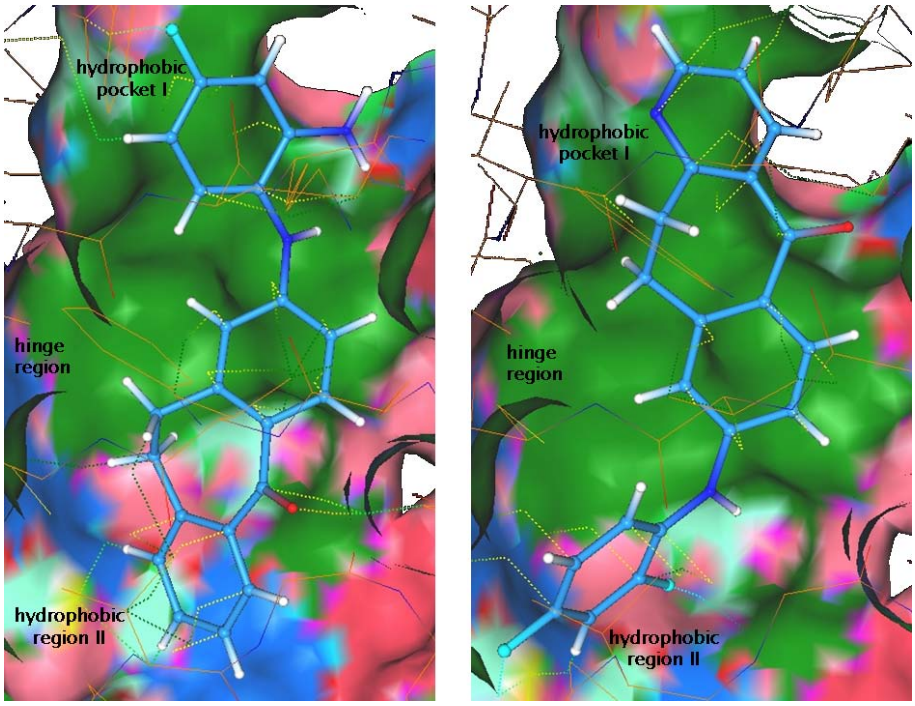

Figure 5.79.: Docking of the Suberones type SG in 278SLS; left rank one (SK541min) and right rank two (SK468min)

Third ranked GA430min was a little shifted to the front (hear hydrophobic region II) and still had its amino-phenol in hydrophobic region II. Just a few compounds were posed with their carbonyl oxygen pointing to the hinge region (SK510min, SK318min, SK539min, SK558min). All the rest of the compounds were posed alike SK541min. In the end the eHITS docking results were not very good.

5.6. MORE2 compounds

The MORE2 compounds were built to test if the amine linker of the amino-phenol could be replaced by an oxygen linker and if the -NH_2 could be replaced by a methoxy group. GLIDE was used for the docking, because due to the above described results it had proved to deliver the best results. The three X-ray strucutures PDB 2I0H, PDB 2QD9 and 278SLS were used, because their conformation mirror the actual induced-fit state during the presence

of the Suberone compounds (278SLS of course is the actual induced-fit state). The docking yielded to three different rankings:

- PDB 2I0H: MORE3min, MORE1min, MORE4min, MORE2min
- PDB 2QD9: MORE2min, MORE3min, MORE1min, MORE4min
- 278SLS: MORE4min, MORE2min, MORE1min, MORE3min

In case of PDB 2I0H all poses were alike. The carbonyl oxygen pointed to the hinge region, but without any H-bonds. The amino-phenol occupied hydrophobic pocket I and only MORE1min was anchored to it by an H-bond between the -NH_2 to the backbone oxygen of Leu104. Two of the results of the PDB 2QD9 ranking (MORE3min and MORE1min) differed , because they had the carbonyl oxygen directed to Lys53, but maintained with their amino-phenol in the hydrophobic pocket I. This also happened to all MORE compounds apart from MORE1min in case of the docking to 278SLS. Figure 5.80 shows the two binding poses. Left is the reasonable pose, whereas the right one with the bad contact between Lys53 and the oxygen, and the ugly contact between Tyr53 and hydrogen (presented through the red dashed line) is rather unlikely.

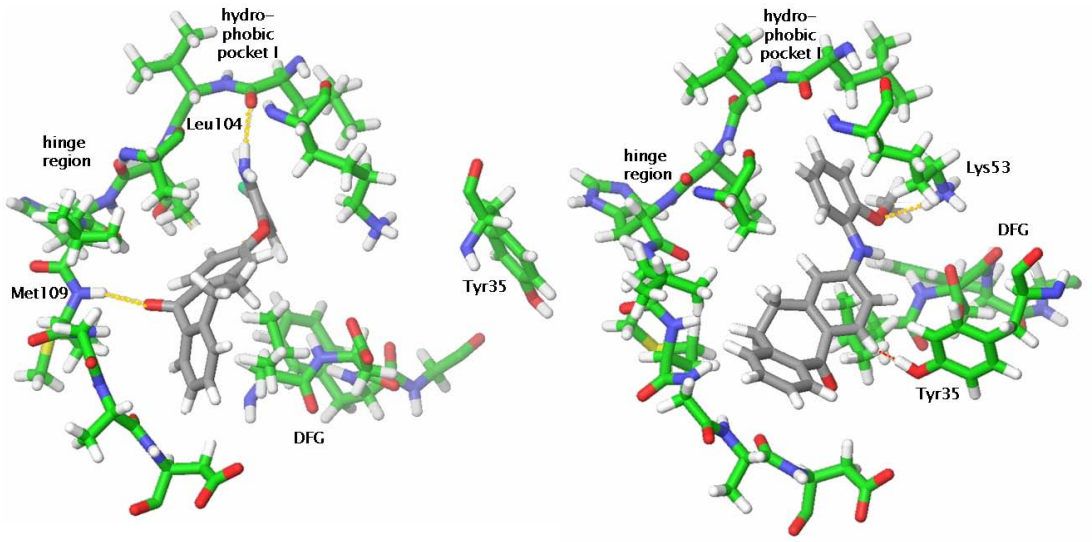

Figure 5.80.: Docking of the MORE2 compounds to PDB 2QD9 and 278SLS (green stick representation); left MORE2min (grey stick representation) in PDB 2QD9; rank one, right MORE3min (grey stick representation) in 278SLS; rank 4

The docking supports the idea that an oxygen linker may also be acceptable in a Suberone compound.

6. Conclusions and discussion

The molecular modeling studies were able to propose a binding mode of the Suberones and X-ray crystallography supplied the evidence. The Suberones bind in the pose proposed by Revesz *et al.* (see figure 6.1 on the next page).

Both Revesz *et al.* and Ottosen *et al.* proposed that the carbonyl oxygen is bound to hinge region via an H-bond to the backbone -NH of Met109. They were contradictory on the position of the amino-phenol (ring C). According to Ottosen *et al.* it was situated in the hydrophobic region II, whereas Revesz *et al.* proposed that it would occupy the hydrophobic pocket I.

However, Revesz *et al.* and Ottosen *et al.* could not generate more details of the binding pose that were actually observed in the X-ray structure (278SLS). The X-ray structure revealed that the hinge region performs a "flip" to be able to form two H-bonds. The backbone -NH of Gly110 is turned towards the inside of the ATP binding site (the "flip"), so that it can interact with the carbonyl oxygen of the Suberones. The carbonyl oxygen also interacts with the backbone -NH of Met109. So the concept of the previous mentioned Linear Binders has to be enhanced. This class of Suberones does not only bind to the hinge region's linker residue Met109, but enforce the "flip". So not only due to the gatekeeper residue Thr106 which determines the width of the entrance of the hydrophobic pocket I, but also the hinge region residue next to Met109 itself contribute to selectivity. Through the existence of Gly110 the ϕ-ψ-rotation is restricted to a certain conformation. Other residues like Asp150 in JNK3 may be unable to perform such a "flip", due to their side chains.

Docking is not able to predict such an interaction, because all programmes that were used (and that also applies for the majority of the available docking programmes) only treat the ligand as flexible, while keeping the protein structure rigid. Docking in a fully flexible protein would need too much CPU- and calculation time. So it is of great consequence in which rigid PDB structure the ligands are docked (apart from the choosing of the applicable docking programme). Choosing a suitable PDB structure was also part of this work. It was evident that there is more to the quality of a structure than only one quality criteria (e.g the R-factor). It has to

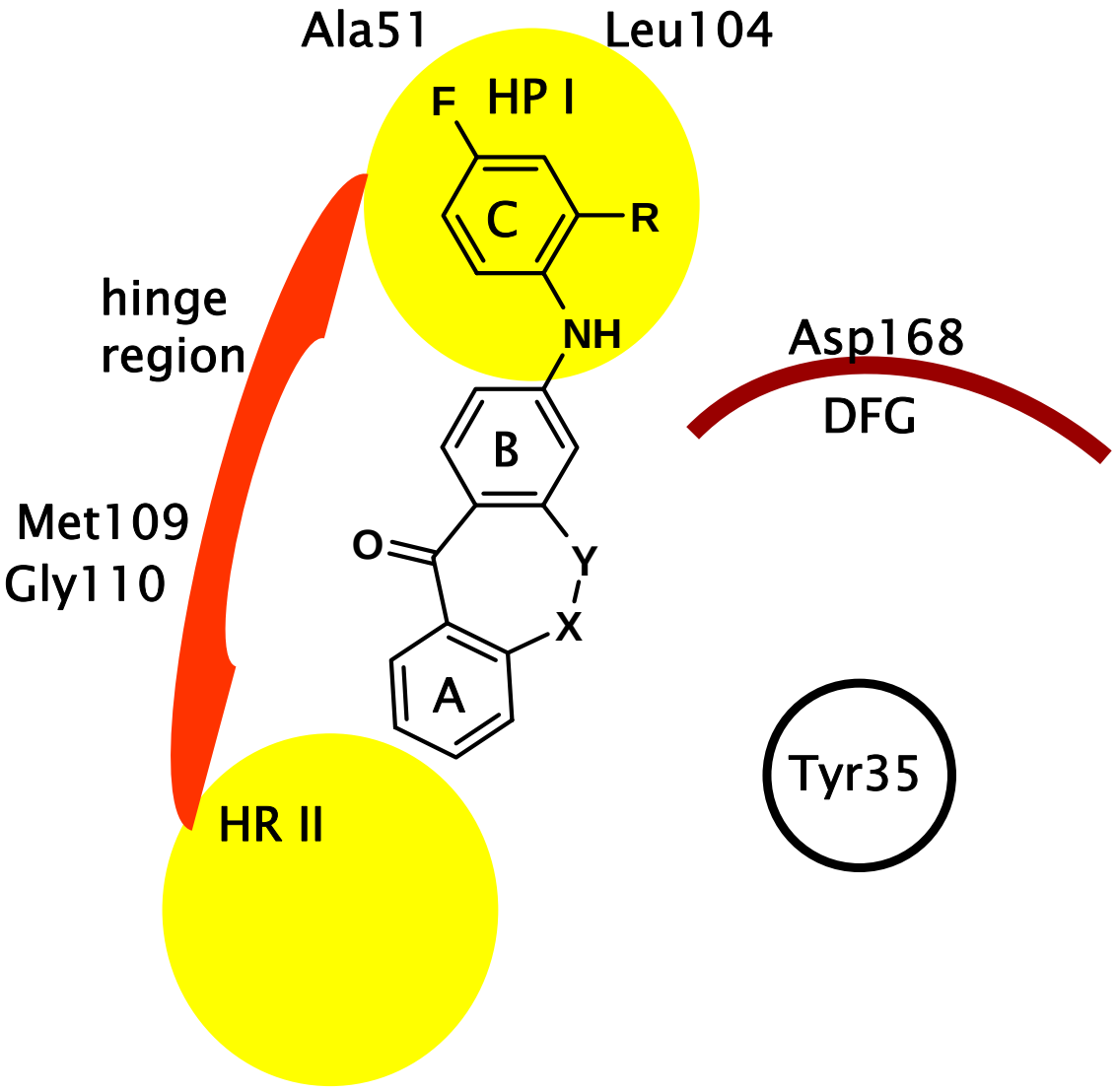

Figure 6.1.: Binding mode of the Suberones proposed by the modeling studies

be a consensus of several aspects. The PDB structure which was used in the former Diploma thesis (PDB 1YWR) e.g. failed the quality standards. Considering the above mentioned rigid docking, the use of several PDB structures is of high importance. Several conformations of the p38α MAP kinase were used here and it came out that different conformations yield to different results (PDB 1W84 in comparison to PDB 2I0H). Thus the ligand determines the induced-fit state of a protein, the native ligand and the database ligands have to be similar and provoke the induced fit. Docking with just one PDB structure, which even may be the unsuitable, may draw wrong conclusions. This was made clear by the use of the several conformations and highlights the need for careful preparations before such a docking study. For example Ottosen *et al.* only proposed their binding mode through docking studies with PDB 1BL7 [46] whose ligand is SB220025 and does not share many constitutional similarities with the Suberone compounds. In the end the Suberone X-ray crystal structure (278SLS) showed that the "flip" makes up about only 2Å in comparison to e.g. PDB 1W84.

The conformations of the ligands seemed not of that importance. The conformations which were generated seemed to meet the requirements, which were needed for the dockings. Measuring the dimensions of the Suberones revealed that active Suberones share certain angles and such upstream calculations and considerations might help to meet a preselection before the actual synthesis. That the calculated conformations of the Suberones completely agreed with the confromation in the protein is not clearly secured, but can be assumed.

The GRID calculations strongly supported that the carbonyl oxygen binds to the hinge region. The position of the -NH_2 however was still unsure. It supported both binding poses by showing that any -NH or -NH_2 groups are favoured in hydrophobic pocket `I` and hydrophobic region `II`. The results also depended on the conformation of the used PDB structure. In the end GRID slightly favoured the hydrophobic pocket `I`, but did not hint to the later in the docking studies observed H-bonds to Ala51 and Leu104.

The docking results strongly depended first on the algorithm of the used docking programme and secondly on the PDB structure. The FlexX results were not as good as the others again. More unlikely poses had to be sorted out. If just FlexX had been used, the proposed binding mode would have been that according to Ottosen *et al.*, because all dockings to the DFG-IN conformations led to that conclusion. Only the docking to PDB 1OZ1 did not favour the one or the other binding mode, while completely failing in proposing any suitable binding modes in PDB 1W84 or PDB 2FSO. FlexX also had huge problems with ligands of smaller molecular weight. It is again not considered to be applicable for docking studies with the p38α MAP kinase. Flexidock could not be used, because of its inability to dock large databases and its

complicated preparations. Docking has to be automatable to deliver good results in a short period of time.

GLIDE was superior to FlexX and Flexidock and proposed many likely poses. It clearly favoured the binding mode according to Revesz *et al.*, apart from the docking to PDB 1OZ1. It also had problems with PDB 1W84, implicating that the use of 1W84 for Suberone docking is not recommendable, although PDB 1W84 is of good quality. eHITS, a not well known often used programme with not so many possibilities to change any settings, yielded acceptable results. It also favoured the binding mode according to Revesz *et al.* and even found the right docking poses in PDB 1W84. Although the results were not preferring one of the two binding modes. eHITS had problems with the dockings to the DFG-OUT conformations in PDB 1W82 and PDB 1WBS. FlexX showed that the Suberone may bind to the DFG-OUT conformation as well, but considering its other results, this could have been mistrusted, if GLIDE had not supported it as well. This possibility was not supported by the X-ray crystallization studies. However, [1] made clear that this can only be proofed by NMR studies.

More studies with JNK3 models were neglected to focus on the DFG-OUT conformation. These might be a task for further studies.

Unfortunately some difficulties emerged, considering any activity predictions or explanations for activity or inactivity. Any rankings of the dockings could not mirror the ranking according to IC_{50} values. A variation of the docking parameters or the use of newer programmes which consider flexibility of the residues may improve those results in further studies. The loss of activity in the isomeres of the 3-amino-6,11-dihydro-dibenzo[b,e]oxepin-11-ones could not be explained by the molecular modeling studies.

Thus water was not present in the docking studies, the observed water mediated H-bond could not be foreseen. The docking studies often proposed H-bonds to Ala51 or Leu104, what could not be observed in 278SLS.

Although now a X-ray crystal structure is available, the first docking studies showed that it will not make the modeling much easier. The particular position of the Gly-rich loop influences the docking results. More dockings should include PDB 2I0H and PDB 2QD9 as well to sort out any results which were too much influenced by the Gly-rich loop.

In conclusion the following propositions can be given (see figure 6.2 on the next page) based on the molecular modeling studies.

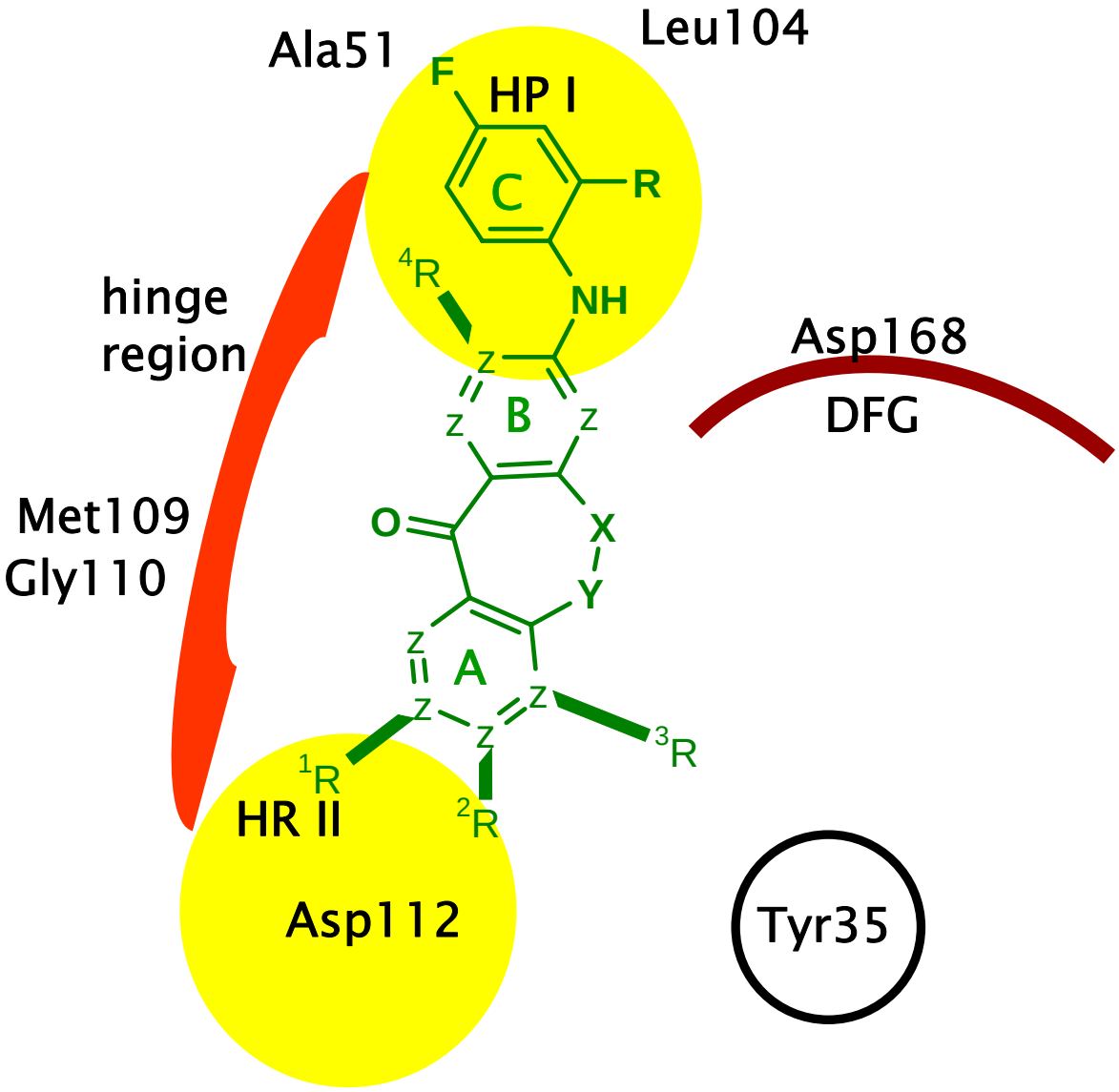

Figure 6.2.: Possible modificatons of the Suberones proposed by the modeling studies

Any variations in the aromatic rings (displayed by the letter Z) may be possible to improve e.g. water solubility by introducing a nitrogen. Subsitituents on R3 should be rigid and follow the other proposals made up by Revesz *et al.*, as are subsituents at the R2 position. Those substituents would point out of the ATP binding pocket and could have effects on drug properties (such as bioavailability). Substituents on R1 if even should be rather small, so that they would not collide with the hinge region. The same applies for substitutents at the R4 position. There, small substituents such as -NH_2 may also be acceptable, maybe would form an additional H-bond to Thr106. Furthermore it would improve selectivity, because Thr106 is not always present there in other kinase structures (e.g. JNK3). The modeling studies showed that the exchange of the amine liker with an oxygen may also head to good ligands.

7. Materials and Methods

7.1. PDB structures

All PDB structures of p38α MAP kinase and JNK3 were downloaded from `http://www.rcsb.org`. The website contains all published PDB structures since its opening in 1971 at Brookhaven National Laboratory. It is the depository of information about the three-dimensional structures of large biological molecules, including proteins and nucleic acids. These are the molecules of life that are found in all organisms including bacteria, yeast, plants, flies, and mice, and in healthy as well as diseased humans [47].

7.2. Quality Check

The tools which were used for checking the quality of the PDB structures are described below.

7.2.1. WHAT IF

The WHAT IF programme [86], [87] can help the user to rapidly check the crystallographic data. A generated document contains a report of findings during the analysis of the given protein. Each reported fact has an assigned severity. Error terms requires immediate attention, while warnings describe less severe problems or uncommon structural features, but still need special attention. A note gives statistical values, plots, or other verbose results of tests and analysis that have been performed. To indicate the normality of a values is expressed as a Z-value or Z-score. This is the number of standard deviations that the score deviates from the expected value. If a Z-score is used in WHAT IF, the accompanying text explains how the expected value and standard deviation were obtained. The first feature that is checked, is "Nomenclature" e. g. (Chain names), followed by "Weight" or if there any missing atoms. Next is "Symmetry related problems", such as rounded coordinates detected, crystallographic symmetry between molecules, extra crystallographic symmetry between the independent molecules or the Matthews coefficient. The Matthews coefficient is defined as the density of the protein

structure in cubic Angstroms per Dalton. Normal values are between 1,5 (tightly packed, little room for solvent) and 4,0 (loosely packed, much space for solvent). The "Geometry" check contains chirality (values around -35 or +35 are expected for chiral atoms, around 0 for planar atoms), bond lengths, bond angles, torsion angles (values for protein residues were taken from Engh and Huber [88]), Ramachandran score and Ramachandran plot, omega check and χ-1/χ-2 score. The cell scaling check finds significant systematic deviation. A reason might be that the unit cell used in the refinement can be different from the best cell calculated. Or the value of λ used for a synchrotron data set can be miscalibrated. Finally, the discrepancy can be caused by a dataset that has not been corrected for significant anisotropic thermal motion. "Rings and Planarity" checks include side-chain planarity and proline puckering (method of Cremer and Pople [89]). The "Structure" checks include inside/outside profile, bumps (if the atoms are closer than the sum of their van der Waals radii minus 0,40 Å), packing quality, backbone (comparison with structures in the WHAT IF database show if they have alternative positions for the backbone) and peptide plane flip. The side chain or "rotamer check" is based on the 3D backbone database in WHAT IF. The position of the water molecules is also checked. During the B-factors check low B-factors, an average B-factors and the distribution are checked. The B-factor or atomic displacement parameter shows the fluctuation of an atom around its average position. The distribution of B-factors of a protein is an important indicator for flexibility and dynamic. An high B-factor indicates great mobility of side chains or single atoms. Therefore B-factors give reliable information about the dynamic of a protein [90]. The final report includes the following contents:

- Atom coordinate problems and/or unexpected atoms
  - Rounded coordinates
- Symmetry related problems
  - Crystallographic symmetry between molecules
  - Matthews coefficient
- Nomenclature related problems
  - Nomenclature
  - Torsion convention problems
  - Heavy atom naming
  - Chirality deviations

  - Dihedral angle distribution
  - Chain names
  - Atomic occupancy factors
  - Missing atoms
  - Extra C-terminal groups
  - Bond lengths
  - Bond length variability
  - Cell scaling
  - Bond angles
  - Bond angle variability
  - Side chain planarity
  - Atoms connected to aromatic rings
  - Unusual PRO puckering amplitudes
  - PRO puckering phases
  - Unusual residues detected by torsion angle evaluation
  - Unusual conformations detected by backbone torsion angle evaluation
  - Ramachandran Z-score
  - Omega angle restraint
  - Chi-1/chi-2 angle correlation Z-score
  - Ramachandran plot

- Accessibility related checks
  - Inside/Outside residue distribution
  - Inside/Outside RMS Z-score plot

- Secondary structure
  - Secondary structure

- Bump checks
  - All atoms away from symmetry axes

  - Interatomic distances
  - Second generation packing environment
  - Residues with abnormal new packing environment
  - Structural average packing Z-score
- 3D-database related check
  - Backbone oxygen evaluation
  - Rotamers
  - Backbone conformations
  - Backbone conformation Z-score
- Water related checks
  - Water contacts
  - Waters which need moving
  - Water molecules without hydrogen bonds
- B-factor analysis
  - Average B-factor
  - Number of buried atoms with low B-factor
  - B-factor distribution
  - B-factor plot
- Hydrogen bond related checks
  - Side chain flips
  - Histidine type assignments
  - Buried unsatisfied hydrogen bond donors
  - Buried hydrogen bond acceptors OK
- Final summary
  - Summary report for users of a structure
  - Summary report for depositors of a structure

7.2.2. ProSA

ProSA [91, 92] is a webinterface for structure research. It is helpful for experimental structure determinations and modeling studies. It helps the user to decide if the overall structure is correct and to identify faulty parts (https://prosa.services.came.sbg.ac.at/prosa.php).

7.2.3. PDBSUM and PROCHECK

PDBsum [73] provides an at-a-glance overview of the of every macromolecular structure deposited in the Protein Data Bank (PDB), giving schematic diagrams of the molecules in each structure and of the interactions between them (http://www.ebi.ac.uk/thornton-srv/databases/pdbsum) PDBsum is linked to PROCHECK [93]. PROCHECK generates an overview of the stereochemical quality of PDB structures, including the following reports :

1. Main Ramachandran plot
2. All-residue Ramachandran plots
3. All-residue chi1-chi2 plots
4. Main-chain parameters
5. Side-chain parameters
6. Residue properties plot
7. Main-chain bond lengths
8. Main-chain bond angles
9. RMS distances from planarity
10. Distorted geometry

A simple output offered by PDBsum generates firstly the Ramachandran Plot statistics, where a good model would be expected to have over 90% the most favoured regions (based on an analysis of 118 structures of resolution of at least 2,0 Å and R-factor no greater than 20,0) and secondly the overall G-factors. Any G-factors below -1,0 may indicate properties that are highy unusual. The main-chain bond-lengths and bond angles are compared with [88] ideal values derived from small-molecule data. The Ramachandran Plot statistics and the overall average G-factor taken from PDBsum are displayed in table 5.7.

7.3. Modeling

7.3.1. SYBYL7.2

The modeling programme SYBYL7.2 [94] was used to inspect all the PDB files of the p38α MAP kinase and JNK3. It visualizes the atom coordinates of the PDB files to create a three-dimensional picture of a protein structure. The tool "Align by Homology" in the "Biopolymer" option facilitates the identification of the conformational differences. One picked PDB structure stays fixed, while the other chosen structures are aligned to the fixed PDB structure. These alignments can be carried out on the C-α atoms, the backbone atoms (N–α-C–O), the side chains atoms or all atoms. A list of the calculated RMSD values is listed on the prompt.

7.3.1.1. Databases

SYBYL7.2 was used create to the databases used for the docking studies. The ligands of the PDB structures where taken out from the PDB files and stored unvaried in a SYBYL database file. All Suberone compounds where build by the Build/Edit panel of SYBYL. An energy minimum was calculated by using the minimizing protocol for small molecule ligands in figure 7.1.

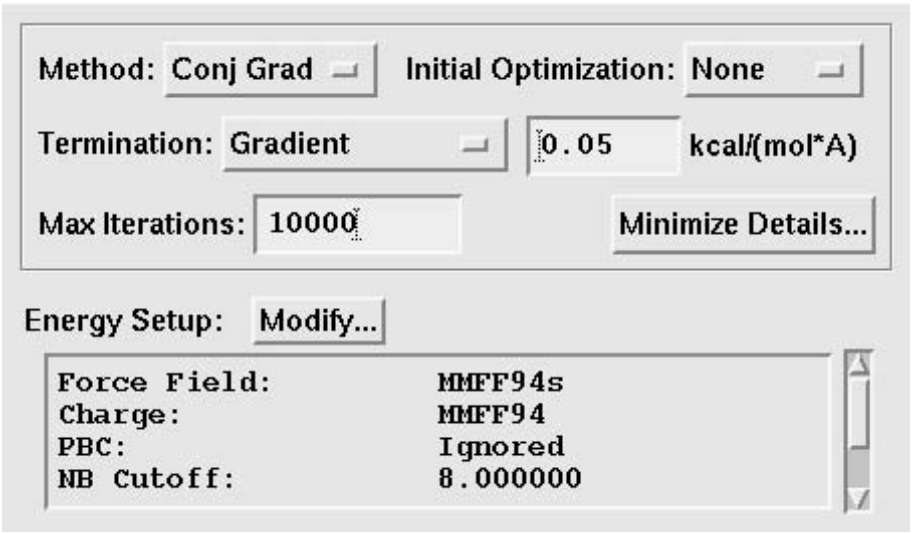

Figure 7.1.: SYBYL minimization protocol

MMFF94s is the best force field for small molecules which is available in SYBYL7.2. The "s" MMFFF94s stands for the "static" variant of the original force field MMFF94. The out-of-plane and torsional parameters were modified to provide nearly planar structures for amide and

unsaturated amine trigonal nitrogens. Terms in the MMFF94 energy equation:

- $E_{MMFF94} = \sum E_{stretch} + \sum E_{bend} + \sum E_{stretch-bend} + \sum E_{OOP} + \sum E_{torsions} + \sum E_{VDW} + \sum E_{elect}$

The method is *Conjugate gradient* which is a good choice for small molecules. No *Simplex* optimization was used. The *Termination Citeria* was set to 0,05 for complete minimization. *Max Iterations* is set to determine the number of cycles before the minimizations stops. 10000 was used to reach the desired complete minimization. [94] The molecules of the database were saved and exported as Mol2, SDF, MDB, HMTL and excel file formats for later usage.

7.3.2. GRID

GRID [95] is a computational procedure for determining energetically favourable interactions between probes with various functional group characteristics and a protein surface (target). The GRID method was first described by [96]. The package GRID2.2 involves the six programmes GREATER, GREAT, GRIN, GRID, GVIEW and GLUE. GREATER is a Graphical User Interface (GUI) for the GRID package (figure 7.2).

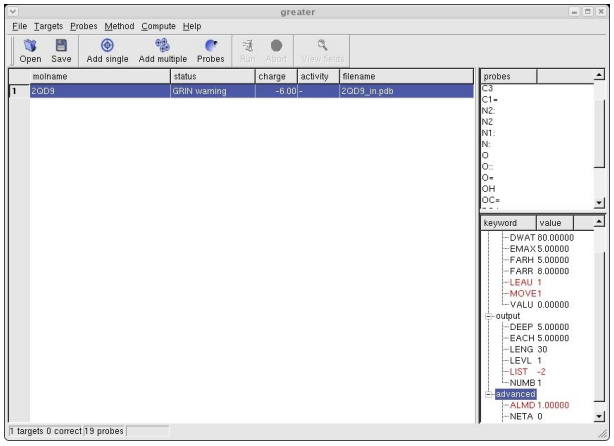

Figure 7.2.: GREATER interface

So the user can access the programmes GRIN, GRID, GREATER and GVIEW. The primary input for GRIN is the coordinates of the atoms in the target molecule. The secondary input for GRIN is a set of "energy variables" which are contained in the GRUB file. Therefore the main function of GRIN is to check the PDB and GRUB files, and merge them so that appropriate energy variables are specified for each atom in the target. The GRIN output file GRINKOUT (GRIN Koordinate OUTput) is a list of target atoms in the correct sequence with their x, y, z

coordinates and the energy variables. It is the input file for GRID. GRID determines where the chosen probes would interact favourably with a protein. Table 7.1 displays the chosen GRID probes, including a short description about the functional groups they represent.

Symbol	**Description**
	single atom
OH2	Water
DRY	The hydrophobic Probe
H	Neutral hydrogen atom
C3	Methyl CH_3 group
C1=	sp^2 CH aromatic or vinyl
N2:	sp^3 NH_2 with lone pair
N2	Neutral flat NH2 eg amide
N1:	sp^3 NH with lone pair
N:	sp^3 N with lone pair
O	sp^2 carbonyl oxygen
O::	sp^2 carboxy oxygen atom
OH	Phenol or carboxy OH
OC=	Ether oxygen
PO4	phosphate dianion
PO4H	phosphate anion
STH	Thiophen or thioether S
F	Organic fluorine atom
MG+2	Magnesium cation
	multi atom
AR.COO-	Aromatic carboxylate
AR.CONH2	Aromatic amide

Table 7.1.: Chosen probes for the GRID calculations

GRID produces two output files called GRIDLONT and GRIDKONT. The last programme of the package is GVIEW which visualizes the structure of the target and the results of the GRID computation simultaneously. The user can check the calculated Molecular Interaction Fields (MIF) and the GRID energy contributions due to atoms of the target. The calculations were mostly carried out with default parameters. During the import of the PDB structures

to GRIN the filtering level was set on semi-automatic. The GRIN warnings were ignored and just accepted, because the errors occurred at atoms outside of the important regions of the box size of the GRID calculation ran over the whole structure, but it the end only the MIF of the ATP binding pocket or the DFG-OUT regions were checked. Before starting the run, the values of the method keywords were varied as follows:

- LEAU determines the way in which water is treated during the computation. Default= 0. LEAU=1 GRID will find and take account of sites for bridging waters.
- MOVE directive controls the flexibility of the target. Default= 0. MOVE=1 as above but flexible side chains are allowed to move.
- ALMD directive controls the printing in the GRIDKONT output file. Default= 0.0 The programme adds to the values of energy of interaction an extra column with the sequential number of the atom interacting more strongly with the probe. When set to -2 an extra record will be prefixed to the start of the GRIDKONT file and it is written in a computer readable binary code [95].

Figure 7.3 gives an overview of the general GRID workflow.

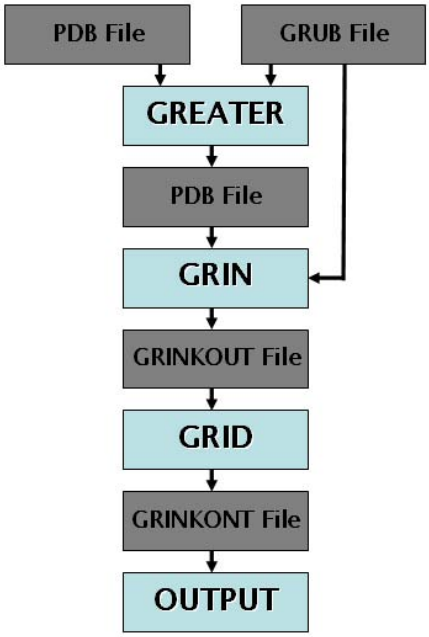

Figure 7.3.: GRID workflow

All PDB structures with the obtained MIF were checked visually with GVIEW.

7.4. Docking

7.4.1. FlexiDock

Flexidock is a docking programme of the SYBYL7.2 modeling package. It's genetic algorithm-based flexible docking provides a means of docking ligands into the active sites. FlexiDock works in torsional space, keeping bond lengths and angles constant. As large van der Waals interactions can only relax via bond rotations, optimization cannot alter chirality and bond chemistry. FlexiDock works on a protein-ligand pair. The protein backbone atoms are fixed in space, but the ligand is mobile. Both the protein side chains and the ligand contain a number of flexible bonds. FlexiDock considers only non-ring single and amid bonds as rotable. But the parameters can be modified. FlexiDock incorporates van der Waals, electrostatic, torsional and constraint energy terms of the Tripos Force Field. With FlexiDock it is possible to determine important atoms and fragments. Genetic algorithms are used by FlexiDock to determine the optimal ligand geometry. Genetic algorithms are robust global optimizers, with performance requirements which scale well with increasing system size. Its principle is to generate a initial population of ligand conformations and interactions. The "Chromosomes" contain sequences of data describing the receptor-ligand interaction's degree of freedom as "genes". After an optimization all ligand poses are scored. Subsequent to the scoring follows the selection of the preferentially good poses for creating the next generation. There the evolution is carried out via genetic operators. During mutation the values of individual genes are changed, during crossover a set of genes is exchanged between the chromosomes. Individual genes are moved to another subpopulation during migration. In the end the fitness function uses a subset of the Tripos Force Field and calculates the energy of the important atoms. Partial scoring is used, as the fitness function improves when complementary site-points are near each other. When each chromosome is scored, each site-point is checked against the set of complementary sites. If the components of the pair are within the site-points radius, the full site score is added to the fitness score (see figure 7.4 on the next page). Before docking a ligand into the protein with FlexiDock, the complex needs charges. In this case the charges are computed with MMFF94s for the small molecule inhibitor and with AmberForceField02 (AmberFF02) for the receptor. In addition, the water molecules have to be removed before using the protein. The FlexiDock input file defines the pocket. The pocket consists of the residues Val30, Ala51, Lys53, Glu71, Leu75, Ile84, Leu86, Leu104, Thr106, Leu108, Met109, Gly110, Ala111, Asp112, Ser154, Ala157, Leu167, Asp168 and Phe169. In the next step the structures are set up. After adding the H atoms to the protein structure, the rotable bonds can be defined. For the receptor

the flexible bonds are the side chains of Lys53, Glu71, Thr106, Met109 and Asp168. Now FlexiDock creates an output-file with 20 solutions. The FlexiDock file contains the ligand and the active site. [94]

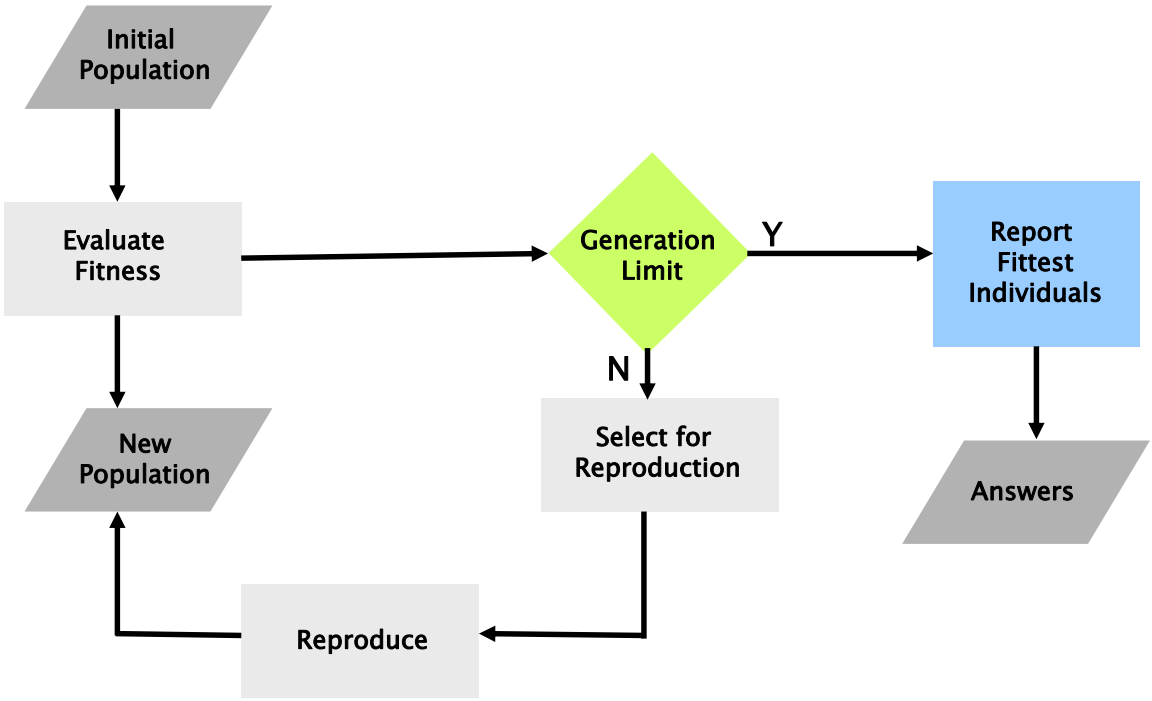

Figure 7.4.: FlexiDock workflow

7.4.2. FlexX

FlexX flexible docking method uses incremental construction algorithmen to place ligands into active sites. The automatically selected base fragment of the ligand is placed into the active site using an algorithmic approach based on a pattern recognition technique called pose clustering. Then the remainder of the ligand is built up incrementally from other fragments. The new fragment is added in all possible conformations to all placements. But only the best conformations are taken on to the next construction step. When adding a new fragment, FlexX searches for matching interactions groups. Distance tolerances of 2Å and angle tolerances of 20° are used to make sure that no possible interactions are missed. The conformational flexibility of the ligand is included by creating general conformations for each fragment and including all in the ligand building step. Placement of the ligand is scored on the basis of protein-ligand interactions (pairwise assignment of interaction geometries). Finally the binding

energy is estimated and the placements are ranked [97]. Figure 7.5 shows the constitution of the FlexX docking algorithm.

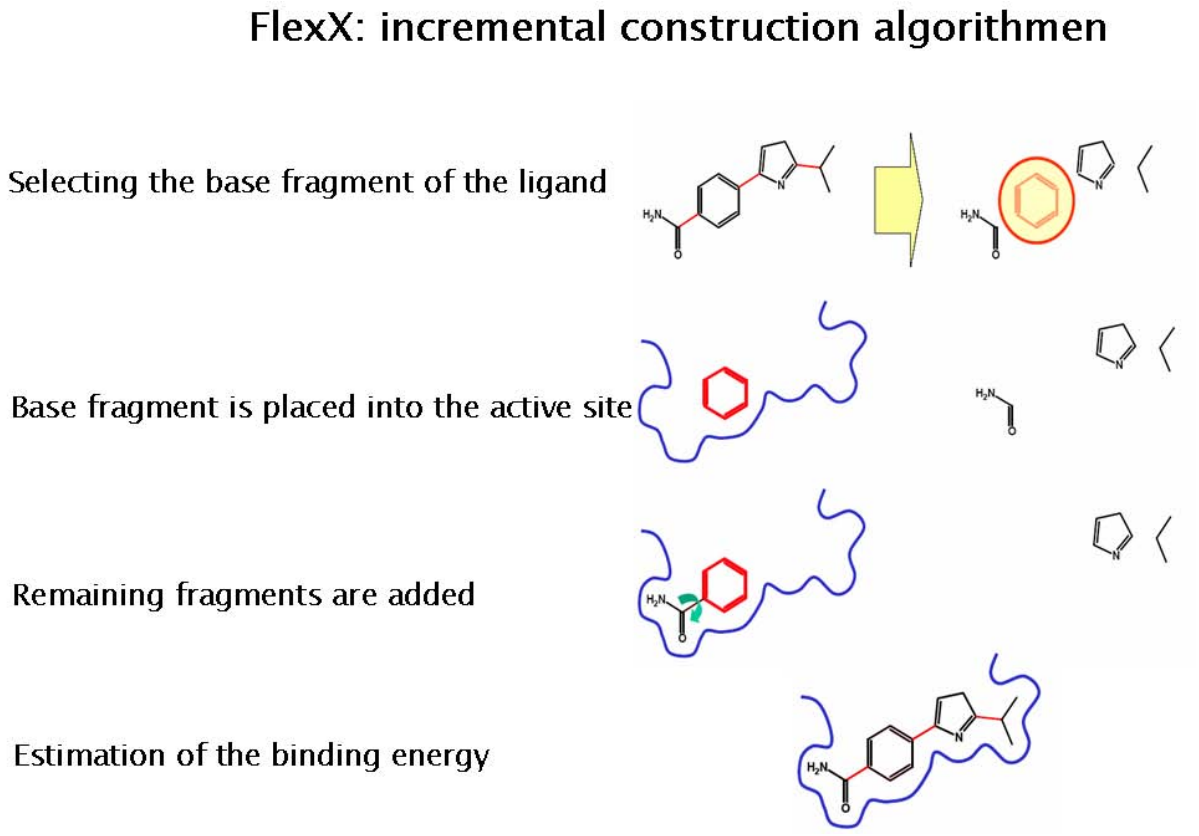

Figure 7.5.: FlexX docking algorithm (lecture slide by O.Kohlbacher)

In the so-called receptor description file (RDF) the docking site and the position of the ligand will be defined. It contains the ionization states (Templates) of the charged amino acids and the torsional angles of the amino acids, which affect the H-bonds in the active site. The original pdb structure of the p38 MAP kinase is used to create the active site file. The defined active site file contains the residues Val30, Ala51, Lys53, Glu71, Leu75, Ile84, Leu86, Leu104, Thr106, Leu108, Met109, Gly110, Ala111, Asp112, Ser154, Ala157, Leu167 and Asp168. The selection radius around the position of the ligand is 5.2Å. For customizing the RDF, the Templates are defined as follows. Asp 112, Asp168 and Glu71 have a negative charge, while Lys53 is positive charged. For the residues Asp112, Asp168, Glu71, Lys53, Ser154 and Thr106 the standard torsions are used. For the ligand and the reference structure the prepared ligand is used. Thus, ligands of PDB structures are often faulty, the atom types and the bonds have to be manually checked, concluding with the addition of the hydrogens. The chosen FlexX option is the serial CScore Calculation, where the relaxed and unrelaxed structures are

calculated. This means that the ligand-protein-complex is minimized and then scored again. The output file contains the 50 best scored conformations according to FlexX.

7.4.3. GLIDE

GLIDE (Grid-based Ligand Docking with Energetics) is a docking programme of Schrödinger [98, 99]. GLIDE searches for favourable interactions between a small ligand molecule and a protein by using a hierarchical series of filters to search for possible locations of the ligand in the active-site region of the receptor. The shape and properties of the receptor are represented on a grid by several different sets of fields that provide progressively more accurate scoring of the ligand. The combination of position and orientation of a ligand relative to the receptor, along with its conformation in flexible docking, is referred to as a ligand pose. Each ligand must be a single molecule, while the receptor may include more than one molecule, e.g., a protein and a co-factor. In this study GLIDE runs in the flexible docking mode, allowing different conformations for the ligand. At first each ligand is divided into a core region and a number of rotamer groups. Each rotamer group is attached to the core by a rotatable bond, but does not contain additional rotatable bonds. The core is what remains when each terminus of the ligand is severed at the "last" rotatable bond. Carbon and nitrogen end groups terminated with hydrogen (-CH_3, -NH_2, -NH_3^+) are not considered rotatable because their conformational variation is of little significance. For each core conformation an exhaustive search of possible locations and orientations is performed over the active site. The search begins with the selection of "site points" on an equally spaced 2Å grid that permeates the active-site region. To make this selection, pre-computed distances from the site point to the receptor surface, evaluated at a series of pre-specified directions and binned in 1Å ranges, are compared to binned distances from the ligand center to the ligand surface. GLIDE positions the ligand center at the site point if there is a good enough match, but skips over the site point if there is not. The second part of the hierarchy begins by examining the placement of atoms that lie within a specified distance of the line drawn between the most widely separated atoms (the ligand diameter). This is done for a pre-specified selection of possible orientations of the ligand diameter. If there are too many steric clashes with the receptor, the orientation is skipped. Next, rotation about the ligand diameter is considered, and the interactions of a subset consisting of all atoms capable of making hydrogen bonds or ligand-metal interactions with the receptor are scored (subset test). If this score is good enough, all interactions with the receptor are scored. The scoring in these three tests is carried out using Schrödinger's own version of ChemScore, an empirical scoring function [100]. ChemScore recognizes favorable

hydrophobic, hydrogen-bonding, and metal-ligation interactions, and penalizes steric clashes (greedy scoring). After that the poses are re-scored according to the top greedy-scoring via a "refinement" procedure, in which the ligand as a whole is allowed to move rigidly by ± 1 Å in the Cartesian directions. The best refined poses are passed on to the third stage in the hierarchy-energy minimization. The energy minimization typically begins on a set of van der Waals and electrostatic grids that have been "smoothed" to reduce the large energy and gradient terms that result from too-close inter-atomic contacts. It finishes on the full-scale OPLS-AA nonbonded energy surface ("annealing") which consists only of rigid-body translations and rotations when external conformations are docked. When conformations are generated internally, however, the optimization also includes torsional motion about the core and end-group rotatable bonds. In the end a small number of the top-ranked poses are then subjected to a Monte-Carlo procedure in which alternative localminima-vcore and rotamer-group torsion angles are examined to try to improve the energy score. Finally, the minimized poses are re-scored using the GLIDEScore scoring function. GLIDEScore is based on ChemScore, but includes another steric-clash term and adds buried polar terms to penalize electrostatic mismatches. The best-docked structure for each ligand is made using a model energy score (Emodel) that combines the energy grid score, the binding affinity predicted by GLIDEScore, and the internal strain energy for the model potential used to direct the conformational-search algorithm. GLIDE can also compute a specially constructed Coulomb-van der Waals interaction-energy score that is formulated to avoid overly rewarding charge-charge interactions at the expense of charge-dipole and dipole-dipole interactions. The user can combine the computed GLIDEScore and "modified" Coulomb-van der Waals score values to give a composite score that usually helps improve enrichment factors in database screening applications. Figure 7.6 on the next page gives an overview of the GLIDE docking hierarchy. A GLIDE constraint is a ligand-receptor interaction requirement. To use GLIDE constraints, the receptor sites for possible ligand interactions must be specify when you set up a receptor grid generation job. To run a ligand docking job, the user has to select GLIDE constraints to apply from the list of receptor constraint sites that were defined for the receptor. In GLIDE constraint docking jobs, GLIDE incorporates satisfaction of these constraints into several of its hierarchical filters, allowing prompt rejection of docked poses that fail to meet the requirements. The XP (extra-precision) mode of GLIDE is a refinement tool designed for use only on good ligand poses. The standard-precision (SP) mode is recommend for the first screening of large databases. Only the top-scored ligands should be docked using XP mode. The XP mode of GLIDE is able to identify ligand poses that would be expected to have unfavorable energies. The presumption is that only active compounds will have available

poses that avoid these penalties while at the same time securing a favorable scoring from the terms in the scoring function that reward e.g. hydrophobic contact between the protein and the ligand, appropriate hydrogen-bonding interactions. The chief purposes of the XP method are to weed out false positives and to provide a better correlation between good poses and good scores. Both modes were tested during this study.

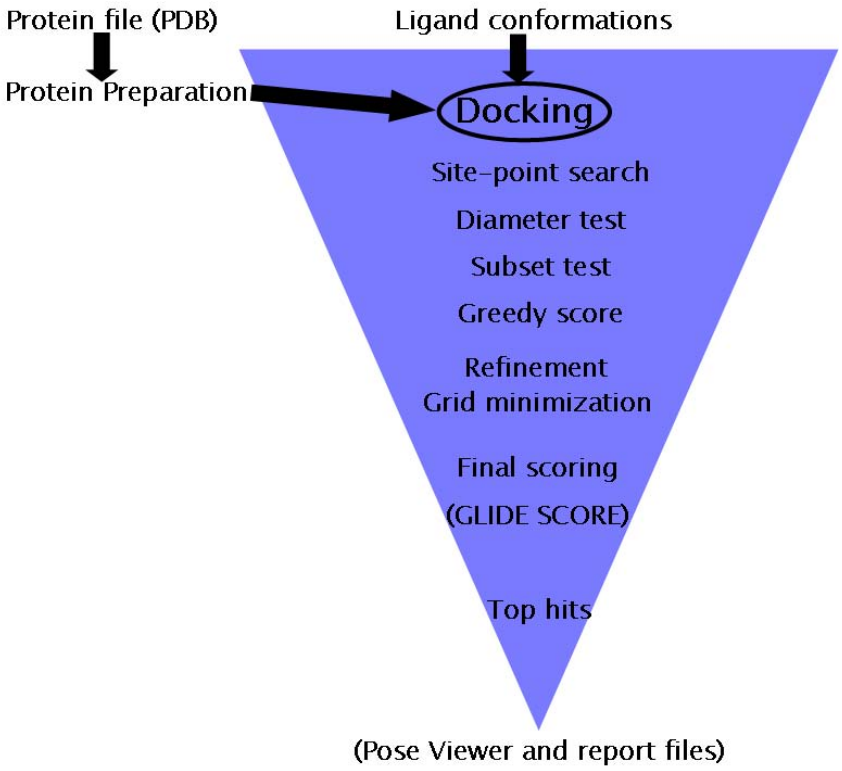

Figure 7.6.: The GLIDE docking hierarchy

All following panels were carried out in Maestro, the unified interface for all Schrödinger software. Before starting to generate the receptor grids for ligand docking, the protein has to be prepared. After deleting the water molecules and the identification of the ligand the protein preparation panel is started.

- Automatic protein preparation is divided into two steps:
  - preparation adds hydrogens and neutralizes side chains that are not close to the binding cavity and do not participate in salt bridges.
  - refinement component performs a restrained impact minimization of the co-crystallized complex, which re-orientates side chain hydroxyl groups and alleviates potential steric clashes

For the PDB 2FSO and PDB 2PKJ, which do not contain a small molecule ligand, the identification of a ligand was enabled through a little indirection. Both PDB structures were loaded in SYBYL and aligned by homology to PDB 2EWA. The ligand of PDB 2EWA was merged into the files of PDB 2FSO and PDB 2PKJ, and saved for the the further usage with GLIDE. This was necessary, because a ligand is required for the later described Receptor Grid Generation. The preparation panel was carried out by default. Just the button of "Neutralization zone around the ligand" was unchecked. The ligands prepared in SYBYL were imported to the workspace and all the hydrogens were added. The structures were stored in a maestro file. Another ligand database was generated by using the LigPrep tool. LigPrep process consists of a series of steps that perform conversions, apply corrections to the structures, generate variations on the structures, eliminate unwanted structures, and optimize the structures. The settings were used by default, apart from "stereoisomers: generate all combinations" and "ionization: generate possible states at target pH 7,4 ($\pm$0,5)" The last step before the actual docking is the Receptor Grid Generation. The Receptor Grid Generation panel has three tabs, which specify the settings for the receptor grid generation job:

- Receptor, where the user picks the ligand molecule, which excludes the ligand from receptor grid generation.
- Site, where an enclosing box is generated around the picked ligand to ensure that the database ligands will be confined to the enclosing box.
- Constraints enable Glide to screen out ligands, conformations, or poses that do not meet these criteria early on in their evaluation for docking suitability.

For each PDB structure a file with and a file without contraints were generated. The chosen contraints were:

- Positional
  - Atoms of the ligand which form H-bonds to the hinge region (e.g. 1W84: N-pyridin)
- H-bond
  - The atoms of a residue with forms H-bonds to the ligand (e.g. 1W84: bb NH of Met109-N pyridin)
- Hydrophobic
  - Identification of hydrophobic cells (e.g. 1W84: 14 hydrophobic cells situated in the hydrophobic region /)

To use Glide constraints they have to be applied during the docking setup. All other options were used by default. The actual docking the Ligand Docking panel has five tabs:

- Settings: the user has to chose the Receptor Grid base name (the generated file of the Receptor Grid Generation)and the docking precison (SP or XP). All ligands were docked flexibly in the receptor grid.
- Ligands: here the source of the ligands is specified and some other parameters which were used by default.
- Constraints: the contraints are activated here; just the hydrophobic contraints were used in the end.
- Similarity: was used by default.
- Output: the user defines the structure of the output; in this study a pose viewer file was generated to check both ligand and receptor and for each ligand at most 50 poses per ligand were written out in the output file. Other options were used by default.

The results were visualized with the help of the pose viewer in maestro.[101] Any lengths of H-bonds or contacts was used by default. All used Schrödinger programmes (Maestro, GLIDE, LigPrep) were from the Schrödinger7.0 version.

7.4.4. eHITS

eHITS by SimBioSys [102, 103] uses a systematic docking algorithm. The ligand is divided into fragments and flexible chains. The fragments are docked independently in the receptor side. The poses of the fragments are found by a fast graph match algorithm. eHITS keeps a number of pre-defined poses and reconnects them with the flexible chains. To obtain the final ligand pose, the programme executes an optimization by using a local energy minimization algorithm. In the end the poses are scored to obtain the final ranking. eHITS' visualizer is called CheVi (Chemical visualizer). After loading the docking the user can decide if he want to keep the water during the docking. If the PDB file contains a ligand the programme needs to know that as well (highlighting complex). The parameters were all used in default. Just the accuracy was varied during the Re-docking and Cross-docking approaches, identifying standard as the most useful one in comparison to accurate and fast. The receptor can be displayed in a surface option which can be colored due to the 25 surface points types (figure 7.7).
The ligand can be displayed in stick representation with or without ligand. The interactions

eHITS Surface Points
Positively charged metal ion point
Positively charged hydrogen, e.g. Arginine
Primary amine hydrogen/lone-pair, e.g. -NH3+ or -NH2
Strong (primary) hydrogen bond donor H (polar-atom-H)
Weak (secondary) hydrogen bond donor H (polarized -C-H)
Lone pair of negatively charged group, e. g. PO^{-3}
Lone pair of an acid group, e. g. carboxylate
Strong (primary) hydrogen bond acceptor lone pair
Weak (secondary) hydrogen bond acceptor lone pair
Donor HO OR acceptor Lp depending on protonation state
Rotatable-hydroxy donor H
Rotatable-hydroxy acceptor Lp
H on aliphatic (chain) hydrophobic carbon
H on hydrophobic carbon in aromatic ring (non-polarized)
H on weak secondary hydrophobic atom (e.g. carbon next to polar)
H/Lp on neutral atom (no recognised activity)
Pi electron of an aromatic ring
Pi electron on polar atom (N/O) in resonance chain, e. g. amide
Pi electron on carbon atom in resonance chain, e.g. amide
Pi electron on sp2 polar atom (N/O) (non-resonating, non-arom)
Pi electron on sp2 carbon atom (non-resonating, non-arom)
Lone electron pair of a halogen atom (F,Cl,I)
Lone electron pair of a sulfur atom
Join external atom point in a ligand rigid fragment
Invalid/unknown type

Figure 7.7.: eHITS surface points

between the ligand and the protein are saved in a separate interaction file which contains e.g. the scores, distances and type of interaction. These interactions can be labeled with numbers and are visualized by coloured hyphens.

7.4.5. Pictures

All pictures of results of FlexX, GLIDE and eHITS were obtained with "The Gimp"(http://gimp.org) and later treated with "Paint.net" (http://getpaint.net). Any 2-D structures of the compounds were created with "IsisDraw(2.4)" and the rest of the 3-D protein structures were made up with "PyMOL" (http://pymol.sourceforge.net).

Bibliography

[1] M. Vogtherr, K. Saxena, S. Hoelder, S. Grimme, M. Betz, U. Schieborr, B. Pescatore, M. Robin, L. Delarbre, T. Langer, K. U. Wendt, and H. Schwalbe. NMR characterization of kinase p38 dynamics in free and ligand-bound forms. *Angew Chem Int Ed Engl*, 45(6):993–997, Jan 2006.

[2] B.M. Swahn, Y. Xue, E. Arzel, E. Kallin, A. Magnus, N. Plobeck, and J. Viklund. Design and synthesis of 2'-anilino-4,4'-bipyridines as selective inhibitors of c-Jun N-terminal kinase-3. *Bioorg. Med. Chem. Lett.*, 16:1397–1401, Mar 2006.

[3] C. Pargellis, L. Tong, L. Churchill, P.F. Cirillo, T. Gilmore, A.G. Graham, P.M. Grob, E.R. Hickey, N. Moss, S. Pav, and J. Regan. Inhibition of p38 MAP kinase by utilizing a novel allosteric binding site. *Nat. Struct. Biol.*, 9:268–272, Apr 2002.

[4] A. L. Gill, M. Frederickson, A. Cleasby, S. J. Woodhead, M. G. Carr, A. J. Woodhead, M. T. Walker, M. S. Congreve, L. A. Devine, D. Tisi, M. O'Reilly, L. C. A. Seavers, D. J. Davis, J. Curry, R. Anthony, A. Padova, C. W. Murray, R. A. E. Carr, and H. Jhoti. Identification of novel p38alpha MAP kinase inhibitors using fragment-based lead generation. *J Med Chem*, 48(2):414–426, Jan 2005.

[5] D. Voet, J. G. Voet, and C. W. Pratt. *Fundamentals of Biochemistry-Life at the molecular level, 2nd Edition*. John Wiley & Sons, Inc., 2006.

[6] S. B. Patel, P. M. Cameron, B. Frantz-Wattley, E. O'Neill, J. W. Becker, and G. Scapin. Lattice stabilization and enhanced diffraction in human p38 alpha crystals by protein engineering. *Biochim Biophys Acta*, 1696(1):67–73, Jan 2004.

[7] K. Pervushin, R. Riek, G. Wider, and K. Wüthrich. Attenuated T2 relaxation by mutual cancellation of dipole-dipole coupling and chemical shift anisotropy indicates an avenue to NMR structures of very large biological macromolecules in solution. *Proc. Natl. Acad. Sci. U.S.A.*, 94:12366–12371, Nov 1997.

[8] G. Manning, D.B. Whyte, R. Martinez, T. Hunter, and S. Sudarsanam. The protein kinase complement of the human genome. *Science*, 298:1912–1934, Dec 2002.

[9] C. Peifer, R. Selig, K. Kinkel, D. Ott, F. Totzke, C. Schächtele, R. Heidenreich, D. Schollmeyer, and S. Laufer. Design, synthesis and biological evaluation of novel 3,4-diaryl-2h-pyrrole-2-ones as vegf-r inhibitors. *J. Med. Chem.*, accepted, 2008.

[10] D. Fabbro, S. Ruetz, E. Buchdunger, S.W. Cowan-Jacob, G. Fendrich, J. Liebetanz, J. Mestan, T. O'Reilly, P. Traxler, B. Chaudhuri, H. Fretz, J. Zimmermann, T. Meyer, G. Caravatti, P. Furet, and P.W. Manley. Protein kinases as targets for anticancer agents: from inhibitors to useful drugs. *Pharmacol. Ther.*, 93:79–98, 2002.

[11] D. R. J. Hauser. *Purinderivate als mögliche ATP-kompetitive Kinase Inhibitoren*. PhD thesis, Pharmazeutisches Institut der Universität Tübingen, 2004.

[12] V. Schattel. Homology modeling of map kinases- implications for selectivity of inhibitors, 2007.

[13] W. F. Waas, H.-H. Lo, and K.N. Dalby. The kinetic mechanism of the dual phosphorylation of the atf-2 transcription factor by p38 mitogen-activated protein (map) kinase alpha - implications for signal/response profiles of mapkinase pathways. *J. Biol. Chem.*, 276:5676–5684, 2001.

[14] J. E. Sullivan, G. A. Holdgate, D. Campbell, D. Timms, S. Gerhardt, J. Breed, A. L. Breeze, A. Bermingham, R. A. Pauptit, R. A. Norman, K. J. Embrey, J. Read, W. S. VanScyoc, and W. H. J. Ward. Prevention of MKK6-dependent activation by binding to p38alpha MAP kinase. *Biochemistry*, 44(50):16475–16490, Dec 2005.

[15] S. Laufer, K. Brune, and S. Gay. *Inflammation and Rheumatic Diseases, The molecular basis of novel therapies*. Georg Thieme Verlag, 2003.

[16] P.L. Kozuch and S.B. Hanauer. Treatment of inflammatory bowel disease: A review of medical therapy. *World J. Gastroenterol.*, 14:354–377, Jan 2008.

[17] U. Feige, Y.L. Hu, J. Gasser, G. Campagnuolo, L. Munyakazi, and B. Bolon. Anti-interleukin-1 and anti-tumor necrosis factor-alpha synergistically inhibit adjuvant arthritis in Lewis rats. *Cell. Mol. Life Sci.*, 57:1457–1470, Sep 2000.

[18] C.A. Wijbrandts, M.G. Dijkgraaf, M.C. Kraan, M. Vinkenoog, T.J. Smeets, H. Dinant, K. Vos, W.F. Lems, G.J. Wolbink, D.E. Sijpkens, B.A. Dijkmans, and P. Tak. The clinical response to infliximab in rheumatoid arthritis is in part dependent on pre-treatment TNFalpha expression in the synovium. *Ann Rheum Dis*, Nov 2007.

[19] T. Frembgen-Kesner and A.H. Elcock. Computational sampling of a cryptic drug binding site in a protein receptor: explicit solvent molecular dynamics and inhibitor docking to p38 MAP kinase. *J. Mol. Biol.*, 359:202–214, May 2006.

[20] M. Bukhtiyarova, M. Karpusas, K. Northrop, H. V .M. Namboodiri, and E. B Springman. Mutagenesis of p38alpha MAP kinase establishes key roles of Phe169 in function and structural dynamics and reveals a novel DFG-OUT state. *Biochemistry*, 46(19):5687–5696, May 2007.

[21] A. Trejo, H. Arzeno, M. Browner, S. Chanda, S. Cheng, D. D. Comer, S. A. Dalrymple, P. Dunten, J. Lafargue, B. Lovejoy, J. Freire-Moar, J. Lim, J. Mcintosh, J. Miller, E. Papp, D. Reuter, R. Roberts, F. Sanpablo, J. Saunders, K. Song, A. Villasenor, S. D. Warren, M. Welch, P. Weller, P. E. Whiteley, L. Zeng, and D. M. Goldstein. Design and synthesis of 4-azaindoles as inhibitors of p38 MAP kinase. *J Med Chem*, 46(22):4702–4713, Oct 2003.

[22] S.R. Natarajan and J.B. Doherty. P38 MAP kinase inhibitors: evolution of imidazole-based and pyrido-pyrimidin-2-one lead classes. *Curr Top Med Chem*, 5:987–1003, 2005.

[23] B.J. Mavunkel, S. Chakravarty, J. J. Perumattam, G. R. Luedtke, X. Liang, D. Lim, Y. Xu, M. Laney, D. Y. Liu, G. F. Schreiner, J. A. Lewicki, and S. Dugar. Indole-based heterocyclic inhibitors of p38alpha MAP kinase: designing a conformationally restricted analogue. *Bioorg Med Chem Lett*, 13(18):3087–3090, Sep 2003.

[24] J. Regan, S. Breitfelder, P. Cirillo, T. Gilmore, A.G. Graham, E. Hickey, B. Klaus, J. Madwed, M. Moriak, N. Moss, C. Pargellis, S. Pav, A. Proto, A. Swinamer, L. Tong, and C. Torcellini. Pyrazole urea-based inhibitors of p38 MAP kinase: from lead compound to clinical candidate. *J. Med. Chem.*, 45:2994–3008, Jul 2002.

[25] R. Diskin, N. Askari, R. Capone, D. Engelberg, and O. Livnah. Active mutants of the human p38alpha mitogen-activated protein kinase. *J Biol Chem*, 279(45):47040–47049, Nov 2004.

[26] B.J. Canagarajah, A. Khokhlatchev, M.H. Cobb, and E.J. Goldsmith. Activation mechanism of the MAP kinase ERK2 by dual phosphorylation. *Cell*, 90:859–869, Sep 1997.

[27] F. Zhang, A. Strand, D. Robbins, M.H. Cobb, and E.J. Goldsmith. Atomic structure of the MAP kinase ERK2 at 2.3 A resolution. *Nature*, 367:704–711, Feb 1994.

[28] S. Bellon, M.J. Fitzgibbon, T. Fox, H.M. Hsiao, and K.P. Wilson. The structure of phosphorylated p38gamma is monomeric and reveals a conserved activation-loop conformation. *Structure*, 7:1057–1065, Sep 1999.

[29] R.M. Angell, F.L. Atkinson, M.J. Brown, T.T. Chuang, J.A. Christopher, M. Cichy-Knight, A.K. Dunn, K.E. Hightower, S. Malkakorpi, J.R. Musgrave, M. Neu, P. Rowland, R.L. Shea, J.L. Smith, D.O. Somers, S.A. Thomas, G. Thompson, and R. Wang. N-(3-Cyano-4,5,6,7-tetrahydro-1-benzothien-2-yl)amides as potent, selective, inhibitors of JNK2 and JNK3. *Bioorg. Med. Chem. Lett.*, 17:1296–1301, Mar 2007.

[30] Z. Han, D.L. Boyle, L. Chang, B. Bennett, M. Karin, L. Yang, A.M. Manning, and G.S. Firestein. c-Jun N-terminal kinase is required for metalloproteinase expression and joint destruction in inflammatory arthritis. *J. Clin. Invest.*, 108:73–81, 2001.

[31] A.M. Manning and R.J. Davis. Targeting JNK for therapeutic benefit: from junk to gold? *Nat Rev Drug Discov*, 2:554–565, Jul 2003.

[32] X. Xie, Y. Gu, T. Fox, J.T. Coll, M.A. Fleming, W. Markland, P.R. Caron, K.P. Wilson, and M.S. Su. Crystal structure of JNK3: a kinase implicated in neuronal apoptosis. *Structure*, 6:983–991, Aug 1998.

[33] G. Scapin, S.B. Patel, J. Lisnock, J.W. Becker, and P.V. LoGrasso. The structure of JNK3 in complex with small molecule inhibitors: structural basis for potency and selectivity. *Chem. Biol.*, 10:705–712, Aug 2003.

[34] Y. Cheng and W.H. Prusoff. Relationship between the inhibition constant (K1) and the concentration of inhibitor which causes 50 per cent inhibition (I50) of an enzymatic reaction. *Biochem. Pharmacol.*, 22:3099–3108, Dec 1973.

[35] E. R. Ottosen, M. D. Sorensen, F. Bjorkling, T. Skak-Nielsen, M. S. Fjording, H. Aaes, and L. Binderup. Synthesis and structure-activity relationship of aminobenzophenones. A novel class of p38 MAP kinase inhibitors with high antiinflammatory activity. *J Med Chem*, 46(26):5651–5662, Dec 2003.

[36] M. Menéndez, J. Laynez, F.J. Medrano, and J.M. Andreu. A thermodynamic study of the interaction of tubulin with colchicine site ligands. *J. Biol. Chem.*, 264:16367–16371, Oct 1989.

[37] L. Revesz, E. Blum, F.E. Di Padova, T. Buhl, R. Feifel, H. Gram, P. Hiestand, U. Manning, and G. Rucklin. SAR of benzoylpyridines and benzophenones as p38alpha MAP kinase inhibitors with oral activity. *Bioorg. Med. Chem. Lett.*, 14:3601–3605, Jul 2004.

[38] M.R. Lee and C. Dominguez. MAP kinase p38 inhibitors: clinical results and an intimate look at their interactions with p38alpha protein. *Curr. Med. Chem.*, 12:2979–2994, 2005.

[39] F.G.; Duffy J.P.; Cochran J.E.; Harrington E.M.;Murcko M.A.; Wilson K. P.; Su M.; Galullo V.P. Bemis, G W.; Salituro. Patent WO9827098A1, Vertex Pharmaceuticals, Inc., June 25 1998.

[40] A. Schlapbach, R. Heng, and F. Di Padova. A novel Pd-catalyzed cyclization reaction of ureas for the synthesis of dihydroquinazolinone p38 kinase inhibitors. *Bioorg. Med. Chem. Lett.*, 14:357–360, Jan 2004.

[41] J. E. Stelmach, L. Liu, S. B. Patel, J. V. Pivnichny, G. Scapin, S. Singh, C. E. C. A. Hop, Z. Wang, J. R. Strauss, P. M. Cameron, E. A. Nichols, S. J. O'Keefe, E. A. O'Neill, D. M. Schmatz, C. D. Schwartz, C. M. Thompson, D. M. Zaller, and J. B. Doherty. Design and synthesis of potent, orally bioavailable dihydroquinazolinone inhibitors of p38 MAP kinase. *Bioorg Med Chem Lett*, 13(2):277–280, Jan 2003.

[42] R. Nieß. *Design, Synthese und biologische Testung von N-Aryl-subsitituierten 2-Aminodibenzosuberonen und 2-Aminodibenzo[a,d]cyclohepten-5-onen als p38 MAP Kinase-Inhibitoren*. PhD thesis, Pharmazeutisches Institut der Universität Tübingen, 2006.

[43] J. S. Hering. *Synthese und biologische Testung von 3- bzw. 8-substituierten 6,11-Dihydro-dibenzo[b,e]oxepin/thiepin-11-onen als neue Klasse von p38-MAP Kinase Inhibitoren*. PhD thesis, Pharmazeutisches Institut der Universität Tübingen, 2005.

[44] S.A. Laufer, G.M. Ahrens, S.C. Karcher, J.S. Hering, and R. Niess. Design, synthesis, and biological evaluation of phenylamino-substituted 6,11-dihydro-dibenzo[b,e]oxepin-11-ones and dibenzo[a,d]cycloheptan-5-ones: novel p38 MAP kinase inhibitors. *J. Med. Chem.*, 49:7912–7915, Dec 2006.

[45] S. Laufer, S. Thuma, C. Peifer, C. Greim, Y. Herweh, A. Albrecht, and F. Dehner. An immunosorbent, nonradioactive p38 MAP kinase assay comparable to standard radioactive liquid-phase assays. *Anal. Biochem.*, 344:135–137, Sep 2005.

[46] Z. Wang, B. J. Canagarajah, J.C. Boehm, S. Kassisa, M. H. Cobb, P. R. Young, S. Abdel-Meguid, J. L. Adams, and E. J. Goldsmith. Structural basis of inhibitor selectivity in MAP kinases. *Structure*, 6(9):1117–1128, Sep 1998.

[47] H.M. Berman, T. Battistuz, T.N. Bhat, W.F. Bluhm, P.E. Bourne, K. Burkhardt, Z. Feng, G.L. Gilliland, L. Iype, S. Jain, P. Fagan, J. Marvin, D. Padilla, V. Ravichandran, B. Schneider, N. Thanki, H. Weissig, J.D. Westbrook, and C. Zardecki. The Protein Data Bank. *Acta Crystallogr. D Biol. Crystallogr.*, 58:899–907, Jun 2002.

[48] A.M. Aronov, C. Baker, G.W. Bemis, J. Cao, G. Chen, P.J. Ford, U.A. Germann, J. Green, M.R. Hale, M. Jacobs, J.W. Janetka, F. Maltais, G. Martinez-Botella, M.N. Namchuk, J. Straub, Q. Tang, and X. Xie. Flipped out: structure-guided design of selective pyrazolylpyrrole ERK inhibitors. *J. Med. Chem.*, 50:1280–1287, Mar 2007.

[49] M. Alam, R.E. Beevers, T. Ceska, R.J. Davenport, K.M. Dickson, M. Fortunato, L. Gowers, A.F. Haughan, L.A. James, M.W. Jones, N. Kinsella, C. Lowe, J.W. Meissner, A.L. Nicolas, B.G. Perry, D.J. Phillips, W.R. Pitt, A. Platt, A.J. Ratcliffe, A. Sharpe, and L.J. Tait. Synthesis and SAR of aminopyrimidines as novel c-Jun N-terminal kinase (JNK) inhibitors. *Bioorg. Med. Chem. Lett.*, 17:3463–3467, Jun 2007.

[50] L. Shewchuk, A. Hassell, B. Wisely, W. Rocque, W. Holmes, J. Veal, and L.F. Kuyper. Binding mode of the 4-anilinoquinazoline class of protein kinase inhibitor: X-ray crystallographic studies of 4-anilinoquinazolines bound to cyclin-dependent kinase 2 and p38 kinase. *J. Med. Chem.*, 43:133–138, Jan 2000.

[51] L. Tong, S. Pav, D.M. White, S. Rogers, K.M. Crane, C.L. Cywin, M.L. Brown, and C.A. Pargellis. A highly specific inhibitor of human p38 MAP kinase binds in the ATP pocket. *Nat. Struct. Biol.*, 4:311–316, Apr 1997.

[52] C.I. Chang, B.E. Xu, R. Akella, M.H. Cobb, and E.J. Goldsmith. Crystal structures of MAP kinase p38 complexed to the docking sites on its nuclear substrate MEF2A and activator MKK3b. *Mol. Cell*, 9:1241–1249, Jun 2002.

[53] C. E. Fitzgerald, S. B. Patel, J. W. Becker, P. M. Cameron, D. Zaller, V. B. Pikounis, S. J. O'Keefe, and G. Scapin. Structural basis for p38alpha MAP kinase quinazolinone and pyridol-pyrimidine inhibitor specificity. *Nat Struct Biol*, 10(9):764–769, Sep 2003.

[54] Z. Wang, P.C. Harkins, R.J. Ulevitch, J. Han, M.H. Cobb, and E.J. Goldsmith. The structure of mitogen-activated protein kinase p38 at 2.1-A resolution. *Proc. Natl. Acad. Sci. U.S.A.*, 94:2327–2332, Mar 1997.

[55] M. J. Hartshorn, C. W. Murray, A. Cleasby, M. Frederickson, I. J. Tickle, and H. Jhoti. Fragment-based lead discovery using X-ray crystallography. *J Med Chem*, 48(2):403–413, Jan 2005.

[56] K. P. Wilson, P. G. McCaffrey, K. Hsiao, S. Pazhanisamy, V. Galullo, G. W. Bemis, M. J. Fitzgibbon, P .R. Caron, M. A. Murcko, and M. S. Su. The structural basis for the specificity of pyridinylimidazole inhibitors of p38 MAP kinase. *Chem Biol*, 4(6):423–431, Jun 1997.

[57] N. Tamayo, L. Liao, M. Goldberg, D. Powers, Y. Tudor, V. Yu, L.M. Wong, B. Henkle, S. Middleton, R. Syed, T. Harvey, G. Jang, R. Hungate, and C. Dominguez. Design and synthesis of potent pyridazine inhibitors of p38 MAP kinase. *Bioorg Med Chem Lett*, 15(9):2409–2413, May 2005.

[58] S. K. Laughlin, M.P. Clark, J. F. Djung, A. Golebiowski, T. A. Brugel, M. Sabat, R. G. Bookland, M. J. Laufersweiler, J. C. VanRens, J. A. Townes, B. De, L. C. Hsieh, S. C. Xu, R. L. Walter, M. J. Mekel, and M.J. Janusz. The development of new isoxazolone based inhibitors of tumor necrosis factor-alpha (TNF-alpha) production. *Bioorg Med Chem Lett*, 15(9):2399–2403, May 2005.

[59] A. Golebiowski, J. A . Townes, M.J. Laufersweiler, T. A. Brugel, M. P. Clark, C. M. Clark, J. F. Djung, S. K. Laughlin, M. P. Sabat, R. G. Bookland, J. C. VanRens, B. De, L. C. Hsieh, M. J. Janusz, R. L. Walter, M. E. Webster, and M. J. Mekel. The development of monocyclic pyrazolone based cytokine synthesis inhibitors. *Bioorg Med Chem Lett*, 15(9):2285–2289, May 2005.

[60] E. L. Michelotti, K. K. Moffett, D. Nguyen, M. J. Kelly, R. Shetty, X. Chai, K. Northrop, V. Namboodiri, B. Campbell, G.A. Flynn, T. Fujimoto, F.P. Hollinger, M. Bukhtiyarova, E. B. Springman, and M. Karpusas. Two classes of p38alpha MAP kinase inhibitors

having a common diphenylether core but exhibiting divergent binding modes. *Bioorg Med Chem Lett*, 15(23):5274–5279, Dec 2005.

[61] K. F. McClure, E. R. Abramov, Y. A .and Laird, J. T. Barberia, W. Cai, T. J. Carty, S. R. Cortina, D. E. Danley, A. J. Dipesa, K. M. Donahue, N. C. Dombroski, M. A .and Elliott, C. A. Gabel, S. Han, T. R. Hynes, P.K. Lemotte, M.N. Mansour, E. S. Marr, M.A. Letavic, J. Pandit, D. B. Ripin, F. J. Sweeney, D. Tan, and Y. Tao. Theoretical and experimental design of atypical kinase inhibitors: application to p38 MAP kinase. *J Med Chem*, 48(18):5728–5737, Sep 2005.

[62] R. Diskin, D. Engelberg, and O. Livnah. High-resolution diffracting crystals of intrinsically active p38alpha MAP kinase: a case study for low-throughput approaches. *Acta Crystallogr D Biol Crystallogr*, 63(Pt 2):260–265, Feb 2007.

[63] D.M. Goldstein, T. Alfredson, J. Bertrand, M.F. Browner, K. Clifford, S.A. Dalrymple, J. Dunn, J. Freire-Moar, S. Harris, S.S. Labadie, J. La Fargue, J.M. Lapierre, S. Larrabee, F. Li, E. Papp, D. McWeeney, C. Ramesha, R. Roberts, D. Rotstein, B. San Pablo, E.B. Sjogren, O.Y. So, F.X. Talamas, W. Tao, A. Trejo, A. Villasenor, M. Welch, T. Welch, P. Weller, P.E. Whiteley, K. Young, and S. Zipfel. Discovery of S-[5-amino-1-(4-fluorophenyl)-1H-pyrazol-4-yl]-[3-(2,3-dihydroxypropoxy)phenyl]methanone (RO3201195), an orally bioavailable and highly selective inhibitor of p38 MAP kinase. *J. Med. Chem.*, 49:1562–1575, Mar 2006.

[64] T.A. Brugel, J.A. Maier, M.P. Clark, M. Sabat, A. Golebiowski, R.G. Bookland, M.J. Laufersweiler, S.K. Laughlin, J.C. Vanrens, B. De, L.C. Hsieh, M.J. Mekel, and M.J. Janusz. Development of N-2,4-pyrimidine-N-phenyl-N'-phenyl ureas as inhibitors of tumor necrosis factor alpha (TNF-alpha) synthesis. Part 1. *Bioorg. Med. Chem. Lett.*, 16:3510–3513, Jul 2006.

[65] J.A. Maier, T.A. Brugel, M.P. Clark, M. Sabat, A. Golebiowski, R.G. Bookland, M.J. Laufersweiler, S.K. Laughlin, J.C. Vanrens, B. De, L.C. Hsieh, K.K. Brown, K. Juergens, R.L. Walter, and M.J. Janusz. Development of N-2,4-pyrimidine-N-phenyl-N'-alkyl ureas as orally active inhibitors of tumor necrosis factor alpha (TNF-alpha) synthesis. Part 2. *Bioorg. Med. Chem. Lett.*, 16:3514–3518, Jul 2006.

[66] M. Sabat, J. C. Vanrens, M. P. Clark, T. A. Brugel, J. Maier, R. G. Bookland, M. J. Laufersweiler, S. K. Laughlin, A. Golebiowski, B. De, L. C. Hsieh, R. L. Walter, M. J.

Mekel, and M. J. Janusz. The development of novel C-2, C-8, and N-9 trisubstituted purines as inhibitors of TNF-alpha production. *Bioorg Med Chem Lett*, 16(16):4360–4365, Aug 2006.

[67] S. R. Natarajan, S. T. Heller, K. Nam, S. B. Singh, G. Scapin, S. Patel, J.E. Thompson, C. E. Fitzgerald, and S. J. O'keefe. p38 MAP kinase inhibitors. Part 6: 2-Arylpyridazin-3-ones as templates for inhibitor design. *Bioorg Med Chem Lett*, 16(22):5809–5813, Nov 2006.

[68] T.G. Murali Dhar, S.T. Wrobleski, S. Lin, J.A. Furch, D.S. Nirschl, Y. Fan, G. Todderud, S. Pitt, A.M. Doweyko, J.S. Sack, A. Mathur, M. McKinnon, J.C. Barrish, J.H. Dodd, G.L. Schieven, and K. Leftheris. Synthesis and SAR of p38alpha MAP kinase inhibitors based on heterobicyclic scaffolds. *Bioorg. Med. Chem. Lett.*, 17:5019–5024, Sep 2007.

[69] G.J. Kleywegt. Validation of protein crystal structures. *Acta Crystallogr. D Biol. Crystallogr.*, 56:249–265, Mar 2000.

[70] K. Kinkel. Computer-chemical contributions to protein-ligand-interactions of the p38 map kinase, 2005.

[71] A. T. Bruenger, J. Kuriyan, and M. Karplus. Crystallographic r factor refinement by molecular dynamics. *Science*, pages 235(4787), 458–60, 1987.

[72] A. T. Bruenger. Free r value: a novel statistical quantity for assessing the accuracy of crystal structures. *Nature*, pages 355(6359), 472–5, 1992.

[73] EMBL-European Bioinformatics Institute (EBI). Technical report, http://www.ebi.ac.uk/thornton-srv/databases/cgi-bin/pdbsum/, 2008.

[74] Kabsch W. and Sander C. Dictionary of protein secondary structure: pattern recognition of hydrogen-bonded and geometrical features. *Biopolymers*, 22:2577–2637, 1983.

[75] C. Peifer, K. Kinkel, M. Abadleh, D. Schollmeyer, and S. Laufer. From five- to six-membered rings: 3,4-diarylquinolinone as lead for novel p38MAP kinase inhibitors. *J. Med. Chem.*, 50:1213–1221, Mar 2007.

[76] M.A. Kastenholz, M. Pastor, G. Cruciani, E.E. Haaksma, and T. Fox. GRID/CPCA: a new computational tool to design selective ligands. *J. Med. Chem.*, 43:3033–3044, Aug 2000.

[77] J.J. Sutherland, R.K. Nandigam, J.A. Erickson, and M. Vieth. Lessons in molecular recognition. 2. Assessing and improving cross-docking accuracy. *J Chem Inf Model*, 47:2293–2302, 2007.

[78] P.C. Hawkins, G.L. Warren, A.G. Skillman, and A. Nicholls. How to do an evaluation: pitfalls and traps. *J Comput Aided Mol Des*, Jan 2008.

[79] J.A. Erickson, M. Jalaie, D.H. Robertson, R.A. Lewis, and M. Vieth. Lessons in molecular recognition: the effects of ligand and protein flexibility on molecular docking accuracy. *J. Med. Chem.*, 47:45–55, Jan 2004.

[80] P.K. Gadakar, S. Phukan, P. Dattatreya, and V.N. Balaji. Pose prediction accuracy in docking studies and enrichment of actives in the active site of GSK-3beta. *J Chem Inf Model*, 47:1446–1459, 2007.

[81] G.B. McGaughey, R.P. Sheridan, C.I. Bayly, J.C. Culberson, C. Kreatsoulas, S. Lindsley, V. Maiorov, J.F. Truchon, and W.D. Cornell. Comparison of topological, shape, and docking methods in virtual screening. *J Chem Inf Model*, 47:1504–1519, 2007.

[82] R. Kim and J. Skolnick. Assessment of programs for ligand binding affinity prediction. *J Comput Chem*, Jan 2008.

[83] J.C. Cole, C.W. Murray, J.W. Nissink, R.D. Taylor, and R. Taylor. Comparing protein-ligand docking programs is difficult. *Proteins*, 60:325–332, Aug 2005.

[84] M. Kontoyianni, L.M. McClellan, and G.S. Sokol. Evaluation of docking performance: comparative data on docking algorithms. *J. Med. Chem.*, 47:558–565, Jan 2004.

[85] Y. Pan, N. Huang, S. Cho, and A.D. MacKerell. Consideration of molecular weight during compound selection in virtual target-based database screening. *J Chem Inf Comput Sci*, 43:267–272, 2003.

[86] G. Vriend. WHAT IF: a molecular modeling and drug design program. *J Mol Graph*, 8(1):52–56, Mar 1990.

[87] G. Vriend, C. Sander, and P. F. Stouten. A novel search method for protein sequence–structure relations using property profiles. *Protein Eng*, 7(1):23–29, Jan 1994.

[88] R.A . Engh and R. Huber. Accurate bond and angle parameters for x-ray protein structure refinement. *Acta Cryst.*, A47:392–400, 1991.

[89] D. Cremer and J. A. Pople. General definition of ring puckering coordinates. *J. Am. Chem. Soc.*, 97:1354–1358, 1975.

[90] Z. Yuan, T.L. Bailey, and R.D. Teasdale. Prediction of protein B-factor profiles. *Proteins*, 58:905–912, Mar 2005.

[91] M.J. Sippl. Recognition of errors in three-dimensional structures of proteins. *Proteins*, 17:355–362, Dec 1993.

[92] M. Wiederstein and M.J. Sippl. ProSA-web: interactive web service for the recognition of errors in three-dimensional structures of proteins. *Nucleic Acids Res.*, 35:W407–410, Jul 2007.

[93] A.L. Morris, M.W. MacArthur, E.G. Hutchinson, and J.M. Thornton. Stereochemical quality of protein structure coordinates. *Proteins*, 12:345–364, Apr 1992.

[94] Tripos. *Receptor-Ligand Modeling for New Modelers*, 2005.

[95] Molecular Discovery Ltd. *GRID manual*, 2004.

[96] P J Goodford. A computational procedure for determining energetically favorable binding sites on biologically important macromolecules. *J Med Chem*, 28(7):849–857, Jul 1985.

[97] Tripos. *SYBYL Interface to the FlexX Suite*, 2004.

[98] R.A. Friesner, J.L. Banks, R.B. Murphy, T.A. Halgren, J.J. Klicic, D.T. Mainz, M.P. Repasky, E.H. Knoll, M. Shelley, J.K. Perry, D.E. Shaw, P. Francis, and P.S. Shenkin. Glide: a new approach for rapid, accurate docking and scoring. 1. Method and assessment of docking accuracy. *J. Med. Chem.*, 47:1739–1749, Mar 2004.

[99] T.A. Halgren, R.B. Murphy, R.A. Friesner, H.S. Beard, L.L. Frye, W.T. Pollard, and J.L. Banks. Glide: a new approach for rapid, accurate docking and scoring. 2. Enrichment factors in database screening. *J. Med. Chem.*, 47:1750–1759, Mar 2004.

[100] M.D. Eldridge, C.W. Murray, T.R. Auton, G.V. Paolini, and R.P. Mee. Empirical scoring functions: I. The development of a fast empirical scoring function to estimate the binding affinity of ligands in receptor complexes. *J. Comput. Aided Mol. Des.*, 11:425–445, Sep 1997.

[101] Schrödinger LLC. *GLIDE 4.0 User Manual*, 2006.

[102] Z. Zsoldos, D. Reid, A. Simon, B.S. Sadjad, and A.P. Johnson. eHiTS: an innovative approach to the docking and scoring function problems. *Curr. Protein Pept. Sci.*, 7:421–435, Oct 2006.

[103] Z. Zsoldos, D. Reid, A. Simon, S.B. Sadjad, and A.P. Johnson. eHiTS: a new fast, exhaustive flexible ligand docking system. *J. Mol. Graph. Model.*, 26:198–212, Jul 2007.

A. Databases

A.1. Ligands for docking

This chapter includes the used ligands for the Docking evaluation.

No.	Structure	Name	PDB	MW	EN (kcal/mol)	IC $_{50}$ nM
1.	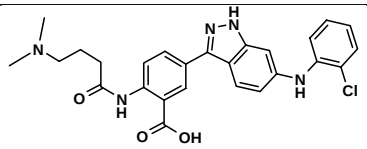	AIZ501	2B1P	491.9720	60.8832	903
2.	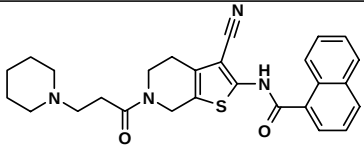	COM2000	2O0U	472.6048	141.8275	$\leq$4.8 [1]
3.	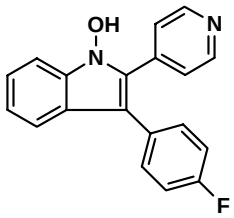	FPH	1OZ1	305.3074	93.3378	1
4.	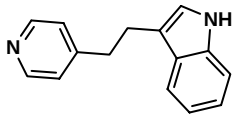	L12	1W84	222.2864	22.5271	n. t.
5.	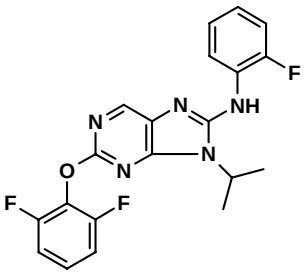	LIE301	2GTN	399.3710	71.9225	n. t.

[1] (pIC$_{50}$corresponds to -log IC$_{50}$, higher values indicate exponentially greater potency)

6.	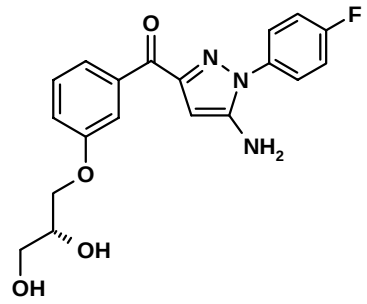	PQB1	2GFS	371.3641	32.9947	200
7.	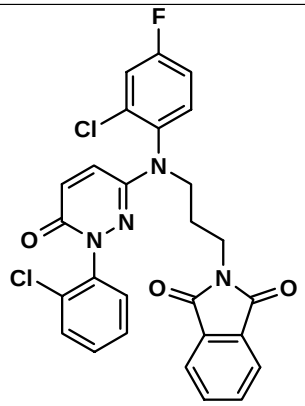	Q222-400	2I0H	537.3720	121.1298	9
8.	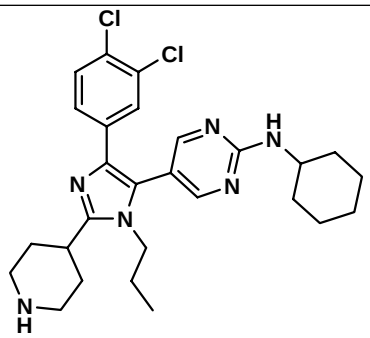	Q880-501	1PMQ	513.508	173.0708	4
9.	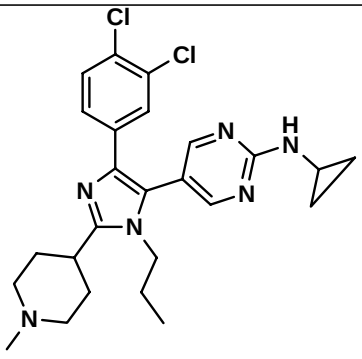	Q984-501	1PMN	485.4546	352.9408	0.2

Table A.1.: Ligands for docking evaluation

A.2. Compounds for docking: Suberones, Revesz and Ottosen compounds

A.2.1. Suberone scaffold type GA

No.	Structure	Name	MW	EN (kcal/mol)	IC $_{50}\mu$M
1.	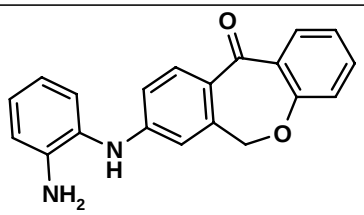	GA1min	316.3551	99.808	3.06 [2]
2.	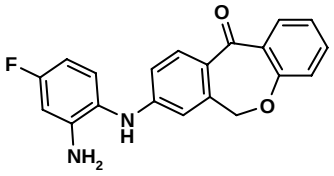	GA2min	319.3308	87.010	-
3.	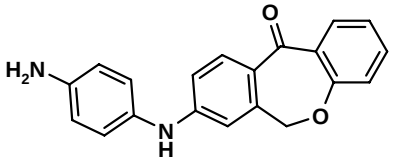	GA3min	316.3551	81.046	$\geq$ 5 [3]
4.	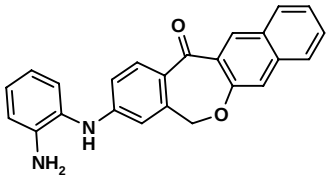	GA4min	366.4141	108.700	-
5.	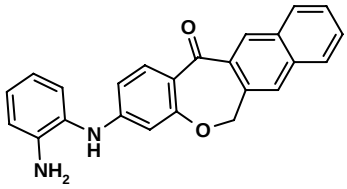	GA5min	366.4141	110.669	-

[2]SB203580 0.064
[3]SB203580 0.064

6.	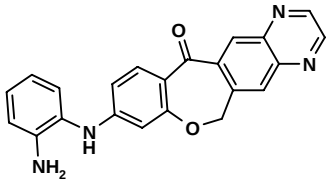	GA6min	368.3901	144.582	-
7.	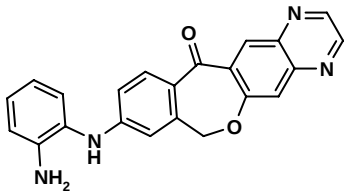	GA7min	368.3901	140.649	-
8.	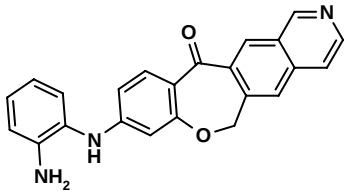	GA8min	367.4021	111.865	-
9.	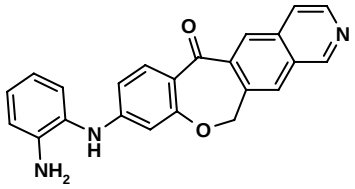	GA9min	367.4021	113.312	-
10.	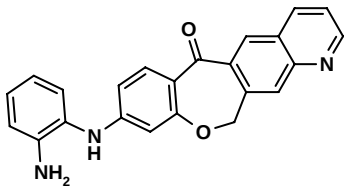	GA10min	367.4021	110.452	-
11.	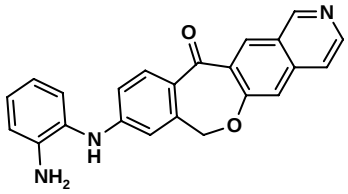	GA11min	367.4021	110.036	-

12.	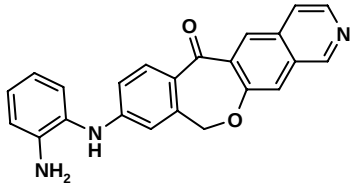	GA12min	367.4021	109.950	-
13.	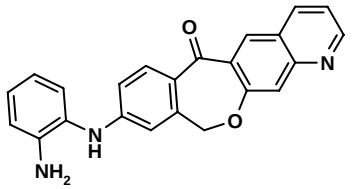	GA13min	367.4021	107.960	-
14.	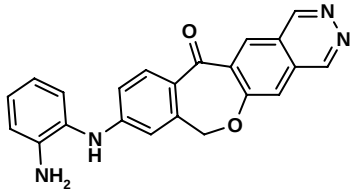	GA14min	368.3901	115.378	-
15.	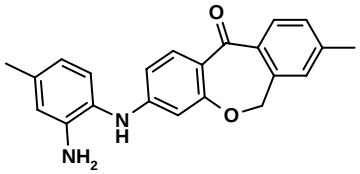	GA15min	368.3901	118.621	-
16.	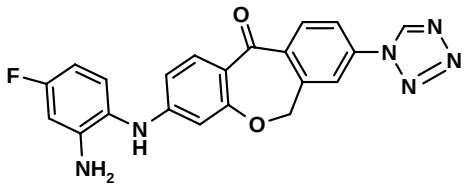	GA16min	384.3927	123.728	- [4]
17.	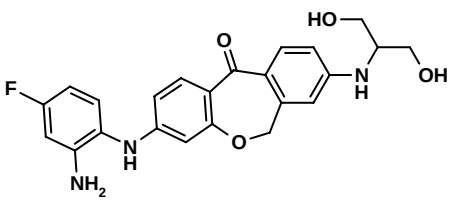	GA17min	405.4486	149.507	-

Table A.2.: Suberone scaffold type GA

[4] Di-fluoro: $\leq$3 SB203580 0.064

A.2.2. Suberone scaffold type JH

No.	Structure	Name	MW	EN (kcal/mol)	IC $_{50}\mu$M
1.	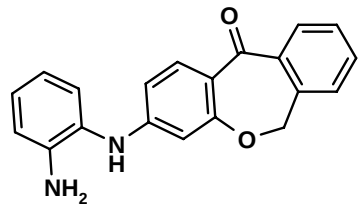	JH30min	316.3551	100.784	1.430 $\pm$ 0.676 [5]
2.	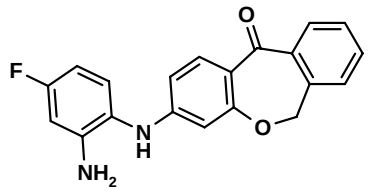	JH31min	334.345	95.963	0.038 $\pm$ 0.016 [6]
3.	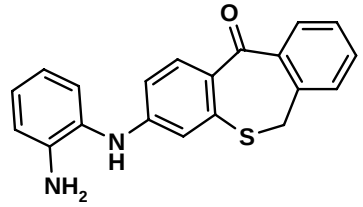	JH46min	332.4211	97.637	1.2 $\pm$ 0.315 [7]
4.	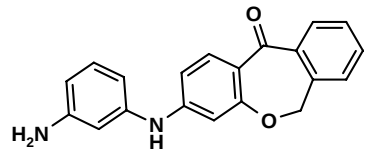	JH126min	316.3551	85.660	7.47 $\pm$ 0.160 [8]

Table A.3.: Suberone scaffold type JH

A.2.3. Suberone scaffold type MORE

No.	Structure	Name	MW	EN (kcal/mol)	IC $_{50}$
1.	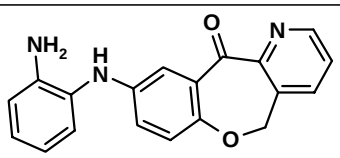	MO1min	317.3430	113.598	-

[5]SB203580 0.4276; n=3
[6]SB203580 0.0631; n=3
[7]SB203580 0.4171; n=3
[8]SB203580 0.4168; n=2

2.	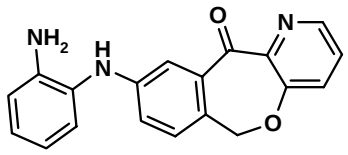	MO2min	317.3400	133.101	-
3.	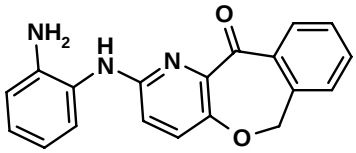	MO3min	317.3430	103.053	-
4.	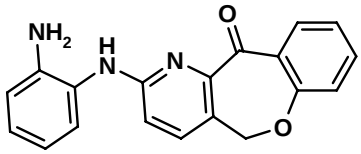	MO4min	317.3430	85.990	-
5.	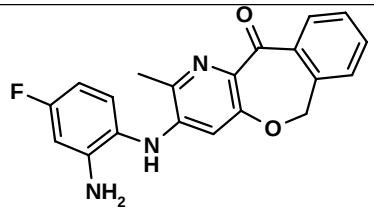	MO5min	349.3602	149.028	-
6.	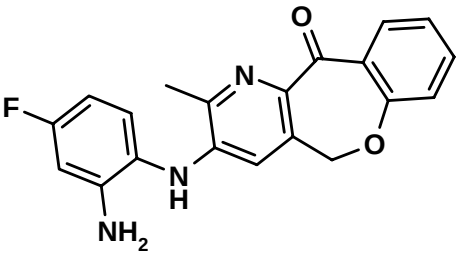	MO6min	349.3602	129.448	-
7.	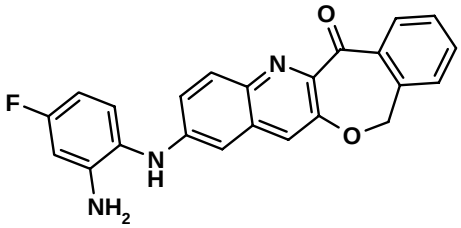	MO7min	385.3925	139.185	-
8.	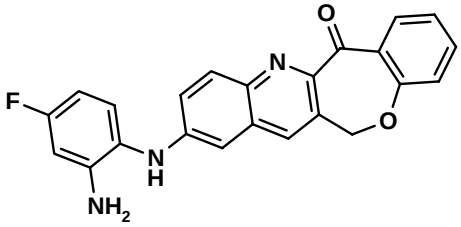	MO8min	385.3925	121.838	-

9.	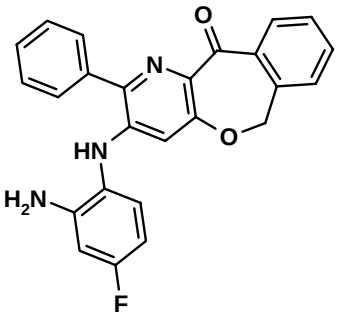	MO9min	411.4300	179.010	-
10.	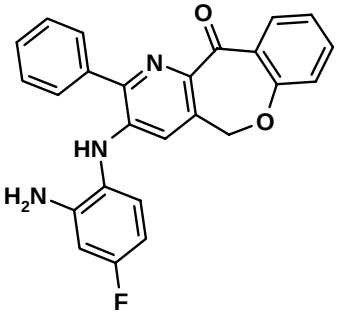	MO10min	411.4300	159.793	-
11.	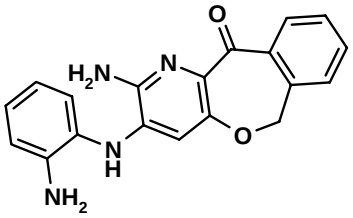	MO11min	332.3577	114.795	-
12.	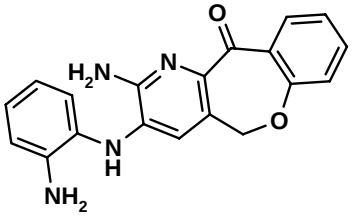	MO12min	332.3577	96.674	-
13.	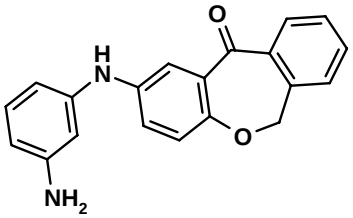	MO13min	316.3551	99.433	-
14.	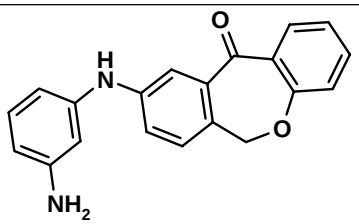	MO14min	316.3551	100.790	-

15.	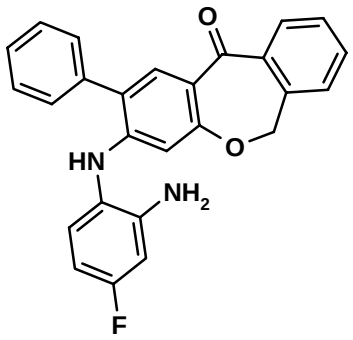	MO15min	410.442	124.550	-
16.	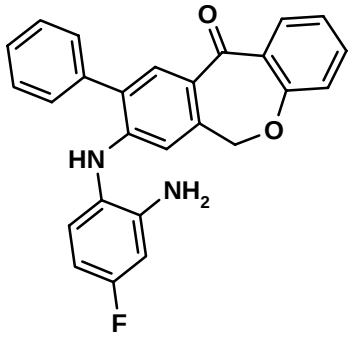	MO16min	410.442	123.790	-
17.	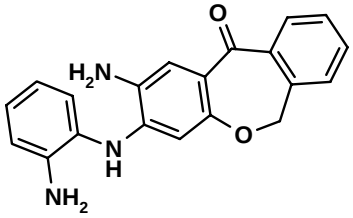	MO17min	331.3697	105.168	-
18.	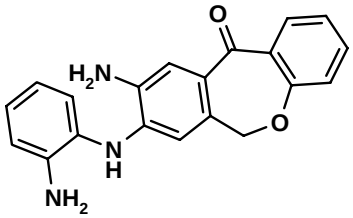	MO18min	331.3697	105.401	-
19.	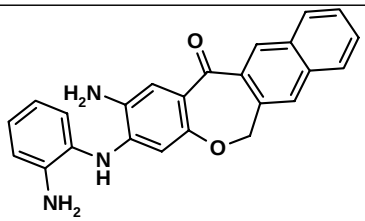	MO19min	381.4287	115.174	-

20.	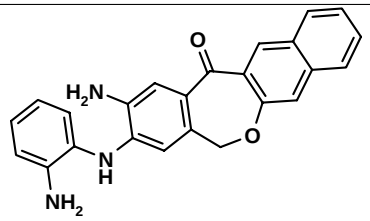	MO20min	381.4287	114.382	-
21.	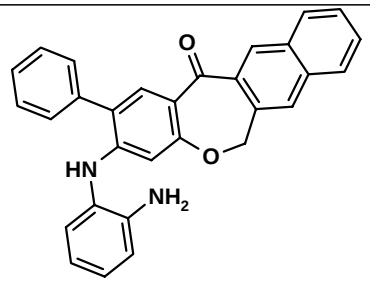	MO21min	442.5105	139.424	-
22.	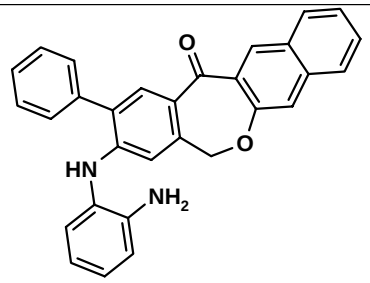	MO22min	442.5105	137.698	-
23.	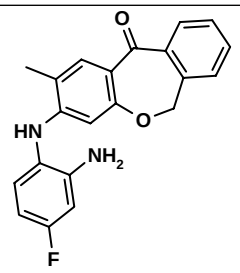	MO23min	348.3722	99.866	-
24.	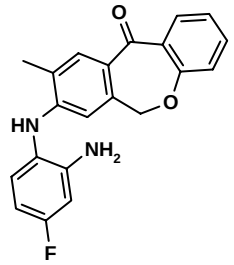	MO24min	348.3722	98.643	-
25.	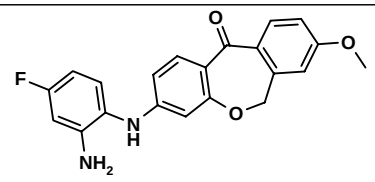	MO25min	364.3710	98.305	-

26.	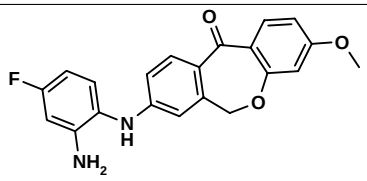	MO26min	364.3710	97.048	-
27.	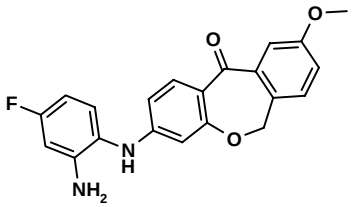	MO27min	364.3716	95.876	-
28.	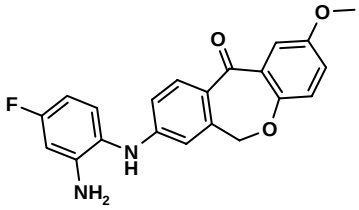	MO28min	364.3716	93.711	-
29.	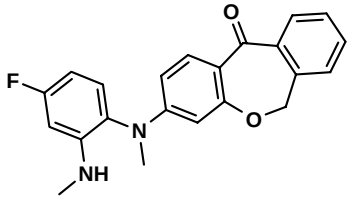	MO29min	362.3989	116.061	-
30.	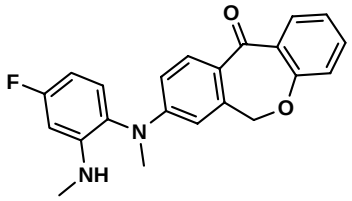	MO30min	362.3989	110.064	-
31.	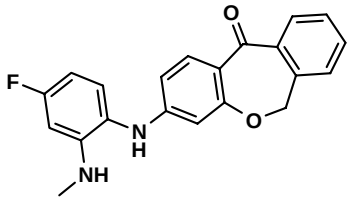	MO31min	348.3722	102.033	-
32.	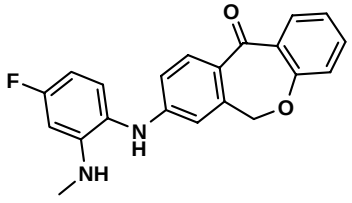	MO32min	348.3722	97.201	-

33.	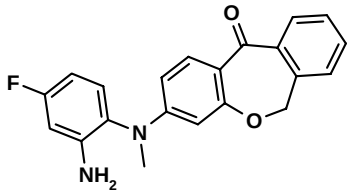	MO33min	348.3722	108.972	-
34.	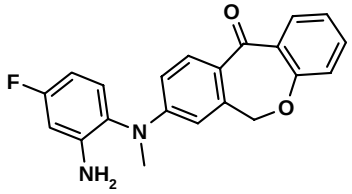	MO34min	348.3722	107.918	-
35.	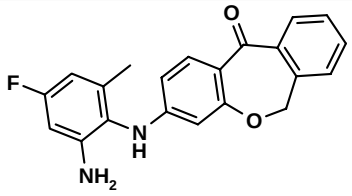	MO35min	348.3722	102.158	-
36.	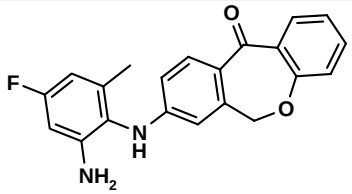	MO36min	348.3722	100.932	-
37.	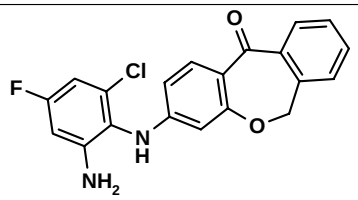	MO37min	368.7908	108.817	-
38.	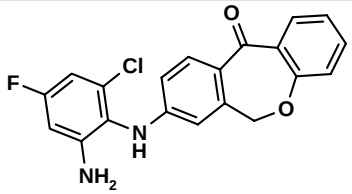	MO38min	368.7908	107.378	-
39.	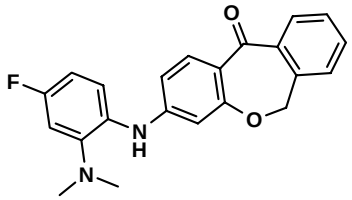	MO39min	362.3989	107.358	-

40.	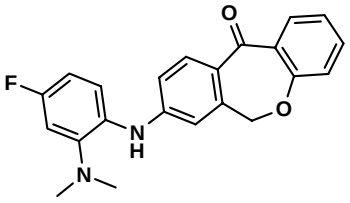	MO40min	362.3989	106.452	-

Table A.4.: Suberone scaffold type MORE

A.2.4. Suberone scaffold type MORE2

No.	Structure	Name	MW	EN (kcal/mol)	IC $_{50}\mu$M
1.	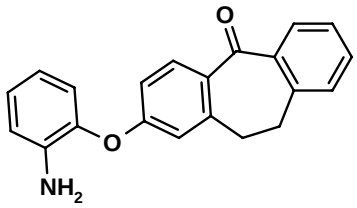	MORE1min	315.3671	118.501	-
2.	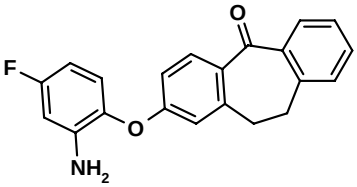	MORE2min	333.3575	114.152	-
3.	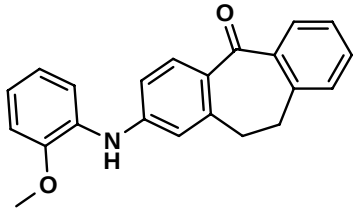	MORE3min	329.3937	112.540	$\leq$0.5 [9]
4.	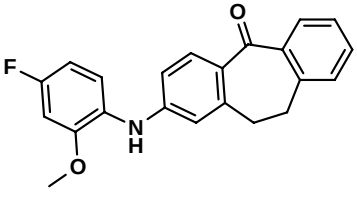	MORE4min	347.3842	104.690	- [10]

Table A.5.: Suberone scaffold type MORE2

[9] SB203580 0.015; with 3-amino subsituent $\leq$0.5; SB203580 0.064

[10] without 3-amino subsituent 0.592; SB203580 0.064

A.2.5. Scaffold type OTTO

No.	Structure	Name	MW	EN (kcal/mol)	IC $_{50}$nM
1.	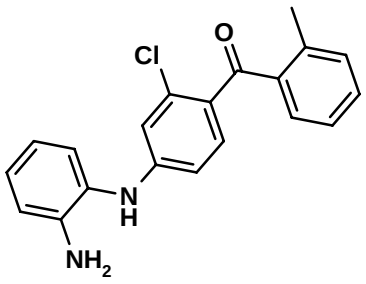	OTTO1min	336.8168	92.262	10± 3
2.	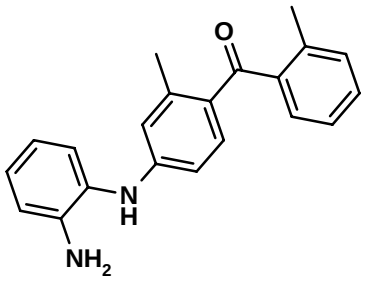	OTTO2min	316.3982	99.596	13± 3
3.	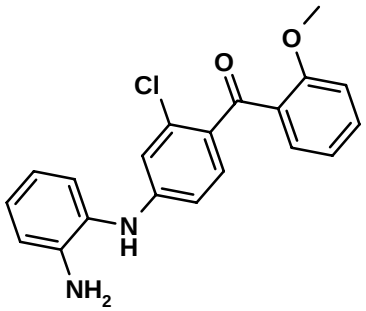	OTTO3min	352.8160	94.007	5± 2
4.	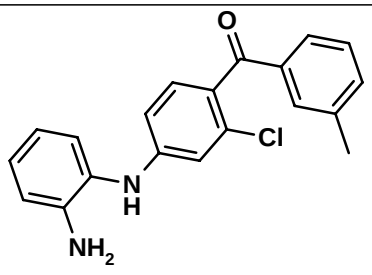	OTTO4min	336.8168	86.192	574± 16

Table A.6.: Scaffold type OTTO

A.2.6. Scaffold type REV

No.	Structure	Name	MW	EN (kcal/mol)	IC $_{50}$nM
1.	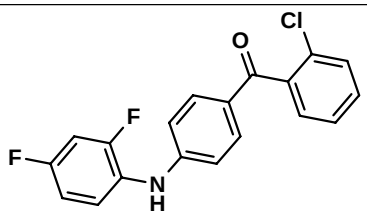	REV1min	343.7563	81.762	11
2.	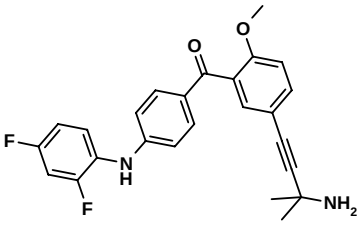	REV2min	420.4534	76.404	14
3.	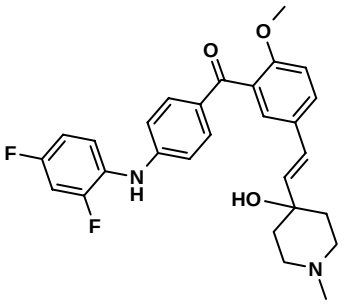	REV3min	478.5329	95.065	1
4.	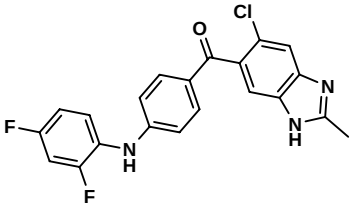	REV4min	397.8072	67.146	0.7
5.	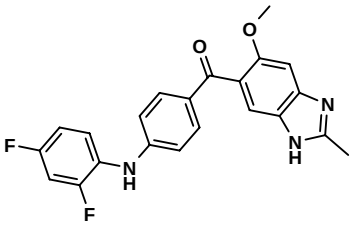	REV5min	393.3881	84.582	5
6.	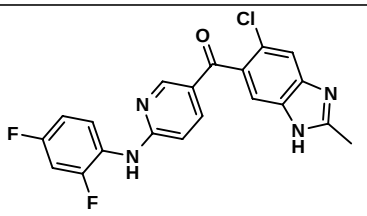	REV6min	398.795	41.062	8

7.	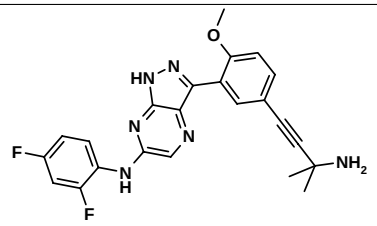	REV7min	434.4434	109.643	10
8.	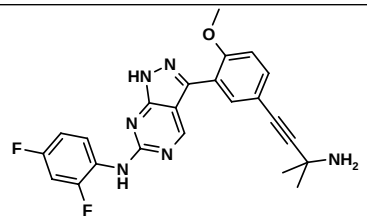	REV8min	434.4434	3.277	12
9.	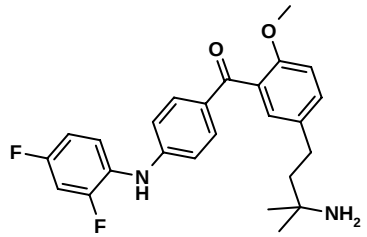	REV9min	424.4852	100.780	113
10.	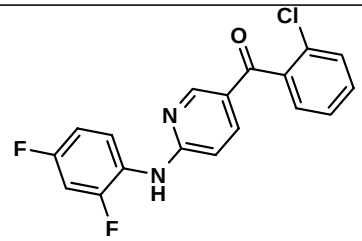	REV10min	344.7443	55.583	100

Table A.7.: Scaffold type REVESZ

A.2.7. Suberone scaffold type RN

No.	Structure	Name	MW	EN (kcal/mol)	IC $_{50}$ μM
1.	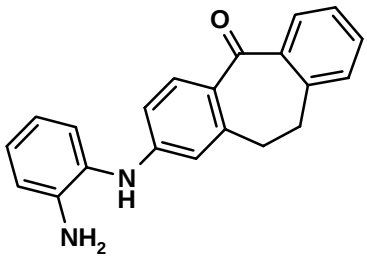	RN13amin	314.3823	104.047	0.087 [11]

[11] SB203580 0.049; n=4

2.	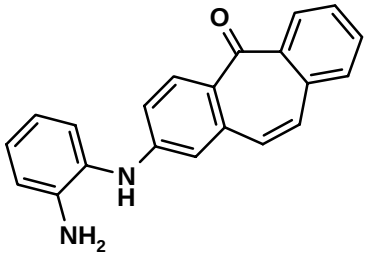	RN14amin	312.3664	132.157	1.06 [12]
3.	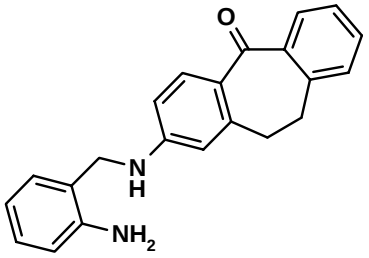	RN14min	328.4090	93.944	3.58 [13]
4.	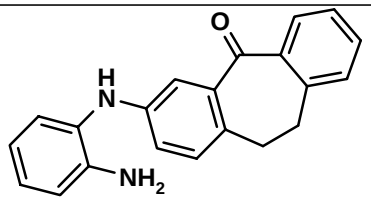	RN15min	314.3823	100.326	31.9 [14]

Table A.8.: Suberone scaffold type RN

A.2.8. Suberone scaffold type SK

No.	Structure	Name	MW	EN (kcal/mol)	IC $_{50}$
1.	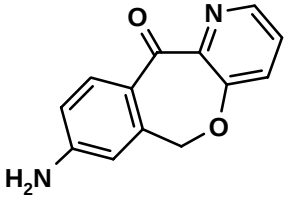	SK1min	226.2319	87.045	-
2.	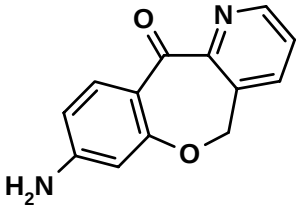	SK2min	226.2319	103.145	-

[12]SB203580 0.049; n=4
[13]SB203580 0.015; n=4
[14]SB203580 0.049; n=4

3.	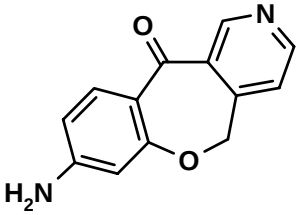	SK3min	226.2319	67.662	-
4.	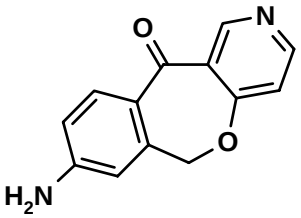	SK4min	226.2319	60.587	-
5.	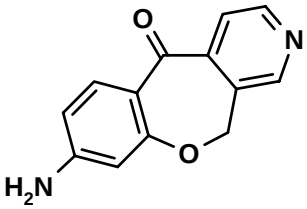	SK5min	226.2319	50.400	-
6.	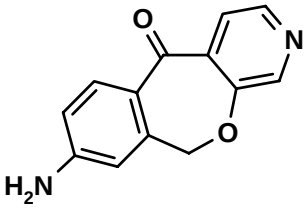	SK6min	226.2319	64.784	-
7.	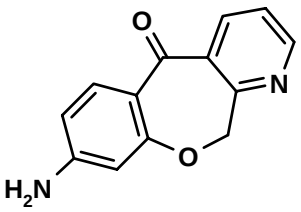	SK7min	226.2319	81.210	-
8.	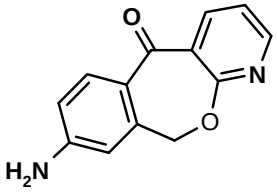	SK8min	226.2319	54.035	-
9.	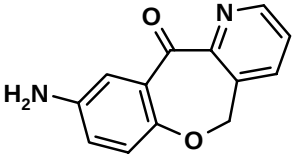	SK9min	226.2319	82.888	-

10.	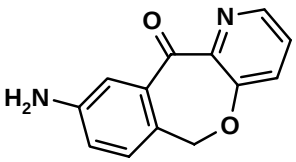	SK10min	226.2319	102.746	-
11.	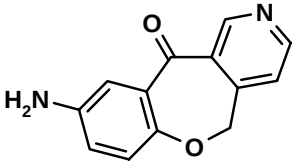	SK11min	226.2319	63.556	-
12.	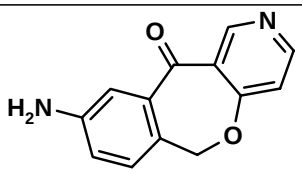	SK12min	226.2319	60.220	-
13.	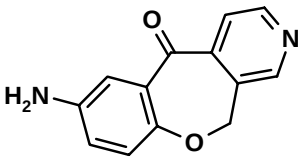	SK13min	226.2319	46.291	-
14.	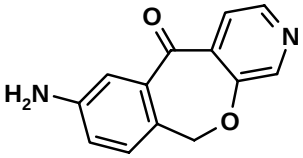	SK14min	226.2319	64.427	-
15.	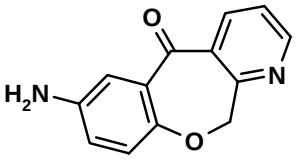	SK15min	226.2319	77.091	-
16.	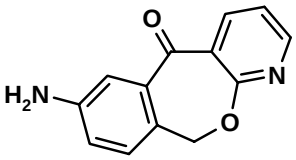	SK16min	226.2319	53.753	-
17.	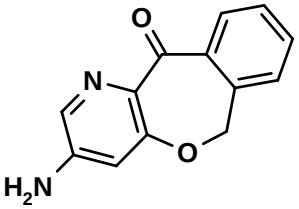	SK17min	225.2240	125.337	-

18.	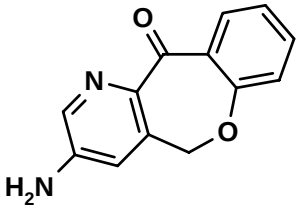	SK18min	226.2319	108.229	-
19.	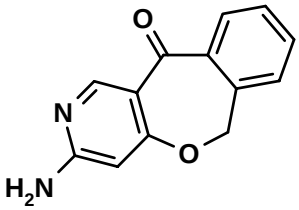	SK19min	226.2319	23.684	-
20.	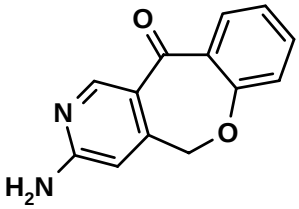	SK20min	226.2319	26.219	-
21.	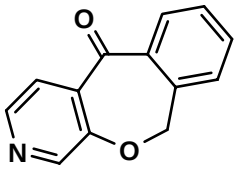	SK21min	211.2172	75.796	-
22.	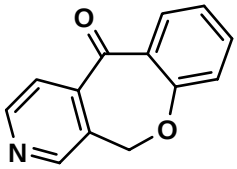	SK22min	211.2172	59.118	-
23.	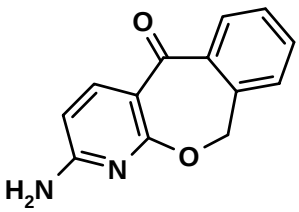	SK23min	226.2319	17.159	-
24.	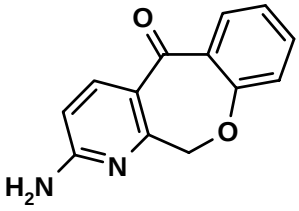	SK24min	226.2319	39.881	-

25.	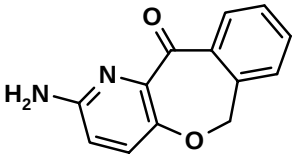	SK25min	226.2319	61.871	-
26.	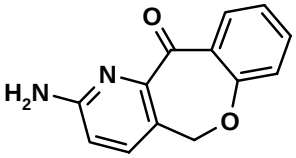	SK26min	226.2319	45.073	-
27.	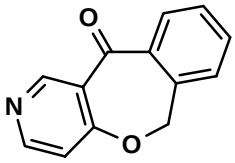	SK27min	211.2172	71.595	-
28.	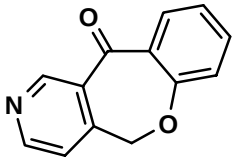	SK28min	211.2172	76.375	-
29.	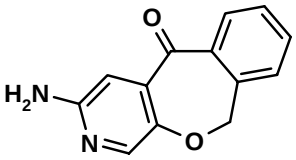	SK29min	226.2319	23.920	-
30.	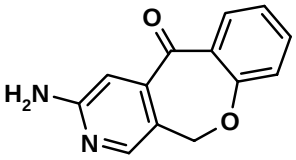	SK30min	226.2319	8.839	-
31.	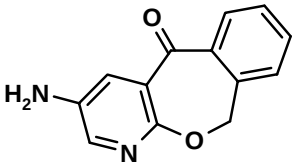	SK31min	225.2240	82.363	-
32.	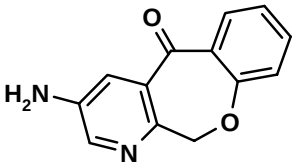	SK32min	226.2319	102.060	-

Table A.9.: Suberone scaffold type SK

A.2.9. Suberone scaffold type SG

No.	Structure	Name	MW	EN (kcal/mol)	IC $_{50}$ µM
1.	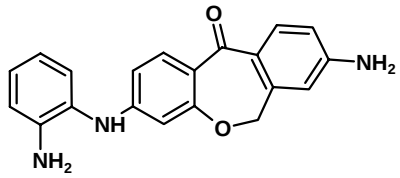	GA425	331.3697	89.778	$\leq$0.5 [15]
2.	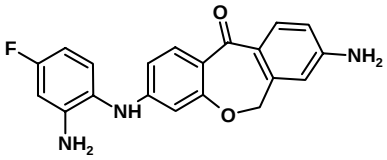	GA430	349.3602	84.954	$\leq$0.5 [16]
3.	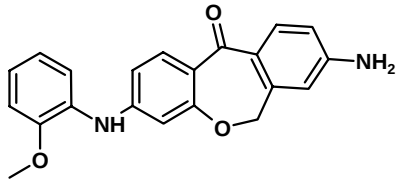	GA553	346.3812	98.304	n.t.
4.	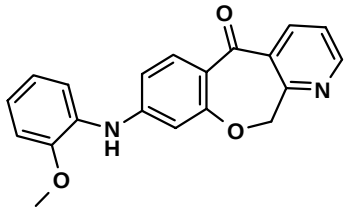	SK288	332.3545	117.665	$\geq$5
5.	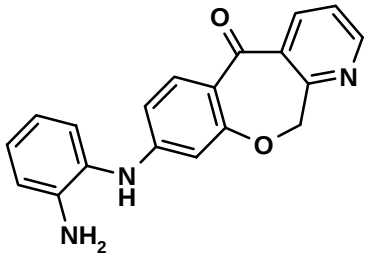	SK316	317.343	109.166	$\geq$1 [17]
6.	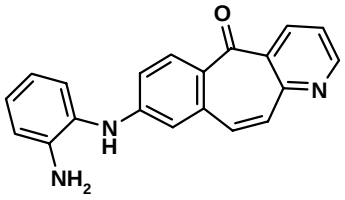	SK318	334.3206	121.536	$\geq$1 [18]

[15] SB203580 0.064
[16] SB203580 0.064
[17] SB203580 0.058
[18] SB203580 0.035

7.	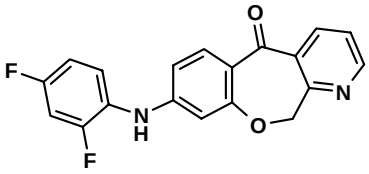	SK345	338.3093	103.493	$\geq$1
8.	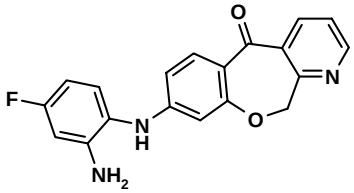	SK362	335.3335	104.375	$\leq$0.5
9.	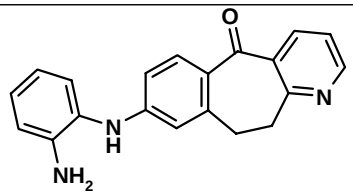	SK383	315.3703	97.914	$\leq$0.5 [19]
10.	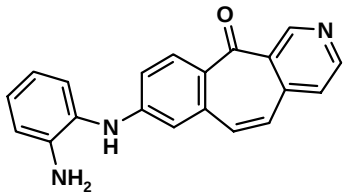	SK436	313.3544	123.494	$\geq$1 [20]
11.	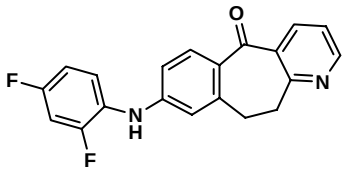	SK468	336.3365	92.189	$\leq$0.5 [21]
12.	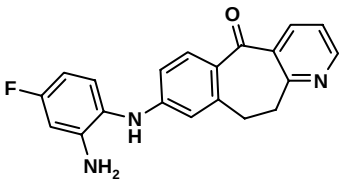	SK508	333.3607	93.107	$\leq$0.5 [22]
13.	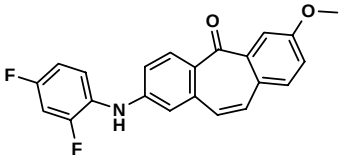	SK510	363.3588	96.193	- [23]

[19] SB203580 0.033
[20] SB203580 0.033
[21] SB203580 0.046
[22] SB203580 0.046
[23] $\geq$10% inhibition at 1μM; SB203580 0.059

14.	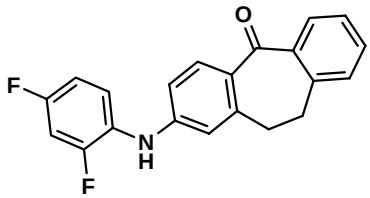	SK539	335.3485	98.236	$\leq$0.5 [24]
15.	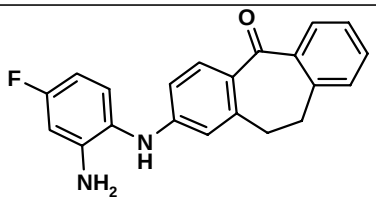	SK541	332.3728	99.260	$\leq$0.5 [25]
16.	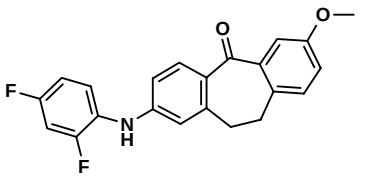	SK558	365.3746	98.130	$\leq$0.5 [26]
17.	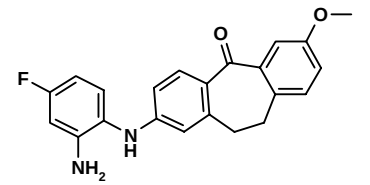	SK568	362.3989	99.177	$\leq$0.5 [27]

Table A.10.: Suberone scaffold type SG

[24] SB203580 0.059
[25] SB203580 0.046
[26] SB203580 0.059
[27] SB203580 0.024

A.2.10. Suberone scaffold type GA

Compound	a in Å	b in Å	c in Å	d in Å	e in Å	f in Å
GA1min	1.494	1.422	1.367	1.413	1.401	12.706
GA2min	1.494	1.422	1.367	1.406	1.405	12.696
GA3min	1.494	1.422	1.367	1.405	1.404	12.696
GA4min	1.494	1.423	1.367	1.413	1.401	12.739
GA5min	1.368	1.422	1.494	1.413	1.400	12.640
GA6min	1.368	1.422	1.494	1.413	1.400	12.648
GA7min	1.494	1.423	1.366	1.413	1.401	12.711
GA8min	1.368	1.422	1.495	1.413	1.400	12.659
GA9min	1.368	1.422	1.495	1.413	1.400	12.651
GA10min	1.368	1.423	1.494	1.413	1.400	12.680
GA11min	1.494	1.423	1.367	1.413	1.401	12.723
GA12min	1.494	1.423	1.367	1.413	1.401	12.795
GA13min	1.494	1.423	1.367	1.413	1.401	12.755
GA14min	1.494	1.423	1.367	1.413	1.400	12.718
GA15min	1.368	1.422	1.495	1.413	1.400	12.721
GA16min	1.366	1.425	1.504	1.413	1.402	12.753
GA17min	1.364	1.426	1.499	1.413	1.402	12.730

Table A.11.: Distances of the Suberone scaffold type GA

A.2.11. Suberone scaffold type JH

Compound	a in Å	b in Å	c in Å	d in Å	e in Å	f in Å
JH30min	1.368	1.423	1.494	1.413	1.400	12.645
JH46min	1.794	1.809	1.496	1.413	1.400	12.486
JH126min	1.368	1.423	1.494	1.407	1.404	12.660
JH31min	1.368	1.423	1.494	1.413	1.401	12.639

Table A.12.: Distances of the Suberone scaffold type JH

A.2.12. Suberone scaffold type MORE

Compound	a in Å	b in Å	c in Å	d in Å	e in Å	f in Å
MO1min	1.367	1.423	1.489	1.414	1.405	12.059
MO2min	1.494	1.423	1.365	1.413	1.405	11.517
MO3min	1.364	1.423	1.495	1.405	1.390	12.082
MO4min	1.488	1.422	1.368	1.405	1.391	11.534
MO5min	1.365	1.423	1.495	1.413	1.403	11.794
MO6min	1.489	1.423	1.368	1.413	1.403	11.678
MO7min	1.365	1.423	1.495	1.413	1.400	15.017
MO8min	1.489	1.422	1.368	1.413	1.401	14.682
MO9min	1.365	1.423	1.494	1.412	1.407	11.779
MO10min	1.489	1.423	1.368	1.411	1.407	11.742
MO11min	1.365	1.423	1.494	1.409	1.404	11.847
MO12min	1.489	1.423	1.368	1.409	1.405	11.830
MO13min	1.366	1.423	1.494	1.414	1.405	12.475
MO14min	1.494	1.423	1.367	1.413	1.405	11.715
MO15min	1.367	1.423	1.494	1.412	1.409	11.831
MO16min	1.494	1.423	1.367	1.412	1.409	11.809
MO17min	1.367	1.422	1.494	1.409	1.407	11.877
MO18min	1.494	1.423	1.367	1.409	1.407	11.891
MO19min	1.367	1.422	1.494	1.409	1.407	11.958
MO20min	1.493	1.423	1.367	1.409	1.407	11.930
MO21min	1.367	1.422	1.494	1.412	1.408	11.857
MO22min	1.494	1.424	1.367	1.409	1.412	11.895
MO23min	1.367	1.423	1.494	1.413	1.404	11.851
MO24min	1.494	1.422	1.367	1.413	1.405	11.731
MO25min	1.368	1.422	1.495	1.413	1.401	12.629
MO26min	1.494	1.423	1.369	1.413	1.401	12.726
MO27min	1.368	1.423	1.494	1.413	1.401	12.663
MO28min	1.494	1.423	1.367	1.413	1.401	12.706
MO29min	1.367	1.422	1.494	1.425	1.409	11.182
MO30min	1.494	1.423	1.367	1.425	1.408	11.164
MO31min	1.368	1.422	1.494	1.412	1.399	11.907

MO32min	1.494	1.423	1.367	1.415	1.401	11.927
MO33min	1.368	1.422	1.494	1.423	1.408	11.125
MO34min	1.494	1.423	1.367	1.422	1.409	11.203
MO35min	1.368	1.422	1.494	1.414	1.401	11.476
MO36min	1.494	1.423	1.367	1.414	1.401	11.451
MO37min	1.368	1.422	1.494	1.416	1.401	11.536
MO38min	1.494	1.423	1.367	1.415	1.402	11.527
MO39min	1.368	1.422	1.494	1.413	1.398	11.936
MO40min	1.494	1.422	1.367	1.413	1.399	12.060

Table A.13.: Distances of the Suberone scaffold type MORE

A.2.13. Suberone scaffold type MORE2

Compound	**a in Å**	**b in Å**	**c in Å**	**d in Å**	**e in Å**	**f in Å**
MORE1min	1.510	1.522	1.499	1.381	1.376	12.042
MORE2min	1.510	1.522	1.500	1.381	1.376	12.044
MORE3min	1.510	1.522	1.500	1.412	1.400	12.634
MORE4min	1.510	1.522	1.500	1.412	1.400	12.635

Table A.14.: Distances of the Suberone scaffold type MORE2

A.2.14. Scaffold OTTOSEN compounds

Compound	**d in Å**	**e in Å**	**f in Å**
OTTO1min	1.413	1.401	12.177
OTTO2min	1.413	1.401	12.224
OTTO3min	1.413	1.401	11.717
OTTO4min	1.413	1.401	11.675

Table A.15.: Distances of the scaffold type OTTOSEN

A.2.15. Scaffold REVESZ compounds

Compound	d in Å	e in Å	f in Å
REV1min	1.408	1.403	12.471
REV2min	1.408	1.404	12.485
REV3min	1.408	1.403	12.443
REV4min	1.408	1.403	12.449
REV5min	1.408	1.403	12.493
REV6min	1.408	1.404	12.481
REV7min	1.408	1.409	12.797
REV8min	1.399	1.391	12.885
REV9min	1.408	1.403	12.475
REV10min	1.408	1.404	12.483

Table A.16.: Distances of the scaffold type REVESZ

A.2.16. Suberone scaffold type RN

Compound	a in Å	b in Å	c in Å	d in Å	e in Å	f in Å
RN13amin	1.510	1.522	1.500	1.413	1.400	12.606
RN14min	1.509	1.522	1.500	1.452	1.377	13.264
RN14amin	1.463	1.341	1.463	1.413	1.401	12.910
RN15min	1.509	1.522	1.500	1.412	1.401	12.610

Table A.17.: Distances of the Suberone scaffold type RN

A.2.17. Suberone scaffold type SG

Compound	a in Å	b in Å	c in Å	d in Å	e in Å	f in Å
GA425min	1.358	1.423	1.494	1.413	1.400	12.684
GA430min	1.368	1.423	1.494	1.413	1.401	12.685
GA553min	1.368	1.423	1.494	1.412	1.400	12.721
SK288min	1.366	1.425	1.497	1.412	1.400	12.691
SK316min	1.366	1.425	1.497	1.413	1.400	12.653
SK318min	1.463	1.342	1.462	1.408	1.403	12.822

SK345min	1.366	1.426	1.496	1.408	1.402	12.669
SK362min	1.366	1.426	1.497	1.413	1.401	12.654
SK383min	1.511	1.519	1.497	1.413	1.400	12.537
SK436min	1.464	1.342	1.464	1.413	1.401	12.863
SK468min	1.511	1.519	1.497	1.408	1.402	12.552
SK508min	1.511	1.519	1.497	1.412	1.400	12.538
SK510min	1.466	1.338	1.465	1.408	1.403	12.490
SK539min	1.500	1.522	1.510	1.408	1.403	12.663
SK541min	1.500	1.522	1.510	1.413	1.402	12.638
SK558min	1.500	1.522	1.510	1.408	1.403	12.670
SK568min	1.500	1.522	1.510	1.413	1.401	12.640

Table A.18.: Distances of the Suberone scaffold type SG

A.2.18. Suberone scaffold type SK

Compound	a in Å	b in Å	c in Å	e in Å
SK1min	1.369	1.432	1.489	1.382
SK2min	1.494	1.423	1.365	1.382
SK3min	1.368	1.432	1.492	1.382
SK4min	1.495	1.424	1.367	1.382
SK5min	1.368	1.423	1.487	1.382
SK6min	1.494	1.423	1.363	1.382
SK7min	1.367	1.425	1.497	1.382
SK8min	1.497	1.420	1.362	1.381
SK9min	1.368	1.423	1.489	-
SK10min	1.494	1.423	1.365	-
SK11min	1.366	1.423	1.492	-
SK12min	1.495	1.424	1.367	-
SK13min	1.367	1.423	1.487	-
SK14min	1.494	1.423	1.363	-
SK15min	1.365	1.425	1.496	-
SK16min	1.497	1.420	1.362	-
SK17min	1.367	1.423	1.494	1.382

SK18min	1.489	1.423	1.369	1.381
SK19min	1.367	1.424	1.495	1.377
SK20min	1.492	1.423	1.367	1.377
SK21min	1.363	1.423	1.495	-
SK22min	1.487	1.423	1.367	-
SK23min	1.363	1.420	1.498	1.377
SK24min	1.496	1.425	1.366	1.376
SK25min	1.363	1.423	1.495	-
SK26min	1.488	1.422	1.368	-
SK27min	1.367	1.424	1.495	-
SK28min	1.492	1.423	1.367	-
SK29min	1.362	1.423	1.495	-
SK30min	1.486	1.423	1.367	-
SK31min	1.362	1.420	1.498	-
SK32min	1.496	1.425	1.366	-

Table A.19.: Distances of the Suberone scaffold type SK

A.3. Comparisons of the different Suberone scaffolds; Angles

A.3.1. Suberone scaffold type GA

Compound	α **in** $^\circ$	β **in** $^\circ$	γ **in** $^\circ$	δ **in** $^\circ$	ϵ **in** $^\circ$	ς **in** $^\circ$
GA1min	120.44	108.52	113.80	113.30	118.81	119.15
GA2min	120.53	108.56	113.90	113.30	118.88	118.98
GA3min	120.50	108.53	113.87	113.28	119.06	118.96
GA4min	120.40	108.44	113.66	113.34	118.84	119.20
GA5min	113.12	114.38	108.63	120.67	118.74	119.31
GA6min	113.12	114.26	108.38	120.77	118.77	119.33
GA7min	120.46	108.61	114.20	113.45	118.80	119.13
GA8min	113.22	114.18	108.54	120.61	118.77	119.34
GA9min	113.21	114.19	108.52	120.67	118.78	119.34

GA10min	113.29	114.12	108.50	120.49	118.81	119.40
GA11min	120.47	108.50	113.94	113.22	118.79	119.14
GA12min	120.45	108.46	113.91	113.23	118.81	119.15
GA13min	120.31	108.47	113.69	113.49	118.79	119.15
GA14min	120.43	108.57	114.00	113.22	118.77	119.16
GA15min	113.42	113.63	108.39	120.42	118.75	119.32
GA16min	116.59	109.60	111.11	117.97	118.90	119.46
GA17min	116.44	109.19	110.87	117.67	119.18	119.19

Table A.20.: Angles of the Suberone scaffold type GA (α-ς)

Compound	η **in** $^\circ$	θ **in** $^\circ$	ι **in** $^\circ$	κ **in** $^\circ$
GA1min	132.20	117.03	118.82	124.12
GA2min	131.79	117.02	118.90	124.06
GA3min	131.87	117.05	118.88	124.05
GA4min	132.11	116.95	118.73	124.30
GA5min	132.35	119.09	117.22	123.66
GA6min	132.26	119.20	117.00	123.77
GA7min	132.22	117.18	118.68	124.12
- GA8min	132.24	119.10	117.01	123.85
GA9min	132.26	119.09	117.06	123.82
GA10min	132.13	119.08	116.94	123.95
GA11min	132.22	117.12	118.66	124.19
GA12min	132.19	117.09	118.70	124.18
GA13min	132.23	117.10	118.48	124.39
GA14min	132.20	117.20	118.54	124.23
GA15min	132.33	118.91	116.98	124.29
- GA16min	132.32	116.74	117.96	125.26
GA17min	131.61	116.84	118.23	124.87

Table A.21.: Angles of the Suberone scaffold type GA (η-κ)

A.3.2. Suberone scaffold type JH

Compound	α in °	β in °	γ in °	δ in °	ϵ in °	ς in °
JH30min	113.15	114.24	108.66	120.66	118.75	119.31
JH46min	112.68	102.65	109.90	120.87	118.77	119.29
JH126min	113.18	114.14	108.66	120.61	118.92	119.18
JH31min	113.15	114.32	108.75	120.67	118.78	119.38

Table A.22.: Angles of the Suberone scaffold type JH (α-ς)

Compound	η in °	θ in °	ι in °	κ in °
JH30min	132.33	119.00	117.19	123.77
JH46min	132.33	119.81	117.18	122.87
JH126min	131.97	118.95	117.16	123.86
JH31min	132.11	118.98	117.22	123.77

Table A.23.: Angles of the Suberone scaffold type JH (η-κ)

A.3.3. Suberone scaffold type MORE

Compound	α in °	β in °	γ in °	δ in °	ϵ in °	ς in °
MO1min	113.12	115.43	108.72	122.18	113.43	114.77
MO2min	120.94	108.89	114.80	113.60	113.47	114.66
MO3min	113.82	114.94	109.01	120.81	116.24	111.70
MO4min	122.25	108.61	115.12	113.00	116.30	111.39
MO5min	113.64	114.78	108.88	120.78	113.34	116.38
MO6min	122.10	108.68	115.34	112.99	111.41	116.38
MO7min	113.65	114.83	108.83	120.79	111.57	116.05
MO8min	122.34	108.70	115.40	135.99	111.57	116.13
MO9min	113.64	114.81	108.81	120.76	111.81	115.30
MO10min	122.08	108.58	115.31	113.05	111.94	115.32
MO11min	113.57	115.09	108.90	120.89	113.13	113.53
MO12min	121.93	108.54	115.15	113.02	113.33	113.55
MO13min	113.35	114.14	108.61	120.59	113.37	114.93
MO14min	120.58	108.55	113.74	113.36	113.47	114.73

MO15min	113.30	114.02	108.56	120.52	111.79	115.12
MO16min	120.54	108.53	114.03	113.31	111.89	115.10
MO17min	113.35	113.92	108.51	120.48	113.32	113.86
MO18min	120.35	108.48	113.75	113.37	113.51	113.86
MO19min	113.52	113.55	108.53	120.29	113.35	113.92
MO20min	120.07	108.32	113.18	113.49	113.52	113.90
MO21min	113.36	113.97	108.51	120.50	111.73	115.37
MO22min	120.02	108.38	112.99	113.65	111.73	115.33
MO23min	113.42	113.72	108.52	120.43	111.51	116.08
MO24min	120.59	108.56	114.14	113.21	111.66	116.12
MO25min	113.12	114.40	108.67	120.64	111.49	115.93
MO26min	120.45	108.45	113.77	113.17	111.71	116.07
MO27min	113.19	114.18	108.65	120.73	111.57	115.95
MO28min	120.53	108.54	113.94	113.32	111.70	116.01
MO29min	113.45	113.72	108.54	120.41	111.44	119.77
MO30min	120.35	108.60	113.85	113.34	112.07	120.08
MO31min	113.23	114.04	108.58	120.57	110.34	115.91
MO32min	120.42	108.56	113.95	113.27	111.65	116.03
MO33min	113.39	113.90	108.57	120.46	112.08	119.83
MO34min	120.41	108.62	113.91	113.31	112.23	119.88
MO35min	113.22	114.20	108.63	120.62	112.29	116.52
MO36min	120.31	108.52	113.69	113.39	112.43	116.40
MO37min	113.18	114.27	108.73	120.64	112.60	116.46
MO38min	120.29	108.45	113.73	113.31	112.53	116.19
MO39min	113.23	113.96	108.56	120.52	109.73	116.09
MO40min	120.37	108.59	113.89	113.28	109.83	115.91

Table A.24.: Angles of the Suberone scaffold type MORE (α-ς)

Compound	η **in** $^\circ$	θ **in** $^\circ$	ι **in** $^\circ$	κ **in** $^\circ$
MO1min	130.78	118.90	119.19	121.90
MO2min	130.66	116.59	120.66	122.72
MO3min	131.98	120.48	116.86	122.62

MO4min	132.30	118.87	118.86	122.26
MO5min	132.13	120.52	116.76	122.68
MO6min	132.03	119.09	118.96	121.94
MO7min	132.15	120.53	116.76	122.67
MO8min	132.16	119.12	119.02	121.85
MO9min	132.69	120.49	116.73	122.74
MO10min	132.50	119.01	119.07	121.91
MO11min	133.29	120.60	116.84	122.52
MO12min	133.06	118.95	118.83	122.20
MO13min	130.73	118.89	117.12	123.96
MO14min	130.75	116.92	118.81	124.25
MO15min	132.77	118.81	117.07	124.09
MO16min	132.65	117.00	119.01	123.97
MO17min	132.82	118.81	117.02	124.15
MO18min	132.62	117.03	118.76	124.19
MO19min	132.70	118.60	116.89	124.50
MO20min	132.58	116.89	118.46	124.63
MO21min	132.40	116.82	117.40	124.13
MO22min	132.64	116.78	118.41	124.80
MO23min	132.24	118.72	117.03	124.23
MO24min	131.97	117.10	119.03	123.84
MO25min	132.29	119.09	117.27	123.61
MO26min	132.01	117.01	118.80	124.17
MO27min	132.27	118.91	117.26	123.81
MO28min	132.10	116.95	119.00	124.03
MO29min	125.79	118.65	117.11	124.21
MO30min	125.73	116.98	118.88	124.11
MO31min	133.71	118.86	117.15	123.96
MO32min	132.13	117.02	118.95	124.00
MO33min	125.85	118.72	117.15	124.11
MO34min	125.94	116.99	118.91	124.08
MO35min	130.46	118.87	117.22	124.88
MO36min	130.45	116.94	118.80	124.24

MO37min	130.77	118.92	117.21	123.85
MO38min	131.00	117.01	118.78	124.18
MO39min	134.02	118.82	117.12	124.03
MO40min	134.02	117.05	118.89	124.03

Table A.25.: Angles of the Suberone scaffold type MORE (η-κ)

A.3.4. Suberone scaffold type MORE2

Compound	α **in** °	β **in** °	γ **in** °	δ **in** °	ϵ **in** °	ς **in** °
MORE1min	115.63	115.86	110.13	119.96	118.32	116.7
MORE2min	115.63	115.9	110.18	119.98	118.22	116.69
MORE3min	115.67	115.96	110.28	120.01	118.61	118.91
MORE4min	115.69	115.97	110.28	120.01	118.54	118.93

Table A.26.: Angles of the Suberone scaffold type MORE2 (α-ς)

Compound	η **in** °	θ **in** °	ι **in** °	κ **in** °
MORE1min	116.8	119.18	116.94	123.8
MORE2min	116.81	119.14	116.98	123.8
MORE3min	133.38	119.23	117.00	123.65
MORE4min	133.37	119.21	117.03	123.65

Table A.27.: Angles of the Suberone scaffold type MORE2 (η-κ)

A.3.5. Scaffold type OTTOSEN

Compound	α **in** °	β **in** °	γ **in** °	δ **in** °	ϵ **in** °	ς **in** °
OTTO1min	-	-	-	-	118.73	118.99
OTTO2min	-	-	-	-	118.78	119.11
OTTO3min	-	-	-	-	118.76	119.02
OTTO4min	-	-	-	-	118.76	119.02

Table A.28.: Angles of the scaffold type OTTOSEN (α-ς)

Compound	η **in** $^\circ$	θ **in** $^\circ$	ι **in** $^\circ$	κ **in** $^\circ$
OTTO1min	132.33	119.83	119.59	120.34
OTTO2min	132.32	120.86	118.75	120.34
OTTO3min	132.36	117.97	119.62	122.41
OTTO4min	132.29	118.02	120.57	121.37

Table A.29.: Angles of the scaffold type OTTOSEN (η-κ)

A.3.6. Scaffold type REVESZ

Compound	α **in** $^\circ$	β **in** $^\circ$	γ **in** $^\circ$	δ **in** $^\circ$	ϵ **in** $^\circ$	ς **in** $^\circ$
REV1min	-	-	-	-	118.86	118.69
REV2min	-	-	-	-	118.89	118.71
REV3min	-	-	-	-	118.92	118.70
REV4min	-	-	-	-	118.89	118.73
REV5min	-	-	-	-	118.90	118.73
REV6min	-	-	-	-	118.62	118.04
REV7min	-	-	-	-	118.67	118.34
REV8min	-	-	-	-	118.41	113.92
REV9min	-	-	-	-	118.88	118.68
REV10min	-	-	-	-	118.69	118.10

Table A.30.: Angles of the scaffold type REVESZ (α-ς)

Compound	η **in** $^\circ$	θ **in** $^\circ$	ι **in** $^\circ$	κ **in** $^\circ$
REV1min	132.95	120.47	118.12	121.36
REV2min	132.93	120.27	117.92	121.79
REV3min	132.83	120.46	118.04	121.49
REV4min	132.80	120.43	118.04	121.47
REV5min	132.87	120.06	117.92	121.99
REV6min	131.56	120.17	118.23	121.54
REV7min	131.31	111.05	121.88	127.03
REV8min	134.75	110.88	120.61	128.49
REV9min	132.96	120.15	118.06	121.77

REV10min	131.41	120.11	118.37	121.48

Table A.31.: Angles of the scaffold type REVESZ(η-κ)

A.3.7. Suberone scaffold type SG

Compound	α **in** °	β **in** °	γ **in** °	δ **in** °	ϵ **in** °	ς **in** °
GA425min	113.21	114.04	108.66	120.48	118.79	119.34
GA430min	113.21	114.07	108.68	120.49	118.71	119.33
GA553min	113.34	113.78	108.57	120.40	118.53	118.90
SK288min	113.61	113.29	109.37	116.65	118.59	118.98
SK316min	113.42	113.70	109.44	116.80	118.79	119.37
SK318min	119.26	111.51	112.24	114.98	118.89	118.80
SK345min	113.50	133.53	109.37	116.76	118.93	119.00
SK362min	113.42	113.71	109.46	116.79	118.73	119.36
SK383min	115.69	115.51	109.82	116.12	118.82	119.37
SK436min	119.12	111.64	111.52	119.57	118.80	119.18
SK468min	115.71	115.4	109.76	116.07	118.92	118.96
SK508min	115.69	115.52	109.84	116.12	118.75	119.35
SK510min	116.94	127.66	127.64	116.96	118.90	118.79
SK539min	120.14	110.27	116.14	115.63	118.95	118.77
SK541min	120.13	110.32	116.21	115.65	118.73	119.12
SK558min	120.15	110.28	116.16	115.72	118.90	118.72
SK568min	120.14	110.3	116.22	115.72	118.72	119.1

Table A.32.: Angles of the Suberone scaffold type SG (α-ς)

Compound	η **in** °	θ **in** °	ι **in** °	κ **in** °
GA425min	132.29	118.87	117.14	124
GA430min	132.27	118.84	117.16	124
GA553min	133.65	118.78	117.07	124.1
SK288min	133.42	118.46	116.62	124.9
SK316min	132.26	118.62	116.67	124.7
SK318min	132.81	116.73	116.57	126.70

SK345min	132.81	118.52	116.70	124.8
SK362min	132.25	118.60	116.69	124.70
SK383min	132.14	119.34	116.71	123.8
SK436min	132.21	116.99	116.58	126.43
SK468min	132.73	119.27	116.69	123.9
SK508min	132.13	119.31	116.72	123.9
SK510min	132.72	119.14	119.40	121.1
SK539min	132.70	116.98	119.40	123.50
SK541min	132.18	117.03	119.37	123.5
SK558min	132.76	116.90	119.47	123.5
SK568min	132.20	116.97	119.47	123.5

Table A.33.: Angles of the Suberone scaffold type SG (η-κ)

A.3.8. Suberone scaffold type SK

Compound	α **in** $^\circ$	β **in** $^\circ$	γ **in** $^\circ$	δ **in** $^\circ$	ϵ **in** $^\circ$	ς **in** $^\circ$
SK1min	113.01	115.37	108.70	122.18	-	120.80
SK2min	120.81	108.94	114.98	113.51	-	120.59
SK3min	113.63	113.24	108.34	120.68	-	120.81
SK4min	120.32	108.98	114.03	113.63	-	120.63
SK5min	113.51	113.45	108.45	121.04	-	120.82
SK6min	120.40	108.81	114.01	114.92	-	120.62
SK7min	113.52	113.49	109.34	116.75	-	120.83
SK8min	118.94	107.94	110.08	112.65	-	120.69
SK9min	113.04	115.63	108.87	122.27	-	-
SK10min	121.08	108.98	115.09	113.47	-	-
SK11min	113.59	113.53	108.40	120.80	-	-
SK12min	120.64	109.01	114.26	113.52	-	-
SK13min	113.46	113.74	108.48	121.17	-	-
SK14min	120.64	108.80	114.01	114.91	-	-
SK15min	113.53	113.65	109.35	116.81	-	-
SK16min	119.16	107.90	110.12	112.62	-	-
SK17min	113.45	115.17	108.35	121.23	-	121.09

SK18min	122.12	108.79	115.57	112.93	-	120.91
SK19min	113.90	113.64	108.91	120.19	-	120.20
SK20min	120.70	108.49	113.63	113.63	-	121.00
SK21min	114.92	114.03	108.83	120.49	-	-
SK22min	120.98	108.44	113.29	113.29	-	-
SK23min	112.61	110.14	107.97	119.69	-	116.69
SK24min	116.60	109.39	113.42	113.53	-	116.59
SK25min	113.71	115.02	109.01	120.89	-	-
SK26min	122.29	108.68	115.29	112.96	-	-
SK27min	113.56	114.22	109.04	120.46	-	-
SK28min	120.73	108.38	113.35	113.55	-	-
SK29min	115.00	114.27	108.95	120.55	-	-
SK30min	121.24	108.40	113.47	113.44	-	-
SK31min	112.76	109.94	107.95	118.93	-	-
SK32min	116.86	109.37	113.62	113.44	-	-

Table A.34.: Angles of the Suberone scaffold type SK (α-ς)

Compound	η **in** $^\circ$	θ **in** $^\circ$	ι **in** $^\circ$	κ **in** $^\circ$
SK1min	120.18	118.96	119.17	121.86
SK2min	120.14	116.80	120.70	122.46
SK3min	120.20	118.71	116.81	124.47
SK4min	120.13	117.51	118.63	123.83
SK5min	120.26	118.74	116.72	124.53
SK6min	120.14	117.34	118.62	124.01
SK7min	120.33	118.57	116.63	124.78
SK8min	120.05	117.42	116.99	125.58
SK9min	-	119.09	119.24	121.65
SK10min	-	116.86	120.78	122.32
SK11min	-	118.93	116.73	124.33
SK12min	-	117.61	118.75	123.61
SK13min	-	118.96	116.67	124.35
SK14min	-	117.37	118.61	123.99

SK15min	-	118.73	116.56	124.70
SK16min	-	117.46	116.95	125.59
SK17min	120.35	120.87	116.99	122.12
SK18min	120.44	119.27	119.02	121.70
SK19min	112.73	118.41	117.49	124.08
SK20min	112.51	116.72	118.79	124.49
SK21min	-	118.64	117.35	123.98
SK22min	-	113.52	116.68	118.68
SK23min	119.05	117.00	117.42	125.58
SK24min	118.75	116.58	118.59	124.81
SK25min	-	120.70	116.82	122.44
SK26min	-	119.11	118.84	122.03
SK27min	-	118.74	117.56	123.67
SK28min	-	116.79	118.78	124.42
SK29min	-	118.81	117.36	123.80
SK30min	-	116.82	118.69	124.47
SK31min	-	116.89	117.43	125.67
SK32min	-	116.65	118.58	124.76

Table A.35.: Angles of the Suberone scaffold type SK (η-κ)

Auflistung meiner Akademischen Lehrer

Prof. Dr. S. Alban	Pharmazeutische Biologie
Prof. Dr. W. Blaschek	Pharmazeutische Biologie
PD Dr. B. Classen	Pharmazeutische Biologie
Prof Dr. B. Clement	Pharmazeutische Chemie
Prof. Dr. R. Daniels	Pharmazeutische Technologie
Prof. Dr. W. Hänsel	Pharmazeutische Chemie
Prof. Dr. D. Heber	Pharmazeutische Chemie
Prof. Dr. T. Herdegen	Pharmakologie
Prof. Dr. K.-A. Kovar	Pharmazeutische Analytik
HD Dr. T. Kunze	Pharmazeutische Chemie
Prof. Dr. S. Laufer	Pharmazeutische Chemie
Prof. Dr. E. Maser	Pharmakologie
Prof. Dr. Dr. h.c. B. W. Müller	Pharmazeutische Technologie
Prof. Dr. H.-J. Schaller	Physikalische Chemie
Apotheker Gerd Stange	Geschichte der Naturwissenschaften
Prof. Dr. H. Steckel	Pharmazeutische Technologie
Prof. Dr. O. Werz	Pharmazeutische Analytik

Lebenslauf

Curriculum Vitae

Persönliche Daten

Katrin Kinkel
Gösstr. 92
72070 Tübingen

Tel.: 0 70 71/ 14 64 37
E-mail: katrin.kinkel@uni-tuebingen.de

Geb. am 16. Mai 1978 in Hannover
Ledig

Schulbildung

09.1984–07.1988	Grundschule Brink
09.1988–07.1990	Orientierungsstufe Brink
08.1990–07.1997	Gymnasium Langenhagen
06.1997	Abitur

Ausbildung zur PTA

09.1997–07.1999	Sabine-Blindow-Schulen, Hannover
08.1999–02.2000	Iris Apotheke, Laatzen

Hochschulstudium

04.2000–06.2004	Studium der Pharmazie an der Christians-Albrechts-Universität zu Kiel

05.08.2005 Drittes Staatsexamen und Approbation zur Apothekerin

Diplom

01.2005–10.2005 Diplomarbeit am Pharmazeutischen Institut mit dem Thema: "Computerchemische Beiträge von Ligand-Protein-Wechselwirkungen der p38 MAP Kinase", unter der Leitung von Prof. Dr. S. Laufer, Abteilung Medizinische Chemie, Universität Tübingen

Promotion

seit 11.2005 Dissertation am Pharmazeutischen Institut mit dem Thema:

"Ermittlung des Bindemodus von Suberon-Inhibitoren in der p38 MAP Kinase mit Methoden des Molecular Modelings"

unter der Leitung von Prof. Dr. S. Laufer, Abteilung Medizinische Chemie, Universität Tübingen